Adenylosuccinate lyase and metabolic fate of fumarate in the intraerythrocytic stages of *Plasmodium falciparum*

A thesis submitted for the award of the degree of

Doctor of Philosophy

By

Vinay Bulusu

July 2010

Molecular Biology and Genetics Unit

Jawaharlal Nehru Centre for Advanced Scientific Research

(Deemed University)

Jakkur, Bangalore 560 064

Adenylosuccinate Lyase and Metabolic Fate of Fumarate in the Intraerythrocytic Stages of *Plasmodium falciparum*

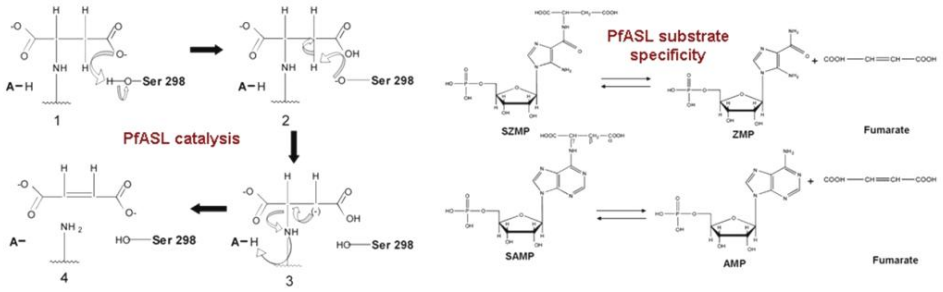

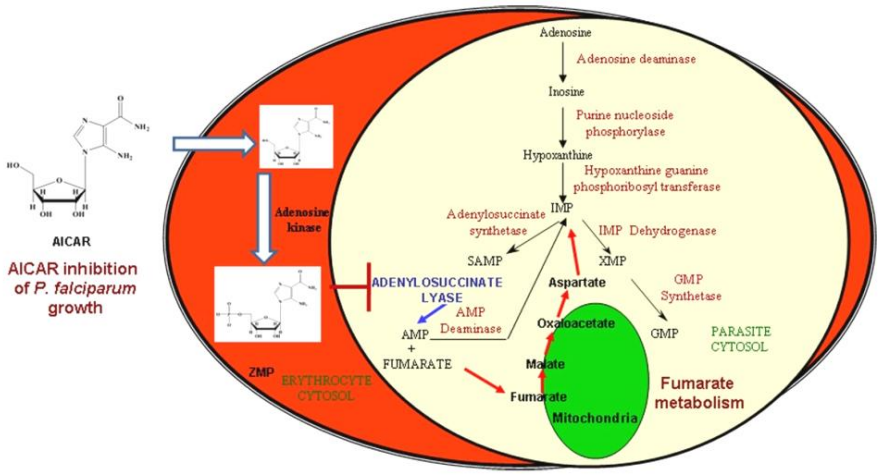

A Thesis Submitted for the Award of the Degree of *Doctor of Philosophy*

By

Vinay Bulusu

July 2010

Molecular Biology and Genetics Unit
Jawaharlal Nehru Centre for Advanced Scientific Research.
(Deemed University)
Jakkur, Bangalore 560 064

Molecular Biology and genetics Unit
JAWAHARLAL NEHRU CENTRE FOR ADVANCED SCIENTIFIC RESEARCH
Jakkur, Bangalore-560 064, India

Prof. Hemalatha Balaram

CERTIFICATE

This is to certify that the work described in this thesis entitled **"Adenylosuccinate lyase and metabolic fate of fumarate in the intraerythrocytic stages of *Plasmodium falciparum*"** is the result of investigations carried out by Mr. Vinay Bulusu in the Molecular Biology and Genetics Unit, Jawaharlal Nehru Centre for Advanced Scientific Research, Bangalore, India under my supervision, and that the results presented in this thesis have not previously formed the basis for the award of any other diploma, degree or fellowship.

Hemalatha Balaram
Professor
Molecular Biology and Genetics Unit
Jawaharlal Nehru Centre for Advanced Scientific Research

09.07.2010

◆Telephone: 91-80-22082812 ◆ Telefax: 91-80-22082766 ◆email: hb@jncasr.ac.in

DECLARATION

I hereby declare that this thesis entitled **"Adenylosuccinate lyase and metabolic fate of fumarate in the intraerythrocytic stages of *Plasmodium falciparum*"** is an authentic record of the research work carried out by me under the supervision of Prof. Hemalatha Balaram at the Molecular Biology and Genetics Unit, Jawaharlal Nehru Centre for Advanced Scientific Research, Bangalore, India and that this work has not been submitted elsewhere for the award of any other degree.

In keeping with the general practice of reporting scientific observations, due acknowledgements have been made wherever the work described has been based on the findings of other investigators. Any omission, which might have occurred by oversight or misjudgement, is regretted.

Vinay Bulusu

09.07.10

ACKNOWLEDGEMENTS

The work done in this thesis would not have been possible without the guidance and support of my supervisor, Prof. Hemalatha Balaram. Her enthusiasm in the subject along with her amazing patience in adversity has propelled me at various stages of my PhD. I am extremely fortunate to have worked with a person who has always been an explorer of new ideas and has given total freedom to pursue the same. I express my sincere gratitude to her and hope that I live up to her expectations in the future.

The Department of Molecular Biology and Genetics Unit, JNCASR, has been a wonderful niche for academic learning. A constant positive pressure mediated through the departmental presentations has always been helpful for the students to foster their research. For this, I would like to thank Prof. Dipankar Chatterjee, Prof. M.R.S Rao who have been the chairmen of the department, Prof. Anuranjan Anand, the current chairman and the department faculty: Prof. Ranga Uday Kumar, Prof. Namita Surolia, Prof. Tapas Kundu, Prof. Maneesha Inamdar and Prof. Kaustuv Sanyal. Their critical comments in my work during the presentations have immensely helped in my research. I would like to thank them and also thank Prof. P. Balaram, Prof. Utpal Tatu, IISc. for the course work.

I would like to acknowledge Dr. Amit Mandal and Dr. Suman Thakur for carrying out the ESI-MS experiments. Dr. Kalyan and Prof. Udgaonkar, NCBS have been extremely helpful in carrying out the transient kinetics using stopped flow apparatus and Dr. Bipasha and Prof. Varadarajan, IISc. for the use of isothermal titration calorimetry. I would like to thank Dr. Vathsala and Prof. G. Padmanabhan, IISc. for the mice experiments and for providing PfHSP 60 antibodies. Mahesh, Debu and Dr. Govindaraju, NCU, JNCASR have been extremely helpful in ^{13}C NMR experiments.

Special thanks to Suma Ma'm, Anitha Ma'm, Roopa and Dr. Prakash who collectively form the backbone of MBGU with their tireless efforts in confocal microscopy facility, DNA sequencing facility, mass spectrometry facility and animal house facility respectively. Their contributions are invaluable in any research coming out of MBGU,

Working in the field of malaria brings a person several names like "Vampire", "Dracula" and "Leech" because of the constant requirement of fresh human erythrocytes for maintaining P. falciparum culture. I am not an exception in this. I would like to acknowledge from the bottom of my heart to Prof Hemalatha Balaram, Dr. Sonali, Dr.

Anand, Dr. Vasudeva, Vidhi, Moumita, Varun and Mahesh for their timely donation of blood to keep my P. falciparum culture going.

A mere "thanks" is a very small word to acknowledge several wonderful people in the laboratory who have helped in many ways in my PhD. My seniors Dr. Chethan, Dr. Sonali, Dr. Subhra, Dr. Mousumi and Shastri have been always there for me in my learning of several lab techniques. My labmate, Javaid and my so-called junior, Bharath have served the role of elder brothers with their constant encouragement and advice in scientific and non-scientific issues. Their fearless attitude has always been an inspiration for me. A special word of thanks to Bopanna for teaching me P. falciparum culture work in his own unorthodox style and my "little sister" Roopa for carrying out the mass spectrometry experiments. The unconditional support of Dr. Vasudeva, Dr. Chethana, Sanjeev, Sourav, Vijay, Moumita, Vidhi, Sonia, Kavita, is highly appreciated.

My batchmates, especially Pavan, Manohar, Sairam, Arif, Gayatri, Shrikanth, have been extremely good and helpful when needed. Ruchika, Gaurav and Mamta (IPIans) have been very helpful and supportive. Special thanks to a special person, Selvi, for all the encouragement and "lectures" to keep me going. Lastly, thanks to all my MBGU and JNC friends for making these last six years a memorable time in my life.

My teachers, Prof. K. Kannan and Prof. N. Raghuram have been very instrumental in shaping my career. Their inspiration and support have played a key role in my reaching this far in my academic career.

I would like to thank the complab, library, academic, admin, security, hostel and other JNCASR staff for maintaining JNCASR a lovely place for carrying out research. Financial support from JNCASR and CSIR-UGC is highly appreciated.

My family: my mother, my brother and bhabhi for their unconditional support and belief in me. Without their support, I would not have reached this far in life. My mother has always been a role model for me and I would like to dedicate this thesis to her.

Vinay Bulusu

List of Abbreviations

ASL	Adenylosuccinate lyase
PfASL	*P. falciparum* adenylosuccinate lyase
SAMP	Adenylosuccinate
SZMP	5-aminoimidazole-4 (N-succinylcarboxamide) ribonucleotide
ZMP	5-aminoimidazole-4-carboxamide ribonucleotide
AICAR	5-aminoimidazole-4-carboxamide ribonucleoside
ADA	Adenosine deaminase
AK	Adenosine kinase
PNP	Purine nucleoside phosphorylase
HGPRT	Hypoxanthine guanine phosphoribosyl transferase
ADSS	Adenylosuccinate synthetase
IMPDH	Inosine monophosphate dehydrogenase
GMPS	Guanosine monophosphate dehydrogenase
FH	Fumarate hydratase
MDH	Malate dehydrogenase
MQO	Malate quinone oxidoreductase
AAT	Aspartate aminotransferase
DTT	Dithiothreitol
IPTG	Isopropyl thio-β-D-galactopyranoside

List of Publications

1. **Bulusu V**, Srinivasan B, Bopanna MP and Balaram H (2009) Elucidation of the substrate specificity, kinetic and catalytic mechanism of adenylosuccinate lyase from Plasmodium falciparum. *Biochim. Biophys. Acta*.**1794**:642-54.

2. Mehrotra S, Bopanna MP, **Bulusu V**, Balaram H. (2010) Adenine metabolism in Plasmodium falciparum. *Exp. Parasitol.* **125**:147-51.

3. **Bulusu V**, Thakur S, Venkatachala R, Balaram H (2010) Mechanism of growth inhibition of intraerythrocytic stages of *Plasmodium falciparum* by 5-aminoimidazole-4-carboxamide ribonucleoside (AICAR) (manuscript in revision)

4. **Bulusu V**, Jayaraman V and Balaram H (2010) Metabolic fate of fumarate in the intraerythrocytic stages of *Plasmodium falciparum* (manuscript under revision)

THESIS SYNOPSIS

Adenylosuccinate lyase and metabolic fate of fumarate in the intraerythrocytic stages of *Plasmodium falciparum*

Student: Vinay Bulusu

PhD. Supervisor: Prof. Hemalatha Balaram

Plasmodium falciparum is a microaerophillic protozoan parasite that causes the most lethal form of malaria in humans. The parasite completes its sexual phase of the life cycle (sporogony) in mosquito, while the asexual phase (schizogony) is completed in human beings. Schizogony further consists of hepatic schizogony (in liver) and erythrocytic schizogony (in erythrocytes). During erythrocytic schizogony, a single merozoite replicates extensively to give rise to 16-32 new merozoites and as a result, the parasite replicates its genome multiple times (Sherman, 1979). Due to this extensive replication, there is an increased demand for nucleotide (pyrimidine and purine) production. Nucleotides are synthesized by salvage and the *de novo* pathways. However, *P. falciparum* lacks the *de novo* purine biosynthetic pathway and the pyrimidine salvage pathway and hence, depends on the purine salvage pathway and the *de novo* pyrimidine pathway to meet its nucleotide requirements (Gardner *et al.*, 2002).

The total dependence on the purine salvage pathway makes the constituent enzymes potential targets for chemotherapeutic interventions. In this pathway, hypoxanthine is phosphoribosylated to IMP by hypoxanthine guanine phosphoribosyltransferase (HGPRT). Adenosine is also salvaged by the parasite, which is then deaminated to inosine by adenosine deaminase (ADA) and subsequently converted to hypoxanthine by purine nucleoside phosphorylase (PNP). IMP formed is then converted to GMP, by the concerted actions of IMP dehydrogenase (IMPDH) and GMP synthetase (GMPS) and, to AMP by adenylosuccinate synthetase (ADSS) and adenylosuccinate lyase (ASL). AMP synthesis is thought to be dependent solely on the concerted actions of adenylosuccinate synthetase (ADSS) and adenylosuccinate lyase (ASL) as other alternate routes for the synthesis of this nucleotide seem to be absent. Previous studies have indicated that *P. falciparum* adenylosuccinate lyase (PfASL) is expressed at a constant level throughout the intraerythrocytic stages of the life cycle (Bozdech *et al.*, 2003)

and, *in silico* knockout and metabolic flux analysis indicate that PfASL is at a critical step in the parasite's metabolism (Fatumo *et al.*, 2009).

Adenylosuccinate lyase (ASL) (E.C. 4.3.2.2) is the only enzyme in the purine biosynthetic pathway that catalyzes two distinct, but chemically similar reactions. The first is the cleavage of 5-aminoimidazole-4(N-succinylcarboxamide) ribonucleotide (SZMP) to 5-aminoimidazole-4-carboxamide ribonucleotide (ZMP) and fumarate that forms the eighth step of the *de novo* purine biosynthetic pathway and the second being the cleavage of succinyl-adenosine monophosphate (SAMP) to adenosine monophosphate (AMP) and fumarate, the final step in AMP synthesis. Previous studies have indicated that ASLs from *Bacillus subtilis* (Palenchar *et al.*, 2003), *Neurospora crassa* (Giles *et al.*, 1957) and *Homo sapiens* (Stone *et al.*, 1993) are able to act upon both substrates with equal efficiency. As the *de novo* purine biosynthetic pathway is absent in *P. falciparum,* it is not known whether PfASL retains the catalytic ability to cleave SAICAR to AICAR and fumarate.

In the purine salvage pathway, the generation of AMP is also accompanied by the generation of a molecule of fumarate. In organisms with a functional TCA cycle, fumarate has been shown to play an anaplerotic role as it replenishes the carbon skeleton. However, during the intraerythrocytic stages of *P. falciparum*, the TCA cycle seems to be dysfunctional for the following reasons: (1) Bulk of the glucose is metabolized to lactate, which is then secreted by the parasite as a metabolic waste (Bryant *et al.*, 1964). As a result, unlike in aerobic cells, in *P. falciparum*, there is minimal carbon flow from the cytoplasm to the TCA cycle in the mitochondrion, (2) pyruvate dehydrogenase, which channels pyruvate into the TCA cycle through acetyl-CoA has been found to localize on the apicoplast membrane in *P. falciparum* (Foth *et al.*, 2005). This is unlike in mammalian cells, where the enzyme is present on the inner mitochondrial membrane and (3) the enzyme isocitrate dehydrogenase generates NADPH rather than NADH, thereby implicating that its main role is to probably act as a redox sensor rather than donate reducing equivalents to the electron transport chain (Wrenger and Muller, 2003) . In view of the dysfunctional TCA cycle, the metabolic fate of fumarate in the intraerythrocytic stages of *P. falciparum* is unknown and needs investigation.

Studies reported in this thesis include (1) the kinetic and catalytic characterization of PfASL, (2) the elucidation of the substrate specifity of PfASL and its use to inhibit AMP synthesis in the parasite and (3) the tracing of the metabolic fate of fumarate in the intraerythrocytic stages of *P. falciparum*.

The thesis is divided into four chapters. The first chapter presents an introduction to *P. falciparum* metabolism with special emphasis on the purine salvage pathway, *de novo* pyrimidine biosynthetic pathway and the TCA cycle.

The second chapter includes kinetic and catalytic characterization of PfASL. The gene encoding adenylosuccinate lyase was amplified from the genomic DNA and cloned in pET28b expression vector. The protein was expressed with a hexahistidine tag at the C-terminus in *E. coli* BL21-CodonPlus™(DE3)-RIL cells. The protein was purified by Ni-NTA affinity chromatography followed by Sephacryl 200 gel filtration chromatography. PfASL was found to exist as a tetramer in solution as probed by pre-calibrated Sephacryl S-300 analytical size exclusion chromatography. Kinetic characterization of PfASL revealed that the enzyme is able to catalyze the reversible cleavage of its substrate, SAMP to AMP and fumarate. Kinetic constants revealed that the enzyme has a forward k_{cat} of 7.5 s^{-1} and a reverse k_{cat} of 2.9 s^{-1}. Product inhibition studies and initial velocity kinetics show that PfASL follows a Uni-Bi Rapid Equilibrium Ordered kinetic model. Transient kinetics using a stopped flow set up did not show any burst in the time course of the reaction implicating the catalytic step to be rate-limiting. Primary kinetic isotope and solvent isotope effect experiments show that of the two bond cleavages in the substrate, SAMP, C-N bond cleavage is the slowest and hence, rate-limiting. Crystal structure of *E. coli* ASL liganded with SAMP implicated Ser 295 as the catalytic base due to its proximity to the C(β)-H group of SAMP. The serine residue is highly conserved across all the ASL sequences. The corresponding serine in PfASL (Ser 298), when mutated to Ala or Cys showed more than 1000 fold drop in specific activity. This indicates that Ser 298 in PfASL catalysis is an indispensable residue and it functions probably by acting as a catalytic base. A homology model of PfASL, generated with *E. coli* ASL as the template shows the proximity of Ser 298 to the C(β)-H group of SAMP. Interestingly, pH kinetics showed two inflections in the k_{cat} vs. pH profile, while only one inflection corresponding to the acid ionization was evident in the k_{cat} / K_m profile. These results indicate that the catalytic base (Ser 298) is ionized only in the enzyme substrate (ES) complex and not in the free enzyme (E). Both in the homology model of PfASL and structure of *E. coli* ASL, we find that the side chain of serine hydroxyl is in close contact (< 4 Å) with the SAMP carboxylic group. This explains our pH kinetics data and we propose a 'substrate assisted catalytic mechanism' in PfASL.

The third chapter describes the ability of PfASL to catalyze the SAICAR cleavage reaction with kinetic parameters similar to those of the SAMP reaction. The presence of this catalytic activity in PfASL is probably a vestigial feature retained in the parasite enzyme as the *de novo* purine biosynthetic pathway is absent. However, this raises the possibility of using AICAR

as a subversive substrate of PfASL that could bring about parasite death. In support of this, we see a dose dependent inhibition of parasite growth in the presence of the cell permeable 5-aminoimidazole-4-carboxamide ribonucleoside (AICAriboside, AICAR) with half maximal inhibition at 167 μM. Our results show that AICAR toxicity is mediated through the erythrocyte where AICAR is phosphorylated to its nucleotide, ZMP, possibly by the action of adenosine kinase. Further, purine metabolite labeling of the parasitized erythrocytes by [^{3}H]-hypoxanthine, in the presence of AICAR, showed a significant decrease in radioactive counts in adenylate (AMP, ADP and ATP) fractions but not in guanylate (GMP, GDP and GTP) fractions. The most dramatic effect on parasite growth was observed when erythrocytes pretreated with AICAR were used in culture. Pretreatment of erythrocytes with AICAR led to significant intracellular accumulation of ZMP and these erythrocytes were incapable of supporting parasite growth and also parasite invasion. These results implicate that, in addition to the purine salvage pathway in *P. falciparum*, AICAR alters the metabolic status of the erythrocytes, which inhibits parasite growth. As AICAR and ZMP are metabolites in the human serum and erythrocytes, our studies reported here throw light on their possible role in the manifestation of malaria susceptibility. Previously, AICAR has been used extensively in rodents and humans at doses as high as 10 – 100 mg kg^{-1} body weight with no significant toxic side effects. This opens up the possibility of using AICAR or its analogues as novel antiparasitic agents.

The fourth chapter delineates the metabolic fate of fumarate, product of ASL catalysis, in the intraerythrocytic stages of *P. falciparum*. From our metabolic labeling studies with ^{14}C-U-aspartic acid and ^{14}C-2,3-fumarate on the parasitized erythrocytes, we find that fumarate is not a metabolic waste, but is incorporated significantly into the nucleic acid and protein fractions. The incorporation is also seen with saponin released free parasites indicating that the enzymes involved in fumarate metabolism are parasite encoded. Metabolite labeling of parasites indicated that ^{14}C-2,3-fumarate labeled only the pyrimidine and not the purine mononucleotides. Further, ^{13}C proton decoupled NMR spectra of the free parasites incubated with ^{13}C-2,3-fumarate showed the formation of malate, aspartate, pyruvate and lactate. All these results implicate that fumarate is converted to aspartate in a pathway involving malate and oxaloacetate as the metabolic intermediates. Bioinformatic analysis followed by biochemical experiments showed that the activity of *P. falciparum* fumarate hydratase, which catalyzes the conversion of fumarate to malate, is localized to the mitochondrial fractions. Previous reports have implicated that *P. falciparum* malate dehydrogenase is localized exclusively to the cytosol (Lang-Unnasch, 1992) and catalyzes preferentially the conversion of oxaloacetate to malate. Malate quinone oxidoreductase, an enzyme present mostly in bacteria catalyzes the conversion of malate to

oxaloacetate. The gene encoding malate quinone oxidoreductase is present in *P. falciparum* genome and we hypothesize that this enzyme catalyzes the conversion of malate to oxaloacetate. The conversion of malate to oxaloacetate is accompanied by the reduction of ubiquinone to ubiquinol, which then feeds the electron transport chain directly at complex III. The last enzyme in the proposed pathway is aspartate aminotransferase, which converts glutamate and oxaloacetate to α-ketoglutarate and aspartate. The gene encoding the enzyme was cloned in pET28b expression vector and the recombinant protein was expressed in C41 DE3 strain of *E. coli*. The protein was purified by Ni-NTA affinity chromatography and gel filtration chromatography and antibodies were raised in mice. Indirect immunofluorescence and digitonin permeabilization showed that PfAAT is localized to the cytosol in *P. falciparum*. This metabolic conversion of fumarate, the end product of purine salvage pathway, to aspartate, which forms the backbone of the pyrimidine ring, might probably represent a mechanism through which purine salvage pathway might regulate the *de novo* pyrimidine biosynthetic pathway.

References

1. Bozdech, Z. *et al.* (2003) *PLoS Biol.* **1**:E5.

2. Bryant, C. *et al.* (1964) *Am. J. Trop. Med. Hyg.* **13**:515-9.

3. Fatumo, S. *et al.* (2009) *Infect. Genet. Evol.* **9**:351-8.

4. Foth, B.J. *et al.* (2005) *Mol. Microbiol.* **55**:39-53.

5. Gardner, M.J. *et al.* (2002) *Nature* **419**:498-511.

6. Giles, N.H. *et al.* (1957) *Proc. Natl. Acad. Sci. U S A* **43**:305-317.

7. Lang-Unnasch N. (1992) *Mol. Biochem. Parasitol.* **50**:17-25.

8. Palenchar, J.B. *et al.* (2003) *Prot. Sci.* **12**:1694-1705.

9. Sherman, I.W. (1979) *Microbiol. Rev.* **43**:453-95.

10. Stone, R.L. *et al.* (1993) *J. Biol. Chem.* **268:**19710-19716.

11. Wrenger, C and Muller, S. (2003) *Eur. J. Biochem.* **270**:1775-83.

TABLE OF CONTENTS

CHAPTER 1

INTRODUCTION

Introduction

Abstract

This chapter gives an introduction on Plasmodium falciparum life cycle and its metabolism. Studying P. falciparum metabolism will not only lead to novel biochemical targets for chemotherapeutic intervention but also stimulate broader scientific interests. Special emphasis is laid on the purine salvage pathway, de novo pyrimidine biosynthetic pathway and the TCA cycle during the asexual stages of the parasite life cycle.

1.1 Malaria

1.1.1 History, Pathogenesis and Epidemiology

Malaria is a vector-borne infectious disease that affects all classes of terrestrial vertebrates including birds, reptiles, rodents and humans (Hayakawa *et al.*, 2008). Charles Laveran, Ettore Marchiafava and Angello Celli identified the agent in the blood of patients suffering from malarial fever and they named this new microorganism as *Plasmodium*. Later on, Ronald Ross found the existence of *Plasmodium* in the midgut of *Culex* mosquito and further, Italian physician Giovanni Battista Grassi found *Plasmodium* in the Anopheles mosquito (Sherman, 1979). Today, over 200 different species of *Plasmodium* and more than 100 different species of mosquitoes, which transmit malaria, are known (Sherman, 1998).

Human malaria is primarily caused by four different species of *Plasmodium*: *Plasmodium ovale*, *Plasmodium malariae*, *Plasmodium vivax* and *Plasmodium*

falciparum (Sherman, 1979). In addition to these, the macaque malarial parasite *Plasmodium knowlesi* has recently, been shown to infect a large number of people in Thailand, Myanmar, the Philippines, and Singapore (Singh *et al.*, 2004; Jongwutiwes *et al.*, 2004; Ng *et al.*, 2008). The most common clinical symptoms of malaria include recurrent fever and chills. However, in extreme cases, caused only by *P. falciparum* infections, patients develop (1) severe anemia due to destruction of erythrocytes, (2) cerebral complications like impaired consciousness, convulsions and long-term neurological deficits, (3) metabolic acidosis and (4) hypoglycemia, which, if left untreated, often results in death (Mackintosh *et al.*, 2004). Unlike other species of *Plasmodia*, only *P. falciparum* causes the severe form of malaria as the knob like structures it develops on the surface of infected erythrocytes enable them to adhere to endothelium and placenta. Adherence protects the infected erythrocytes from clearance and also leads to their sequestration in the blood vessels, which in turn causes an obstruction in the flow of nutrients and oxygen to the local tissue. The parasite protein that mediates adhesion is the Eythrocyte Membrane Protein 1 (EMP1), expressed predominantly on the infected erythrocyte surface (Newbold *et al.*, 1999) and encoded by the *var* gene family. The infected erythrocytes also adhere to the uninfected erythrocytes forming rosettes (David *et al.*, 1988); the formation of which is directly proportional to the severity of malaria (Carlson *et al.*, 1990).

The burden of morbidity and mortality caused by this parasite is huge. Each year, 300 to 500 million people worldwide are infected by this disease out of which 1.5 to 2.7 million die (Sherman, 1979). Almost all the malarial deaths occur as a consequence of *P. falciparum* infection. Majority of these cases are concentrated in the Sub-Saharan Africa

and a few in South East Asia. Besides these endemic areas, global travel and migration have contributed to a steady occurrence of the disease in nonendemic areas also (Franco *et al.*, 2006).

1.1.2 Life Cycle of *P. falciparum*

The life cycle of *P. falciparum* involves an *Anopheles* mosquito vector and a human host (Fig. 1.1). The parasite completes its sexual phase of the life cycle, also known as sporogony in the mosquito while the asexual phase, schizogony is completed in the human host. During a blood meal, the female *Anopheles* mosquitoes transfer *P. falciparum* sporozoites directly into the human bloodstream, which circulate briefly before invading hepatocytes, where an asexual life cycle ensues. This exo-erythrocytic or hepatic schizogony lasts for 10–12 days after which, infected hepatocytes rupture releasing thousands of daughter merozoites back into the blood. The merozoites then invade circulating erythrocytes and initiate the intraerythrocytic cycle of asexual replication, which follows a 48 h cycle (Haldar *et al.*, 2007). During the erythrocytic schizogony, the parasite undergoes distinct morphological and biochemical changes through the ring (0-24 h), trophozoite (24-32 h) and schizont stages (32-48 h). This phase of the life cycle produces 16-32 parasites from a single merozoite and is responsible for most of the observed clinical symptoms. In response to stress or other cues, some parasites inside the erythrocytes differentiate into male or female gametocytes, which upon ingestion by a feeding female mosquito fuse and undergo a complex process of sexual development eventually forming infective sporozoites that can

be introduced back into the human host during the next blood meal, thereby ensuring the continuation of the parasite life cycle.

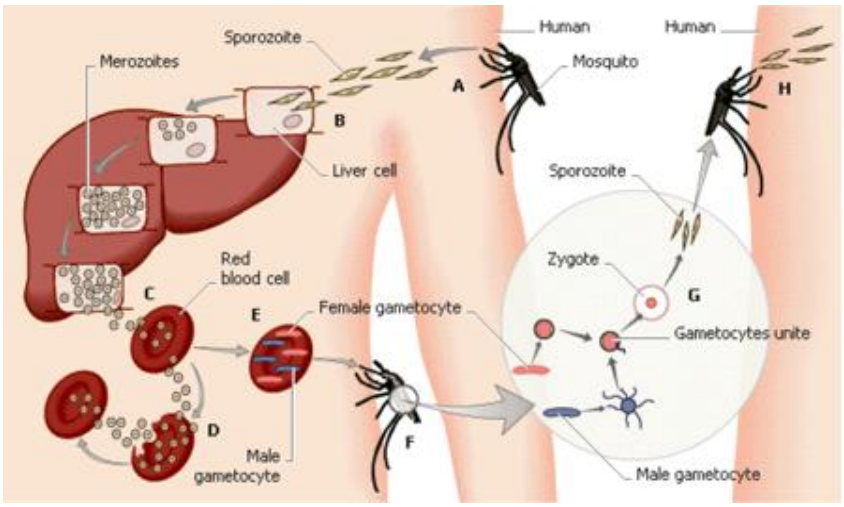

Image adapted from: http://www.coalitionagainstmalaria.org.uk

Fig. 1.1: Life cycle of *P. falciparum*

(A) Blood meal of female Anopheles mosquito resulting in the injection of infective sporozoites into the human blood stream; (B) Invasion of the liver by sporozoites and their development into merozoites; (C) Lysis of infected hepatocytes and release of merozoites into the blood stream; (D) Invasion of circulating erythrocytes by merozoites to initiate erythrocytic schizogony; (E) Development of the merozoites into male and female gametocytes; (F) Blood meal of female Anopheles mosquito resulting in the ingestion of gametocytes; (G) Fusion of male and female gametocytes to form zygote and further development into sporozoites; (H) Injection of sporozoites by the mosquito into a new human host.

1.1.2.1 Erythrocytic Schizogony

The erythrocytic schizogony begins when merozoites emerge from liver and invade erythrocytes. Most of the clinical symptoms occur as a consequence of this phase of the parasite's life cycle. The parasites undergo distinct morphological and biochemical changes through three different forms, ring, trophozoite and schizont (Fig. 1.2).

1.1.2.2 Erythrocytic invasion

Initial interaction of the merozoite causes a wave of deformation across the erythrocyte membrane after which, the merozoite reorients itself so that its apical end (containing specialized apical secretory organelles known as the micronemes, rhoptries, and dense granules) is in apposition to the erythrocyte (Hadley, 1986). Invagination of the erythrocyte membrane results in the engulfment of the merozoite surrounded by a vacuolar membrane. It was observed that merozoites of *P. lophurae*, preferentially invaded duck rather than chicken erythrocytes (McGhee, 1953) suggesting that malaria parasites recognize species specific molecules on host erythrocytes. This explains, in part, the species-specificity of malarial infections. The major ligands involved in the attachment of the parasite on the erythrocyte membrane are the merozoite surface proteins (MSPs) and the major erythrocyte glycoprotein band 3, but additional parasite ligands and host receptors might also be involved (Haldar *et al.*, 2007).

1.1.2.3 Ring stage

After invasion of the erythrocyte, the parasite develops into a thin biconcave disc and appears in the form a ring in Giemsa stained smears (Bannister and Mitchell, 2003). At the ring stage, the parasite starts consuming hemoglobin to obtain amino acids and also to generate space for its growth. At the end of the ring stage, the parasite starts secretion of molecules to the erythrocyte surface that are involved in (1) sequestration of infected erythrocytes to the vascular endothelium and (2) attachment of infected erythrocytes to normal erythrocytes, a process known as resetting (David *et al.*, 1988). Therefore, Giemsa stained smears of peripheral blood of a *P. falciparum* infected patient

will show the presence of only rings as the mature forms adhere to the vascular endothelium and hence, get sequestered. The ring stage lasts for 18-20 h following infection.

1.1.2.4 Trophozoite stage

In the trophozoite stage, the parasite is round in shape and is metabolically more active. This stage lasts for 8-10 h after the completion of the ring stage. The host hemoglobin is ingested and is cleaved by a large number of proteases to generate amino acids and heme. As free heme is toxic to the parasite, it is polymerized to hemozoin, which is visible as a black pigment in Giemsa stained smears. Protein and nucleic acid synthesis are initiated at this stage. In addition to this, the parasite develops (1) knob like structures on the erythrocyte surface and (2) tubulovesicular network from the parasite plasma membrane to the erythrocyte membrane for the transport of ions and other nutrients (Bannister and Mitchell, 2003) into the parasite cytoplasm.

1.1.2.5 Schizont stage

The parasite undergoes a series of nuclear divisions to generate 16 – 32 nuclei within a common cytoplasm. Each nucleus then moves into merozoite buds formed at the periphery and eventually pinch off with the residual cytoplasm into a merozoite. The erythrocyte membrane and parasitophorous membrane are lysed by specific proteases, followed by the egress of the daughter merozoites.

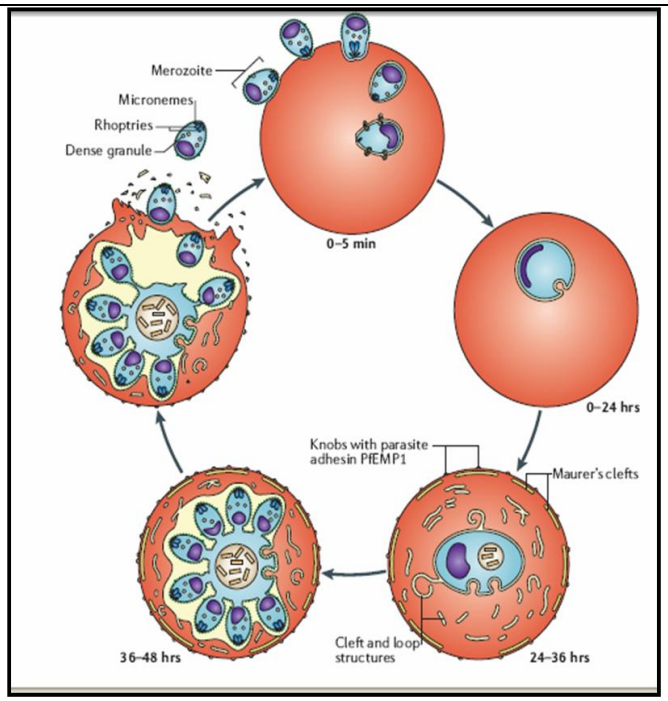

Image adapted from Haldar *et al.*, (2006) *Nat. Rev. Microbiol.* **4**:922-32

Fig. 1.2: Stages of *P. falciparum* erythrocytic schizogony

A single merozoite invades an erythrocyte and multiplies extensively to generate 16-32 new merozoites at the end of erythrocytic schizogony. During this phase, the erythrocyte membrane is extensively modified by parasite proteins.

1.2 Strategies to combat malaria

A variety of strategies have been used by the World Health Organization (WHO) with the aim of controlling malaria. The most important of them has been to reduce the transmission rate of the disease in malaria endemic countries by (1) controlling the number of breeding sites for mosquitoes by the use of insecticides, (2) eliminating sites of stagnant bodies of water, (3) use of biological agents like fish (*Gambusia affinis*) that feed directly on the mosquito larva or using bacterial endotoxins derived from *Bacillus sphaericus* and *Bacillus thuringiensis israelensis* (Collins and Paskewitz, 1995) and (4)

improving residential areas to separate humans from mosquitoes by the use of insecticide impregnated bed nets. Though this helped decline the incidence of malaria in North America and parts of Europe (Marshall and Taylor, 2009), a major portion of Africa still suffers an annual mortality rate of one million from this infection alone (Hay *et al.*, 2005).

1.2.1 Malaria vaccines

Over the last ten years, increased vaccination programs by the WHO have been successful in reducing the number of cases of polio, measles, tetanus, diphtheria and tuberculosis across the globe (Hinman, 1999). However, the development of an effective vaccine against malaria has been extremely difficult. The ones, which have met partial success, have been broadly classified into three categories based on their mode of action: (1) Erythrocytic stage vaccines, (2) Transmission blocking vaccines and (3) Pre-erythrocytic stage vaccines (Targett and Greenwood, 2008). The first category of vaccines target antigens such as Merozoite Surface protein (MSP) and Ring Infected Erythrocyte Surface Antigen (RESA), which are involved in the erythrocyte invasion by the merozoites. However, due to the polymorphism of these antigens together with the redundancy of the invasion process, the success of these vaccines has been less with only few progressing to the Phase I and Phase II clinical trials. The transmission blocking vaccines (TBVs) target either parasite antigens expressed in the sexual phase of the life cycle or they target mosquito antigens (Dinglasan and Jacobs-Lorena, 2008). The antibodies generated in the immunized individuals are taken up during the blood meal by the mosquitoes, which then inhibit the subsequent parasite development in the mosquito

midgut. The TBVs however, do not protect the immunized individual from contracting malaria. The pre-erythrocytic stage vaccines aim at inhibiting the invasion of erythrocytes by the parasites and hence, the disease. It has been shown that when infectious mosquitoes are irradiated, the sporozoites are altered such that they remain capable of invading liver in the human host, but do not develop further and invade erythrocytes (Nussenzweig *et al.,* 1967). Thus, infection of human volunteers with such irradiated mosquitoes will expose them to liver-stage antigens and thereby, resulting in the generation of pre-erythrocytic immunity. However, the requirement of a large number of bites by irradiated mosquitoes in order to successfully induce immunity reduces the plausibility of this method for routine immunization. Recently, the inoculation of intact sporozoites along with the administration of chloroquine, a drug that inhibits the erythrocytic stages and not the liver stages of *P. falciparum* has been shown to confer protective immunity in humans (Roestenberg *et al.,* 2009). The pre erythrocytic stage vaccines target surface proteins, especially the circumsporozoite protein (CSP). The most successful candidate in this category and also amongst the various malaria vaccines is the RTS, S vaccine. The vaccine consists of a tandem repeat tetra-peptide (R) and C-terminal T-cell epitope containing (T) regions of CSP fused to the hepatitis B surface antigen (S), plus unfused S antigen (Targett and Greenwood, 2008). The vaccine is currently in Phase III clinical trial involving 16,000 children under the age of two at eleven sites in seven African countries, the largest ever in the history of malaria vaccine (Nayar, 2009).

1.2.2 Malaria drugs

The bark of the Cinchona tree was used to treat malaria centuries ago and the active agent, known, as quinine was isolated in 1820 (Sherman, 1979). A derivative of

quinine called chloroquine was widely used thereafter due to its safety, efficacy and low cost. Although the exact mechanism of action of chloroquine is not known, there is a general consensus that it binds to the ferriprotoporphyrin IX (Ginsburg *et al.*, 1999) and interferes with heme polmerization, thereby leading to parasite death. The other effective antimalarial compound, artemisinin (also known as qinghaosu) was isolated from a Chinese medicinal plant and was used for a long time to treat malarial fevers (Eastman and Fidock, 2009). Artemisinin is thought to alkylate and hydroxylate the parasite proteins and also generate reactive oxygen species (ROS), all of which combine to result in parasite death (Salter and Cerami, 1992). Due to the emergence of drug resistance in *P. falciparum* to these first line anti-malarials, there is an increased search for new therapeutic molecules. Over the years, biochemical investigations on *P. falciparum* metabolism have led to the identification of novel chemical molecules, which inhibit parasite growth under *in vitro* conditions, and several of them, also under *in vivo* conditions. Some of these are highlighted in Table 1.1.

Molecule	Biochemical target	Side effects	Clinical use
Chloroquine	Exact mode of action still unknown but the accepted mechanism is binding to Ferriprotoporphyrin IX and inhibiting heme polymerization to hemozoin. (Salter and Cerami, 1992)	Cardiotoxicity at low doses and long-term use has been associated with toxic side effects like retinopathy, encephalopathy, neuropathy, myopathy, and impairment of auditory function (Fragasso *et al.*, 2009)	Used extensively alone or in combination as an antimalarial agent.
Amodiaquine	Similar mode of action as chloroquine	Severe hepatotoxicity and life-threatening agranulocytosis (Schlitzer, 2008)	Used against low level chloroquine-resistant *P. falciparum*
Quinine	Similar mode of action as chloroquine	Multiple side effects with some severe in nature, like the release of insulin resulting in severe hypoglycemia (Schlitzer, 2008)	Used as a therapeutic option for the treatment of severe malaria. (Schlitzer, 2008)
Mefloquine	Similar mode of action as chloroquine	Neuropsychiatric side effects, such as insomnia,depression, and panic attacks (Schlitzer, 2008)	Used in combination with artesunate
Primaquine	Exact mechanism not known but is believed to act on the electron transport chain. Active against sexual stages and the liver stages of *P. falciparum* (Schlitzer, 2008)	Hemolysis in humans with glucose-6-phosphate-dehydrogenase (G6PD) deficiency (Schlitzer, 2008)	Used in combination with chloroquine
Atovaquone	Ubiquinol-cytochrome c reductase in the electron transport chain (Mather *et al.*, 2005)	No severe toxic side effects	Used in combination with proguanil (Srivastava and Vaidya, 1999)

Doxycyclin	Inhibits mitochondrial protein synthesis (Pradines *et al.*, 2000)	Incorporation in developing bones in pregnant women and children (Schlitzer, 2008)	Used in combination with quinine or artesunate
Clindamycin	Inhibits mitochondrial protein synthesis (Pradines *et al.*, 2000)	No severe side effects	Used as an alternative to doxycyclin
Artemisinine	Induces the formation of oxidative free radicals , which modify parasite proteins (Schlitzer, 2008)	No severe side effects	Used in the form of its derivatives, artesunate and artemether
Pyrimethamine	Dihydrofolate reductase in the synthesis of tetrahydrofolate (Falco *et al.*, 1951)	Prolonged prophylactic use causes toxic epidermal necrolysis	Used in combination with sulfadoxine
Chlorproguanil	Metabolized to chlorcycloguanil, which is an inhibitor of dihydrofolate reductase (Nzila, 2006)	No severe side effects	Used in combination with dapsone
Proguanil	Metabolized to cycloguanil which is an inhibitor of dihydrofolate reductase in the synthesis of tetrahydrofolate (Nzila, 2006)		Used in combination with atovaquone

Table 1.1: Inhibitors with defined molecular targets that inhibit *P. falciparum* growth

1.3 *P. falciparum* metabolism

Much of the biochemical understanding of the parasite's metabolism has been obtained from studies carried out on the intraerythrocytic (IEC) stages of the life cycle due to the importance of these stages in the pathology of human malaria and also due to technical difficulties in culturing other stages of the *P. falciparum* life cycle. *P. falciparum* is a facultative anaerobe requiring a reduced oxygen environment for its optimal growth. The metabolism of the parasite was therefore predicted to be different from its aerobic human host. Indeed, sequencing of the *P. falciparum* genome revealed that many of the enzymes performing critical metabolic functions like amino acid biosynthesis, fatty acid degradation are completely absent (Gardner *et al.*, 2002). This explained the previous findings that some of the nutrients like pantothenate and isoleucine are indispensable for the parasite growth under *in vitro* conditions (Divo *et al.*, 1985). On the other hand, metabolic pathways not present in the humans were also found, some of which include shikimate pathway (Roberts *et al.*, 1998), Type II fatty acid biosynthesis (Surolia and Surolia, 2001) and Vitamin B1 and B6 biosynthesis (Müller and Kappes, 2007), which have been targeted for anti-malarial chemotherapy. Further detailed studies on *P. falciparum* metabolism would enable us to have a better understanding of the diversity in metabolism across different species, which in turn, would bring out novel targets for chemotherapeutic intervention.

1.3.1 Glycolysis

During the intraerythrocytic stages, energy metabolism of *P. falciparum* is mainly through the breakdown of glucose by glycolysis (Bryant *et al.*, 1964). Parasitized

erythrocytes have been shown to take up glucose 100 times more than the uninfected erythrocytes (Kirk *et al.,* 1996). Bulk of the glucose taken up gets metabolized to lactate, which is then secreted out by the parasite as a metabolic waste (Bryant *et al.*, 1964). It is for this reason that in severe malaria, patients develop hypoglycemia and lactic acidosis (White *et al.*, 1983; Agbenyega *et al.*, 2000). Thus, in contrast to aerobic metabolism, where pyruvate generated at the end of glycolysis is acted upon by the mitochondrial multienzyme complex pyruvate dehydrogenase to acetyl-CoA, *P. falciparum* converts bulk of the pyruvate to lactate by lactate dehydrogenase (E.C. 1.1.1.27). In this process, the parasite recycles its NAD^+ pool to allow continuous operation of glycolysis.

1.3.2 Tricarboxylic acid (TCA) cycle

In aerobic metabolism, the function of the TCA cycle is to breakdown acetyl-CoA into CO_2 and generate the reducing equivalents, NADH and $FADH_2$. In addition to this, the TCA cycle also serves several biosynthetic roles by acting as a sink or as a source of carbon skeletons for many biochemical reactions. The genes encoding all the enzymes of the TCA cycle were found to be present in the *P. falciparum* genome (Gardner *et al.*, 2002). Acetyl-CoA represents the major entry point of the carbon skeleton into the TCA cycle (Fig. 1.3).

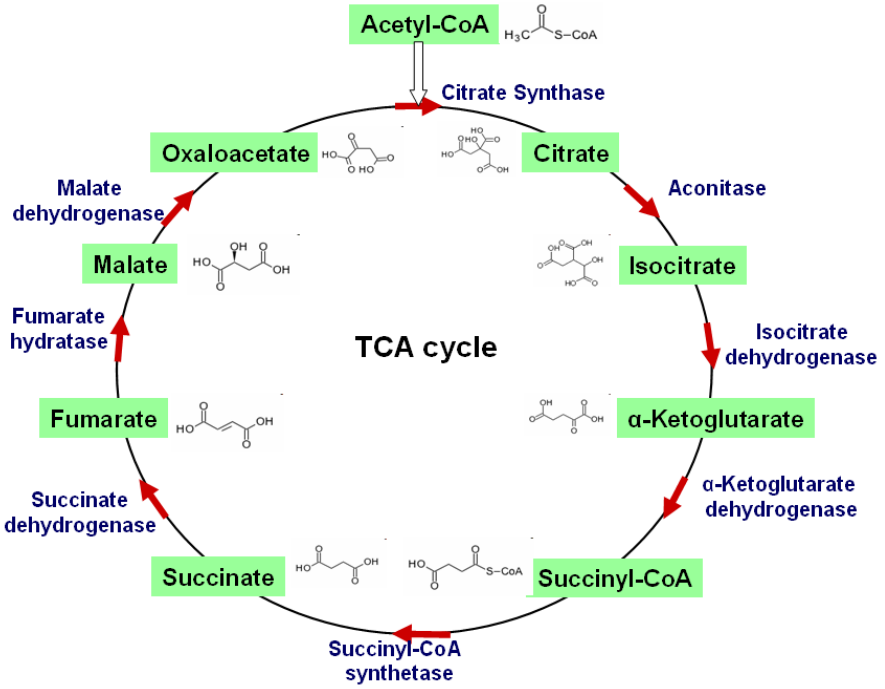

Fig. 1.3: Tricarboxylic acid cycle in aerobic respiration

Acetyl-CoA is combined with oxaloacetate by citrate synthase to form citrate and initiate the cycle. Citrate then undergoes a series of reactions to regenerate back oxaloacetate. The structures of the intermediates were obtained from KEGG database (Kanehisa and Goto, 2000).

Acetyl-CoA is generated by three different metabolic pathways: (1) Breakdown of pyruvate by pyruvate dehydrogenase; (2) β oxidation of fatty acids and (3) breakdown of branched chain amino acids such as leucine, valine and isoleucine. The TCA cycle however, seems to be dysfunctional as a cycle in the parasite during the intraerythrocytic stages. When *P. falciparum* cultures were incubated with ^{14}C-U-labelled glucose, bulk of the label was excreted as lactate into the culture medium with very little ^{14}C getting incorporated in the tricarboxylic acids (Bryant *et al.*, 1964). These observations were supported by a study in which free *P. falciparum* parasites were incubated with 1-[^{13}C]-glucose (Lian *et al.*, 2009). The authors found ^{13}C enrichment at the C-3 position of

lactate, pyruvate and glycerol, but not in any of the TCA cycle intermediates. These results indicated that in *P. falciparum*, glycolysis is not connected with the TCA cycle and the parasite obtains most of its energy from the breakdown of blood glucose to lactate. This is unlike in *Trypanosoma cruzi*, which is a pathogenic protozoan responsible for the Chagas disease. *T. cruzi* intact cells upon incubation with 1-[^{13}C]-glucose showed ^{13}C enrichment at the C-2 position of succinate (Frydman *et al.*, 1990). This indicates that unlike in *P. falciparum*, there exists a carbon flow from cytoplasm to the mitochondria in *T. cruzi*.

These findings were later explained by studies that showed that *P. falciparum* pyruvate dehydrogenase was localized on the apicoplast membrane (Foth *et al.*, 2005). Further, deletion of the E1α or E3 subunit genes of pyruvate dehydrogenase in the rodent malaria parasite, *P. yoelli* caused no defect in blood stage development, mosquito stage development or early liver stage development (Pei *et al.*, 2010). However, the knockout parasites could not initiate the blood stage infection as they were unable to develop into exo-erythrocytic merozoites. This phenotype is similar to that observed for deletions of genes (Pf FabI) involved in Type II fatty acid synthesis (Yu *et al.*, 2008). Thus, these results indicate that the sole role of PDH is probably to provide acetyl-CoA for FAS II rather than the TCA cycle (Fig. 1.4). β oxidation of fatty acids seems to be absent in *Plasmodium spp.* as no genes for this metabolic process were found in any of the Plasmodial genomes sequenced thus far (Gardner *et al.*, 2002). Breakdown of branched chain amino acids involves transamination by a branched chain aminotransferase and decarboxylation by a branched-chain α-keto acid dehydrogenase complex. However, further steps of this catabolic process that lead to acetyl-CoA generation are doubtful as

homologues of enzymes involved in this process are absent in the *P. falciparum* genome (van Dooren *et al.*, 2006).

In addition to the limiting mitochondrial concentration of acetyl-CoA to continuously feed the TCA cycle, certain enzymes of the pathway have features that make them very unlikely to function as *bona fide* TCA cycle enzymes. Pf isocitrate dehydrogenase, for example, utilizes $NADP^+$ instead of the usual NAD^+ as a cofactor to catalyze the conversion of isocitrate to α-ketoglutarate. It also gets upregulated during oxidative stress (Wrenger and Muller, 2003). The enzyme, therefore, appears to be involved in maintenance of redox balance in the cell by providing NADPH rather than serving the electron transport chain with the reducing equivalent, NADH. Thus, it appears that during the erythrocytic stages, ATP synthesis in *P. falciparum* takes place mainly by substrate level phosphorylation through glycolysis with a minor contribution from oxidative phosphorylation (Vaidya and Mather, 2009).

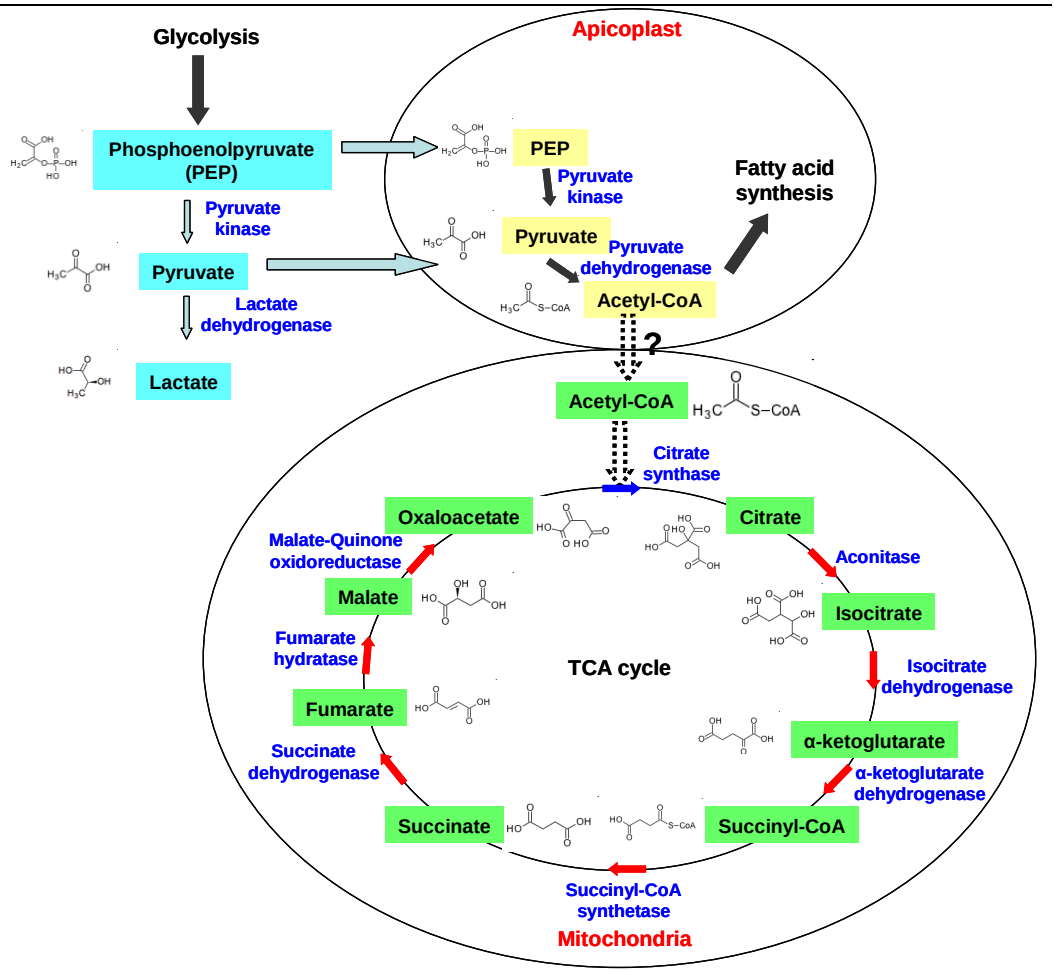

Fig. 1.4: Dysfunctional TCA cycle in *Plasmodium falciparum*

Bulk of the glucose gets metabolized to lactate by glycolysis. Pyruvate is converted to acetyl-CoA in the apicoplast by pyruvate dehydrogenase, which feeds the fatty acid synthesis. Pyruvate is not chanelled into mitochondria and hence, there is insufficient acetyl-CoA to drive the formation of citrate. As apicoplast remain in physical association with the mitochondrion during the intraerythrocytic stages of P. falciparum (van Dooren et al., 2005), there might be a possibility of acetyl-CoA channeling from the apicoplast to the mitochondrion. Metabolite structures are adapted from the KEGG database (Kanehisa and Goto, 2000).

During other stages of the parasite's life cycle in the mosquito and the human liver, glucose availability might be limiting and hence, the parasite might rely on more than just glycolysis for energy generation. In support of this, proteomic studies on *P. falciparum* life cycle showed the presence of peptides corresponding to the TCA cycle

enzymes citrate synthase, aconitase, isocitrate dehydrogenase, succinate dehydrogenase, fumarate hydratase and the iron sulfur subunit of succinate dehydrogenase in the sexual stages (Florens *et al.*, 2002). Transcriptome analysis of the parasites isolated from blood samples of patients suggested three distinct physiological states of *P. falciparum* (Daily *et al.*, 2007). These three states are (1) active growth based on glycolytic metabolism similar to the known profile *in vitro*, (2) starvation response accompanied by the metabolism of alternative carbon sources like lactic acid, glycerol present in the patient's blood. and (3) an environmental non-nutritional stress response. The starvation response showed induction of genes associated with oxidative phosphorylation, mitochondrial respiration and biogenesis. This indicates that under *in vivo* conditions, parasites display physiological diversity depending on the availability of nutrients and oxygen. However, reexamination of the data by Lemieux *et al.* suggested a continuous rather than a discrete clustering of gene expression data sets (Lemieux *et al.*, 2009). This implicated the presence of a significant proportion of sexually committed but phenotypically indistinguishable parasite populations. Due to limited biochemical knowledge, it is not known to what extent is the contribution of TCA cycle and a functional mitochondrion in general, to the parasite survival during the non-erythrocytic stages.

1.3.3 Electron transport chain

The mitochondrial electron transport chain (ETC) transfers electrons between four protein complexes, Complex I-IV, mediated through electron carriers. In aerobic respiration, the mitochondrial ETC is generally composed of four integral membrane enzyme complexes in the mitochondrial inner membrane: NADH:ubiquinone

oxidoreductase (Complex I), succinate:ubiquinone oxidoreductase (Complex II), ubiquinol:cytochrome *c* oxidoreductase (Complex III, or cytochrome bc_1), and cytochrome *c* oxidase (Complex IV). Ubiquinone (Coenzyme Q, CoQ) and cytochrome *c* function as electron carriers between these complexes. This process of electron transfer is coupled to the translocation of protons from the mitochondrial matrix to the intermembrane space, which therefore, generates a proton gradient across the inner mitochondrial membrane, which is used, in aerobic respiration to generate ATP in a process known as oxidative phosphorylation. Complex I, which is a multisubunit protein complex in mammals, is replaced by a single subunit type II NADH dehydrogenase in *Plasmodium spp.* (Fisher *et al.*, 2007). *P. falciparum* complex I is rotenone insensitive (Biagini *et al.*, 2006) and does not pump protons like the mammalian counterpart. Complex II or Succinate ubiquinone oxidoreductase (SQR) is an enzyme common to both the TCA cycle and the ETC. In aerobic respiration, oxidation of succinate to fumarate causes the reduction of ubiquinone, which then feeds the Complex III of ETC. In anaerobic respiration, complex II plays an important role in PEPCK-succinate pathway by carrying out the reverse reaction involving reduction of fumarate to succinate (Kita *et al.*, 2002). In this pathway, phosphoenolpyruvate is converted to oxaloacetate by phosphoenolpyruvate carboxykinase (E.C. 4.1.1.32), which is then converted to fumarate by the reverse reactions of malate dehydrogenase and fumarate hydratase. Complex III or ubiquinol:cytochrome *c* oxidoreductase catalyzes the reduction of cytochrome c along with the oxidation of CoQ. *Plasmodium spp.* showed complex III activity (Fry & Beesley, 1991), and inhibitors such as antimycin, have been shown to inhibit both complex III activity and the consumption of oxygen, which functions as the terminal

acceptor of electrons in the electron transport chain (Fry & Beesley, 1991; Uyemura *et al.*, 2000, 2004; Krungkrai, 2004). Complex III inhibitors were also shown to collapse membrane potential in *Plasmodium* parasites, supporting the role of a functional, proton-translocating complex III in *Plasmodium* (Srivastava *et al.*, 1997, Uyemura *et al.*, 2000, 2004). Reduced cytochrome c donates electrons to complex IV, which then reduces molecular oxygen and hence, serves as the terminal oxidase of the electron transport chain. Complex IV inhibitors depolarize the mitochondrial membrane potential and also reduce oxygen consumption in *Plasmodium spp.* (Srivastava *et al.*, 1997; Uyemura *et al.*, 2000) implicating the functionality of complex IV in the parasite. The proton gradient across the mitochondrial inner membrane is harnessed by ATP synthase to generate ATP from ADP and Pi. Oligomycin, a specific inhibitor of ATP synthase reduces the oxygen uptake and also affects the mitochondrial membrane potential in *Plasmodium spp*. (Uyemura *et al.*, 2000, 2004). However, oligomycin had a negligible effect on the overall cellular ATP levels in the parasite (Fry *et al.*, 1990). Thus, the role of ATP synthase in contributing to the cellular ATP pool in asexual stages and in other parts of the life cycle is not yet clear (van Dooren *et al.*, 2006).

1.3.4 Nucleotide metabolism

Apart from being the building blocks for the nucleic acids, DNA and RNA, nucleotides also constitute cofactors like NAD^+, $NADP^+$ and $FADH_2$ that are vital for many of the enzymatic reactions and serve as secondary messengers in the form of cyclic AMP (cAMP) and cyclic GMP (cGMP). Purine and pyrimidine nucleotides can be

obtained either exclusively by *de novo* synthesis or by direct acquisition through salvage pathways or by both the pathways.

1.3.4.1 Pyrimidine biosynthesis

It was found that *Plasmodium spp.* incubated with [^{3}H]-uridine, [^{3}H]-thymidine, [^{14}C]-thymine, [^{14}C]-thymidine, [^{14}C]-uracil, or [^{14}C]-uridine did not show radioactive incorporation in the nucleic acid pool (Bungener and Nielsen, 1968; Polet and Barr, 1968). On the other hand, *Plasmodium spp.* could incorporate [^{3}H]-orotate (Polet and Barr, 1968) into their nucleic acids. These results implicated that *Plasmodium spp.* lack the pyrimidine salvage pathway and depend on the *de novo* pathway for the generation of pyrimidine nucleotides. Further, the genome sequence of *P. falciparum* failed to uncover genes for the enzymes in the pyrimidine salvage pathway (Gardner *et al.*, 2002). As erythrocytes do not contain significant amounts of pyrimidine nucleotides (Hassan and Coombs, 1988), *Plasmodium spp.* might have retained the enzymes for the *de novo* synthesis of pyrimidines. The pathway includes six steps to synthesize uridine monophosphate (UMP) (Fig. 1.5) and all of the enzymes required for the biosynthesis of UMP were shown to be present in *P. falciparum* (Booden and Hull., 1973) (Gero *et al.*, 1984). The gene for the first enzyme of the pathway, carbamoyl phosphate synthetase II (E.C. 6.3.5.5), which catalyzes the formation of carbamoyl phosphate was characterized (Flores *et al.*, 1994) and was found to contain two large inserts not found in the enzyme from the human host. Subsequently, these inserts were found to be the target of ribozyme mediated inhibition of *P. falciparum* proliferation *in vitro* (Flores *et al.*, 1997). The second enzyme of the pathway is aspartate transcarbamylase (E.C. 2.1.3.2) whose activity

has been found in crude extracts of *P. berghei* (Hill *et al.*, 1981). The enzyme adds a molecule of aspartic acid to carbamoyl phosphate to generate carbamoyl aspartate and liberating phosphate. N-(phosphonacetyl)-L-aspartate (PALA) was found to be a potent inhibitor of this enzyme with a K_i of 0.48 µM. Dihydroorotase (DHOase; EC 3.5.2.3), the next enzyme in the pathway converts carbamoyl aspartate to dihydroorotate, has been cloned from *P. falciparum* (Christopherson *et al.*, 2004). The enzyme has been characterized biochemically (Krungkrai *et al.*, 2008) and was found to have both the mammalian (Type I) and *E. coli* (Type II) enzyme features. Dihydroorotate dehydrogenase catalyzes the fourth step involving the dehydrogenation of dihydroorotate to generate orotate. The reducing equivalents are transferred to ubiquinone (CoQ), which then feeds the electrons directly to ubiquinol cytochrome c reductase (complex III) through ubiquinol ($CoQH_2$). Napthoquinones, which target complex III at the step of electron transfer, have been found to deplete UTP levels in the parasite. Atovaquone, a hydroxynapthoquinone has a potent effect on *P. falciparum* growth and is being used in clinics in combination with proguanil for treatment of malaria. PfDHODH was purified, characterized and localized to the mitochondrial membrane (Krungkrai, 1995) and a series of potent and species-specific inhibitors of *P. falciparum* DHODH were identified (Patel *et al.*, 2008) (Davies *et al.*, 2009). Orotate formed is then phosphoribosylated to orotidine 5' monophosphate by the enzyme orotate phosphoribosyltransferase (OPRT) (E.C. 2.4.2.10). *P. falciparum* has a monofunctional OPRT (Krungkrai *et al.*, 2004[a]). On the other hand, humans have a bifunctional enzyme with both OPRT and orotidine monophosphate decarboxylase (OMPDA) activities in a single polypeptide (Wittman *et al.*, 2008). However, *P. falciparum* OMPDA remain associated with OPRT in a tight

heteroduplex when purified from *P. falciparum* lysate (Krungkrai *et al.*, 2004[b]). UMP gets phosphorylated to UTP in two steps catalyzed by UMP kinase (UMPK) (E.C. 2.7.4.14) and nucleoside diphosphate kinase (NDK) (E.C. 2.7.4.6). The activities for both of these enzymes could be found in *P. falciparum* lysates (Reyes *et al.*, 1982). Pf NDK has also been cloned, expressed and functionally characterized (Kandeel *et al.*, 2009). UTP is converted to CTP by CTP synthetase (E.C. 6.3.4.2), whose activity has been obtained from *P. falciparum* lysate (Perignon *et al.*, 1994). The gene encoding CTP synthetase has been cloned, expressed and purified and was found to contain two novel inserts in its coding sequence (Yuan *et al.*, 2005).

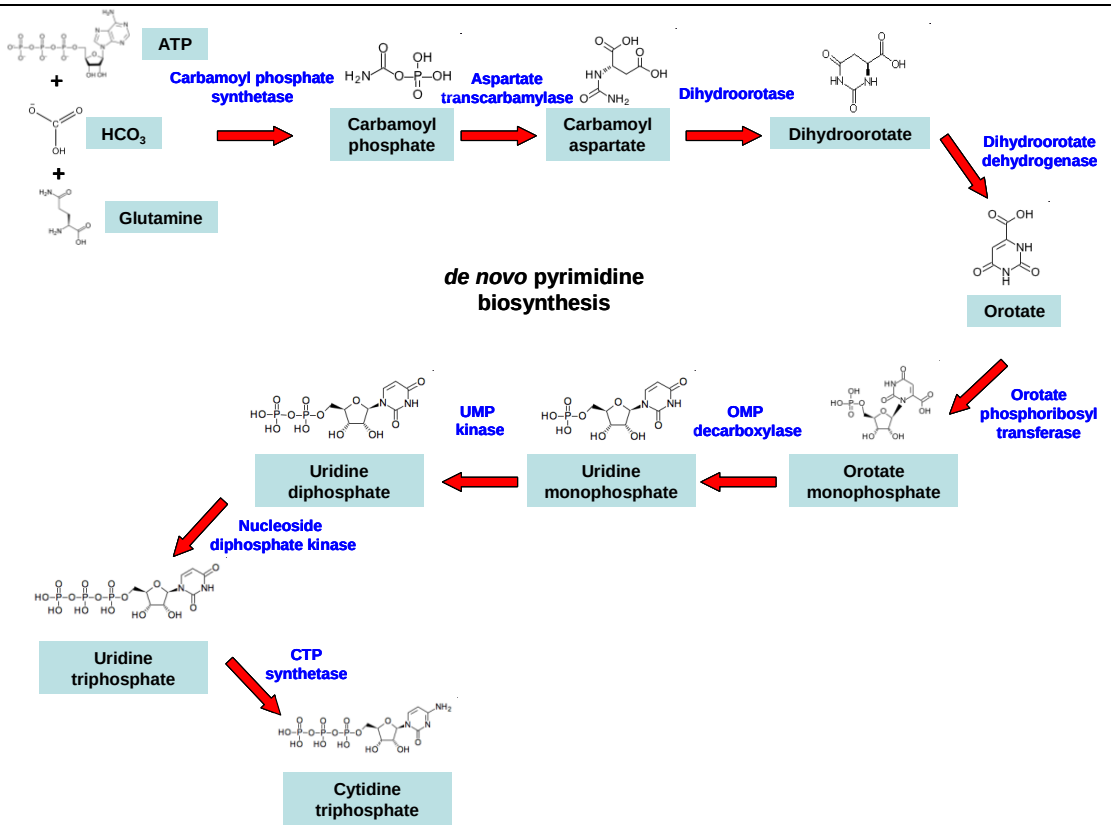

Fig. 1.5: *de novo* pyrimidine biosynthetic pathway

UMP is synthesized from simple precursor molecules bicarbonate, glutamine and aspartate by a series of six enzyme catalyzed reactions. UMP is then converted to UTP and then to CTP. Hence, unlike UMP, CMP cannot be produced directly. Metabolite structures are adapted from KEGG database (Kanehisa and Goto, 2000)

1.3.4.2 Purine synthesis

Parasitic protozoans lack the *de novo* purine biosynthetic pathway and hence, depend only on purine salvage pathway to replenish the purine nucleotide pool. There exists a great diversity in the mechanisms of purine salvage amongst protozoan parasites. *Giardia lamblia*, synthesizes the purines, AMP and GMP by direct phosphoribosylation of adenine and guanine by adenine phosphoribosyltransferase and guanine phosphoribosyltransferase, respectively (Wang and Aldritt, 1983). *Cryptosporidium parvum* on the other hand, uses adenosine as the sole purine source and converts it

directly into AMP by the action of adenosine kinase (E.C. 2.7.1.20) (Striepen *et al.*, 2004). AMP is deaminated by AMP deaminase (E.C. 3.5.4.6) to generate inosine monophosphate (IMP), which is then converted to GMP by the concerted actions of IMP dehydrogenase (E.C. 1.1.1.205) and GMP synthetase (E.C. 6.3.4.1). In contrast to these two parasites, *Toxoplasma* (Chaudhary *et al.*, 2004) and *Plasmodium spp.* (Hyde, 2004) can utilize a wide range of purine nucleobases and nucleosides. Sequencing of *P. falciparum* genome has failed to uncover any genes encoding enzymes involved in the *de novo* biosynthesis of purine nucleosides or nucleobases (Gardner *et al.*, 2002). This explains the early biochemical experiments, which showed that *Plasmodium spp.* could incorporate the radiolabeled purines, [^{3}H]-adenosine and [^{3}H]-hypoxanthine significantly into the nucleic acid pool (Bungener and Nielsen, 1968). Other purine bases such as adenine, guanosine, inosine, guanine have also been shown to be taken up and incorporated into the nucleic acids, but as compared to adenosine and hypoxanthine, both the uptake and incorporation were lower (Van Dyke *et al.*, 1970; El Bissati *et al.*, 2008). It is believed that ATP in the erythrocytes is completely broken down to hypoxanthine, which is then salvaged to form AMP and GMP in the parasite (Roth *et al.*, 1989). It was also found that supplementation of the culture medium with 100-400 µM hypoxanthine increased the parasite yield (Zolg *et al.*, 1982; Divo and Jensen, 1982; Freese *et al.*, 1988) and depletion of serum and erythrocyte hypoxanthine pools by the addition of xanthine oxidase (E.C. 1.17.3.2) resulted in complete parasite death (Berman *et al.*, 1991) suggesting that hypoxanthine is an important source of purines in *P. falciparum*.

Erythrocytes being metabolically inactive have a modest nutrient requirement and limited nutrient transport ability. In contrast, the parasite in the erythrocyte has higher

metabolic activity and requires a constant supply of nutrients. Thus, upon infection, the parasite induces the formation of New Permeation Pathways (NPP) in the erythrocyte membrane, which permits the uptake of low molecular weight solutes such as amino acids, nucleobases, monosaccharides and various monocarboxylates (Saliba and Kirk, 2001). Hence, most of the nutrients including purines can cross the erythrocytic membrane and also the parasitophorous vacuolar membrane. However, the parasite plasma membrane permits only selective uptake of the nutrients by parasite encoded specific transporters. Purine uptake takes place essentially by the transporter PfENT1 (*P. falciparum* Equilibrative Nucleoside/Nucleobase Transporter 1), which has a broad specificity for hypoxanthine, adenosine, guanine, guanosine, adenine, xanthine and inosine (Carter *et al.*, 2000; Rager *et al.*, 2001; Downie *et al.*, 2008; El Bissati *et al.*, 2008; Quashie *et al.*, 2008). Genetic knockout of PfENT1 resulted in the loss of parasite viability, which could be recovered only in the presence of excess non-physiological concentrations of hypoxanthine, inosine and adenosine (El Bissati *et al.*, 2006) implicating the pivotal role of PfENT1 in purine salvage in *P. falciparum*.

Purine nucleobase/nucleoside transport is followed by the action of several enzymes to generate AMP and GMP. The enzymatic activities for adenosine deaminase (ADA) (E.C. 3.5.4.4), purine nucleoside phosphorylase (PNP) (E.C. 2.4.2.1) and phosphoribosyltransferase (PRT) were obtained from the *P. falciparum* lysate (Reyes *et al.*, 1982). The complete dependence of *P. falciparum* on the purine salvage pathway (Fig. 1.6) makes the constituent enzymes potential candidates for antimalarial chemotherapy (Gherardi and Sarciron, 2007; Downie *et al.*, 2008). Adenosine deaminase (ADA), which deaminates adenosine to inosine has been characterized from *P.*

falciparum (Daddona *et al.*, 1984) and was found to catalyze the conversion of methylthioadenosine to methylthioinosine, a feature not present in the human counterpart (Ting *et al.*, 2005). This catalytic specificity of malarial ADAs permitted the development of methylthiocoformycin (MT-coformycin) to act as a *Plasmodium*-specific transition state analogue. MT-Coformycin was found to be a subnanomolar inhibitor of PfADA and more importantly showed more than 20000-fold selectivity for PfADA relative to human ADA (Tyler *et al.*, 2007). Purine nucleoside phosphorylase (PNP) is the next enzyme that catalyzes the phosphorolysis of inosine to hypoxanthine. *P. falciparum* PNP was found to have a very low sequence identity of 20 % with the human PNP (Kicska *et al.*, 2002). Immucillins, which are transition state analogue inhibitors of the human PNP were found to inhibit *P. falciparum* PNP with Immucillin H being the most potent inhibitor with a K_m/K_i ratio of 9000 (Kicska *et al.*, 2002[a]). Immucillin H was then shown to have a potent inhibitory activity on the *in vitro* growth of *P. falciparum* with an IC_{50} of 35 nM (Kicska *et al.*, 2002[b]). Crystal structure of *P. falciparum* PNP in complex with Immucillin H revealed the presence of a solvent filled cavity near the 5′-hydroxyl group of Immucillin H, which suggested that PfPNP can accept additional functional groups at the 5′-carbon (Shi *et al.*, 2004). This explained the earlier observation that PfPNP could accept methylthioinosine as well as inosine as substrates (Ting *et al.*, 2005). The extended substrate specificity enabled the development of 5′-Methylthio-Immucillin-H (MT-ImmH), which had ~ 100 times more affinity to PfPNP than to the human PNP (Shi *et al.*, 2004). Interestingly, PNP knockout *P. yoelli* transgenic parasites were unable to complete a full life cycle and mice injected with such parasites were resistant to a subsequent challenge of wild type *P. yoelli* (Ting *et al.*,

2008). Further, PNP deleted *P. falciparum* transgenic parasites showed growth defects under physiological concentrations of hypoxanthine implicating the important role of PNP in parasite survival (Madrid *et al.*, 2008). Hypoxanthine formed is phosphoribosylated to inosine monophosphate (IMP) by the action of hypoxanthine guanine phosphoribosyltransferase (HGPRT). *P. falciparum* HGPRT, in addition to hypoxanthine and guanine also catalyze the phosphoribosylation of xanthine, a feature that is absent in human HGPRT (Keough *et al.*, 1999). It was found that the substrate specificity of human HGPRT could be extended to catalyze xanthine phosphoribosylation by a non active site mutation of Phe36 to Leu36 (Raman *et al.*, 2004). Purine analogues such as 6-chloroguanine, 8-azaguanine, 8-azahypoxanthine, 6-thioxanthine and allopurinol were found to be good substrates for PfHGPRT and more interestingly, these bases were not converted to their nucleotides by the human HGPRT (Keough *et al.*, 2006). IMP is converted to guanosine monophosphate (GMP) through xanthosine monophosphate (XMP) by the concerted actions of IMP dehydrogenase (IMPDH) and GMP synthetase (GMPS). *P. falciparum* IMPDH has not been characterized, but the enzyme from the related apicomplexan, *C. parvum* has been targeted for the development of species specific inhibitors (Umejiego *et al.*, 2004; Umejiego *et al.*, 2008). The gene encoding *P. falciparum* GMP synthetase has been isolated and found to have a unique 20 amino acid insertion in the Glutamine Amidotransferase (GAT) domain (McConkey, 2000). Biochemical characterization of PfGMPS has shown that (1) the enzyme exists as a dimer in solution, unlike other eukaryotic GMP synthetases that are monomeric (2) the enzyme is not inhibited by decoynine unlike the human GMP synthetase (Nakamura and Lou, 1995) (3) the enzyme has the highest leaky glutamine hydrolyzing activity (Bhat *et*

al., 2008). All these features were significantly different from the human GMPS making PfGMPS a good target for chemotherapeutic interventions. IMP is also converted to AMP by the concerted actions of adenylosuccinate synthetase (ADSS) and adenylosuccinate lyase (ASL). Gene encoding PfADSS has been cloned, expressed and purified (Jayalakshmi *et al.*, 2002) and was found to catalyze the reaction through a unique kinetic mechanism (Raman *et al.*, 2004). Crystal structure of fully ligated PfADSS identified unique substrate interactions and highlighted differences in the dimer interface (Eaazhisai *et al.*, 2004). Hadacidin, a specific inhibitor of ADSS (Shigeura and Gordon, 1962) was shown to inhibit PfADSS enzyme activity with a K_i of 5.6 μM (Raman *et al.*, 2004), which also showed a potent inhibitory activity on the *in vitro* growth of *P. falciparum* (Webster *et al.*, 1984; Mehrotra *et al.*, 2010). The gene encoding PfASL was found to have a very low homology to the human ASL (15 % sequence identity) (Marshall and Coppel, 1997). Previous studies have also indicated that PfASL is expressed at a constant level throughout the intraerythrocytic stages of the life cycle (Bozdech *et al.*, 2003) and, *in silico* knockout followed by metabolic flux analysis indicate that PfASL is at a critical step in the parasite's metabolism (Fatumo *et al.*, 2009). Further, ASL is not subjected to positive selection (Kedzierski *et al.*, 2002), which makes it a good target for development of antimalarials. However, PfASL has not been studied and forms an aspect of the studies reported in this thesis.

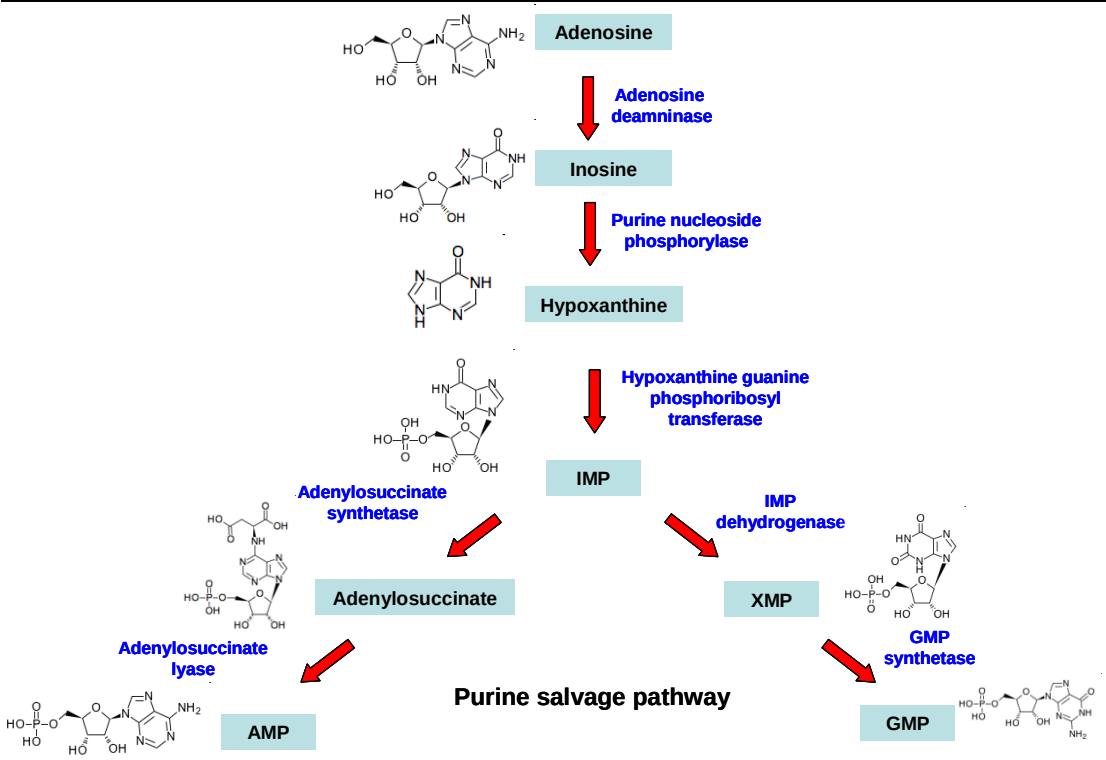

Fig. 1.6: Purine salvage pathway

Hypoxanthine is phosphoribosylated to IMP, which then branches out to form AMP and GMP. Adenosine can also be salvaged by P. falciparum, which after deamination and phosphorolysis generates hypoxanthine. Metabolite structures are adapted from KEGG database (Kanehisa and Goto, 2000).

1.3.5 Metabolic bypass mechanisms of purine salvage pathway

In addition to the above described pathway, purine nucleobases and nucleosides can be converted to their nucleotide monosphosphates by other alternate mechanisms. Adenosine, for example can be directly phosphorylated to AMP by the action of adenosine kinase. Adenine and guanine can get phosphoribosylated to AMP and GMP by adenine and guanine phosphoribosyltransferases. *P. falciparum* lacks a homologue of adenosine kinase in its genome (Gardner *et al.*, 2002) and hence, salvage of adenosine to form AMP is not possible in *P. falciparum*. Guanine can be salvaged by *P. falciparum* to GMP as recombinant PfHGPRT could catalyze the phosphoribosylation of guanine to

GMP (Keough *et al.*, 2006). The presence of a weak adenine phosphoribosyltransferase (APRT) activity in the parasite lysate (Reyes *et al.*, 1982) and a recent report suggesting the incorporation of [^{3}H]-adenine into the nucleic acid pool of free parasites (Mehrotra *et al.*, 2010) suggests the presence of an APRT like activity in *P. falciparum*. However, no gene that encodes APRT has been annotated thus far, in *P. falciparum* genome. Cassera *et al.* have shown that the erythrocytic AMP can also serve as an alternate purine source in *P. falciparum* (Cassera *et al.*, 2008).

1.3.6 Metabolic cross talk of purine salvage pathway

Because of the presence of metabolites that are common to other metabolic pathways, the purine salvage pathway is interconnected and regulated by many other metabolic pathways. In *P. falciparum*, such interconnections are conserved although in some cases, they are varied.

1.3.6.1 Polyamine synthesis

Polyamine synthesis pathway generates methylthioadenosine (MTA) for the synthesis of spermidine (Pegg, 2009) (Fig. 1.7). In most organisms, MTA is converted to adenine and methylthioriboside 5'phosphate (MTR-1-P) by the action of methylthioadenosine phosphorylase (MTAP) (E.C. 2.4.2.28). Adenine is then acted upon by adenine phosphoribosyltransferase to generate AMP. In *P. falciparum*, however, it was found that MTA is acted upon by *P. falciparum* adenosine deaminase to generate methylthioinosine (MTI), a metabolite that is not present in the humans. MTI further undergoes phosphorolysis by *P. falciparum* purine nucleoside phosphorylase to generate

hypoxanthine (Ting *et al.*, 2005) (Fig. 1.7). The extended substrate specificity of PfADA and PfPNP led to the development of methylthiocoformycin and 5' methylthio-immucillin H as highly potent and selective antimalarials (Tyler *et al.*, 2007; Ting *et al.*, 2005). Further, MTA analogs have been synthesized that have antimalarial activity (Sufrin *et al.,* 1995). Methylthioriboside 5' phosphate (MTR-1-P) formed as a result of the phosphorolysis reactions is converted to methionine in a series of four enzyme catalyzed steps. The final step is the transamination of α-ketomethylthiobutyrate to generate methionine by aminotransferases (Albers, 2009). This methionine regeneration pathway has been partially characterized for a number of organisms, including protozoan parasites like *Trypanosomatids* (Berger *et al.,* 1996). In *P. falciparum,* it was found that aspartate aminotransferase carries out transamination of α-ketomethylthiobutyrate to generate methionine using aspartate, glutamate, histidine, tryptophan, phenylalanine, and tyrosine as effective amino donors (Berger *et al.*, 2001) indicating a functional methionine recycling in *P. falciparum.*

H. sapiens

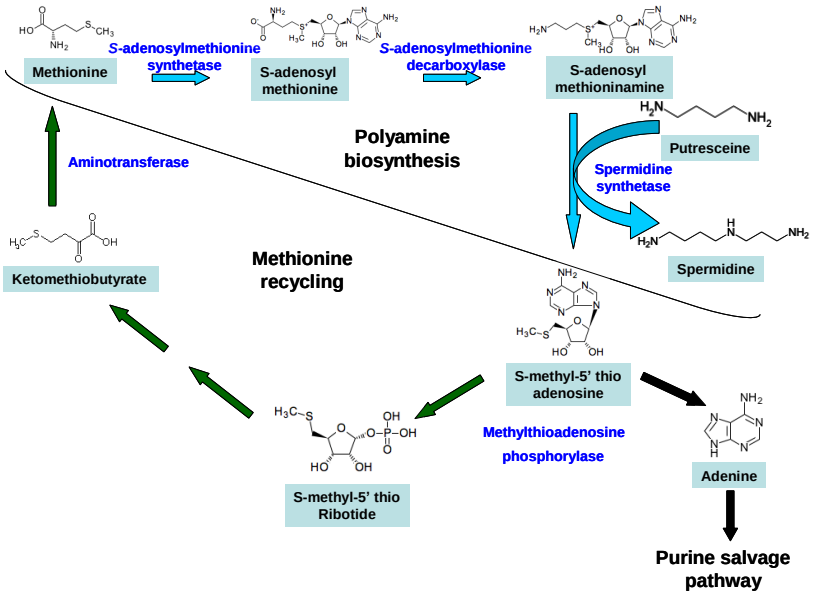

P. falciparum

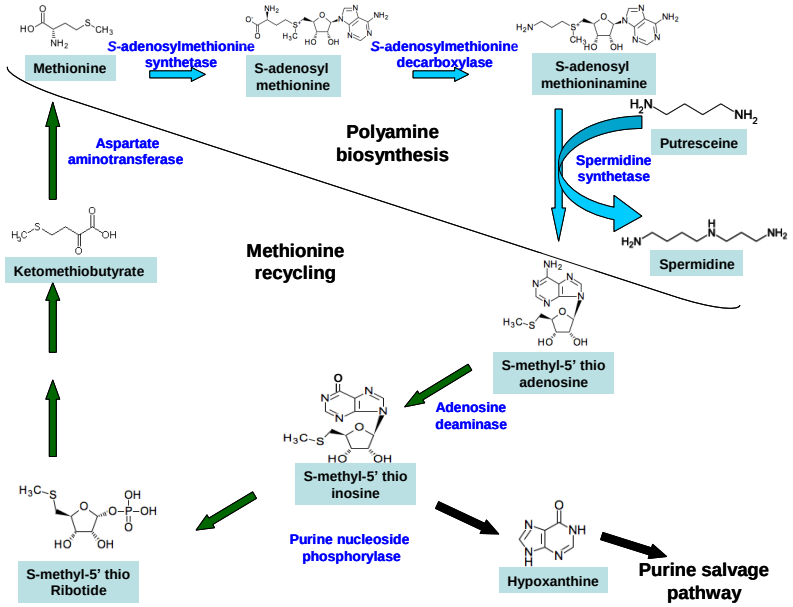

Fig. 1.7: Metabolic cross talk of polyamine biosynthesis in *H. sapiens* and *P. falciparum*

Methylthioadenosine (MTA) gets converted to adenine and methylthioribotide in H. sapiens while in P. falciparum, MTA is deaminated to methylthioinosine by adenosine deaminase. The purine salvage pathway is replenished by adenine in H. sapiens, while in P. falciparum, the pathway is replenished by hypoxanthine.

1.3.6.2 Pentose phosphate pathway

The pentose phosphate pathway (PPP) or otherwise known as the hexose monophosphate shunt (HMPS) provides NADPH for maintaining redox balance and ribose 5' phosphate for nucleotide biosynthesis. Ribose 5' phosphate is converted to phosphoribosyl pyrophosphate (PRPP) by PRPP synthetase (E.C. 2.7.6.1), which then enters the purine salvage pathway. Levels of PRPP and ribose-5-P have been shown to regulate purine salvage pathway in rat liver (Kim *et al.,* 1992). In the oxidative arm of the pentose phosphate pathway, the C-1 of glucose is removed as CO_2. The operation of a functional pentose phosphate pathway in *P. falciparum* is demonstrated by the production of $^{14}CO_2$ by free parasites and parasitized erythrocytes upon incubation with [^{14}C]-1-D-glucose. The evolution of $^{14}CO_2$ was found to be stage dependent and was highest in the trophozoites (Atamna *et al.,* 1994). It was noticed that the PRPP content of *P. falciparum* infected erythrocytes increased to as much as 56 times the PRPP content of the uninfected erythrocytes from 24-48 h post infection and was also maximal in the trophozoite stage (Roth *et al.*, 1986). Ribose 5' phosphate could also be synthesized from fructose-6-phosphate and glyceraldehyde-3-phosphate in the reverse direction of the non-oxidative arm of the pentose phosphate pathway. This pathway has also been shown to be functional in *P. falciparum* as parasites incubated with [^{14}C]-1-D-glucose and [^{14}C]-6-D-glucose showed similar radioactive incorporation in the nucleic acid pool (Atamna *et al.,* 1994).

1.3.6.3 TCA cycle

AMP formed from the purine salvage pathway is deaminated to IMP by AMP deaminase and this constitutes the purine nucleotide cycle. The purine nucleotide cycle is a cyclic series of reactions involving the transfer of the amino group of aspartate to the 6-oxo-group of IMP to generate adenylosuccinate, which is broken down to AMP and fumarate. AMP is then deaminated back to IMP to start the cycle again. Under conditions of excess ATP demand such as during vigorous exercise, the purine nucleotide cycle plays an important role of AMP deamination to IMP and hence, driving the adenylate kinase reaction towards ATP formation (Aragon and Lowenstein, 1980). *P. falciparum* genome contains genes for all the three enzymes constituting the purine nucleotide cycle. Free parasites incubated with [^{33}P]-AMP produced radiolabelled IMP indicating an active AMP deaminase (Cassera *et al.*, 2008). Further, it has been seen that parasitized erythrocytes secrete substantial amounts of ammonia into the media at a rate of 0.8 fmol h^{-1} per parasite (Zeuthen *et al.*, 2006). All these observations support the existence of the purine nucleotide cycle in *P. falciparum*, although the exact function is unknown.

In the purine salvage pathway, a molecule of fumarate is generated along with the synthesis of a molecule of AMP. In organisms with an aerobic respiration, fumarate has been shown to replenish the TCA cycle (Aragon and Lowenstein, 1980; Aragon *et al.*, 1981). However, as mentioned before, the TCA cycle in *P. falciparum* seems to be different from the conventional TCA cycle. Hence, the metabolic fate of fumarate is unknown and needs investigation.

1.4 Objectives

The work done in this thesis aims at carrying out the biochemical, kinetic and catalytic characterization of adenylosuccinate lyase from *P. falciparum*. Crystal structures of ASLs have been solved from *Thermotoga maritima* (Toth and Eates, 2000), *Pyrobacullum aerophillum* (Toth *et al.,* 2000), *Escherichia coli* (Tsai *et al.*, 2007), *Plasmodium vivax* (PDB I.D: 2QGA, 2HVG) and *Homo sapiens* (PDB I.D: 2J91). However, aspects related to kinetics of ASL such as order of product release, identification of the rate limiting step(s) are still not clear.

ASL is the only enzyme that catalyzes two distinct, but chemically similar reactions involving the cleavage of succinyl-adenosine monophosphate (SAMP) to adenosine monophosphate (AMP) and fumarate (Ratner, 1972) and the second being the eighth step of the *de novo* purine biosynthetic pathway, which involves the cleavage of 5-aminoimidazole-4 (N-succinylcarboxamide) ribonucleotide (SZMP) to 5-aminoimidazole-4-carboxamide ribonucleotide (ZMP) and fumarate. In the absence of the *de novo* purine biosynthetic pathway, it is not known whether PfASL has retained the catalytic ability to cleave SZMP. Hence, it was interesting to study the enzyme from *P. falciparum*.

The other facet of the thesis is to delineate the metabolic fate of fumarate, which is an end product of the purine salvage pathway in the intraerythrocytic stages of *P. falciparum*. In *P. falciparum* it is known that TCA cycle is dysfunctional as a cycle in the intraerythrocytic stages and there is minimal carbon flow from the cytoplasm to the mitochondria. Hence, the metabolic fate of fumarate was unknown and has been delineated.

CHAPTER 2

Kinetic and Catalytic Characterization of Recombinant Adenylosuccinate lyase from *Plasmodium falciparum*

Kinetic and Catalytic Characterization of Recombinant Adenylosuccinate lyase from *Plasmodium falciparum*

Abstract

This chapter presents the detailed biochemical and kinetic characterization of the recombinant adenylosuccinate lyase from Plasmodium falciparum (PfASL). The enzyme exists as a tetramer in solution. Initial velocity, product inhibition, pre-steady state kinetics and kinetic isotope effect studies indicate that PfASL exhibits a Uni-Bi rapid equilibrium ordered reaction in which, the overall rate is limited by the C-N bond cleavage in the substrate, SAMP. pH kinetics and mutagenesis suggest that the substrate carboxylic group activates the catalytic base, Ser 298 in the enzyme susbtrate complex to deprotonate the C (β)-H of SAMP. A brief introduction to kinetic and catalytic mechanisms exhibited by enzymes is presented.

2.1 Introduction

2.1.1 Enzymes

Enzymes are biological catalysts that accelerate the rate of various complex biochemical reactions constituting a living cell. In the absence of enzymes, most of these reactions would proceed at time scales, far larger than the life span of an organism (Radzicka and Wolfenden, 1997). Enzymes can accelerate the rate of a reaction by a factor as high as 10^{19} and this enhancement in the reaction rate over the corresponding uncatalyzed rate has been termed the "proficiency" of an enzyme (Radzicka and

Wolfenden, 1997). Linus Pauling proposed that the enhancement in the reaction rate by an enzyme arises due to the enzyme's ability to bind the "distorted substrate" or the "transition state" more tightly than the normal substrate or the ground state. It then follows that antibodies generated against the transition state structure of a reaction would ideally possess similar complimentary sites as would be present in the enzyme catalyzing that particular reaction and hence, would also lead to similar rate accelerations. These antibodies termed as the 'catalytic antibodies' did lead to rate accelerations over the uncatalyzed rate (10^4-10^6), but the fold increase in the rate was found to be well below that of an enzyme catalyzed reaction (10^{12}-10^{20}) (Schwartz and Schramm, 2009). Thus, tight binding of the transition state by the enzyme is one of, but not the sole reason to explain the proficiency of an enzyme. Recently, increasing theoretical and experimental studies have indicated that enzyme dynamics (both short range and long range) play vital role in the overall enzyme catalysis (Eisenmesser *et al.*, 2002, Antoniou *et al.*, 2006).

2.1.2 Enzyme Specificity

Enzymes are highly specific to their substrates. Emil Fischer suggested the "lock and key" hypothesis to explain this specificity. According to this hypothesis, a substrate fits into an enzyme just like a key fits into a lock. Enzymes were assumed to be rigid molecules with a definite geometric shape, which does not change during the course of catalysis. Although this model explains the enzyme's specificity, but a major drawback was that it could not explain the stabilization of the transition state by the enzyme. The "induced fit" model given by Daniel Koshland suggested that enzymes alter their active site shape based on the interactions with the substrate and as a consequence, position the

key functional groups to enable the enzyme to perform catalysis (Koshland, 1958). This model therefore, assumes that enzymes are dynamic and not rigid and hence, could also account for the stabilization of the transition state. The concept of 'one enzyme-one substrate' has been constantly challenged with the findings that many enzymes in addition to their primary reaction(s) are able to catalyze other secondary reaction(s). This extended ability of the enzymes has been termed 'promiscuity' (Khersonsky *et al.*, 2006, Nobeli *et al.*, 2009). It seems that catalytic promiscuity is an inherent feature that can be further improved by 'tinkering' with the enzyme. Such a 'directed evolution' would then enable us to engineer enzymes with altered specificities, which can be exploited in various aspects of metabolic engineering.

2.1.3 Enzyme catalysis

Enzymes catalyze biochemical reactions by different chemical mechanisms that can be classified into:

2.1.3.1 Acid-Base catalysis

The enzyme's active site contains an acidic and/or a basic group, which are involved in the donation or abstraction of a proton, respectively from either the substrate or the transition state. pH versus activity profile of such enzymes is usually a bell shaped curve (Fig. 2.1), with the activity falling on either side of the pH optima. The half inflection point on the left of the pH optima gives the pK_a of the basic group while that to the right gives the pK_a of the acidic group on the enzyme.

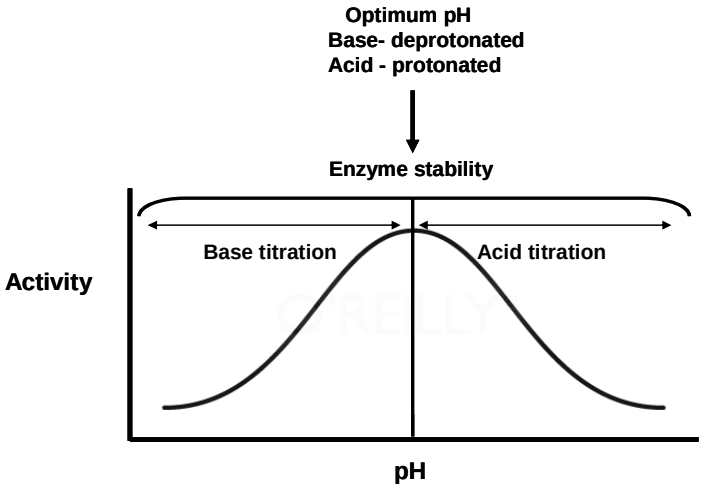

Fig. 2.1: pH dependent enzyme catalysis

The enzyme activity drops on either side of the pH optima. Enzyme stability is not affected in the pH range studied indicating that the drop in activity is due to true titration of the basic and acidic groups.

2.1.3.2 Covalent catalysis

The enzyme forms a transient covalent bond with the substrate by means of a nucleophilic reaction (here, a nucleophile refers to an enzyme side chain group such as the thiol group of cysteine). This is followed by the withdrawal of electrons from the reaction centre by the electrophilic catalyst and finally the elimination of the catalyst by a reaction that is the reverse of the initial nucleophilic attack.

2.1.3.3 Metal ion catalysis

Metal ions participate in enzyme catalysis by (1) electrostatic stabilization of the negative charge (s) in either the substrate or the transition state of a reaction; (2) mediating oxidation-reduction processes through reversible changes in the metal ion's oxidation state and (3) orienting substrates properly for an efficient reaction. Na^{+}, Mg^{2+}, Ca^{2+} and Zn^{2+} are the most common metals found in enzyme catalysis.

2.1.3.4 Electrostatic catalysis

Enzymes occlude water from their active sites thereby causing a reduction in the local dielectric constant. Electrostatics in the active site of such enzymes would be then more similar to that in an organic solvent than in aqueous solutions. Such charge distributions would guide polar substrates into the active sites so that the rates of these enzymatic reactions are greater than their apparent diffusion controlled limits and also serve to stabilize the transition states of the reactions.

2.1.4 Enzyme Kinetics

Reactions catalyzed by enzymes are kinetically described under two main assumptions: (1) Rapid equilibrium and (2) Steady state.

2.1.4.1 Rapid equilibrium

The rapid equilibrium treatment of enzyme reactions was given by Henri, Michaelis and Menten. In this, the free enzyme, E and the free substrate, S are assumed to be in equilibrium with the enzyme substrate complex, ES. This equilibrium is established as the breakdown of ES to E and product, P occurs much slower than the dissociation of ES to E and S (Fig. 2.2). Hence, the overall rate of the reaction is determined by the catalytic step (Segel, 1975).

2.1.4.2 Steady state

In case of many enzymes, the breakdown of ES complex to E + P is so rapid that free E and S do not attain equilibrium with the ES complex. As a consequence, steps other than catalysis including substrate binding, product release and also the

conformational changes in the enzyme will now influence the rate of reaction. The step which is the slowest amongst these will determine the rate of reaction. The steady state treatment of enzyme reactions was given Briggs and Haldane.

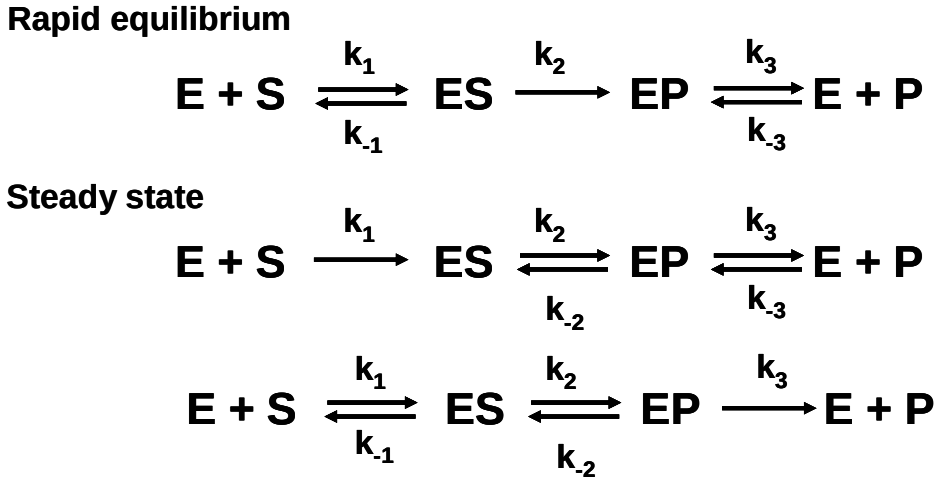

Fig. 2.2: Rapid equilibrium versus Steady state models

2.1.5 Elucidation of the kinetic mechanism

A detailed kinetic mechanism of an enzyme is elucidated by (1) Initial velocity kinetics (2) Product inhibition studies (3) Pre-steady state or transient kinetics and (4) Isotope effect studies.

2.1.5.1 Initial velocity kinetics

In multisubstrate enzymes, the real K_m and V_{max} of one substrate is obtained when all the other substrates are kept saturating (i.e. [S] ~ 9-10 times the K_m). Thus, the effects of the saturating substrates on the overall reaction are minimal. In initial velocity kinetics, velocity measurements are obtained with one substrate varying at different fixed sub-

saturating concentrations ([S] ~ 0.5 – 5 times the K_m) of the other substrate. For example, in a reaction involving two substrates A and B, velocity measurements are obtained at varying concentrations of A at different fixed concentrations of B and also, at varying concentrations of B at different fixed concentrations of A. Based on the pattern of lines in the Lineweaver-Burk (LB) plot, the kinetic model is then determined as either 'ping-pong' or 'sequential'.

Ping-Pong Mechanism

The kinetic mechanism is said to be Ping-Pong if the lines in the LB plot are parallel (Fig. 2.3A). In a Ping-Pong mechanism, the first substrate to bind the enzyme is catalyzed so that a portion of the substrate remains attached to the enzyme with rest falling off before the binding of the second substrate. In other words, no ternary complex is formed.

Sequential mechanism

In a sequential mechanism, the LB plot is characterized by a set of intersecting lines (Fig. 2.3B). Product formation takes place only after the formation of the ternary complex. The pattern of intersection is a characteristic of either a steady state or a rapid equilibrium model.

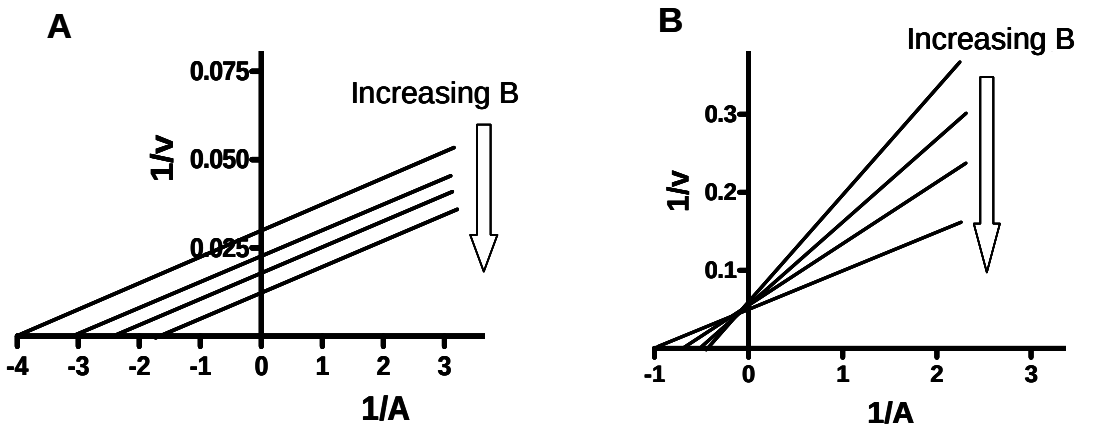

Fig. 2.3: Lineweaver-Burk plots of initial velocity kinetics data
(A) Ping-Pong reaction and (B) Sequential mechanism

2.1.5.2 Product inhibition studies

In multisubstrate enzymes, substrate binding can be (1) ordered, in which binding of one substrate may facilitate the binding of another, or (2) random in which either of the substrates can bind to the free enzyme followed by another to form the central enzyme substrate complex. Likewise, product release can also be ordered or random. The order of substrate binding or product release is probed by product inhibition studies in which, substrate(s) concentration is varied at different fixed concentrations of product(s). LB plots of the velocity measurements would then implicate the type of inhibition as competitive, non competitive, uncompetitive or mixed.

Competitive inhibition

A product P is said to be a competitive inhibitor of a substrate S if the 1 / v versus the 1 / S plot at different fixed concentrations of P gives an intersection pattern on the vertical axis. The competitive inhibitor competes for the active site of the substrate and hence, the inhibition is relieved at high substrate concentrations. In other words, a

competitive inhibitor decreases the K_m of the substrate without affecting the V_{max} of the reaction.

Non- competitive inhibition

A non-competitive inhibitor binds to the enzyme with an affinity that is independent of the substrate concentration. As a consequence, the inhibitor decreases the $V_{max.}$ of the reaction but does not effect the K_m of the substrate. The 1 / v versus the 1 / S plot at different fixed concentrations of P gives an intersection pattern on the horizontal axis.

Uncompetitive inhibition

Inhibitor whose binding is facilitated by the substrate is an uncompetitive inhibitor. The 1 / v versus the 1 / S plot at different fixed concentrations of P gives a parallel pattern. An uncompetitive inhibitor lowers the K_m of the substrate and decreases the $V_{max.}$ of the reaction.

Mixed inhibition

A mixed inhibitor binds the enzyme with an affinity, which is increased in the presence of the substrate. The 1 / v versus the 1 / S plot at different fixed concentrations of P gives an intersection in the second quadrant. A mixed inhibitor increases the K_m of the substrate and decreases the $V_{max.}$ of the reaction. Product inhibition profiles indicate the nature of binding of substrates and release of products from the enzyme.

2.1.5.3 Pre-Steady State Kinetics

Steady state in an enzyme reaction is a state in which the concentration of the different reaction intermediates remains constant with time. In the pre-steady state, the concentration of the intermediates increases linearly with time before attaining the respective steady state concentrations. Study of an enzymatic reaction during this pre-steady state is known as pre-steady state kinetics or transient kinetics. As most of the enzymes carry out multiple turnovers of the substrate in a second, transient kinetics requires the use of a 'stopped flow' or a 'quenched flow' apparatus, which have detection limits in the millisecond time scales. The appearance of a burst followed by a constant steady state rate in the time course of an enzymatic reaction indicates the build up of an intermediate at a step subsequent to catalysis.

2.1.5.4 Isotope effects

Isotopes such as ^{2}H, ^{13}C, ^{15}N, ^{18}O are excellent tools in understanding the kinetic and chemical mechanism of an enzyme catalyzed reaction. The naturally abundant counterparts, ^{1}H, ^{12}C, ^{14}N, ^{16}O are replaced with the heavy isotopes in the molecule undergoing reaction. A change in the rate or equilibrium constant of a reaction upon substitution of a heavier isotope with a lighter one at or adjacent to the position of bond cleavage is defined as the isotope effect. Isotopes are isosteric and isoelectronic, but differ in the absolute mass and hence, isotope effects reflect true changes in vibrational frequencies of reactants as they are converted to products in the rate-determining transition states (Kyte, 1995). Change in the rate of a reaction upon substitution of hydrogen with a deuterium atom at the bond undergoing cleavage is called deuterium

kinetic isotope effect (KIE). Most of the reported KIE studies on enzymes result from replacement of hydrogen on carbon by deuterium. An isotope effect of 3–8 is expected for reactions if protium is replaced by deuterium and the removal of a hydron is rate limiting in the enzyme catalysis (Kyte, 1995). Change in the rate of a reaction upon replacement of H_2O with D_2O is called solvent deuterium isotope effect (Showen and Showen, 1982).

2.1.6 Adenylosuccinate lyase

Adenylosuccinate lyase (ASL) (E.C. 4.3.2.2) is the enzyme that catalyzes the final step in the purine nucleotide biosynthetic pathway. The reaction involves the cleavage of succinyl-adenosine monophosphate (SAMP) to adenosine monophosphate (AMP) and fumarate (Ratner, 1972). Besides this, ASL also catalyzes the eighth step of the *de novo* purine biosynthetic pathway, which involves the cleavage of 5-aminoimidazole-4 (N-succinylcarboxamide) ribonucleotide (SZMP) to 5-aminoimidazole-4-carboxamide ribonucleotide (ZMP) and fumarate (Fig. 2.4). Hence, ASL is the only enzyme that catalyzes two distinct, but chemically similar reactions in the purine biosynthetic pathway.

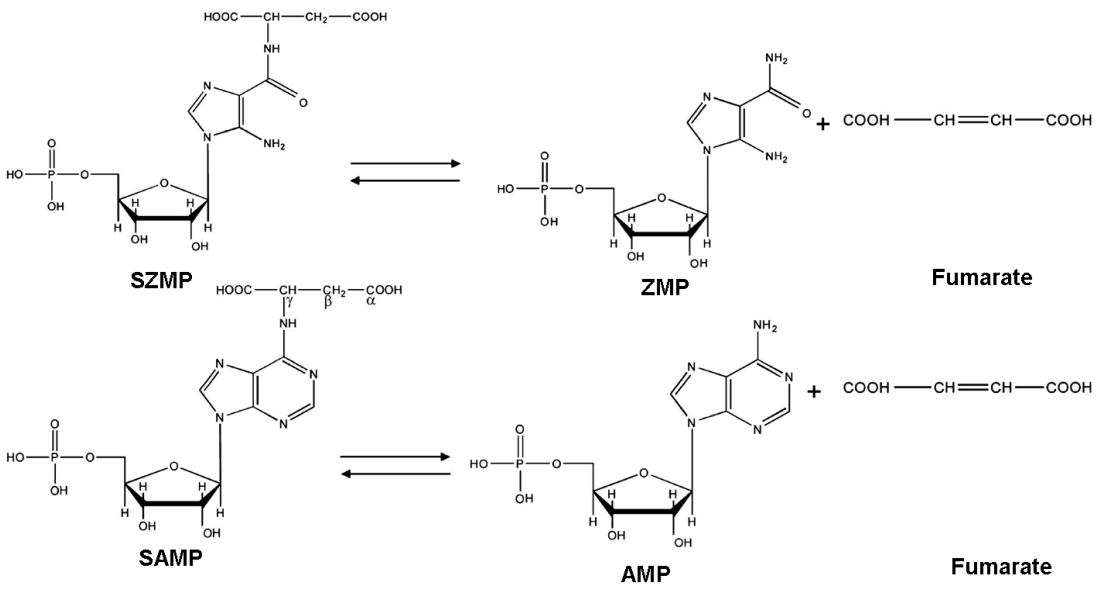

Fig. 2.4: Reactions catalyzed by adenylosuccinate lyase.

SZMP: 5-succinylamino-imidazole-carboxamideribonucelotide; ZMP: 5-amino-imidazole-carboxamideribonucleotide; SAMP: Succinyl-adenosine monophosphate; AMP: adenosine monophosphate. α, β, γ indicate the carbon labeling in SAMP.

2.1.6.1 Structural features

Adenylosuccinate lyase is a member of a superfamily of enzymes that includes class II fumarase, aspartase and arginosuccinate lyase. It is interesting to note that these enzymes have low amino acid sequence identity (25 %), but have an overall similar three dimensional fold (Toth and Yeates, 2000; Weaver *et al.*, 1995; Simpson *et al.*, 1994; Shi *et al.*, 1997; Turner *et al*., 1997). Multiple sequence alignment indicates that these enzymes possess the signature sequence "SSxxPxKxNxxxxE" (Fig. 2.5), where 'X' represents any amino acid. The crystal structures of ASLs have been solved from *Thermotoga maritima* (Toth and Eates, 2000), *Pyrobacullum aerophillum* (Toth *et al.*, 2000), *Escherichia coli* (Tsai *et al.*, 2007), *Plasmodium vivax* (PDB I.D: 2QGA, 2HVG)

and *Homo sapiens* (PDB I.D: 2J91). The enzyme exists as a homotetramer in the asymmetric unit. Further, ASLs from *B. subtilis* (Palenchar and Colman, 2003) and *H. sapiens* (Stone *et al.*, 1993) have been shown to exist as tetramers in solution. Interestingly, *B. subtilis* ASL mutant enzymes with mutations at different catalytic residues are able to complement the loss of function by forming a hybrid active enzyme when mixed together (Lee *et al.*, 1999; Brosius and Colman, 2002; Palenchar *et al.*, 2003). Such an intersubunit complementation can be found in multisubunit enzymes if the active site is constituted by residues coming from different subunits. Other members of this superfamily like arginosuccinate lyase (Turner *et al.*, 1997) have also shown this phenomenon. Further experiments in *B. subtilis* ASL indicated that the active site is formed from residues coming from three different subunits (Brosius and Colman, 2002). Thus, the active form of ASL has been implicated as a tetramer, each molecule of which contains four equivalent active sites.

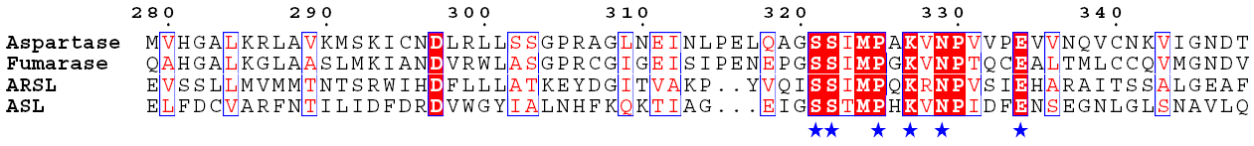

Fig. 2.5: Multiple sequence alignment of proteins representing the ASL superfamily

Protein sequences corresponding to E.coli aspartase (NCBI ID: AAA23499.1); E. coli Fumarate hydratase C (NP_416128.1); Bacillus cereus Arginosuccinate lyase (ARSL) (YP_002368361.1) and E. coli adenylosuccinate lyase (ASL) (AP_001757) were obtained from NCBI protein database and aligned using CLUSTALW (Higgins et al., 1994). The alignment file was submitted to ESPRIPT to indicate the conserved sequence motif (in blue stars).

2.1.6.2 Kinetic and catalytic mechanism

The cleavage of SAMP to AMP and fumarate by ASL has been shown to follow an Ordered Uni-Bi mechanism in which, following cleavage of SAMP, fumarate leaves

the enzyme first followed by AMP. It has been proposed that the overall rate is determined by a step that follows catalysis (Bridger and Cohen, 1968). Catalysis involves abstraction of the methylene proton at the β position of succinyl group (C(β)-H) of SAMP by a general base on ASL, followed by the protonation of the imino nitrogen by a general acid leading to the formation of AMP and fumarate. In *B. subtilis* ASL, a conserved histidine (H141) has been shown to play the role of the catalytic base (Lee *et al.*, 1997) while another conserved histidine (H68) has been implicated as the catalytic acid (Lee *et al.*, 1999). However, liganded and unliganded crystal structures of *E. coli* adenylosuccinate lyase (Tsai *et al*., 2007) implicate a conserved histidine (H171) that was originally thought to be the base seems to be acting as an acid due to its proximity to the imino group of SAMP while a conserved serine (S295) has been proposed to be the catalytic base owing to its proximity to the C (β)-H of SAMP.

2.1.6.3 Physiological role of ASL

Adenylosuccinate lyase deficiency causes an autosomal recessive disorder in which, patients display heterogenous symptoms like psychomotor retardation, muscle wasting, growth failure, seizures, epileptic and autistic features (Spiegel *et al.*, 2006). The body fluids (blood, urine and cerebrospinal fluid) of these patients contain elevated levels of succinyl purines namely succinylamino imidazole carboxamide ribonucleoside (SAICA riboside) and succinyl adenosine (S-Ado). It is proposed that the increased concentrations of these nucleosides are due to an initial cellular accumulation of the substrates, SAICAR and SAMP due to the enzyme's defect. This is followed by dephosphorylation of these nucleotides by a 5' nucleotidase to the corresponding

nucleosides, which being cell permeable, diffuse into the body fluids. It is still not known clearly as to how the deficiency of ASL leads to such pleiotropic effects.

2.1.6.4 *P. falciparum* ASL

An earlier report by Marshall *et al*. (Marshall and Coppel, 1997) shows *P. falciparum* ASL sequence to be significantly different from the human homolog. Sequence similarity of PfASL with that of *H. sapiens* ASL is 15 % while with *E. coli* ASL is 42 % indicating that the parasitic enzyme is more closely related to the bacterial enzyme. Phylogenetic analysis of the different *Plasmodium spp*. with ASL as a query indicated that all the substitutions in the ASL gene locus are synonymous (Kedzierski *et al.*, 2002). This suggested that ASL is not subjected to positive selection unlike the genes that encode surface antigens. Transcriptome analysis suggested a constant expression profile of PfASL across the intraerythrocytic developmental stages of *P. falciparum* (Bozdech *et al.*, 2003). Further, an *in silico* knockout analysis of the different *P. falciparum* genes revealed PfASL as a 'choke point' or otherwise an essential gene for parasite survival (Fatumo *et al.*, 2009). All these features highlight PfASL as a putative drug target and thereby necessitate its detailed biochemical characterization.

2.2 MATERIALS AND METHODS

2.2.1 Materials

All chemical reagents used were of high quality and obtained from Sigma Chemicals Co., USA unless mentioned otherwise. Restriction enzymes, Pfx DNA polymerase and T4 DNA ligase were from Invitrogen, USA and Bangalore Genei Pvt. Ltd., India and were used according to the manufacturers' instructions. Gel filtration matrices were from Amersham Biosciences, UK. Primers were custom synthesized at Microsynth, Switzerland. Media components were from Himedia, Mumbai, India.

2.2.2 Cloning, expression and purification of PfASL

PfASL gene was amplified using parasite genomic DNA as template and with a forward primer ($PfASL_{fwd.}$) with *Nco*I and *BamH*I sites and a reverse primer ($PfASL_{rev.}$) with *Hind*III and *Xho*I restriction sites. A nonconserved valine was substituted with proline (V3P) to facilitate the introduction of *BamH* I site. Amplification yielded a single DNA fragment corresponding to 1.4 kb that was digested with *Nco*I and *Xho*I and cloned in pET28b expression vector. The identity of the clone was confirmed by sequencing. The protein was expressed with a hexahistidine tag at the C-terminus in *E. coli* BL21-CodonPlus™(DE3)-RIL cells (Stratagene, USA). Transformed cultures were grown in terrific broth containing kanamycin (50 μg ml^{-1}) and chloramphenicol (40 μg ml^{-1}) and induced with IPTG at a final concentration of 0.75 mM. Induction was carried out at 16 °C for 12 h. For protein purification, the cell pellets were resuspended in lysis buffer containing 50 mM potassium phosphate, pH 7.4, 100 mM NaCl, 2 mM dithiothreitol (DTT) and 10 % glycerol, lysed using French press and centrifuged. The supernatant was

incubated with nickel nitrilotriacetic acid (Ni-NTA) agarose beads (Novagen) after which the beads were washed extensively with wash buffer (50 mM potassium phosphate, pH 7.4, 100 mM NaCl, 30 mM imidazole, 2 mM DTT, 10% glycerol). Bound PfASL was eluted with elution buffer, pH 7.4 (wash buffer containing 200 mM imidazole). The eluted protein was concentrated and further purified on Sephacryl 200 gel filtration column pre-equilibrated with 50 mM potassium phosphate, pH 7.4, 100 mM NaCl, 2 mM DTT, 1 mM EDTA and 10% glycerol. The eluted protein was again concentrated and used for further experiments. Protein concentrations were determined by the method of Bradford (Bradford, 1976) with bovine serum albumin (BSA) as a protein standard.

PfASL$_{fwd.}$ $^{5'}$GCT**CCATGGATCC**ACATGTGAACCAACTGAAAAAC$^{3'}$

PfASL$_{rev.}$ $^{5'}$ACG**AAGCTT**TTA**CTCGAG**ATTTTTTTTTTATATATTCC
TGTGAGAAGTGCT**CCAC** $^{3'}$

2.2.3 Western blotting

The proteins were separated on a 10 % SDS-polyacrylamide gel and were transferred onto a PVDF membrane using a Hoefer wet transfer apparatus (Hoefer®, Inc., MA, USA). The PVDF membrane was activated with methanol for 10 min. before use. The PVDF membrane was then blocked for 12 h at 4 ºC with blocking solution containing 5 % skim milk in 1 X PBS. The membrane was then incubated with monoclonal anti-hexahistidine antibodies conjugated with horse raddish peroxidase (HRP) (Sigma Chemical Co., St. Louis, USA) in 2.5 % skim milk solution at dilutions of 1:5000 for 3 h at 4 ºC. The membrane was washed thrice with washing solution containing 0.1 % Tween 20 in 1 X PBS. Louis, USA) following which, the membrane

was developed using the chromogenic substrate, 3-amino-9-ethyl-carbazole (Sigma Chemical Co., St. Louis, USA).

2.2.4 Analytical gel filtration

Oligomeric status of PfASL was determined at 25 °C using a pre-calibrated Sephacryl S-300 gel filtration column connected to an AKTA HPLC system in buffer containing 50 mM sodium phosphate, pH 7.0, and 150 mM NaCl. Elution profile of PfASL and molecular weight markers from the column was monitored at 220 nm. V_o or void volume of the column was determined by the use of blue dextran. Molecular weight markers used are: 1. apoferritin, 440 kDa; 2. amylase, 200 kDa; 3.alcohol dehydrogenase, 150 kDa; 4. bovine serum albumin, 66 kDa; 5. carbonic anhydrase, 29 kDa and 6. cytochrome C, 12.4 kDa. Purified recombinant PfASL was loaded onto the column at two different concentrations 1 and 0.25 mg ml^{-1} (20 and 5 μM).

2.2.5 Activity measurements

All assays were done in 50 mM potassium phosphate, pH 7.4, in a final reaction volume of 250 μl using a double beam Hitachi UV 2010 spectrophotometer (Hitachi High Technologies America, Inc., San Jose, CA, USA). Enzyme activities were determined using a saturating SAMP concentration of 200 μM in 50 mM potassium phosphate, pH 7.4 at 25 °C. 1 μg of wild type enzyme and 100 μg of the mutant enzymes were used in a final assay volume of 250 μl. Assays were initiated with the addition of substrate to the sample cuvette after zeroing the absorbance reading with respect to the reference cuvette. PfASL activity for SAMP cleavage to AMP and fumarate was

monitored as a continuous time dependent decrease in absorbance at 290 nm. Amount of substrate consumed was estimated using the difference extinction coefficient of 4.05 $mM^{-1}cm^{-1}$ (Tornheim and Lowenstein, 1972). Specific activity was defined as μmoles of substrate converted to product in 1 min by a milligram of enzyme. To estimate the kinetic parameters, data was fitted to the Michaelis–Menten equation

$$v = \{V_{max}\ [S]\} / \{K_m + [S]\} \qquad \text{(Eqn. 1)}$$

Unless mentioned otherwise, all the data were fitted using GraphPad Prism, version 4.0 (GraphPad Software, Inc., San Diego, CA). Assays were done with three different batches of PfASL with each data point being measured in duplicate.

2.2.6. Order of reaction

2.2.6.1 Product inhibition studies

Product inhibition plots were generated by varying SAMP concentrations at fixed concentrations of either AMP or fumarate. K_i values were obtained by non-linear fits to appropriate inhibition models described below. Standard error and 95% confidence intervals were used as criteria for selecting best fits. The equations for the different inhibitions used were

Competitive

$$v = V_{max}[S] / \{K_m(1+[I]/K_i) + [S]\} \quad \text{(Eqn.2)}$$

Noncompetitive

$$v = V_{max}[S] / \{K_m(1+[I]/K_i) + [S](1+[I]/K_i)\} \quad \text{(Eqn.3)}$$

Uncompetitive

$$v = V_{max}[S] / \{K_m + [S](1+[I]/K_i)\} \quad \text{(Eqn. 4)}$$

where, v is the velocity of the reaction, V_{max} is the maximum velocity, [S] is the substrate concentration, [I] is the inhibitor concentration. K_m is the Michaelis–Menten constant and K_i is the inhibition constant. From the primary linear plot of 1/v versus 1/ [SAMP] at different fumarate concentrations, the values for the slopes and the y-intercept were obtained. Secondary plots of slopes versus fumarate concentrations and y-intercept values versus fumarate concentrations were plotted to obtain the inhibition constants K_{is} and K_{ii} respectively.

2.2.6.2 Initial velocity kinetics

Initial velocity plots were generated by varying AMP at different fixed concentrations of fumarate and by varying fumarate at different fixed concentrations of AMP. The maximum concentration of AMP and fumarate was kept at five times the K_m to maintain sub-saturating conditions. The specific activity values obtained at substrate concentrations near the K_m values were approximate values as the measurements were obscured by the approach of equilibrium. However, initial slopes representing less than 10 % product formation were taken for the specific activity calculations. A global fit of

the data by non-linear regression analysis to the rapid equilibrium ordered bireactant kinetic model was done. The equations used were

$$v = V_{max}\,[A] / \{K_a\,(K_b/[B]) + [A]\,(1+K_b/[B])\} \quad \text{(Eqn. 5)}$$

$$v = V_{max}\,[B] / \{K_b\,(1+K_a/[A]) + [B]\} \quad \text{(Eqn. 6)}$$

where A is the first and B is the second substrate to bind the enzyme E, K_a is the dissociation constant of A from E.A, and K_b is the dissociation constant of B from E.A.B.

2.2.7 Transient Kinetics

Fast reaction kinetics of PfASL in the direction of SAMP cleavage was monitored in a quartz cuvette of pathlength 0.2 cm using a BioLogic SFM 4 stopped flow device (dead time, 10 ms and flow rate, 5 ml s^{-1}) attached to a spectrophotometer (Bio-Logic SAS, France). In order to monitor multiple turnovers, SAMP was maintained at a concentration 20 times greater than the enzyme. Three separate syringes connected to the mixer and the flow cell were filled individually with enzyme, substrate or buffer and incubated at 25 °C for 30 minutes. The contents of the syringes were mixed in the required amounts to obtain the final concentrations (50 mM potassium phosphate, pH 7.4, 100 µM SAMP and 5 µM PfASL) in the flow cell. Progress of the reaction was monitored as decrease in absorbance at 280 nm with a difference extinction coefficient of 10 $mM^{-1}cm^{-1}$ (Tornheim and Lowenstein, 1972). Each data point was acquired at an interval of 10 ms with the total data acquisition time being 20 s. The plot of turnovers versus time was analyzed by the linear regression analysis. Curve fitting was done using GraphPad Prism software, version 4.0.

2.2.8 Preparation of [^{2}H]-SAMP

[^{2}H] SAMP was synthesized by allowing AMP to react with fumarate in D_2O in the presence of PfASL. Stock solutions of AMP (50 mM) and fumarate (100 mM) were prepared in H_2O. After adjusting the pH of these stock solutions to 7.0, the solutions were lyophilized and redissolved in D_2O. 4 mg of purified PfASL was dialyzed extensively against buffer containing 10 mM Tris, pH 7.4, 10 mM NaCl, and 0.5 mM DTT and lyophilized. The latter was dissolved in D_2O and was again lyophilized. This lyophilized powder was added to the reaction mixture in D_2O containing AMP and fumarate at final concentrations of 20 mM and 75 mM, respectively in a total volume of 1 ml. Reaction was allowed to progress for 4 hrs at 37 ˚C. Progress of the reaction was monitored by thin layer chromatography on PEI cellulose with 0.5 M LiCl as the mobile phase (Van den Bergh *et al.*, 1991). For purification of ^{2}H-SAMP, the reaction mixture was passed through a Microsep® centrifugal device, 10K cutoff (Pall life Sciences, USA) to remove the enzyme. The flow-through was loaded on a DEAE anion exchange column and products were eluted with a linear gradient (10-500 mM) of ammonium bicarbonate, pH 8. Under these conditions, SAMP eluted after AMP and fumarate. The fraction corresponding to SAMP was lyophilized, resuspended in water and desalted by passing through Dowex-50W (HCR-W2) cation exchange resin (Sigma Co., USA).

2.2.9 Solvent isotope effect and proton inventory

PfASL activity was monitored in 50 mM potassium phosphate buffer, pH 7.4 (prepared either in H_2O or D_2O) with varying SAMP concentrations to obtain the kinetic parameters, k_{cat} and K_m. The solvent isotope effect values were calculated as

$$^{D}k_{cat} = k_{cat} \text{ in } H_2O / k_{cat} \text{ in } D_2O$$

$$^{D}k_{cat}/K_m = (k_{cat} / K_m) \text{ in } H_2O / (k_{cat} / K_m) \text{ in } D_2O$$

The lyophilized enzyme was incubated in D_2O for 60 minutes on ice prior to the assay to allow complete exchange of protons with deuterons. For proton inventory studies, PfASL activity measurements were carried out at different mole fractions of D_2O in H_2O. Data were fitted to the Gross-Butler equation (Showen and Showen, 1982) describing a linear proton inventory:

$$^{n}k = {}^{D}k(1- n + n\phi^{T}) \qquad \text{(Eqn. 7)}$$

where ^{n}k is the ratio of the rate constants (k_{cat} or k_{cat}/K_m) measured in different fractional concentrations of D_2O compared with 100 % D_2O, ^{D}k is the solvent deuterium isotope effect (the ratio of the rate constants (k_{cat} or k_{cat}/K_m) in H_2O and D_2O), n is the fractional concentration of D_2O, ϕ^{T} is the corresponding deuterium fractionation factor for the exchangeable protonic sites relative to bulk water.

2.2.10 Isothermal titration calorimetry

Binding constants and the associated thermodynamic parameters were determined using a VP-Isothermal Titration Calorimeter (ITC) (Microcal, Inc., Northampton, MA, USA). PfASL was extensively dialyzed against 50 mM potassium phosphate (pH 7.4) containing 100 mM NaCl, 10 % glycerol and 1 mM EDTA prior to use. Stock solutions of ligands were made in the same buffer. Titrations were done at 25 ºC by stepwise addition of small volumes (5 µl) of ligand stock (AMP at a concentration of 5 mM) to PfASL (160 µM) in the sample cell. A control experiment was performed in which the ligands at the same concentration were titrated against buffer alone in the sample cell in

order to obtain the heat of dilution. The raw calorimetric signals were integrated and corrected for the heat of dilution of AMP. The resulting corrected binding isotherms were subjected to nonlinear least squares analysis using ORIGIN software and fit to a single-site model to obtain the association constant, K_A, the binding enthalpy, ΔH^{o}, and the stoichiometry of the interaction, n. The Gibbs free energy, ΔG^{o} and the dissociation constant K_d were calculated using the following equations:

$$\Delta G^{o} = \Delta H^{o} - T\Delta S \qquad \text{(Eqn. 8)}$$

$$K_d = 1 / K_A \qquad \text{(Eqn. 9)}$$

2.2.11 pH Kinetics

pH dependence of PfASL specific activity was monitored over the pH range 6.0 – 9.0 with varying SAMP concentrations. The kinetic parameters, k_{cat} and k_{cat}/K_m obtained from each plot at different pH values were plotted as a function of pH to equations 9 and 10 describing double and single ionization(s), respectively.

$$y = c / \{1 + ([H]/K_1) + (K_2/[H])\} \qquad \text{(Eqn. 10)}$$

$$y = c / \{(1 + (K_2/[H])\} \qquad \text{(Eqn. 11)}$$

where y is the pH dependent parameter, c is the pH independent value of the parameter, [H] is the hydrogen ion concentration and K_1 and K_2 are the ionization constants for the ionizable groups involved in catalysis. pH of the assay mixture was adjusted with 50 mM potassium phosphate buffer and temperature kept constant at 25˚C.

2.2.12 Homology modeling of PfASL

The sequences of ASL from *P. falciparum* (AAC32788), *P. vivax* (AAL60072), *E. coli* (BAA35953), *B. subtilis* (NP_388526) and *H. sapiens* (AAC60603) were downloaded from the non-redundant database at NCBI. Multiple sequence alignments were generated using CLUSTALW (Higgins *et al.*, 1994). The coordinate files for the structures of *E. coli* ASL (Protein data bank code: 2ptr) and *P. vivax* ASL (Protein data bank code: 2qga) were downloaded from protein data bank (www.rcsb.org). Homology models of PfASL were generated, using *E. coli* ASL structure liganded to SAMP (Protein data bank code: 2ptr) and *P. vivax* ASL (Protein data bank code: 2qga) (data not shown) as templates, using MODELLER 9v4 (Sali and Blundell, 1993). The stereochemical quality of the models was verified using WHAT IF (Vriend, 1990) and Verify3D (Luthy *et al.*, 1992). Molecular visualization and structure analysis was done by PyMOL software (DeLano Scientific)

2.2.13 Construction of S298A and S298C PfASL mutants

Site directed mutants of the wild type PfASL were generated by the quick change PCR method using a single mutagenic oligonucleotide method (Shenoy and Visweswariah, 2003). Primers $^{5'}$AAAGAAATTGGCGCGAGTACCATGCCACCATAAAG $^{3'}$ and $^{5'}$AAAGAAATTGGCTGCAGTACCATGCCACCATAAAG $^{3'}$ were used for the generation of S298A and S298C mutants, respectively using wild type gene as a template. PCR product was digested with *Dpn* I and transformed into DH5α strain of *E.coli*. The site of mutation was confirmed by DNA sequencing. Conditions for the

expression and purification of the mutant proteins were kept same as that for the wild type enzyme.

2.3 RESULTS AND DISCUSSION

2.3.1 Expression and Purification of PfASL

The pET 28b plasmid containing PfASL gene insert was transformed into BL21DE3 strain of *E. coli* and protein expression was checked at different IPTG concentrations at 37 ºC. Recombinant PfASL expression could not be obtained even at IPTG concentration as high as 1 mM. *P. falciparum* genome has the highest A+T content of all the genomes sequenced thus far (Gardner *et al.*, 2002). Such a nucleotide compositional bias has resulted in a preferential codon usage by *P. falciparum*. Thus, the lack of expression could be because of the presence of rare codons in the gene sequence of PfASL. Therefore, PfASL expression was checked in *E. coli* BL21-CodonPlus™(DE3)-RIL cells (Stratagene, USA), which contains plasmid encoding rare tRNAs for arginine (*argU*), isoleucine (*ileY*), and leucine (*leuW*). PfASL expression was obtained at different IPTG concentrations. However, soluble PfASL could not be obtained after IPTG induction at 37 ºC for 6 h as most of the expressed protein went into the insoluble fraction. Solubility of PfASL was significantly improved when induction was carried out at a temperature of 16 ºC for a period of 12 h at an IPTG concentration of 0.75 mM. The expressed protein was purified by Ni-NTA affinity chromatography followed by size exclusion chromatography (Fig. 2.6A). The presence of histidine tag in PfASL was confirmed by western blotting with monoclonal anti-hexa-histidine

antibodies (Sigma Co., USA) (Fig. 2.6B). MALDI-TOF-MS of PfASL gave a molecular mass of 56235 Da with the expected mass being 56239 Da (Fig. 2.6C).

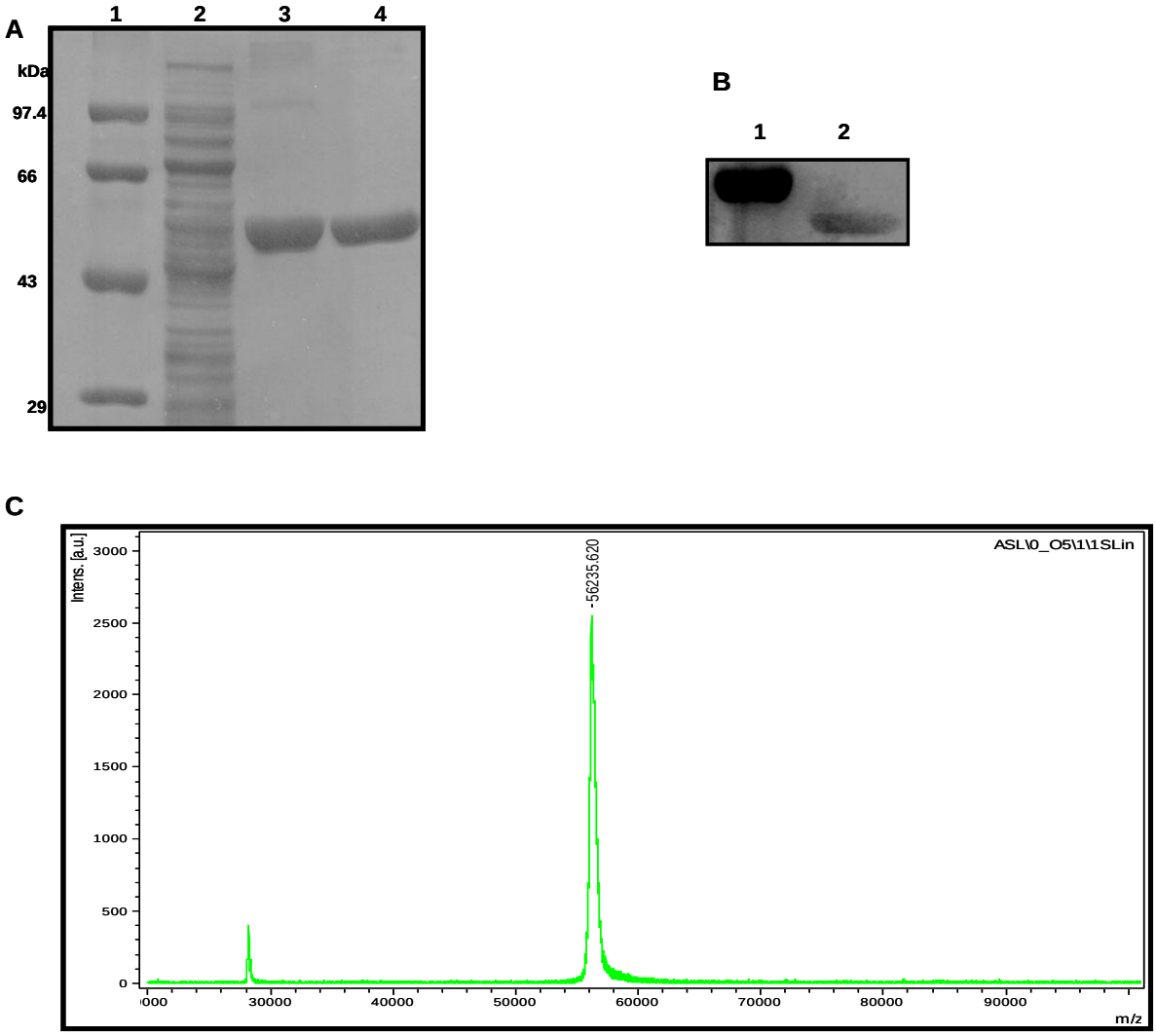

Fig. 2.6: Expression and purification of PfASL

(A) SDS-PAGE analysis of Pf ASL purification. Recombinant Pf ASL was purified from bacterial lysate by Ni-NTA affinity chromatography followed by gel filtration chromatography. Lane 1, Protein molecular weight marker; Lane 2, Crude extract of E. coli lysate; Lane 3, Protein fraction eluted from Ni-NTA affinity column; Lane 4, Protein fraction eluted from sephacryl S-200 gel filtration column. (B) Western Blot analysis of a standard hexa-histidine tagged protein (1) and (2) PfASL. (C) MALDI-TOF-MS analysis of purified PfASL. Mass spectrum was acquired on a Ultraflex II Bruker Daltonics MALDI-TOF-TOF mass spectrometer. The expected molecular mass of the recombinant PfASL was 56239Da.

2.3.2 Quarternary structure of PfASL

The quaternary structure of PfASL was examined using a pre-calibrated Sephacryl 300 (S-300) column. The enzyme eluted as a tetramer at a concentration of 20 µM and no shift in the oligomeric status was seen at a lower protein concentration of 5 µM (Fig. 2.7). Addition of 1 M NaCl did not change the elution profile of PfASL indicating that the tetrameric interface is probably dominated by hydrophobic interactions. Previously, ASLs from *B. subtilis* (Palenchar and Colman, 2003), human (Stone *et al.*, 1993) and other members of the superfamily have also been shown to exist as tetramers.

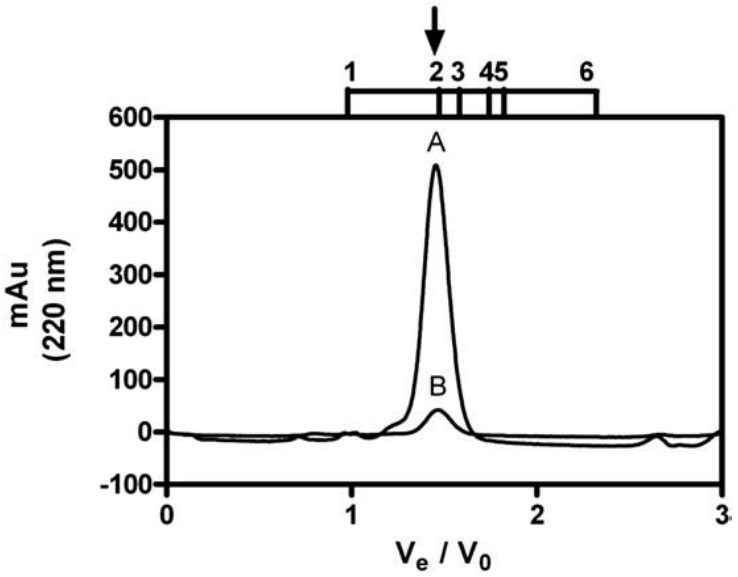

Fig. 2.7: Oligomeric status of PfASL

Elution profile of PfASL from Sephacryl 300 (S-300) gel filtration column as monitored at 220 nm. Scale above the peak corresponds to the elution of the molecular weight markers and the arrow corresponds to the elution of PfASL.. Molecular weight markers are: 1. apoferritin, 440 kDa; 2. amylase, 200 kDa; 3.alcohol dehydrogenase, 150 kDa; 4. bovine serum albumin, 66 kDa; 5. carbonic anhydrase, 29 kDa and 6. cytochrome C, 12.4 kDa. PfASL loaded onto the column was eluted with a buffer containing 50 mM sodium phosphate, pH 7.0, and 150 mM NaCl. The flow rate of the buffer was maintained at 0.5 ml min^{-1}. PfASL concentrations examined were 1 (A) and 0.25 (B) mg ml^{-1} (20 and 5 µM respectively).

2.3.3 Kinetic measurements of PfASL activity

PfASL readily catalyzed the reversible breakdown of SAMP with the forward reaction liberating AMP and fumarate and the reverse reaction catalyzing their condensation. The velocities versus substrate curves for PfASL were fitted to the Michaelis-Menten equation (Eqn. 1) (Fig. 2.8). As can be seen from the curves, PfASL exhibits no cooperativity in catalyzing the reaction. Summarized in Table I are the kinetic parameters of the PfASL catalyzed forward and reverse reactions. PfASL exhibited similar, low K_m values for SAMP and AMP and a high K_m for fumarate. Comparison of the k_{cat} values of the forward and reverse reactions indicates that PfASL catalyzes the forward reaction three times faster than the reverse reaction.

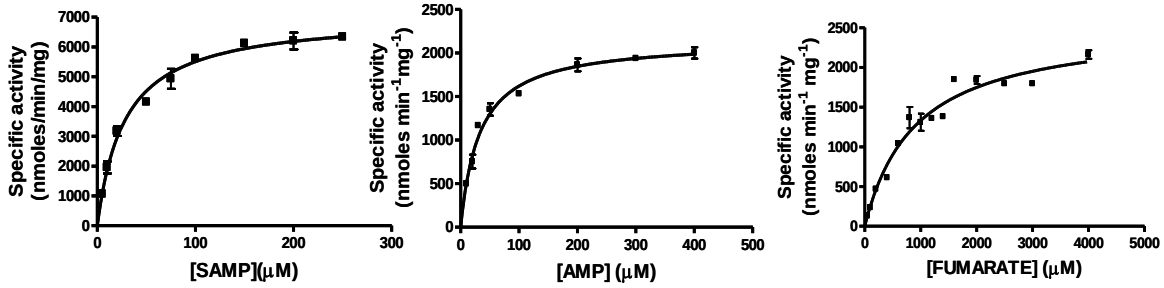

Fig. 2.8: Velocity versus substrate curves for PfASL catalyzed forward and reverse reactions

PfASL activity was monitored as a continuous decrease (forward reaction) or increase (reverse reaction) in absorbance at 290 nm. All assays were done in 50 mM potassium phosphate, pH 7.4, in a final reaction volume of 250 μl using a double beam Hitachi UV 2010 spectrophotometer (Hitachi High Technologies America, Inc., San Jose, CA, USA). Data were fit to Michaelis-Menten equation to obtain the kinetic parameters listed in Table I.

Substrate	K_m (μM)	k_{cat} (s^{-1})
SAMP	32.0 ± 1.7	7.5 ± 0.7
AMP	34.0 ±1.6	2.9 ± 0.4
Fumarate	760 ± 70	2.9 ± 0.4

Table 2.1: Kinetic parameters of PfASL for SAMP cleavage and formation [a].

[a]All enzyme assays were done at 25 °C in 50 mM potassium phosphate, pH 7.4. Enzyme activity was monitored as a time dependent decrease (SAMP breakdown) or increase (SAMP formation) in absorbance at 290 nm and calculated using a difference extinction coefficient of 4.05 mM^{-1} cm^{-1}. Values reported were obtained from the fit of the data to Eqn. 1. Assays were done with three different batches of PfASL with each data point being measured in duplicates.

2.3.4 Initial velocity kinetics

Reciprocal plot of velocities with AMP varying (40 μM to 200 μM) at different fixed concentrations of fumarate (400 μM to 3200 μM) showed convergence above the horizontal axis and beyond the vertical axis in the second quadrant (Fig. 2.9A). This indicates that AMP increases the binding affinity of fumarate to the enzyme. Also, there is an increase in apparent maximum velocities (reciprocals of the vertical intercepts, where AMP concentration is infinite) with fumarate concentration. Both these observations indicate that fumarate could be the second substrate to bind the enzyme after the binding of AMP. This was further confirmed by the reciprocal plot of velocity with concentrations of fumarate varying at different fixed concentrations of AMP (Fig. 2.9B). Both these plots indicated a Rapid Equilibrium Ordered Bi-Uni model and not a Steady State Ordered model where both the plots would have intersected in the second quadrant.

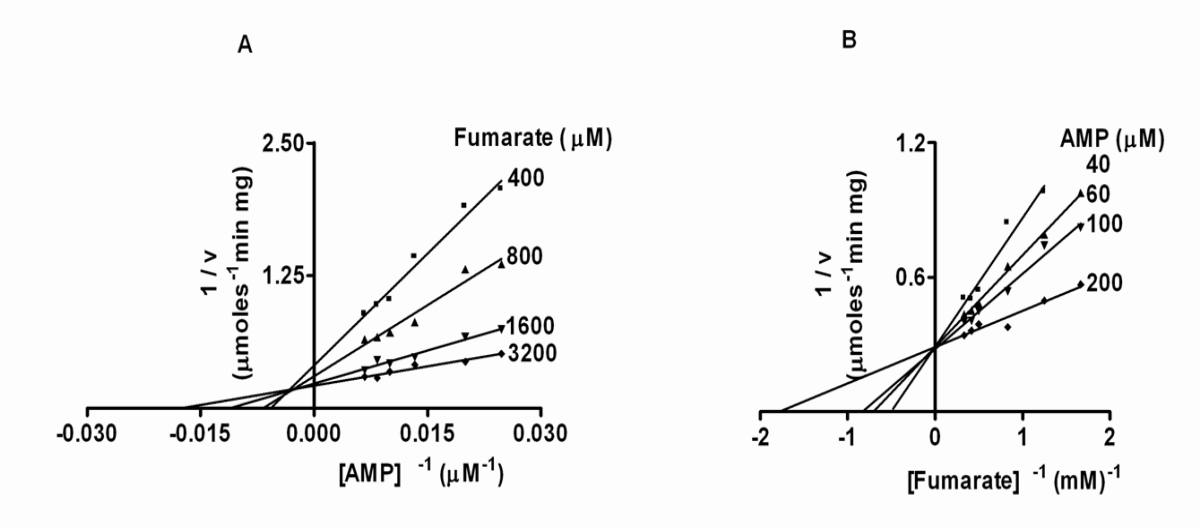

Fig. 2.9: Initial velocity kinetics of PfASL in the direction of SAMP formation from AMP and fumarate

Each plot corresponds to the activity of PfASL in the direction of SAMP formation with (A) AMP varying at different fixed concentrations of fumarate and (B) fumarate varying at different fixed concentrations of AMP. Each line is a theoretical line based on curve fitting. All assays were done at 25°C in 50 mM potassium phosphate, pH 7.4. AMP and fumarate were kept at sub-saturating concentrations with the maximum of each being maintained at around five times the respective K_m values.

A global fit of the data to the non-linear equations (Eqn. 5 and Eqn. 6) describing a Rapid Equilibrium Ordered kinetic model gave the kinetic parameters listed in Table II. The dissociation constant for AMP (K_a) from the enzyme AMP complex was obtained as 0.3 ± 0.15 mM, which was significantly higher than the K_m value for AMP (34.0 ± 1.6 μM). The lower K_m value indicates an increased affinity of AMP towards the enzyme under conditions of catalysis. In other words, the presence of fumarate shifts the equilibrium towards increased product (SAMP) formation and therefore, increased affinity of AMP to the enzyme. Examination of the double reciprocal plot of 1/v vs 1/fumarate at different fixed concentrations of AMP brings out two kinetic aspects of catalysis by PfASL, (1) the decrease in apparent K_b for fumarate with increase in AMP

concentration supports the presence of rapid equilibrium between E.AMP.FUMARATE and FUMARATE and, (2) absence of change in $V_{max.}$ with increase in AMP concentration eliminates rapid equilibrium between E.AMP.FUMARATE and E.SAMP thereby indicating that the process of chemical conversion is rate limiting. This is possible only if the three different enzyme forms, E, E.AMP and E.AMP.FUMARATE exist in a rapid equilibrium as shown in Fig. 2.10.

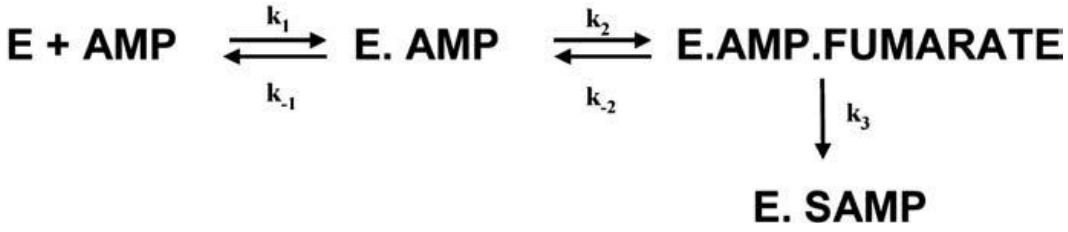

Fig. 2.10 Kinetic scheme for PfASL catalysis

Kinetic parameter	Definition	Value from the fit (mM)
K_a	k_{-1}/k_1	0.3 ± 0.15
K_b	k_{-2}/k_2	0.5 ± 0.02

Table 2.2: Kinetic parameters of PfASL catalysis from initial velocity kinetics[a]

[a]*PfASL activity was examined in the reverse direction keeping AMP and fumarate at sub-saturating concentrations at 25 °C in 50 mM potassium phosphate, pH 7.4. Data were fitted to equations 5 and 6 that describe a Rapid Equilibrium Ordered model as shown in Fig. 2.10*

2.3.5 Product inhibition studies

The effect of products, AMP and fumarate on the rate of SAMP cleavage was determined in order to validate the kinetic mechanism. Reciprocal plot of velocities versus SAMP concentrations at different fixed AMP (0-200 µM) concentrations gave an intersection on the vertical axis indicative of a competitive inhibition (Fig. 2.11A). Data were also fitted to equation for competitive inhibition (Eqn. 2) to obtain a K_i value of 93 ± 8 µM. The reciprocal plot of velocities with the same range of SAMP concentrations at different fixed fumarate (0-4 mM) concentrations gave a set of lines that intersect in the third quadrant (Fig. 2.11B). This is typical of noncompetitive inhibition that was further confirmed by comparing non-linear fits of the data to non-competitive (Eqn. 3) and uncompetitive (Eqn. 4) inhibition models. Best fit was obtained for non-competitive model with a K_i value of 3.7 ± 0.2 mM thereby showing that fumarate can bind to both the free and bound forms of the enzyme. However, the high K_{is} (11.7 mM) value as compared to K_{ii} (2.9 mM) indicates that the affinity of fumarate is high for the AMP bound form of enzyme as compared to the free form. Thus, initial velocity and product inhibition studies indicate that PfASL follows a Rapid Equilibrium Ordered Bi-Uni mechanism in the reverse direction in which AMP binds first to the enzyme followed by fumarate.

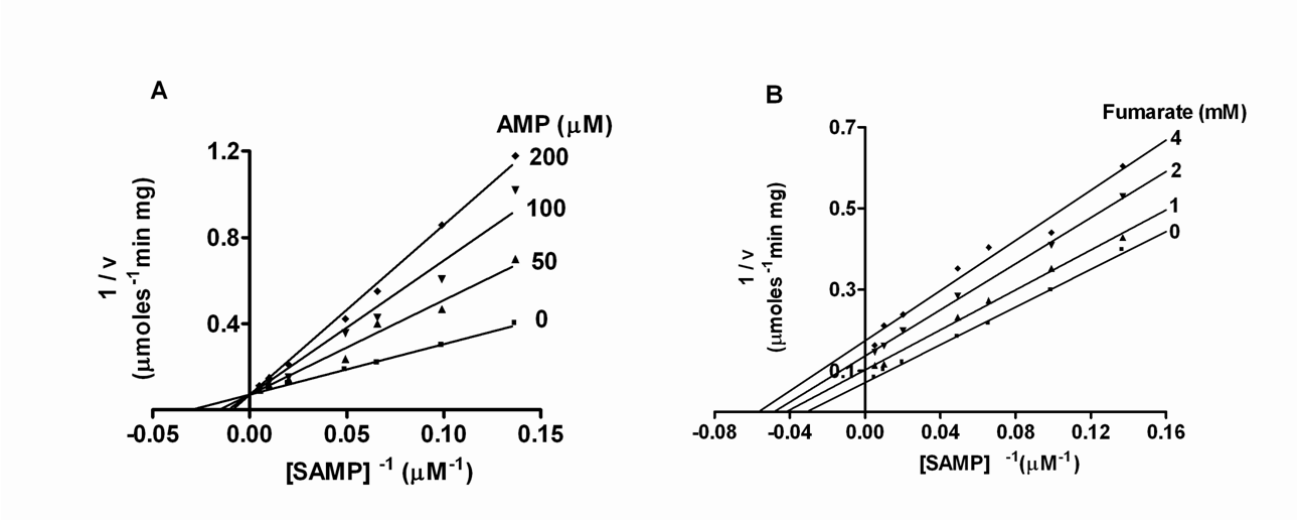

Fig. 2.11: Product inhibition of PfASL in the direction of SAMP breakdown to AMP and fumarate

PfASL activity was measured at varying SAMP concentrations and at different fixed concentrations of (A) AMP and (B) fumarate. Each line is a theoretical line based on curve fitting. All assays were done at 25 °C in 50 mM potassium phosphate, pH 7.4.

2.3.6 Thermodynamics of binary complex formation

The dissociation constant of AMP from PfASL.AMP complex from initial velocity kinetics is an approximate value that needs further confirmation. Thus, thermodynamic characterization of the binding of AMP to PfASL in the absence of fumarate was carried out by isothermal titration calorimetry. The raw calorimetric signals from the ITC titration were integrated and corrected for the heat of dilution of AMP. The resulting enthalpy change was plotted with respect to the molar ratio of AMP and PfASL as shown in Fig. 2.12. The binding of AMP to PfASL occurred at a single site with weak affinity as indicated by the high value of the dissociation constant ($K_{d\ AMP}$ = 170 μM). The dissociation constant for AMP (K_a) from the enzyme AMP complex as monitored by initial velocity kinetics and verified by equilibrium binding measurements by isothermal calorimetry (0.3 ± 0.15 mM and 0.17 ± 0.01 mM, respectively) were significantly higher

than the K_m value for AMP (34.0 ± 1.6 μM) thereby validating the kinetic model in Fig. 2.10.

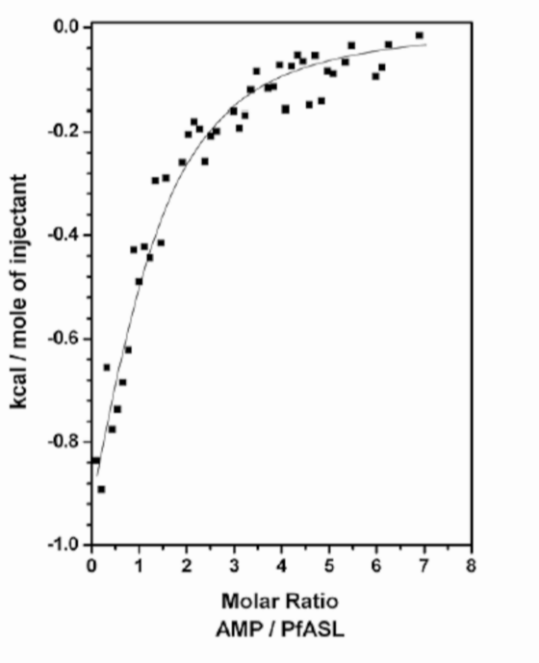

Fig. 2.12: Thermodynamic characterization of the interaction of PfASL with AMP

PfASL (160 μM) was titrated with 5 μl volumes of AMP at 5 mM stock concentration in 50 mM potassium phosphate, pH 7.4 containing 100 mM NaCl and 10% glycerol, at 25 °C. The raw calorimetric signals from the ITC titration were integrated and corrected for the heat of dilution. The resulting enthalpy change was plotted with respect to the molar ratio of ligand and protein. Data were fitted to the single site binding model (using the software ORIGIN) after correction for the heat of dilution of ligand. The dissociation constant of AMP from E.AMP complex was found to be 0.17 ± 0.01 mM.

2.3.7 Transient kinetics

Multiple turn over experiment with SAMP being held in excess (100 μM) over the enzyme (5 μM) was done in the direction of SAMP cleavage in order to probe the rate-limiting step in catalysis. Under steady state conditions, PfASL catalyzes 7 turnovers in a second. Hence, to monitor the first turnover, we measured the reaction in the millisecond time scale with a stopped flow device attached to a spectrophotometer. The reaction trace did not show any burst (Fig. 2.13A) and the plot of turnovers with respect

to time was linear. A catalytic rate of 4.0 ± 0.03 s^{-1} was obtained. The same batch of enzyme was assayed at a concentration of 70 nM with substrate being held at 100 μM under steady state conditions (Fig. 2.13B). A similar catalytic rate of 6.5 ± 0.03 s^{-1} was obtained from the plot of turnovers versus time. The transient kinetic data in the direction of SAMP breakdown reconfirms the model proposed from initial velocity kinetics. The absence of a 'burst' in the reaction trace indicates that the rate limiting step is that of catalysis with step(s) subsequent to it occurring at a faster rate. Moreover, absence of a lag in the reaction trace rules out a steady state step prior to catalysis. Taken together, these results are consistent with a Rapid Equilibrium Uni-Bi Ordered kinetic model with the catalytic step being rate limiting as shown in the Fig. 2.10.

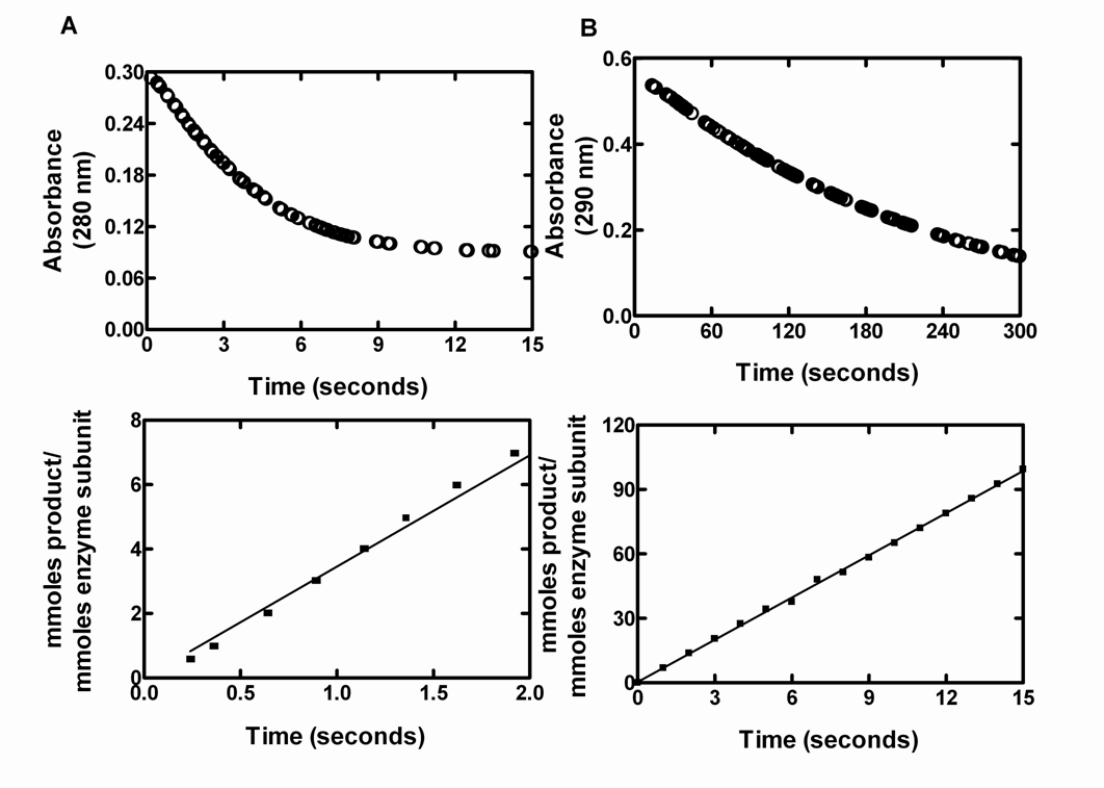

Fig. 2.13: Transient and steady state kinetics of PfASL in the direction of SAMP breakdown

(A) Reaction trace of SAMP disappearance with respect to time as monitored at 280 nm. Final reaction volume of 300 µl contained 100 µM SAMP, 5 µM PfASL and 50 mM potassium phosphate, pH 7.4 and the reaction was carried out at 25 °C. (B) Reaction trace showing SAMP disappearance with respect to time as monitored at 290 nm. Final reaction volume of 250 µl contained 100 µM SAMP, 73 nM PfASL and 50 mM potassium phosphate, pH 7.4. (C) and (D) Turnovers, defined as mmole product formed per mmole PfASL subunit plotted with respect to time, are shown in the lower panel

2.3.8 Preparation and characterization of [^{2}H]-SAMP and primary kinetic isotope effect.

Elimination reactions that result in alkene formation can be of the type E1, E2 or E1cB. E1 mechanism involves the formation of a carbocation intermediate followed by proton abstraction from the substrate, with the latter becoming rate-limiting in catalysis.

In E2 elimination, the two bond cleavages, C-H and C-X (in this case, C-N) take place in a single transition state and hence, a concerted mechanism. In E1cB reactions a strong base abstracts the α proton generating a carbanion intermediate followed by an electron pair expelling the leaving group in a rate limiting step leading to double bond formation. In this mechanism, only the C-N bond cleavage takes place in the transition state and thus, in contrast to E2 mechanism, which is a concerted mechanism, E1cb mechanism is step–wise (Kyte, 1995). ASL catalysis involves the cleavage of two chemically distinct bonds, the C (β)–H bond of the succinyl group and the C (γ)–N bond joining the succinyl group to the adenylate portion of SAMP. In order to determine which of these two bond cleavages is slower, PfASL activity was compared across two substrates, SAMP and [^{2}H]-SAMP. In the latter, the succinyl C–H bond is replaced by a C–D bond. The reaction mixture in D_2O as described in materials and methods section was analyzed by Proton NMR spectroscopy on a Bruker DRX 500 NMR instrument for the incorporation of deuterium at the C-(β) position of SAMP. The ^{1}H-NMR spectra of the standard SAMP is shown in Fig. 2.14A. Peak assignments were done by comparing the chemical shifts of standards from literature. The incorporation of deuterium in place of a hydrogen atom at the C-(β) position of SAMP in [^{2}H]-SAMP is evident from the loss of splitting pattern in the region of 2-3 ppm of the reaction mixture (Fig. 2.14B).

A

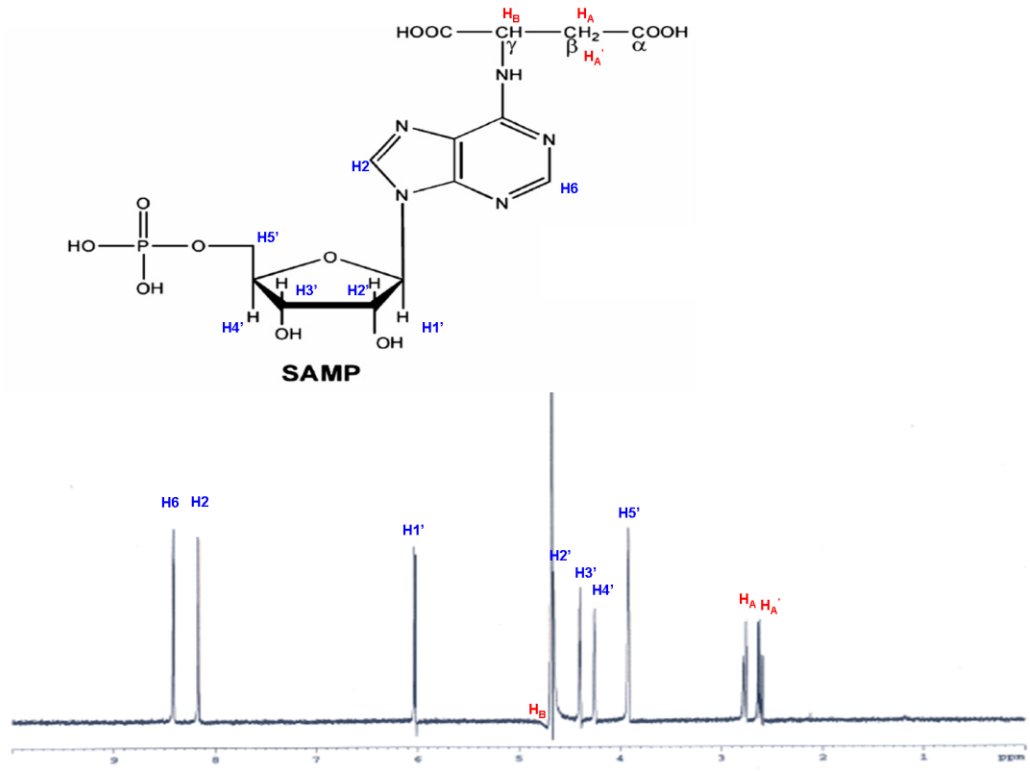

B

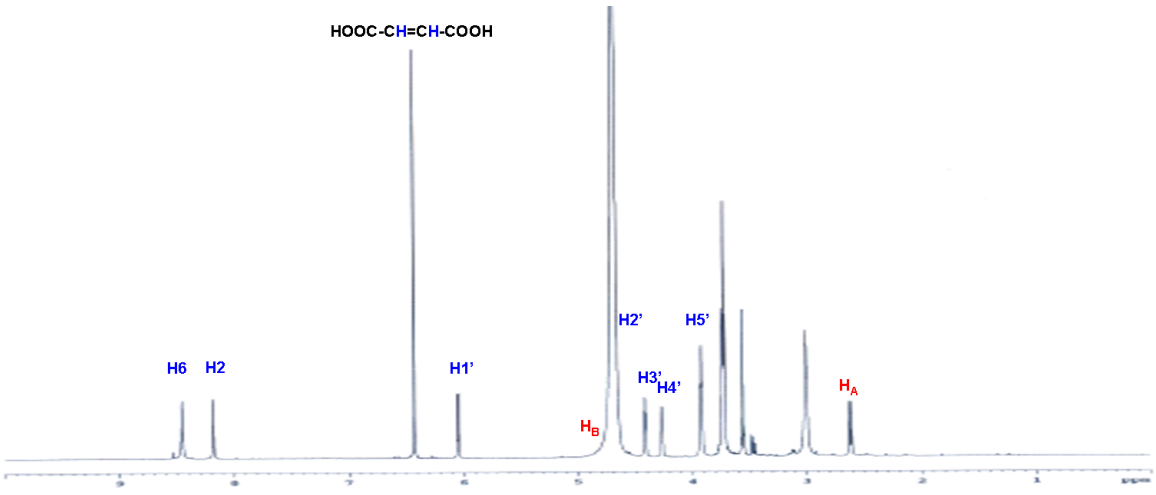

Fig. 2.14: NMR spectrum of standard and synthesized adenylosuccinate

500 MHz ^{1}H- NMR spectrum of (A) standard SAMP and(B) [^{2}H]-SAMP synthesized from AMP and fumarate, in $^{2}H_2O$, by PfASL.

The primary kinetic isotope effect (KIE), defined as the ratio of the kinetic parameters, k_{cat} or k_{cat}/K_m for SAMP and [^{2}H]-SAMP, is only 1.3 at pH 7.4. An isotope effect of 3–8 is expected for reactions that follow E2 elimination, if protium is replaced by deuterium and the removal of a hydron is rate limiting (Kyte, 1995). However, it has been debated earlier that KIE values lower than 2 are also possible (Westheimer, 1961). This occurs when more than one step determines the rate in the overall reaction. To rule out this possibility, the variation of KIE was checked with respect to pH. The KIE showed only a minor variation from 0.8 at pH 6.6 to 1.4 at pH 8.2 (Table III). If more than one step would be rate determining, then it is highly unlikely that the activation energies for the different energy maxima in the reaction coordinate are affected equally by pH and hence, produce a constant KIE. Thus, C–H bond cleavage occurs rapidly and it is the C–N bond cleavage that determines the overall rate in PfASL catalysis.

pH	**(^{D}k$_{cat}$)[b]**	**(^{D}k$_{cat}$/K$_m$)[c]**
6.6	0.8	0.95
7.4	1.3	0.7
7.8	1.6	1.4
8.2	1.4	0.9

Table 2.3: Primary kinetic isotope effects for the conversion of SAMP to AMP catalyzed by PfASL[a]

[a] PfASL activity was monitored with varying concentrations of SAMP and [^{2}H]-SAMP at 25°C in 50 mM potassium phosphate buffer at different pH values. Values reported were obtained from the fit of the data to Eqn. (1).

[b] $^Dk_{cat}$ is defined as (^{1}H SAMP k_{cat})/(^{2}H SAMP k_{cat}).

[c] $^Dk_{cat}/K_m$ is defined as (^{1}H SAMP k_{cat}/K_m)/(^{2}H SAMP k_{cat}/K_m).

2.3.9 Solvent isotope effects and proton inventory

Solvent isotope effects were studied to probe the transfer of the proton(s) (to the leaving group nitrogen) as being involved in a rate-limiting step in catalysis. Plot of velocity data in either H_2O or D_2O with varying SAMP concentrations is shown in Fig. 2.15A. The solvent isotope effect values were obtained as $^{D}k_{cat}$ of 1.8 ± 0.3 and $^{D}k_{cat}/K_m$ of 1.02 ± 0.5, where $^{D}k_{cat}$ and $^{D}k_{cat}/K_m$ represent the ratios, k_{cat} in H_2O / k_{cat} in D_2O and (k_{cat} / K_m) in H_2O / (k_{cat} / K_m) in D_2O respectively. PfASL activity measured in different fractional concentrations of D_2O compared with 100% D_2O gave a straight line (Fig. 2.15B) indicating that a single proton is transferred in the slowest step of the entire reaction (Showen and Showen, 1982). Data was fitted to Eqn. 7 to obtain the deuterium fractionation factor ϕ^T = 0.7 and ^{D}v, the solvent deuterium isotope effect, of 1.5.

A

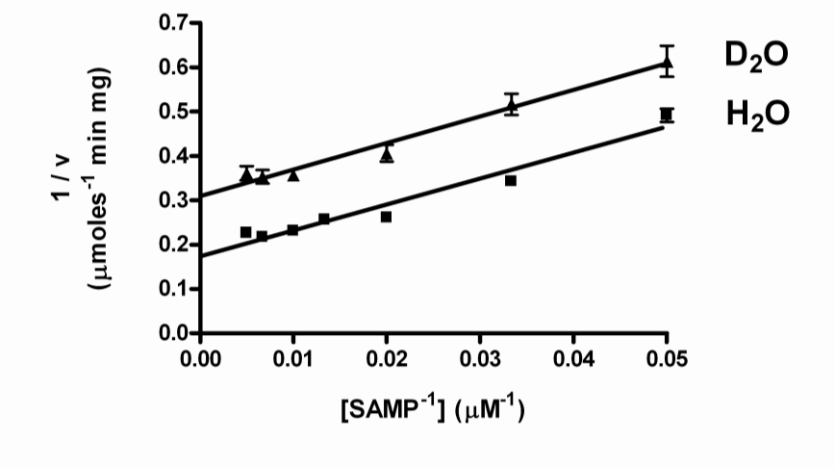

B

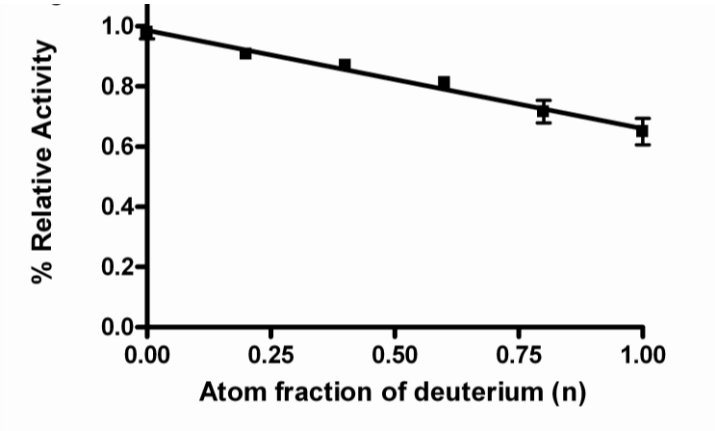

Fig. 2.15: Solvent deuterium kinetic isotope effect and proton inventory

(A) PfASL activity was determined with varying SAMP concentrations in either H_2O or D_2O. PfASL activity was monitored in 50 mM potassium phosphate buffer, pH 7.4 (prepared either in H2O or D2O) with varying SAMP concentrations. Data were fitted by linear regression using GraphPad prism Software, version 4.0 (GraphPad Software, Inc., San Diego, CA). (B) PfASL activity (monitored at a saturating SAMP concentration of 200 μM) as a function of mole fraction of D2O. Data were fitted to the Gross–Butler equation describing a linear proton inventory (Eq. (7)).

Our solvent deuterium isotope effect and proton inventory data suggests that a single proton is transferred in a rate-determining step from the solvent through the enzyme to SAMP. Thus, we conclude from these results that the process of C-N bond cleavage is rate limiting and hence, an E1cb mechanism. Previously, the existence of a carbanion like intermediate in ASL catalysis has been shown indirectly by the tight binding of the nitro analogue of SAMP (a mimic of the carbanion form of SAMP) to the yeast ASL (Porter *et al*., 1983). Also, other members of this superfamily of enzymes such as aspartase (Nuiry *et al.*, 1984) and arginosuccinate lyase (Wu *et al.*, 1998) have been reported to catalyse the reaction through a carbanion like transition state intermediate.

The faster cleavage of the C-H bond over the C-N bond in PfASL catalysis is contrary to the expectation. This is because of the poor acidity of the α proton (C-H) of carboxylate anions. The weak acidity of the α protons of carboxylate anions is because of the poor stability of the resultant carbanion species (Larsen *et al*., 2001). The simple strategy for increasing the acidity of these protons would therefore be to increase the stability of the resultant carbanion species. Indeed, enzymes do so by two mechanisms: Stabilization by metal ions and stabilization by hydrogen bonds (March, 1992). As metal ions do not play any role in the catalysis by ASL, the stabilization of the carbanion intermediate by hydrogen bonds with groups on the enzyme becomes a possible option. Indeed, Tsai *et al*. (Tsai *et al.*, 2007) highlighted the occurrence of such strong hydrogen bonds in the structure of *E. coli* ASL liganded to SAMP (Protein data bank I.D: 2ptr). Thr122, Ser123, Ser296 and His91 (*E. coli* ASL numbering) are the residues involved in hydrogen bonding with the α-carboxylate group of SAMP and hence, aid in the stabilization of the carbanion intermediate. Similar interactions must be operating in PfASL also as all the implicated residues are conserved across the two enzymes.

2.3.10 Activity of Ser298 mutants

It has been shown in *E. coli* ASL that a conserved serine, S295, may probably act as the catalytic base (Tsai *et al.*, 2007) due to its proximity to the C (β)-H group of the substrate. The corresponding serine in PfASL is S298. In order to probe the role of this residue in PfASL catalysis, S298A mutant was generated (Fig. 2.16). The specific activity of S298A mutant at 9.5×10^{-3} μmol $min^{-1}mg^{-1}$ was 1000 fold lower than that of wild type activity. Also, the specific activity remained unchanged upon variation of pH.

The presence of poor residual activity in S298A mutant could possibly arise from the binding of the substrate to a highly structured active site environment favorable enough for proton abstraction. In order to examine whether the thiol from cysteine can replace serine hydroxyl in PfASL catalysis, S298C mutant was generated (Fig. 2.16). However, the S298C mutant displayed a complete loss of activity indicating (1) a preferential requirement for a hydroxyl as compared to a thiol for proton abstraction and/or (2) disruption of the active site environment because of geometric and electrostatic perturbations on substitution of a poorly reactive hydroxyl with a highly reactive thiol group. These results indicate the indispensability of Ser 298 to PfASL catalysis, probably functioning as a base.

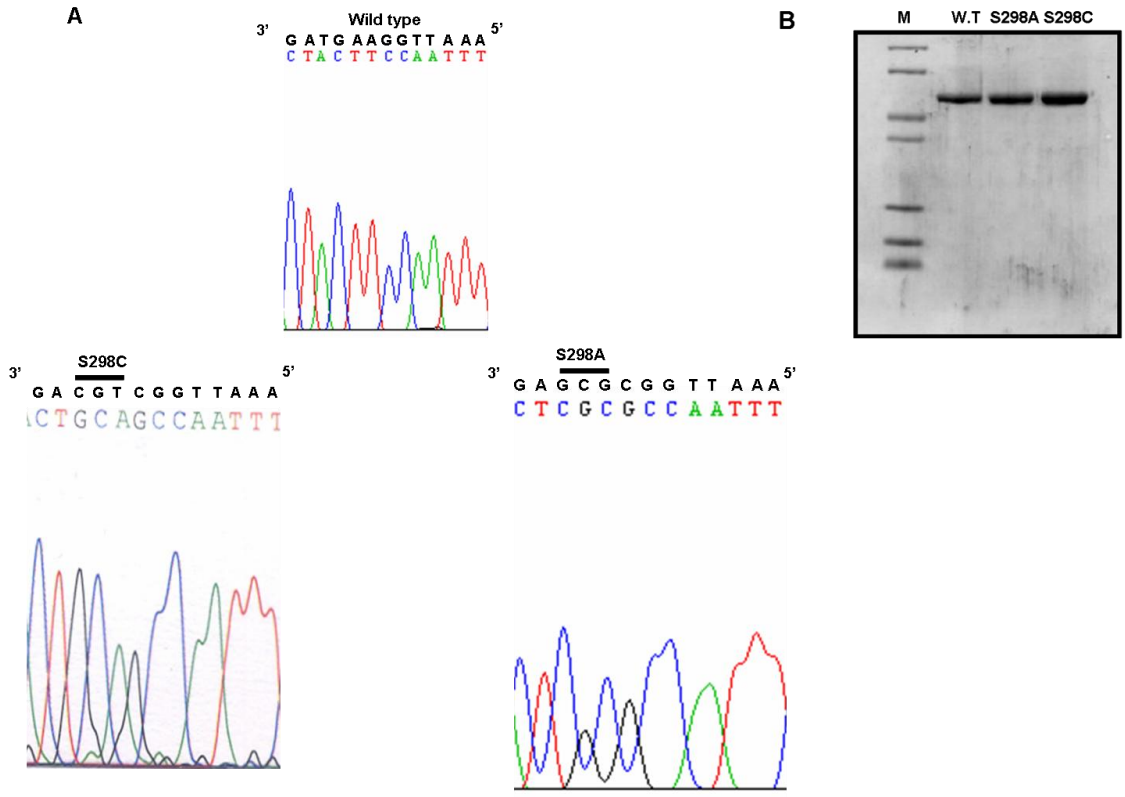

Fig. 2.16: Site directed mutagenesis of Ser 298 to Cys and Ala

(A) Sequencing chromatograms confirming the mutagenesis of Ser 298 to Cys and Ala. (B) SDS-PAGE analysis of the mutant enzymes and the wild type enzyme.

Serine can function as a catalytic base only if its side chain –OH is ionized to form an oxyanion species, which being a very strong nucleophile can easily abstract a proton. As the pK_a of the β-OH group of serine is around 15, its ionization at the physiological pH becomes likely only in the presence of a neighboring basic group. However, no obvious groups on the enzyme, which could serve to abstract the hydroxyl proton of serine, were detected in the structure of *E. coli* ASL complexed to SAMP other than the backbone amide nitrogens of Thr297 and Met298 (Tsai *et al.*, 2007). It is well known that the electrons on the nitrogen atom in a peptide bond –C(O) –NH- are not

freely available for reactivity as they are involved in the resonance stabilization of the peptide unit. Hence, the poor nucleophilicity of the peptide amide group makes it a bad candidate for the abstraction of the proton from serine hydroxyl group.

2.3.11 Effect of pH on PfASL catalysis

The effect of pH on PfASL kinetic parameters, k_{cat} and k_{cat}/K_m, for the cleavage of SAMP to AMP and fumarate was monitored over a pH range of 6.0 to 9.0. k_{cat} is a first order rate constant and its variation with pH describes the ionization processes taking place in the catalytic complex (ES complex). On the other hand, k_{cat}/K_m is a second order rate constant that describes the ionization(s) of either the free substrate (S) or the free enzyme (E) towards the catalytic complex formation. Pre-incubation of the enzyme in different pH buffers (6.0 – 9.0) did not cause any irreversible loss in activity. Hence, the inflections observed in the pH profile can be approximated to the true ionizations of the enzyme's catalytic groups. The plot of k_{cat} versus pH was obtained as a bell shaped curve with both the acidic and the alkaline limbs (Fig. 2.17). The apparent pKa values, pK_1 of 6.45 ± 0.02 and pK_2 of 8.73 ± 0.01, were obtained by fitting the data to Eqn. 10 describing a double ionization process. In contrast to the k_{cat} profile, the k_{cat}/K_m profile exhibited only the alkaline limb (Fig. 2.17). Data were fitted to Eqn. 11 describing a single ionization process to obtain a pK value of 7.4 ± 0.05. This ionization could be occurring in either the free substrate or free enzyme. The possibility of the former could be ruled out as the spectral properties of SAMP (Carter and Cohen, 1956) do not highlight any ionisation (other than the secondary phosphate ionization at pH 6.7) taking place in the pH range studied here. Hence, it can be inferred that this ionization is taking place in the free enzyme. From both these profiles, the implication is that the group

corresponding to $pK_{1,}$ which acts as a catalytic base at the optimum pH is getting ionized only in the catalytic complex (ES complex) but not in the free enzyme. This in turn indicates that the substrate or SAMP assists in this ionization. On the other hand, the group corresponding to pK_2 shows a significant change in its pK_a value, from 7.4 to 8.6, when the enzyme binds the substrate.

A

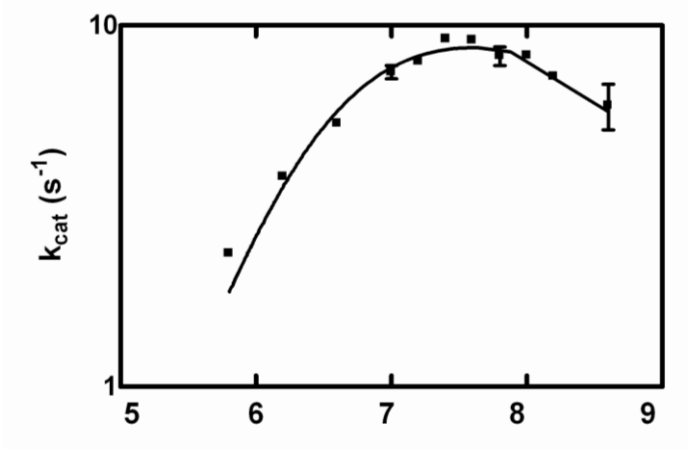

B

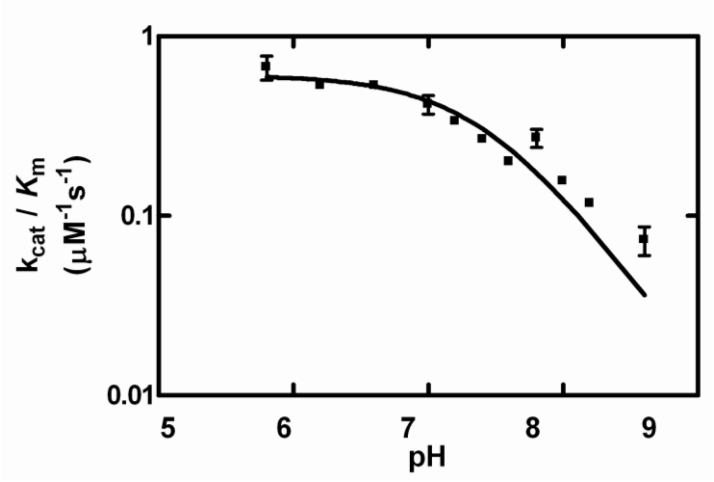

Fig. 2.17: pH kinetics of PfASL catalysis

PfASL activity was determined at different concentrations of SAMP over a range of pH values (5.8–8.8). Data at each pH value was fitted to Eq. (1) to obtain the kinetic parameters, kcat and kcat/Km. Data were fit to equations that describe either a double ionization process (A) (Eq. (10)) or a single ionization process (B) (Eq. (11)). Each line is a theoretical line based on curve fitting. pH was maintained at the desired value using 50 mM potassium phosphate buffer in a final reaction volume of 250 µl.

A closer examination of the liganded *E. coli* ASL structure highlighted the presence of the alpha carboxylate oxygens of SAMP in close proximity to the serine hydroxyl (3.8 Å) with a network of hydrogen bonds from the latter through the substrate and into the functional groups in the protein (Fig. 2.18A). The extensive hydrogen-bonding network of the enzyme residues with the substrate α-carboxylic group could be expected to serve two purposes: (a) to stabilize the carbanion intermediate (b) to serve as a probable sink for the proton abstracted by the substrate carboxylic group from serine 295. Modelling of the *P. falciparum* structure on the *E. coli* enzyme led to a modelled loop orientation similar to that seen in *E. coli* structure with serine 298 in close proximity to C(β)-H of SAMP (Fig. 2.18B). However, modelling of PfASL structure on the available *P. vivax* ASL structure (Protein data bank code: 2qga) in which the catalytic loop has not been mapped led to a modelled loop in an orientation different from that seen in the *E. coli* ASL. These differences in loop conformation observed in the two modelled structures of PfASL emphasize the high mobility of the loop.

A

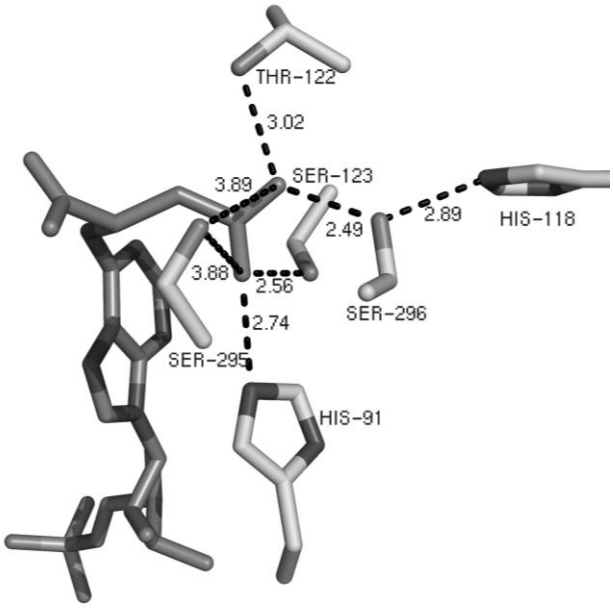

B

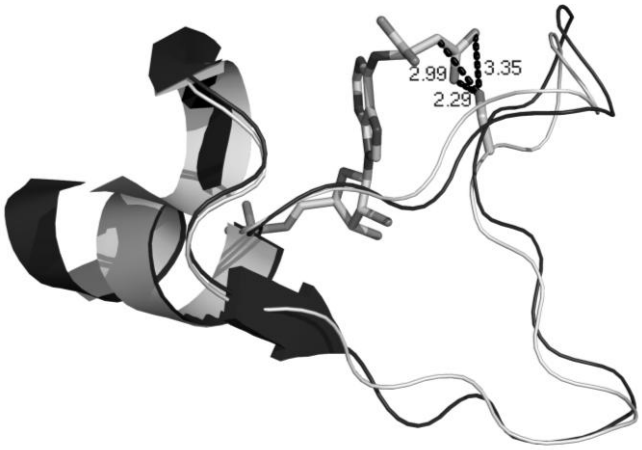

Fig. 2.18: The catalytic loop and the environment of the catalytic serine in adenylosuccinate lyase.

(A) Hydrogen bonding network originating from Ser295 in E. coli ASL. Only the side chains are shown for clarity. Dotted lines represent hydrogen bonds and numbers correspond to the interatomic distances in angstrom (Å). (B) Structural superposition of the catalytic loop of modeled PfASL (light) and E. coli ASL (dark) (2ptr). Also shown in the model structure of PfASL are the contacts of the side chain hydroxyl of the putative catalytic base Ser 298 with the C (β)–H of SAMP (2.99 Å) and the carboxylate oxygens of SAMP (2.29 Å and 3.35 Å respectively). Modelling of PfASL was done as described in the materials and methods using MODELLER 9v4 with E. coli ASL as a template. The figure was generated using PyMol v0.99 (DeLano Scientific).

Thus, in PfASL catalysis, stabilization of the oxyanion of Ser298 by the SAMP carboxylic groups could be the mechanism involved in priming S298 β-OH to facilitate proton abstraction as shown in Fig. 2.19. This is also supported by the observation that the group corresponding to pK_1 in *B. subtilis* ASL has been proposed to be a free acid (Brosius and Colman, 2000) that could be either a phosphate or a carboxylic group.

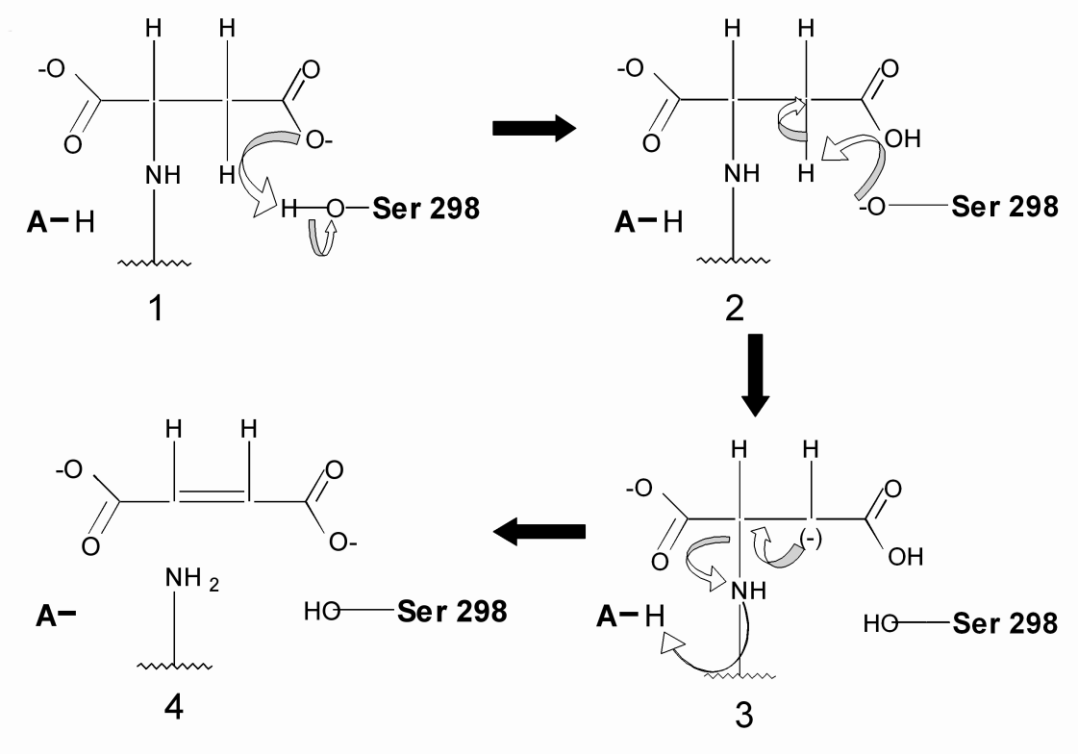

Fig. 2.19: Catalytic scheme for PfASL.

However, whether the phenomenon of substrate dependent base ionisation seen in PfASL hold true for other ASLs is not clear. An important aspect is the variation seen in the behaviour of kinetic parameters with respect to pH for ASLs from different species. *E. coli* ASL, for example shows a 3-5 fold higher activity at pH 8.5 than at a pH value of 7.4 (Tsai *et al.*, 2007), while ASLs from *B. subtilis* (Palenchar *et al.*, 2003) and *H.*

sapiens (Stone *et al.*, 1993) show optimum activity at pH 7.4. A second difference is the bell shaped curve seen in the k_{cat}/K_m vs pH profile in the human ASL (Stone *et al.*, 1993). Finally, the model of the missing signature loop in ASL structures from *B. subtilis* and *H. sapiens* showed dramatic variations in the orientation of the loop (Sivendran and Colman, 2008). These variations may reflect the true differences across ASLs from different organisms.

2.4 CONCLUSIONS

Recombinant adenylosuccinate lyase from *P. falciparum* has been characterized and aspects related to kinetics and catalysis have been delineated in detail. The enzyme exhibits a Uni-Bi Rapid Equilibrium Ordered Kinetic model with the overall rate being limited by the C-N bond cleavage step. The enzyme has also been shown to exhibit a 'substrate assisted catalysis' in which the substrate carboxylic group assists in the ionization of the catalytic base, Ser 298.

CHAPTER 3

Substrate specificity of PfASL and inhibition of *in vitro* growth of *P. falciparum* by AICAR

Substrate specificity of PfASL and inhibition of *in vitro* growth of *P. falciparum* by AICAR

Abstract

This chapter describes the specificity of PfASL to catalyze the reversible cleavage of 5-aminoimidazole-4(N-succinylcarboxamide) ribonucleotide (SZMP) to 5-aminoimidazole-4-carboxamide ribonucleotide (ZMP) and fumarate. This reaction forms the eighth step of the de novo purine biosynthetic pathway. P. falciparum lacks the de novo purine biosynthetic pathway, and hence, the retention of this catalytic ability is probably a vestigial feature in the parasite metabolism. Our results show that PfASL has retained this catalytic activity. Since PfASL has retained the ability to catalyze the reaction on SZMP, the effect of the cell permeable 5-aminoimidazole-4-carboxamide ribonucleoside (AICAR) on the in vitro growth of the parasite was examined and found to inhibit cell proliferation. The mechanism of inhibition is through the erythrocyte, where AICAR gets converted to ZMP leading to inhibition of adenylate synthesis. Besides this, AICAR pretreated erythrocytes were resistant to parasite invasion and growth.

3.1 INTRODUCTION

Unlike the human host, *P. falciparum* is a purine auxotroph that depends on an external source of purines for its survival (Sherman, 1979). Thus, pathways of purine transport and metabolism are attractive targets for antimalarial chemotherapy (Downie *et al.*, 2008). Biochemical studies on purine transporters and purine salvage pathway enzymes have

led to the identification and development of several compounds, which inhibit these two processes and also inhibit parasite growth. Of particular interest are the purine nucleoside analogues, which have also been implicated for chemotherapy against toxoplasmosis (el Kouni, 2007), tuberculosis (Parker and Long, 2007), HIV (el Kouni, 2002) and cancer (Galmarini *et al.*, 2002). These analogues are membrane permeable, which after entering cells get phosphorylated to their nucleotides. These nucleotides then exhibit toxicity by inhibiting the target enzyme(s). A class of nucleoside analogues without a free 3' hydroxyl group exhibit toxicity by a different mechanism. These nucleosides are converted to the corresponding nucleoside triphosphates, which are incorporated into the nucleic acids. However, these triphosphates cannot form a 3'-5' phosphodiester linkage which leads to inhibition of DNA or RNA strand elongation resulting in chain termination (el Kouni, 2002).

Nucleoside analogues (Table 3.1) have been shown to inhibit the *in vitro* growth of malarial parasites (McCormick *et al.*, 1974; Queen *et al.*, 1990; Coomber *et al.*, 1994) Recently, it was found that a subset of such analogues known as tubercidins is transported by PfENT1 (Riegelhaupt *et al.*, 2010). However, the detailed mechanism of action of many of these molecules at the level of individual enzymes in *P. falciparum* has not been elucidated.

Adenylosuccinate lyase (ASL) (E.C. 4.3.2.2) is the only enzyme in the purine biosynthetic pathway that catalyzes two distinct, but chemically similar reactions. The first is the cleavage of succinyl-adenosine monophosphate (SAMP) to adenosine monophosphate (AMP) and fumarate, the final step in AMP synthesis and the second being the cleavage of 5-aminoimidazole-4-(N-succinylcarboxamide) ribonucleotide (SZMP) to 5-aminoimidazole-4-carboxamide ribonucleotide (ZMP) and fumarate that forms the eighth step of the *de novo* purine biosynthetic pathway (Ratner, 1972). Previously, ASLs from *Bacillus subtilis*

(Palenchar *et al.*, 2003), *Neurospora crassa* (Giles *et al.*, 1957) and *Homo sapiens* (Stone *et al.*, 1992) were found to act upon both the substrates with equal efficiency. This could be a consequence of the nature of interaction of ASLs with the ligands, indicating that fully active ASLs do not selectively loose one activity while retaining the other.

Compound	**Type**	**IC_{50} (µM)**	**Putative/Validated site(s) of action**
Tubercidin[a]	Purine nucleoside	3.7	Target (s) not known
Sangivamycin[a]	"	0.2	Target (s) not known
ImmucillinH[b]	"	0.06	Purine nucleoside phosphorylase
5'-Methylthio-ImmucillinH[b]	"	0.05	Purine nucleoside phosphorylase
6-chloropurine riboside[c]	"	n.d[f]	Target (s) not known
6-mercaptopurine riboside[c]	"	n.d[f]	Target (s) not known
Bredinin[d]	"	50	IMP dehydrogenase GMP synthetase
8-azaguanine[c]	Purine base	n.d[f]	Target (s) not known
8-azahypoxanthine[a]	"	12	Target (s) not known
6-mercaptopurine[a]	"	6.2	Target (s) not known
6-thioguanine[a]	"	18	Target (s) not known
Mycophenolic acid[a]		4	IMP dehydrogenase
Azaserine[a]	Glutamine analogue	20	GMP synthetase
Acivicin[a]	"	1	"
Hadacidin[e]	Aspartate analogue	133	Adenylosuccinate synthetase

Table 3.1: List of a few compounds which inhibit *in vitro* growth of *P. falciparum* by targeting enzymes in the purine salvage pathway.

[a] *Data taken from Queen et al., 1990 (Queen et al., 1990)*
[b] *Data taken from Ting et al., 2005 (Ting et al., 2005)*
[c] *Data taken from McCormick et al., 1974 (McCormick et al., 1974)* [d]
[d] *Data taken from Webster and Whaun, 1982 (Webster and Whaun, 1982)*
[e] *Data taken from Mehrotra et al., 2010 (Mehrotra et al., 2010)*
[f] *n.d – not determined.*

Patients with mutations in adenylosuccinate lyase show accumulation of succinyl purines namely succinylimidazole carboxamide ribonucleoside (SAICA riboside) and succinyl adenosine (S-Ado) in their body fluids (Jaeken and Van den Berghe, 1984; Spiegel *et al.*, 2006). Interestingly, a correlation between the severity of psychomotor retardation and the ratio of succinyl purines (S-Ado: SAICA riboside) in the body fluids was noted (Van den Bergh *et al.* 1993). It was found that patients displaying severe phenotype show a ratio of 1 while patients displaying a mild psychomotor delay show a ratio of 2-4. This indicates that certain changes in the enzyme's primary sequence do lead to differential effects on the two substrates and hence, leading to differential accumulation of the succinyl purines.

Due to the absence of *de novo* purine biosynthetic pathway in *P. falciparum*, it was proposed that PfASL probably catalyzes the cleavage of SAMP to AMP and fumarate and not the cleavage of 5-aminoimidazole-4-(N-succinylcarboxamide) ribonucleotide (SZMP) to 5-aminoimidazole-4-carboxamide ribonucleotide (ZMP) and fumarate (Marshall and Coppel, 1997). However, no biochemical evidence supports this hypothesis and it was interesting to test the catalytic ability of PfASL towards the cleavage of SZMP to ZMP and fumarate. In view of the absence of a *de novo* purine biosynthetic pathway, the catalytic ability of PfASL towards the cleavage of SZMP to ZMP and fumarate might not be of any physiological significance to *P. falciparum*. However, if retained, this feature of PfASL catalysis could be exploited in the development of AICAR as a putative novel antimalarial compound.

3.2 MATERIALS AND METHODS

All chemical reagents used were of high quality and obtained from Sigma Chemical Co., St. Louis, USA. [^{3}H]-Hypoxanthine (19.2 Ci mmol^{-1}) was obtained from GE Healthcare, UK. Human O^+ erythrocytes and O^+ serum for culturing parasites were obtained from healthy volunteers from a local hospital. Hadacidin was a kind gift from Developmental Therapeutics Program, National Cancer Institute, NIH, Bethesda, MD. AICAR and hadacidin stock solutions of 200 mM and 100 mM, respectively were made in sterile distilled water.

3.2.1 Isothermal titration calorimetry

Binding constants and the associated thermodynamic parameters were determined using a VP-Isothermal Titration Calorimeter (ITC) (Microcal, Inc., Northampton, MA, USA). PfASL was extensively dialyzed against 50 mM potassium phosphate (pH 7.4) containing 100 mM NaCl, 10 % glycerol and 1 mM EDTA prior to use. Stock solution of ZMP was made in the same buffer. Titrations were done at 25 ºC by stepwise addition of small volumes (5 µl) of AMP or ZMP stock (at a concentration of 5 mM) to PfASL (160 µM) in the sample cell. A control experiment was performed in which AMP or ZMP at the same concentration was titrated against buffer alone in the sample cell in order to obtain the heat of dilution. The raw calorimetric signals were integrated and corrected for the heat of dilution of AMP or ZMP. The resulting corrected binding isotherms were subjected to nonlinear least squares analysis using ORIGIN software and fit to a single-site model to obtain the association constant, K_A, the binding enthalpy, ΔH^{o}, and the stoichiometry of the interaction, n. The Gibbs free energy, ΔG^{o} and the dissociation constant K_d were calculated using the following equations:

$$\Delta G^{o} = \Delta H^{o} - T\Delta S \quad (1)$$

$$K_d = 1 / K_A \quad (2)$$

3.2.2 SZMP reaction and synthesis

SZMP was synthesized from ZMP and fumarate as described previously (Palenchar *et al.*, 2003), with minor modifications, using PfASL. The reaction was carried out in 50 mM potassium phosphate, pH 7.4 containing 10 mM ZMP, 75 mM fumarate and 0.04 mg of Pf ASL in a final reaction volume of 1 ml. The reaction mixture was incubated for 4 hrs at 37 ˚C. Progress of the reaction was monitored by thin layer chromatography on PEI cellulose with 0.5 M LiCl as the mobile phase. For purification of SAICAR, the reaction mixture was passed through a Microsep® centrifugal device, 10 KDa cutoff (Pall life Sciences, USA) to remove the enzyme. The flow-through was loaded on a Diethylaminoethane (DEAE) anion exchange column and products were eluted with a linear gradient (10-500 mM) of ammonium bicarbonate, pH 8. Under these conditions, SZMP eluted after ZMP and fumarate. The fraction corresponding to SZMP was lyophilized, resuspended in water and desalted by passing through Dowex-50W (HCR-W2) cation exchange resin (Sigma Co., USA). The product was confirmed to be SZMP by mass spectrometry (ESI-MS, Bruker Daltonics, Bremen, Germany) in the positive ion mode.

3.2.3 Kinetics of PfASL towards SZMP reaction

PfASL activity for SZMP cleavage to ZMP and fumarate was monitored as a time dependent decrease in absorbance at 267 nm and difference extinction coefficient of 0.7

$mM^{-1}cm^{-1}$ was used to quantify the amount of substrate consumed (Woodward and Braymer, 1966). To estimate the kinetic parameters, data was fitted to the Michaelis-Menten equation

$$v = V_{max}[S] / K_m + [S] \qquad (3)$$

Data were fitted using GraphPad Prism, version 4.0 (GraphPad Software, Inc., San Diego, CA). The reverse reaction of condensation of ZMP and fumarate to SZMP could not be monitored due to the poor sensitivity of the assay**.**

3.2.4 Inhibition of SAMP cleavage activity of PfASL by ZMP

Product inhibition plots were generated by varying SAMP concentrations at fixed concentrations of ZMP. K_i values were obtained by non-linear fits to competitive inhibition model described in Chapter 2. Standard error and 95 % confidence intervals were used as criteria for selecting best fits.

3.2.5 *In vitro* culture of intraerythrocytic stages of *P. falciparum*

3.2.5.1 RPMI + HEPES media

Complete RPMI-1640 medium was used to maintain the 3D7 strain of *P. falciparum* in human O^{+ve} erythrocytes. For the preparation of 480 ml of media, 5.2 g of RPMI-1640 (Roosewell Park Memorial Institute-1640) (Catalog No. R6504, Sigma Chemical Co., USA) and 3 g of HEPES (4-(2-hydroxyethyl)-1-piperazineethanesulfonic acid) (Catalog No. H3375, Sigma Chemical Co., USA) was dissolved in sterile distilled water and was passed through a 0.2 µm cellulose acetate membrane (Sartorius AG, Goettingen, Germany) using Nalgene® bottle top filtration setup (Nalgene, Rochester,

USA). Gentamycin was added to a final concentration of 12.5 µg ml^{-1} to avoid bacterial contamination. 0.5-1 ml of the filtrate was added to sterile Luria Bertoni (LB) media (Himedia Laboratories, Pvt. Ltd. Mumbai, India) and was incubated at 37 ºC in a shaker incubator for 12 h to check for any bacterial contamination during media preparation. The media was prepared after every three weeks and was stored at 4 ºC.

3.2.5.2 Sodium bicarbonate solution

5 % sodium bicarbonate ($NaHCO_3$) solution was prepared by dissolving 2.5 g of $NaHCO_3$ (Catalog No. S5761, Sigma Chemical Co., USA) in 50 ml of sterile distilled water and was sterilized by autoclaving. The solution was stored at 4 ºC till further use.

3.2.5.3 Incomplete and complete media

To prepare 50 ml of complete media, 42.8 ml of RPMI + HEPES media and 2.2 ml of 5 % $NaHCO_3$ were mixed. This is incomplete media, which is used to wash cells (erythrocytes and parasitized erythrocytes). To prepare complete media, 5 ml of heat inactivated human O^{+ve} serum (preparation is mentioned below) was added to obtain a final serum concentration of 10 %. Complete media was prepared fresh each time before media change.

3.2.5.4 Processing of human O^{+ve} serum for *P. falciparum* culture

O^{+ve} blood was collected from healthy individuals at a nearby blood bank. The blood was stored at 4 °C for 24 h after which, the serum was collected in sterile 50 ml Falcon tubes. The tubes were centrifuged at 2000 rpm for 30 min to remove small

amounts of RBC debris. The serum was then pooled into sterile 100 ml reagent bottles and heat inactivated at 55 °C for 1h. Heat inactivation of the serum was carried out to inactivate the heat labile immune complement in the serum, which if present, could lead to undesirable hemolysis. The heat inactivated serum was then stored at -20 °C till further use.

3.2.5.5 Processing of human O^{+ve} erythrocytes for *P. falciparum* culture

5-10 ml of O^{+ve} blood was collected from healthy individuals at a nearby hospital in 25 ml of sterile ACD solution (0.5 g glucose, 0.2 g sodium citrate dehydrate, 0.01375 g citric acid and 0.105 g sodium chloride). The blood was centrifuged at 2000 rpm for 15 min to remove the buffy coat. The erythrocyte pellet was washed thrice with incomplete medium and was resuspended in complete medium (incomplete medium + 10 % serum) to a final hematocrit of 50 %. This erythrocyte stock solution was stored at 4 °C and was used in the subculture of *P. falciparum* till a maximum period of two weeks.

3.2.5.6 Maintenance and assessment of *in vitro P. falciparum* culture

The 3D7 strain of *P. falciparum* was cultured *in vitro* as described previously (Trager and Jensen, 1976). Parasites were maintained in human O^{+} erythrocytes at 5 % hematocrit (Hemtocrit = Volume of the erythrocyte cell pellet / total culture volume) in complete RPMI 1640 medium. The culture was grown in sterile glass vials at 37 ºC in a glass candle jar. Medium was changed every 24 h. The media was prewarmed at 37 ºC for 15 min. before adding to the culture. After every 48 h, 100-200 µl of the parasite culture was taken in an eppendorff tube and centrifuged at 2000 rpm to adjust the

hematocrit to approximately 50 %. A small drop of this suspension was then placed at the end of a clean glass slide and a thin smear was made with the help of another glass slide. The smear was air dried and was fixed in methanol. Giemsa stain was added to Giemsa staining buffer (0.11 g of disodium hydrogen phosphate and 0.07 g of potassium dihydrogen phosphate was dissolved in 100 ml of sterile distilled water and sterilized by autoclaving) in the ratio of 1:3 and then layered over the smear for 15-30 min. The slide was washed in running tap water, dried and was examined under light microscope at 100X under oil immersion. Parasitemia was estimated by dividing the number of parasitized erythrocytes in a field by the total number of erythrocytes (including the parasitized erythrocytes) in that particular field. Atleast ten different fields were examined to obtain an averaged parasitemia. Subculturing was done when the parasitemia reached 8-10 %. Erythrocytes from the 50 % hematocrit stock solution were diluted to a final hematocrit of 5 % and were added to the culture such that the final parasitemia is adjusted to 1-2 %.

3.2.6 Synchronization of *P. falciparum* culture

For synchronization, the parasite culture was treated with 5 % D-sorbitol solution. Sorbitol solution was prepared by dissolving 0.5 g sorbitol (Catalog No. S-1876, Sigma Chemical Co., USA) in 10 ml of sterile distilled water and was filter sterilized by passing through a 0.2 µm Acrodisc® syringe filter (Pall Life Sciences, Ann Arbor, USA). Parasite culture containing predominantly ring infected erythrocytes was initially washed thrice with 1X Phosphate Buffered Saline (PBS) (0.8 g of NaCl, 0.02 g of KCl, 0.144 g of Na_2HPO_4 and 0.024 g of KH_2PO_4 was dissolved in 100 ml of sterile distilled water and

was further sterilized by autoclaving). 5 volumes of sterile 5 % D-sorbitol solution was added to the cell pellet and was incubated for 5 min. Trophozoite and schizont infected erythrocytes due to their increased permeability readily take up sorbitol and get lysed while normal erythrocytes and ring infected erythrocytes are impermeable to sorbitol and hence are not affected (Lambros and Vanderberg, 1979). After incubation, parasite culture was centrifuged at 2000 rpm for 10 min. and the cell pellet again washed thrice with 1X PBS. Following washing, the cell pellet was diluted to 5 % hematocrit with complete medium and was introduced back into the glass vial in the candle jar. 100-200 µl of this culture was taken separately for preparing Giemsa stained smears, which were examined under light microscope. The procedure was repeated after 48 h to achieve a more synchronous parasite culture. After two rounds of sorbitol treatment, a highly synchronous parasite culture containing more than 95 % ring infected erythrocytes was obtained. Synchrony was maintained for atleast 48 h post the second round of sorbitol treatment.

3.2.7 Percoll enrichment of parasitized erythrocytes

9 ml of percoll solution (Pharmacia Biotech AB, Uppsala, Sweden) was mixed with 1 ml of 10X PBS to obtain 90 % percoll solution in 1X PBS, which was further diluted to 70 % with 1X PBS. Parasite culture predominantly in the mature stages (trophozoites or schizonts) was washed thrice in 1X PBS and was resuspended to 10 % suspension in the same solution. Equal volume of this cell suspension was layered over 70 % percoll solution in a sterile 50 ml Falcon tube. The tube was centrifuged at 1500 rpm for 30 min, 25 ºC. Parasitized erythrocytes containing trophozoites and schizonts

formed a distinct band in the middle of the 70 % percoll solution, which was removed and kept separately. These cells were washed thrice with 1X PBS and resuspended in complete medium to a final hematocrit of 5 %. Giemsa stained smears made on glass slides were examined under microscope to calculate parasitemia. Uninfected erythrocytes and ring infected erythrocytes settled at the bottom of the 70 % percoll solution, which were introduced back into the glass vial and kept in glass candle jar. Percoll treatment of parasite culture routinely gave enrichment in parasitemia of 85-90 %.

3.2.8 Saponin lysis of parasitized erythrocytes

Culture with parasites predominantly in the trophozoite stage was centrifuged and washed with 1X PBS thrice. 2 volumes of 0.15 % saponin (Cat. S-1252, Sigma Chemical Co., USA) solution was added to the cell pellet and was incubated for 5 min. followed by the addition of 5 volumes of 1X PBS. The suspension was centrifuged at 4000 rpm for 30 min. and parasite pellet was washed 4-5 times in 1X PBS. The parasite pellet was resuspended in complete medium and was checked for erythrocyte contamination by microscopic examination of Giemsa stained smears under the microscope. Treatment of parasitized erythrocytes with saponin released intact free parasites with negligible erythrocyte contamination.

3.2.9 Parasite growth assays

3.2.9.1 Growth inhibition studies of parasitized erythrocytes

Growth inhibition assays for *P. falciparum* were done in a 96 well flat bottomed plate as described by Desjardins *et al.* (Desjardins *et al.* 1979). AICAriboside (AICAR)

was dissolved in water and the compound serially diluted 2-fold over the concentration range 4000-2 µM. Each well contained 250 µl of cell suspension with 2 % parasitemia and 2 % hematocrit in complete media. Parasitized and nonparasitized erythrocytes and solvent controls were incorporated in all the tests. The plates were incubated at 37 ºC in a candle jar. After 24 h, each well was pulsed with 10 µl of 1X PBS containing 1 µCi of [^{3}H]-hypoxanthine, and plates were incubated for another 12 h. The contents of each well were then harvested onto glass fiber filters using a Combi-12 automated cell harvester (Molecular Devices, Sunnyvale, CA), washed extensively with distilled water and dried. The incorporated radioactivity was measured as disintegrations per minute using a Wallac 1409 (Wallac Oy, Turku, Finland) liquid scintillation counter. The experiments were done in duplicate and repeated twice. For drug treated cultures the percent radioactivity incorporated with respect to the control was plotted against the logarithm of the drug concentration. The concentration causing 50 % inhibition of radioisotope incorporation (IC_{50}) was determined by interpolation. A parallel experiment by microscopy, using Giemsa-stained smears, was also conducted to confirm the toxicity of drugs.

3.2.9.2 Metabolic viability studies on free parasites

The viability of saponin released erythrocyte free parasites can only be maintained for shorter periods of time and hence were incubated with the drug for 2 h after which, each well was pulsed with 10 µl of 1X PBS containing 1 µCi of [^{3}H]-hypoxanthine, and plates were incubated for another 8 h. Metabolic viability of saponin released free parasites in the presence of AICAR, ZMP or hadacidin was monitored by

[^{3}H]-hypoxanthine incorporation. Each well contained 200 µl of cell suspension**.** Free parasites treated with sterile distilled water served as controls and were incorporated in all the tests. After 8 h, the contents of each well were then harvested onto glass fiber filters using a Combi-12 automated cell harvester (Molecular Devices, Sunnyvale, CA), washed extensively with distilled water and dried. The incorporated radioactivity was measured as disintegrations per minute using a Wallac 1409 (Wallac Oy, Turku, Finland) liquid scintillation counter. The experiments were done in duplicate and repeated thrice. The percent radioactivity incorporated in the drug treated cultures was calculated with respect to the control culture and plotted.

3.2.10 Stage specificity of AICAR on the intraerythrocytic stages of *P. falciparum*

Synchronized ring stage parasites were treated with 1 mM AICAR. The stage and the percent parasitemia in the culture was estimated at time t = 0, 24, 36 and 48 h by microscopic examination of Giemsa stained smears. Parasitized erythrocytes that were not treated with AICAR served as controls.

3.2.11 Growth and invasion of AICAR pretreated erythrocytes by *P. falciparum*

Fresh erythrocytes were diluted to a final hematocrit of 5 % after washing thrice in complete RPMI 1640 medium. This cell suspension was incubated with (treated) or without (control) 1 mM AICAR at 37 ºC for 24 h in a 96 well plate kept in a glass candle jar. After incubation, the cells were washed 4-5 times with complete RPMI medium to remove excess AICAR and reconstituted again in complete medium to a final hematocrit of 5 %. For the purpose of infecting AICAR treated erythrocytes, parasitized erythrocytes

were enriched to 85-90 % parasitemia by centrifugation on a 70 % percoll solution and washed thrice in complete RPMI medium. The enriched parasitized erythrocyte pellet was diluted with complete medium to achieve a final hematocrit of 5 %. The parasitemia of the enriched culture was reduced to 1-2 % by addition of either AICAR treated or untreated erythrocytes and growth was monitored every 12 h over a total period of 96 h by microscopic examination of Giemsa stained smears. The viability of the culture was also assessed at the end of 96 h by the addition of 1 µCi of [^{3}H]-hypoxanthine and monitoring the incorporation after 12 h. Erythrocyte invasion assays were done as described earlier (Sharma *et al.*, 1996) with minor modifications. Briefly, culture containing parasites, predominantly in the schizont stages, were first enriched by centrifugation on a 70 % percoll solution**.** These were then used to infect AICAR pretreated erythrocytes using an initial parasitemia of 4-5 %. Untreated erythrocytes served as controls. Invasion was quantified by the appearance of merozoite or ring infected erythrocytes after 24 h. Invasion efficiency was calculated as the ratio of parasitemia (calculated only for rings and merozoites) after 24 h to the initial parasitemia. Rabbit erythrocytes, known to be refractory to *P. falciparum* invasion (Breuer *et al.*, 1983) were used to correct for invasion of carried over erythrocytes from percoll enriched culture by *P. falciparum* merozoites.

3.2.12 Mass spectrometric analysis of cell extracts

Cells (erythrocytes, free parasites or percoll enriched parasitized erythrocytes) were treated with 1 mM AICAR in complete medium for 2 h at 37 °C. For percoll enriched parasitized erythrocytes, AICAR treatment was followed by treatment with 0.15

% saponin solution to release free parasites. The parasite pellet was extensively washed and processed. Cells not treated with AICAR served as controls. Erythrocytes and free parasites were directly washed thrice with 1X PBS after incubation with AICAR. After washing, the cells were resuspended in 2 volumes of distilled water and were lysed by repeated freeze thawing. Soluble metabolites were extracted from the lysate using reported protocols (Cassera *et al.*, 2008). The cell lysate was treated with 0.5 M $HClO_4$ (1:6 ratio) for 30 min. on ice and was then centrifuged at 13000 rpm for 30 min. to obtain acid soluble supernatant. This was neutralized with 5 M KOH and was again centrifuged at 13000 rpm for 15 min. to remove the precipitate. The supernatant was lyophilized and stored at –80 ºC till further use. For MALDI-TOF MS spectral acquisition, the samples were mixed with the matrix dihydroxybenzoic acid (prepared in 50 % acetonitrile and 0.1 % TFA) in a 1:1 ratio. MALDI-TOF mass spectra were recorded in the positive ion mode on an Ultra-Flex II Bruker Daltonics mass spectrometer (Bruker Daltonics, Bremen, Germany). For ESI-MS/MS, the samples were dissolved in 1:1 mixture of acetonitrile and water containing 0.1% formic acid and was directly injected using a syringe pump (Cole-Parmer, Vernon Hills, IL) operated at a flow rate of 200 to 240 µL h^{-1} and spectra were recorded using an Esquire 3000-plus mass spectrometer (Bruker Daltonics, Bremen, Germany) consisting of two octupoles followed by an ion trap. For ESI-MS/MS, helium was used as the collision gas for collision induced dissociation (CID) experiments. The data were processed using Esquire data analysis software, version 3.1.

3.2.13 Metabolic labeling and chromatographic separation of purine nucleotides

Parasite culture was enriched to 80-90 % parasitemia by centrifugation on 70 % percoll solution and washed thrice with complete RPMI medium. The enriched culture was resuspended in complete medium to 5 % hematocrit and was treated with 4 mM AICAR or 1 mM hadacidin for 2 h. After this, 5 µCi of [^{3}H]-hypoxanthine was added to the culture and incubated for further 4 h at 37 ºC in a glass candle jar. Thereafter, the cells were washed thrice with 1X PBS, resuspended in distilled water and lysed by repeated (3 times) rapid freeze-thawing. Soluble metabolites were extracted from the lysate as described in the above section and stored at –80 ºC till further analysis. A combination of ion-pair reverse phase HPLC and Q-sepharose anion exchange chromatography was used to separate purine nucleoside mono, di- and triphosphates. Ion-pair reverse phase HPLC was carried out using a C-18 column (Genesis C18, 4µm, 150mm X 4.6mm, Grace Davison Discovery Sciences^{TM}, Illinois, USA) using solution A (100 mM potassium phosphate, pH 6.0 containing 8 mM tetrabutylammonium bisulfate (TBAHS) (Spectrochem, India) and solution B (100 mM potassium phosphate, pH 6.0 containing 8 mM TBAHS and 30% acetonitrile) as mobile phases. The cell extracts from treated or untreated cultures were resuspended in solution A and spiked with the nucleotide standards IMP, GMP, AMP, GDP, ADP, GTP and ATP. After injection of the sample, the column was washed with two column volumes of solution A followed by a gradient of 0 % to 100 % solution B in 60 min. The flow rate was set at 0.7 ml min^{-1} and the absorbance of the eluate monitored simultaneously at 254 and 280 nm. Under these conditions, four distinct peaks were observed, which were in the order of elution: (1) IMP and GMP, (2) AMP and GDP, (3) ADP and GTP, and (4) ATP. Fractions under the

IMP+GMP and ATP peaks were collected, concentrated and counted on a Wallac 1409 (Wallac Oy, Turku, Finland) liquid scintillation counter. Fractions under peaks corresponding to AMP+GDP and ADP+GTP were concentrated by lyophillization and further resolved by Q-sepharose (GE healthcare, UK) anion exchange chromatography. Briefly, the column was equilibrated with Solution C (10 mM KH_2PO_4, pH 3.0) and nucleotides eluted with a linear gradient of 0-50 % Solution D (500 mM KH_2PO_4, 800 mM KCl, pH 3.0) in 90 min. The individual peaks were collected, concentrated and counted on a Wallac 1409 (Wallac Oy, Turku, Finland) liquid scintillation counter.

3.2.14 Statistical analysis

Statistical analysis of the difference between the control and treated samples was estimated by two-tailed paired t-test using GraphPad Prism software, version 4.0. The difference in mean values was considered significant if the p values of the paired t-test were less than 0.05.

3.3 RESULTS AND DISCUSSION

3.3.1. Binding of ZMP by PfASL

The condensation of ZMP and fumarate to SZMP was monitored in a continuous spectrophotometric assay at 267 nm with PfASL concentration similar to that used for AMP to SAMP conversion (0.5 – 1 μg). However, no measurable activity was obtained with any improvement even upon using 10-fold excess of PfASL (10 μg). This could be due to the inability of PfASL to bind ZMP. In order to probe this, we monitored the binding of ZMP to PfASL using Isothermal Titration Calorimetry (ITC). The raw

calorimetric signals from the ITC titration (Fig. 3.1A&B) were integrated and corrected for the heat of dilution. The resulting enthalpy change was plotted with respect to the molar ratio of ZMP and protein as shown in (Fig. 3.1C&D). Binding isotherm of AMP is shown for comparison. The associated thermodynamic parameters for the interaction are listed in Table 3.1. The binding of ZMP to PfASL occurred at a single site with weak affinity as indicated by the high value of the dissociation constant ($K_{dissoc.ZMP}$=170 μM). This value was similar to the dissociation constant for the PfASL.AMP complex ($K_{dissoc.AMP}$=170 μM) (Table 3.2). A slightly greater enthalpy change was observed in the interaction of AMP with PfASL. This could imply additional protein-ligand interactions in AMP.PfASL complex that are absent in AICAR.PfASL complex. AICAR has an incomplete purine ring and thus, is more flexible than AMP in solution. This inherent flexibility could explain the marginal increased entropy change upon binding of AICAR to PfASL. Most importantly, the overall free energy change associated with the binding of these two ligands was similar ($\Delta G^o = -5.1$ kcal mol^{-1}). Product inhibition studies with SAMP concentration varying at different fixed concentrations of ZMP showed ZMP to be a competitive inhibitor of PfASL with a K_i of 246 ± 26 μM (Fig. 3.1 E).

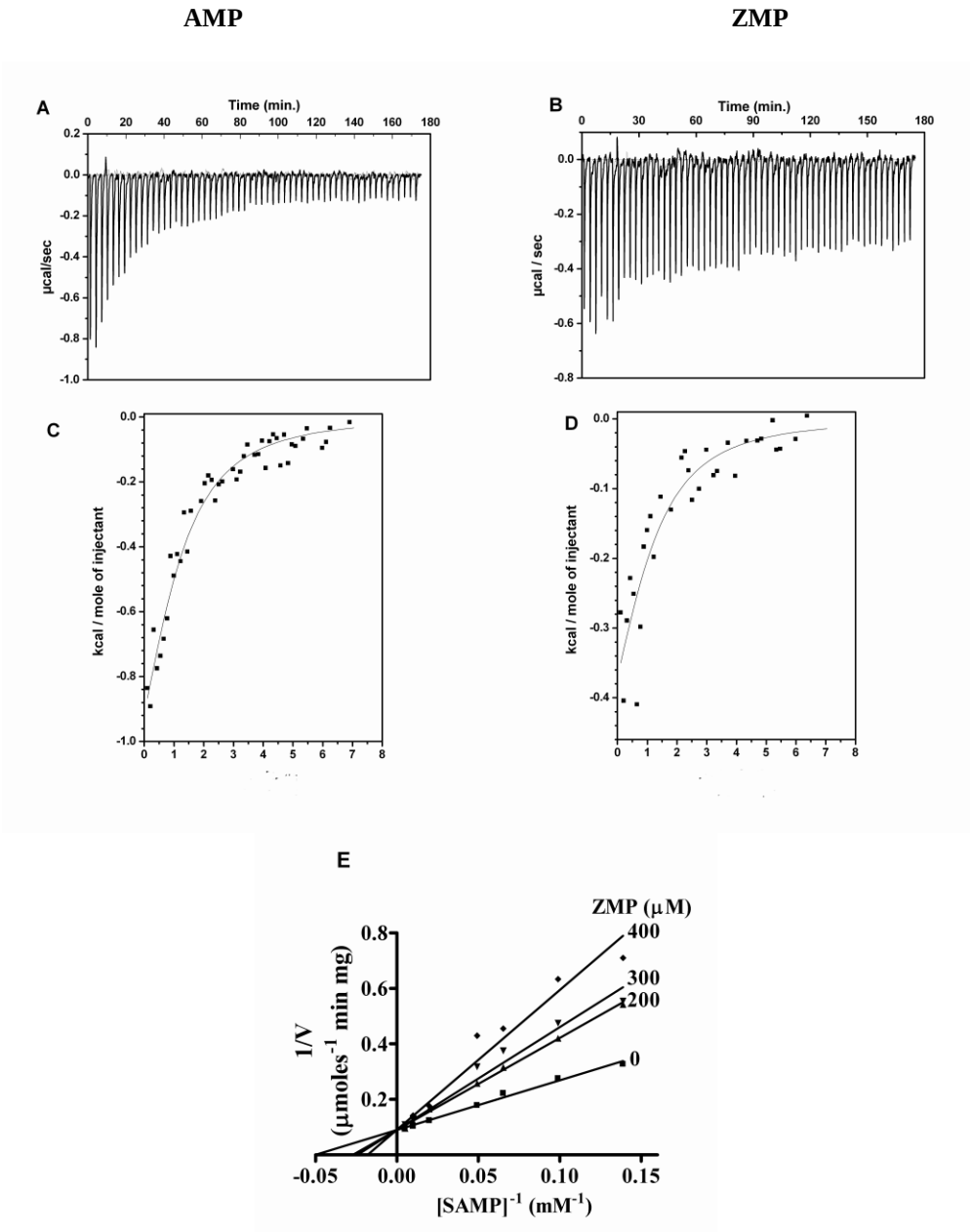

Fig. 3.1: Binding of AMP and ZMP to PfASL by ITC and ZMP inhibition of SAMP reaction

PfASL (160 µM) was titrated with 5 µl volumes of AMP (A) or ZMP (B) each at 5 mM stock concentration in 50 mM potassium phosphate, pH 7.4 containing 100 mM NaCl and 10 % glycerol, at 25 °C. The resulting enthalpy change was plotted with respect to the molar ratio of (C) AMP and (D) ZMP and PfASL. Data were fitted to the single site binding model (using the software ORIGIN) after correction for the heat of dilution of ligand. (E) Line weaver Burk plot of PfASL activity at different fixed concentrations of ZMP.

Ligand	Stoichiometry (n)	Dissociation Constant (K_d)[b] (mM)	Enthalpy change (ΔH^o) (kcal mol^{-1})	Entropy change (ΔS^o) (cal K^{-1} mol^{-1})	Free energy change (ΔG^o)[c] (Kcal mol^{-1})
AMP	1.0	0.17	-1.8 ± 0.08	10	-5.15
AICAR	1.0	0.17	-0.75 ± 0.09	14	-5.13

Table 3.2: **Comparison of the thermodynamic parameters associated with the binding of AMP and AICAR to PfASL[a].**

[a] *The enzyme was maintained at a concentration of 160 µM and titrated with 5 µl volumes of AMP and AICAR at a constant temperature of 25 ºC. The resulting heat changes were recorded on a VP-ITC. The values reported are obtained from the fit of the data in Fig. 3.1 to the single site binding model using ORIGIN software.*
[b] *Dissociation constants were calculated from the association constants by equation 2.*
$K_{d\ AMP} = 1 / K_{A\ AMP} = 1 / 5.9 = 0.17$ *mM*
$K_{d\ AICAR} = 1 / K_{A\ AICAR} = 1 / 5.9 = 0.17$ *mM*
[c] *Free energy change (ΔG^o) was calculated from equation 1.*

3.3.2. PfASL retains the ability to catalyze SZMP reaction

Binding of ZMP to PfASL prompted a large-scale synthesis of SZMP from ZMP and fumarate using PfASL. Thin-layer chromatography of the reaction mixture showed the appearance of a new spot that could correspond to SZMP. Purification of this compound from the reaction mixture was done on DEAE-ion exchange column with a linear gradient of ammonium bicarbonate (pH 8.0). The peak that eluted after ZMP and fumarate (Fig. 3.2A) was found by ESI-MS (Bruker Daltonics, Bremen, Germany) to have a mass of 455 ± 0.4 Da corresponding to the monoprotonated mass of SZMP (Fig. 3.2B). As the sensitivity of the assay for SZMP reaction was lower than the SAMP reaction, enzyme amount was increased to 1–2 µg to obtain reliable activity measurements. The K_m and k_{cat} values obtained for SZMP cleavage were 40.0 ± 8 µM and 7.0 ± 0.7 s^{-1} respectively, which were similar to the kinetic parameters for SAMP cleavage reaction (Table 3.3). However, the kinetic parameters for the reverse reaction (ZMP + fumarate) could not be determined due to the poor sensitivity of the assay.

A

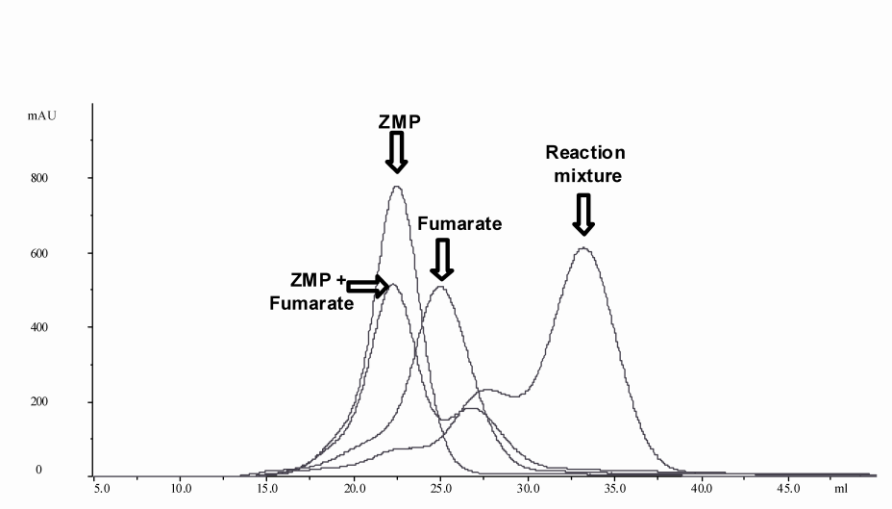

B

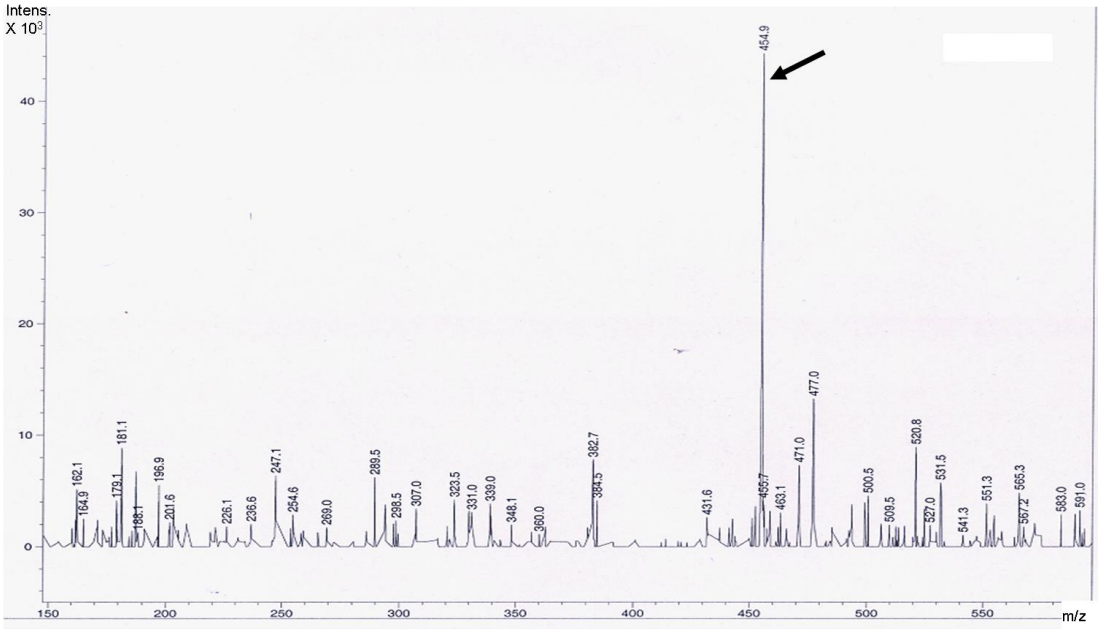

Fig. 3.2: Synthesis, purification and characterization of SZMP

SZMP was synthesized from ZMP and fumarate using PfASL as described in materials and methods. Reaction mixture was purified using DEAE anion exchange chromatography (A) Elution profile of standard samples containing ZMP alone, fumarate alone and ZMP + fumarate show a clear separation of peaks. Reaction mixture of ZMP, fumarate incubated with PfASL shows a distinct peak, which was collected and lyophilized. (B) Electrospray ionization mass spectrum (ESI-MS) of the purified SZMP in the positive ionization mode. The peak at 454.9 Da corresponds to the monoprotonated form of SZMP (Molecular mass: 454 Da).

Substrate	K_m (μM)	k_{cat} (s^{-1})	k_{cat}/K_m (s^{-1} μM^{-1})
SZMP[b]	40 ± 8	7 ± 0.7	0.17 ± 0.03
SAMP[c]	32 ± 1.7	7.5 ± 0.7	0.23 ± 0.02

Table 3.3: **Comparison of the kinetic parameters associated with the cleavage of SZMP and SAMP by PfASL[a].**

[a]*All enzyme assays were done at 25 °C in 50 mM potassium phosphate, pH 7.4.*

[b]*PfASL activity towards SZMP cleavage was monitored as a time dependent decrease in absorbance at 267 nm and calculated using a difference extinction coefficient of 0.7 mM^{-1} cm^{-1}. Values reported were obtained from the fit of the data to equation 1. Assays were done with three different batches of PfASL with each data point being measured in duplicate.*

[c] *Kinetic parameters for SAMP cleavage reaction are taken from Chapter 2 for comparison.*

3.3.3 AICAR, but not ZMP inhibits the *in vitro* growth of *P. falciparum*

The significance of the retention of SZMP catalytic activity in PfASL is not clear in the absence of the *de novo* purine biosynthetic pathway and also the subsequent enzyme for the metabolism of ZMP, AICAR transformylase (E.C. 2.1.2.3) is absent from *P. falciparum* genome (Gardner *et al.*, 2002). In organisms that have a functional *de novo* purine biosynthetic pathway, AICAR transformylase converts ZMP to IMP. Thus, in *P. falciparum*, ZMP represents a 'non-utilizable metabolic block' and hence, can be used as a novel putative anti-malarial. Therefore, the effect of ZMP (dissolved in water) on the *in vitro* growth of *P. falciparum* was tested in a 24 h growth assay. We did not see any change in parasitemia after 24 h of incubation with 1 mM of ZMP in comparison to the control culture (treated with sterile distilled water). It is known that nucleotides are cell impermeable due to the presence of negatively charged phosphate group. Hence, the lack of toxicity of ZMP could be because of the impermeability of this nucleotide. Therefore, the effect of cell permeable AICAriboside (AICAR) on the *in vitro* growth of *P.*

falciparum was monitored (by incorporation of [^{3}H]-hypoxanthine into the genomic DNA). Asynchronous parasite culture with 2 % parasitemia and 2 % hematocrit was treated with increasing concentrations of AICAR and growth was monitored as described in materials and methods. It was found that AICAR inhibited the parasite growth in a dose dependent manner with half-maximal inhibitory concentration (IC_{50}) of 167 ± 5 μM (Fig. 3.3). The result was also validated by following parasite growth through microscopic examination of Giemsa stained smears.

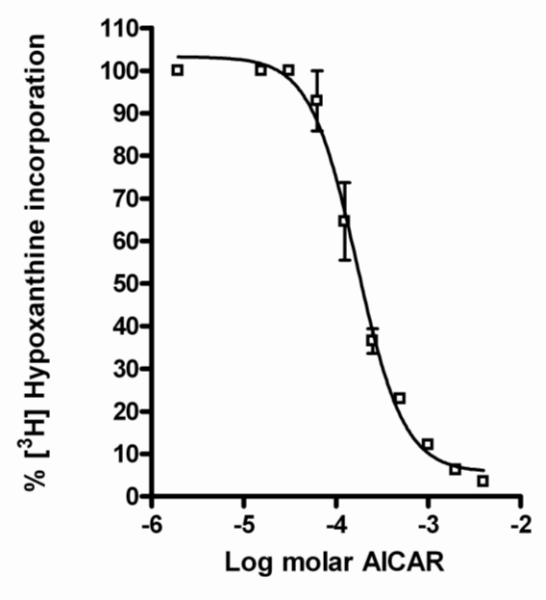

Fig. 3.3: Effect of AICAR on uptake of [^{3}H]-hypoxanthine by parasitized erythrocytes in culture.

Culture containing parasitized erythrocytes (2 % hematocrit, 2% parasitemia) was treated with increasing concentrations of AICAR for 24 h, followed by the addition of 1 μCi of [^{3}H] hypoxanthine to each well. The cells were harvested after another 12 h and [^{3}H]-hypoxanthine incorporation was quantified by scintillation counting. Counts obtained in culture with no drug were set at 100 % and the drop in counts in drug treated cultures was expressed as % of the untreated culture. The graph represents mean of two independent experiments each done in duplicate.

3.3.4 AICAR arrests *P. falciparum* growth at the mature stages

To assess the stage specificity of AICAR action, *P. falciparum* culture was synchronized using 5 % sorbitol followed by treatment of the ring stage parasite culture with AICAR. After 48 h of incubation, microscopic examination of the Giemsa stained smears showed that control cultures without AICAR showed completion of one intraerythrocytic asexual life cycle with parasites being predominantly in the ring stage. However, the growth of the parasites treated with AICAR was totally arrested at the late trophozoite and early schizont stages (Fig. 3.4).

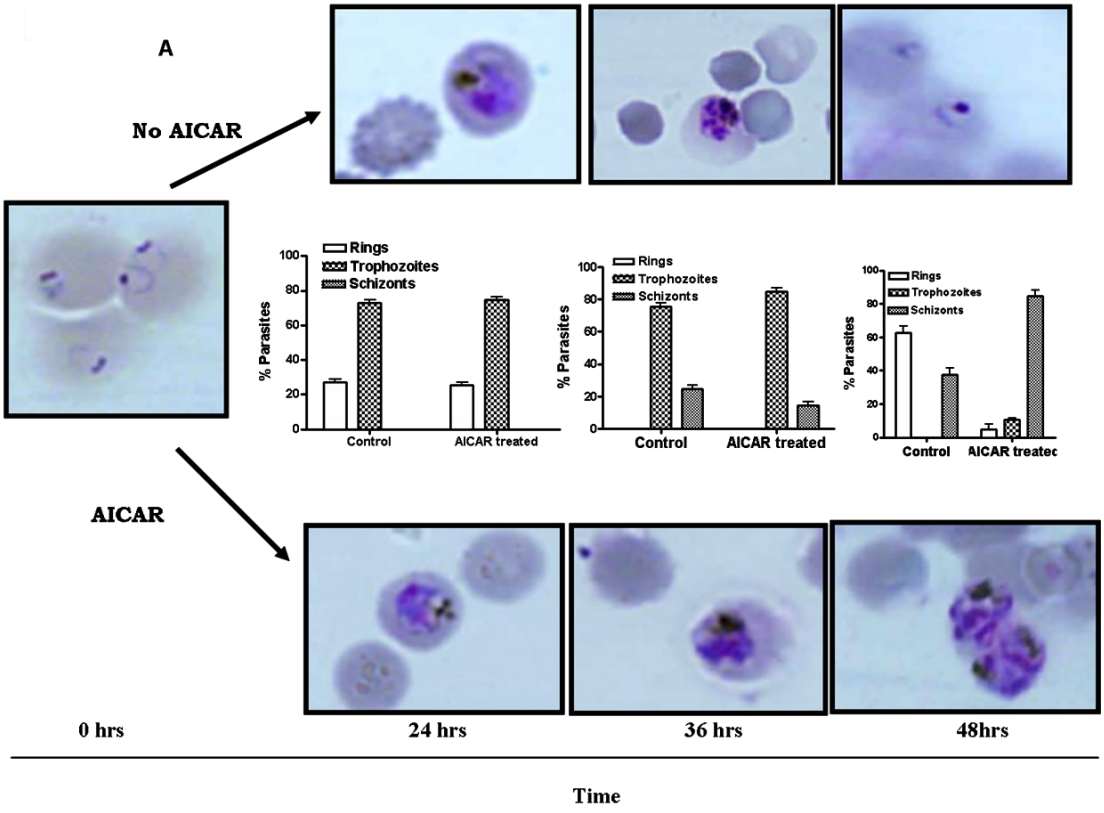

Fig. 3.4: Stage specificity of inhibition of *P. falciparum* growth by AICAR.

Synchronized P. falciparum culture, with parasites in the ring stage, was treated with 1 mM AICAR. Culture treated with the same volume of sterile distilled water served as control. Shown are microscopy images of Giemsa stained smears made at 0 h, 24 h, 36 h and 48 h post treatment. Inset: Plot of % ring/trophozoite/schizont stages of the parasite in control and AICAR treated cultures at each time point. The experiment was repeated twice and found to be reproducible.

3.3.5 Toxicity of AICAR is mediated through the erythrocyte

The toxicity of AICAR on the *in vitro* growth of intraerythrocytic *P. falciparum* does not imply that the mode of action of this compound is solely through parasite encoded enzyme(s). To evaluate this, AICAR toxicity was examined on saponin released erythrocyte free parasites. Hadacidin is a specific inhibitor of adenylosuccinate synthetase (ADSS) (Shigeura and Gordon, 1962) and has been shown to have a potent effect on the growth of *P. falciparum* (Webster *et al.*, 1984). Since hadacidin directly acts on PfADSS and inhibits the purine salvage pathway, this was used as a positive control in the experiments. The free parasites were treated with different concentrations of AICAR or 1 mM hadacidin for 2 h followed by incubation with 1 μCi of [^{3}H]-hypoxanthine for 8 h. The metabolic viability of saponin-released parasites was quantified by measuring the incorporation of [^{3}H]-hypoxanthine into the nucleic acid pool. Interestingly, AICAR had no effect on the incorporation of [^{3}H]-hypoxanthine even at very high concentrations of 2 and 4 mM (> 10 times the IC_{50} value) (Fig.3.5A). On the other hand, hadacidin treated saponin released free parasites showed a dramatic drop in the incorporated counts compared to the control (free parasites treated with the same volume of sterile distilled water). The data were consistent over three independent experiments, each done in duplicate.

In drug titration experiments carried out to obtain the IC_{50} value, parasitized erythrocytes were treated for 24 h with AICAR followed by the addition of [^{3}H]-hypoxanthine and further incubation for 12 h. Hence, the absence of toxicity of AICAR on free parasites could be because of a shorter duration of incubation (10 h) of the drug with free parasites. To check this, parasitized erythrocytes were treated with different

concentrations of AICAR or 1 mM hadacidin for 2 h followed by incubation with 1 μCi of [^{3}H]-hypoxanthine for 8 h. After a total incubation time of 10 h, hadacidin and AICAR treated parasitized erythrocytes showed a dose dependent decrease in the incorporation of [^{3}H]-hypoxanthine (Fig. 3.5B). These observations indicate that the toxicity of AICAR is essentially mediated through the erythrocyte.

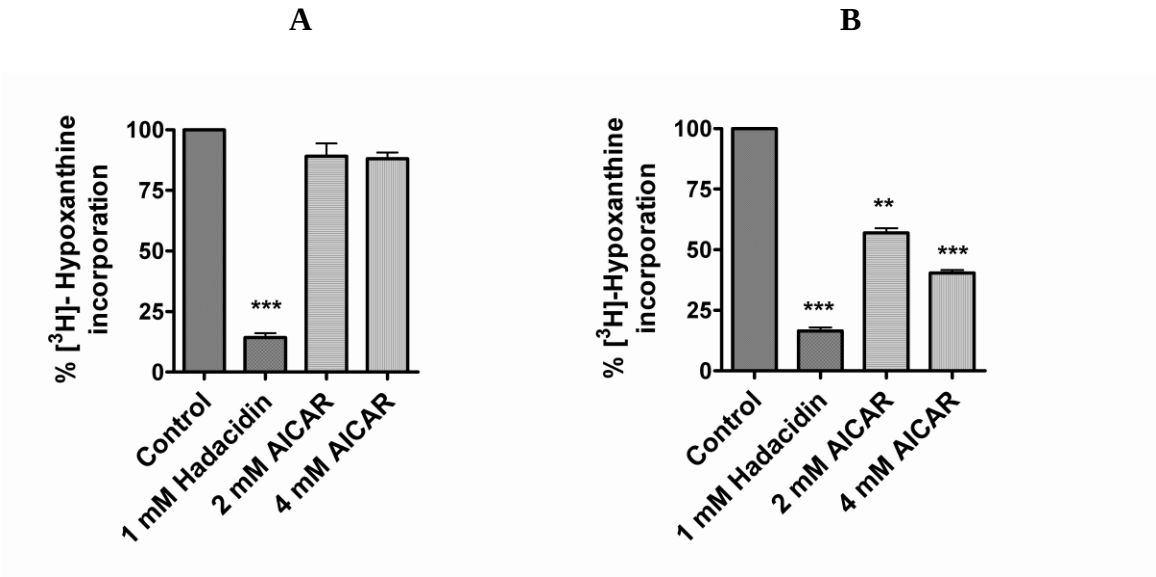

Fig. 3.5: Effect of AICAR on [^{3}H]-hypoxanthine incorporation by free parasites and parasitized erythrocytes

*(A) [^{3}H]-hypoxanthine incorporation in the presence or absence of increasing concentrations of either AICAR or 1 mM hadacidin by erythrocyte free parasites. (B) [^{3}H]-hypoxanthine incorporation in the presence or absence of increasing concentrations of either AICAR or 1 mM hadacidin by parasitized erythrocytes. Controls involved cells that were not treated with either AICAR or hadacidin but were pulsed with [^{3}H]-hypoxanthine and processed in a manner similar to that of the treated samples. The percent radioactivity incorporated by drug treated cultures was calculated with respect to the radioactivity incorporation in the untreated culture. Two-tailed paired t-test was carried out to test the statistical significance of the difference in radioactivity incorporation between control and treated samples using Graph Pad Prism software, version 4.0. ** indicates $p < 0.005$ and *** indicates $p < 0.0005$. The experiments were done in duplicate and repeated thrice.*

3.3.6 Intracellular fate of AICAR

To check the intracellular fate of AICAR, three different kinds of cell types were used: (a) erythrocytes, (b) percoll enriched parasitized erythrocytes and (c) saponin released erythrocyte free parasites. Each cell type was incubated for 2 h with 1 mM AICAR, after which soluble metabolites were extracted from the different cell types as described in the methods section and analyzed by MALDI-TOF mass spectrometry.

Molecular mass of AICAR is 258 Da while the mass of its phosphorylated form, ZMP is 338 Da. The MALDI-TOF mass spectrum of a standard sample of ZMP in the positive ion mode gave a molecular ion peak at 338.9 Da as shown in Fig. 3.6A. Lysate of erythrocytes treated with AICAR showed a dominant molecular ion peak at 338.9 Da (Fig. 3.6B). However, this peak was not observed in the lysate of free parasites treated with AICAR (Fig. 3.6C) or in the free parasites alone (Fig. 3.6D). These results indicate that the conversion of AICAR to ZMP takes place only in the erythrocyte but not in the parasite cytosol. In mammalian cells, the conversion of AICAR to ZMP has been shown to be mediated through adenosine kinase (Zimmerman and Deeprose, 1978). The conversion of AICAR to ZMP in the erythrocyte compartment of parasitized erythrocyte is in agreement with the fact that human erythrocytes contain an active adenosine kinase (Hawkins and Bagnara, 1987). However, a functional annotation of the gene encoding adenosine kinase is absent in *P. falciparum* genome (Gardner *et al.*, 2002). This explains the observation of the absence of ZMP in the lysate of free parasites treated with AICAR.

To address the question whether ZMP formed in the erythrocyte compartment of the parasitized erythrocyte is transported into the parasite cytosol, percoll enriched parasitized erythrocytes were first incubated with AICAR for 2 h and were then treated

with 0.15 % saponin to obtain free parasites. We used percoll enriched parasitized erythrocytes rather than the normal parasite culture to reduce the large background of uninfected erythrocytes that are present in *in vitro* cultures of *P. falciparum*. The isolated parasites were thoroughly washed to remove any contaminating erythrocyte metabolite pool and were then lysed and processed for mass spectrometric analysis. Interestingly, the lysate of these parasites showed the molecular ion peak of 338.9 (Fig. 3.6E). The presence of ZMP in the parasite lysate indicates the uptake of ZMP by the parasite from the erythrocyte compartment.

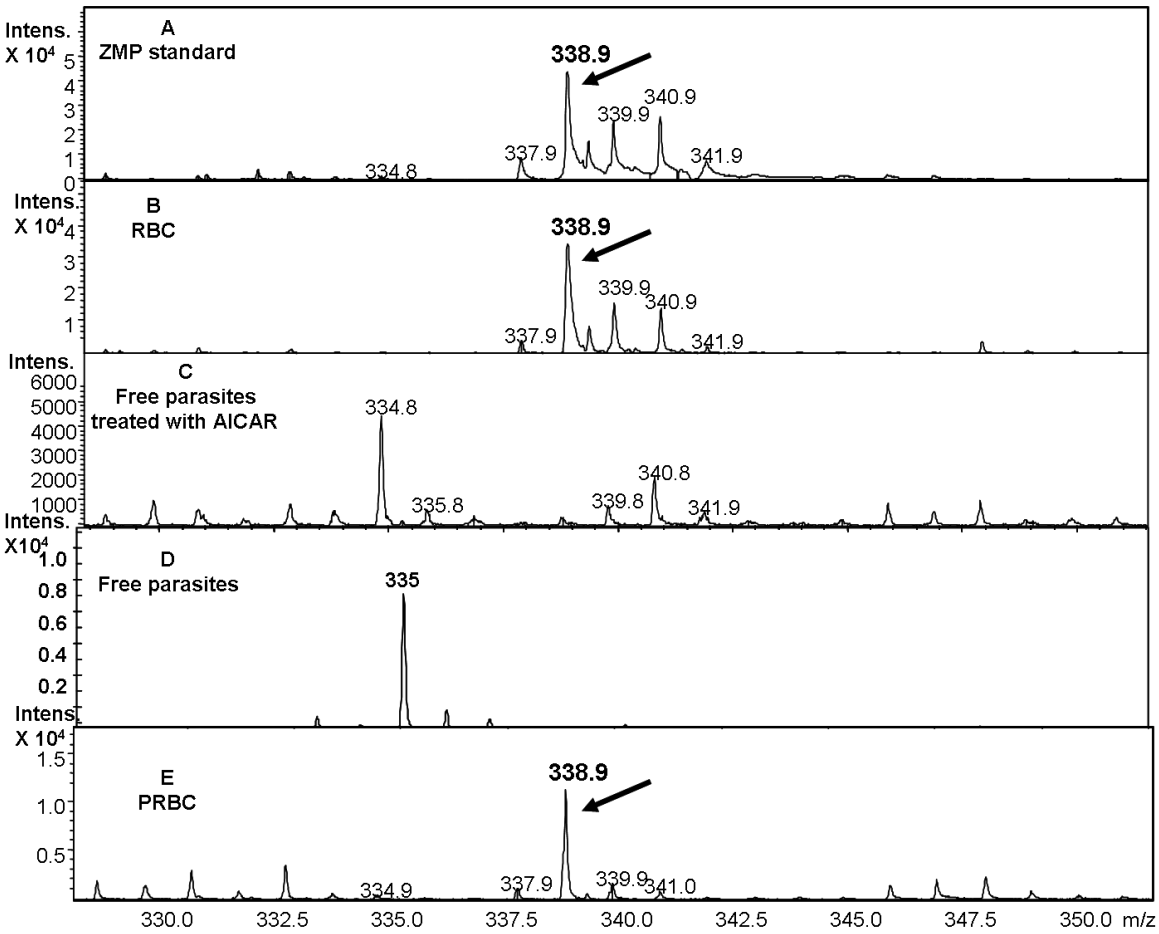

Fig. 3.6: MALDI-TOF MS spectra of cell lysates

(A) 5-aminoimidazole-4-carboxamide ribonucleotide (ZMP) standard, (B) lysate of erythrocytes treated with AICAR, (C) lysate of free parasites treated with AICAR, (D) lysate of free parasites not treated with AICAR and, (E) lysate of saponin released parasites isolated from percoll enriched AICAR treated parasitized culture. Arrow indicates the molecular ion peak of 338.9 Da corresponding to ZMP. Peak at 335 Da is a matrix peak. All cell types were treated with 1 mM AICAR for 2 h at 37 ºC. Samples were processed as described in the methods section. Neutralized samples were mixed in a ratio of 1:1 with dihydroxybenzoic acid (prepared in 50 % acetonitrile and 0.1 % TFA), spotted on MALDI target plate and then analyzed on an Ultra-Flex II Bruker Daltonics, MALDI-TOF mass spectrometer. Experiments were repeated twice and found to be reproducible.

3.3.7. ESI-MS/MS of the molecular ion peak of 338.9 Da

To further confirm the identity of the molecular ion peak at 338.9 Da, ESI-MS/MS analysis was done. The fragmentation pattern of standard ZMP is shown in Fig. 3.7A. Similar fragmentation was done on the molecular ion (338.9 Da) obtained from erythrocyte lysate (Fig. 3.7B) and from the lysate of parasites isolated from AICAR treated percoll enriched parasitized erythrocytes (Fig. 3.7C). As can be seen in Fig. 3.7, the MS/MS spectra of these samples clearly matched the fragmentation pattern of the standard ZMP. Together, the above results indicate that the conversion of AICAR to ZMP takes place exclusively in the erythrocyte and not in the parasite cytosol. Previously, incubation of erythrocytes with 10 mM AICAR led to the accumulation of the di and triphosphorylated forms of ZMP (Friedecky *et al.*, 2005). However, these forms, ZDP and ZTP were not detected in our MALDI experiments.

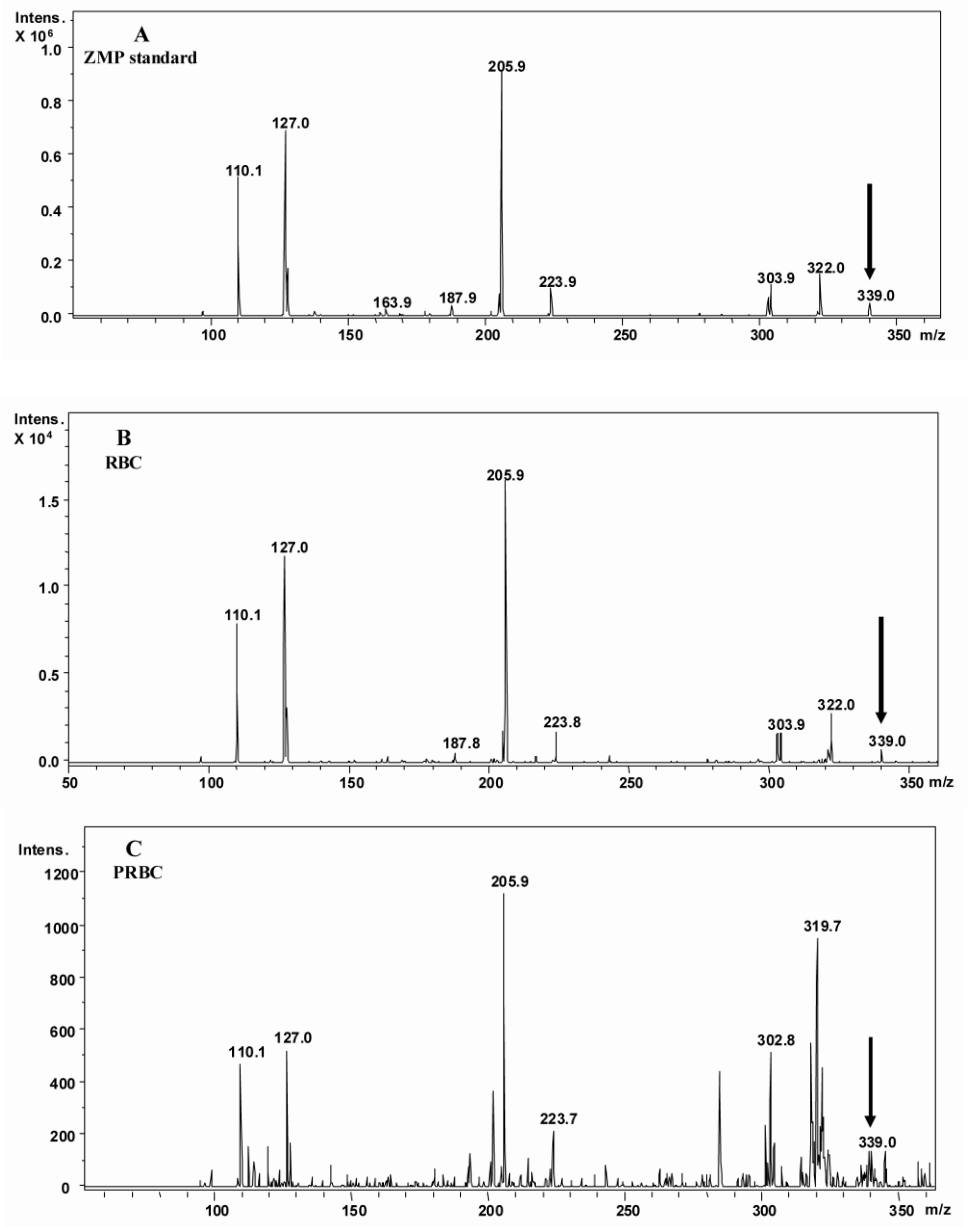

Fig. 3.7: ESI-MS/MS spectra of ZMP standard and cell extracts.

ESI-MS/MS of (A) standard sample of ZMP, (B) lysate of erythrocytes treated with 1 mM AICAR, (C) lysate of parasites, which were isolated from percoll enriched and AICAR treated parasitized erythrocytes. The mass of the parent ion that was fragmented was 339 Da indicated by the arrow. ESI-MS mass spectra were recorded in positive ion mode using an Esquire 3000-plus mass spectrometer (Bruker Daltonics, Bremen, Germany). Direct injection of cell extracts or standard sample was achieved using a syringe pump (Cole-Parmer, Vernon Hills, IL) operated at a flow rate of 200 to 240 µL h^{-1}. Aliquots of the cell extract were mixed with 50 % acetonitrile water mixture containing 0.1 % formic acid and spectra acquired in the positive ion mode. Helium was used as the collision gas for collision induced dissociation (CID). The data were processed using Esquire data analysis software, version 3.1.

These results can be explained by an initial neutral loss of the ribotide residue (−132 Da) giving rise to the protonated 5-amino-imidazole-4-carboxamide (*m*/*z* 127) that subsequently releases ammonia (−17 Da) to yield the cation of imidazole-4-carboxamide with *m*/*z* 110 (Fig. 3.8).

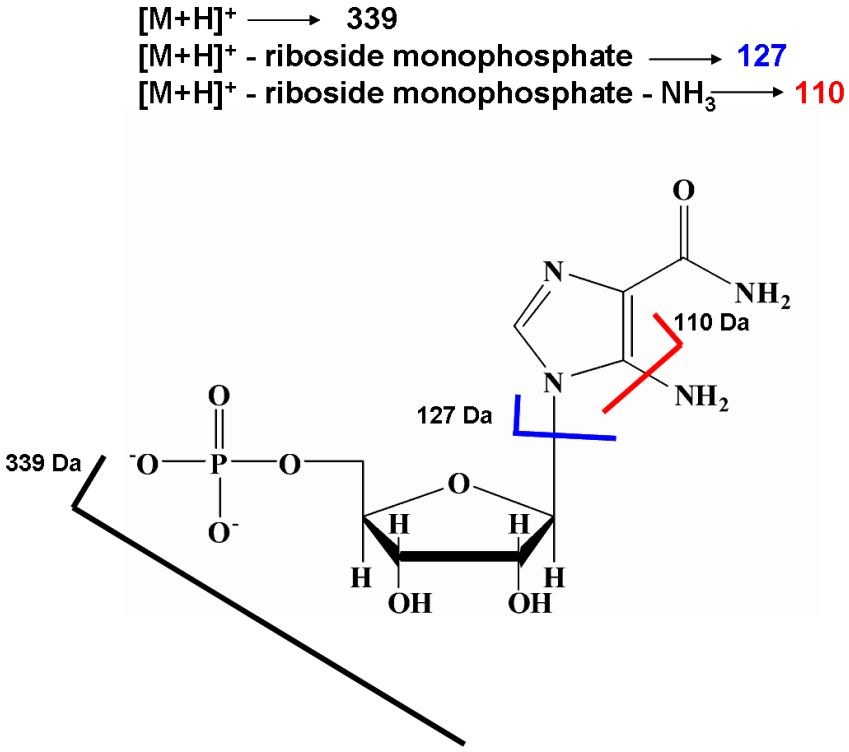

Fig. 3.8: Dissociation pattern of ZMP

The molecular ion peak of 339 Da corresponds to the monoprotonated form ($[M+H]^+$) of ZMP. Fragmentation at the glycosidic bond releases the ribotide and generates the protonated purine base with a molecular ion peak of 127 Da. The subsequent loss of an amino group generates the molecular ion peak of 110 Da.

The other molecular ion peaks of 322 and 304 Da originate due to the consecutive losses of an ammonia (-17 Da) and a water (-18 Da) molecule.

The molecular ion peak of 223 probably arises due to the loss of two molecules of water (-36 Da) from the molecular ion peak of AICAR and the abundant peak at 206 Da

results from the additional loss of an ammonia (-17 Da) molecule. It may be possible that during the MS/MS fragmentation, the phosphodiester bond linking the 5' CH_2OH group of the riboside with the phosphate may get cleaved and generate AICAR. However, we do not see the product peak of AICAR (expected $[M+H]^+$ peak of 259 Da) in MS/MS spectrum of ZMP. Therefore, to verify that the peaks at 223 and 206 Da arise from AICAR, ESI-MS/MS of AICAR standard was done in a similar manner as that for ZMP (Fig. 3.9). Upon fragmentation, the molecular ion peak of 259 Da gave product peaks of 242, 223 and 205 Da corresponding to the initial loss of an ammonia molecule followed by successive losses of water molecules.

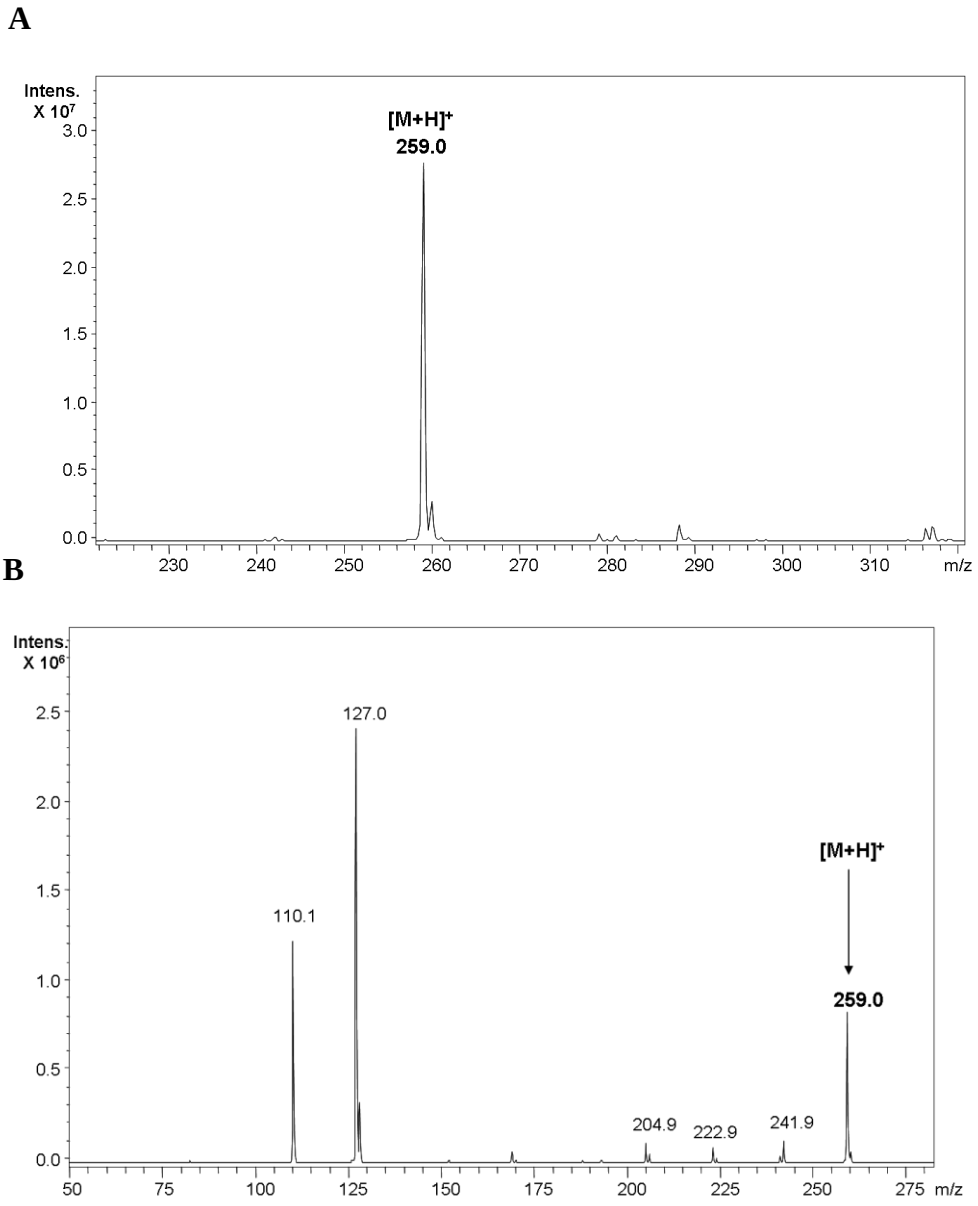

Fig. 3.9: ESI-MS/MS spectra of AICAR standard.

(A) ESI-MS of a standard sample of AICAR (B) ESI-MS/MS of the molecular ion of 259 Da. ESI-MS mass spectra were recorded in positive ion mode using an Esquire 3000-plus mass spectrometer (Bruker Daltonics, Bremen, Germany). Direct injection of cell extracts or standard sample was achieved using a syringe pump (Cole-Parmer, Vernon Hills, IL) operated at a flow rate of 200 to 240 µL h^{-1}. Aliquots of the cell extract were mixed with 50 % acetonitrile water mixture containing 0.1 % formic acid and spectra acquired in the positive ion mode. Helium was used as the collision gas for collision induced dissociation (CID). The data were processed using Esquire data analysis software, version 3.1.

3.3.8 ZMP is not taken up by free parasites

Free parasites were incubated with or without 1 mM ZMP for 2 h and cell extracts were prepared and analyzed by MALDI-TOF MS in the same manner as done with AICAR incubated parasites. Interestingly, lysate of both control and ZMP treated free parasites did not show the 338.9 Da molecular ion peak (Fig. 3.10A&B). The failure in detection could be because of the poor ionization of ZMP and hence, ZMP was added to the parasite lysate and spotted on the MALDI target plate. This sample gave the molecular ion peak of 338.9 Da (Fig. 3.10C). To estimate the sensitivity of MALDI measurements, a standard curve of peak intensity versus different ZMP concentrations was generated. Each spot of matrix and ZMP on the MALDI target plate also contained 200 pmoles of AMP as an internal standard. The MH^+ molecular ion peak of ZMP could be detected even at a concentration of 100 pmoles. This indicates even if ZMP is taken up by free parasites, the concentration is below the MALDI detection limit.

As mentioned earlier, ZMP did not show any effect on parasitized erythrocytes after incubation for 24 h. Free parasites treated with different concentrations of ZMP for 2 h followed by incubation with 1 μCi of [^{3}H]-hypoxanthine for 8 h also showed no drop in radioactive counts as compared to the untreated parasites while parasites treated with hadacidin showed a significant drop in [^{3}H]-hypoxanthine incorporation (Fig. 3.10D). This indicates that the uptake of ZMP by erythrocytes and free parasites is poor and hence, insufficient to cause toxicity.

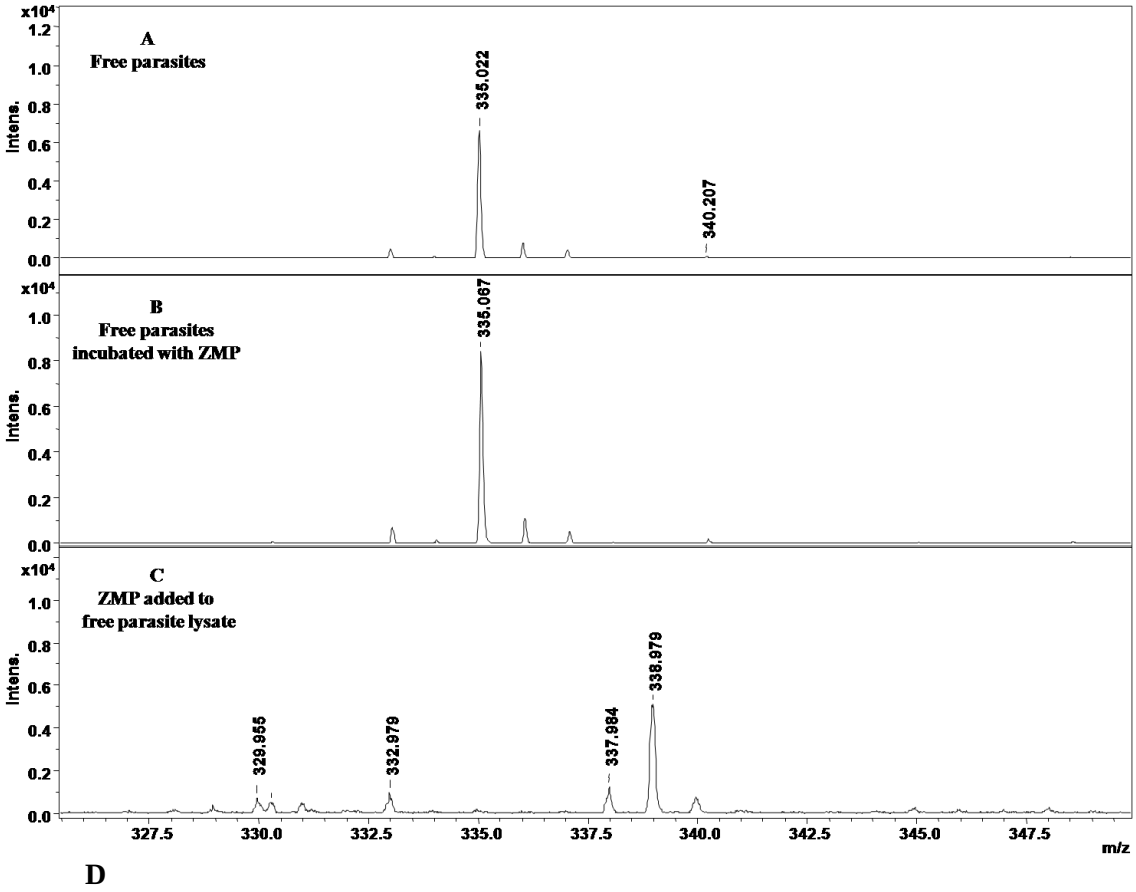

Fig. 3.10: ZMP uptake and effect on [^{3}H]-hypoxanthine incorporation by free parasites

(A-B) MALDI-TOF MS analysis of cell lysates of free parasites incubated in the absence or in the presence of ZMP. (C) ZMP standard was added to the parasite lysate and spectra acquired. (D) [^{3}H]-hypoxanthine incorporation in the presence or absence of increasing concentrations of either ZMP or 1 mM hadacidin by erythrocyte free parasites. Parasite viability after drug treatment was measured by % [^{3}H]-hypoxanthine incorporation with respect to the control.

However, the molecular ion peak of ZMP is seen in the parasite lysate obtained from AICAR treated percoll enriched parasitized erythrocytes (Fig. 3.6E). How can the presence of ZMP in the parasite compartment of parasitized erythrocytes be explained if the free parasites themselves do not seem to take up ZMP? Although no concrete experimental evidence exists to explain the transport of ZMP, some hypotheses are proposed. It was found that *Xenopus laevis* oocytes expressing *P. falciparum* purine nucleobase/nucleoside transporter PfENT1 take up [^{3}H]- tubercidins (Riegelhaupt *et al.*, 2010). These tubercidins also inhibited the uptake of [^{3}H]-hypoxanthine in a dose dependent manner. The same study also showed that [^{3}H]-Immucillins are not transported by PfENT1 and Immucillins do not inhibit the uptake of [^{3}H]-hypoxanthine. The latter result is concordant with our observations where AICAR and ZMP seem to be having no affect on [^{3}H]-hypoxanthine incorporation by free parasites. It is proposed that PfENT1 is not the only transport pathway for nucleosides and nucleobases in the parasite plasma membrane because PfENT1 knockout parasites can incorporate exogenous purines, albeit at supraphysiological concentration (El Bissati *et al.*, 2006; ElBissati *et al.*, 2008). In addition to PfENT1, there are three additional putative nucleoside transporters in *P. falciparum* genome (Martin *et al.*, 2005) that have not yet been characterized. Recently, one of these transporters, PfNT2 has been found to be localized to the endoplasmic reticulum of *P. falciparum* (Downie *et al.*, 2010). It might be that one or more of these transporters is or are involved in the uptake of ZMP and the poor uptake of ZMP by free parasites could be due to the disruption of the tertiary structure of these transporters by the harsh treatment with saponin used in the isolation of parasites from parasitized erythrocytes. Thus, it could be that possible that only in the context of a ‘parasitized

erythrocyte' is that transporter functional on the parasite plasma membrane. Further biochemical studies are needed to have a better understanding of this process.

The uptake of ZMP by the parasite from the erythrocyte compartment could also be explained through the non-specific process of endocytosis by the intraerythrocytic parasite. Endocytosis is a very active process during the intraerythrocytic stages of *P. falciparum* involved in the uptake of hemoglobin, which serves as a source of amino acids and iron (Saliba and Kirk, 2001). It is proposed that this process also provides a mean for other nutrients present in the erythrocyte cytosol to enter the parasite. However, the extent to which it contributes to nutrient uptake has not been determined (Saliba and Kirk, 2001).

3.3.9 ZMP accumulation in intraerythrocytic *P. falciparum* leads to decreased production of AMP, ADP and ATP

ZMP inhibits the enzymatic activity of recombinant purified PfASL and therefore, its *in vivo* effects on purine nucleotide synthesis in intraerythrocytic parasites was monitored through purine metabolite labeling with [^{3}H]-hypoxanthine in the presence or absence of AICAR. Percoll enriched parasitized erythrocytes (80-90 % parasitemia) were treated with/without 4 mM AICAR or 1 mM hadacidin for 2 h followed by addition of 5 µCi of [^{3}H]-hypoxanthine and further incubated for 4 h at 37 ºC. AICAR was used at 4 mM to ensure that the concentration of the phosphorylated product, ZMP is not limiting. The samples were processed and analyzed as described in the materials and methods section. Purine nucleotide standards including IMP, GMP, AMP, GDP, ADP, GTP and ATP could not be separated completely by ion pair RP-HPLC (Fig. 3.11A) and hence,

coeluted peaks of AMP+GDP and ADP+GTP were separated further by using Q-sepharose anion exchange chromatography (Fig. 3.11A) Fractions under different peaks were collected and counted for radioactivity and compared across the drug treated and control samples. The data are summarized in Fig. 3.11B. AICAR treatment led to a significant drop in radioactive counts in fractions corresponding to ATP, ADP and AMP with the counts associated with GDP and GTP remaining unaffected. Hadacidin treatment also led to a similar profile. Apart from a reduction in the adenylate pools, an increase in the IMP/GMP counts was noticed upon treatment with AICAR and hadacidin in comparison to the control sample. Under the HPLC conditions described here, IMP and GMP could not be separated and the net increase in counts could be a contribution from both the nucleotides. However, GTP counts remained the same across the three conditions and therefore, the increase in the IMP/GMP counts could be mainly due to the accumulation of IMP in the presence of hadacidin or AICAR (through ZMP) suggesting that the action of these molecules is at a site downstream of IMP synthesis. Thus, all these results implicate the site of action of AICAR (through ZMP) to be on the adenylate arm of the purine salvage pathway and specifically on PfASL.

A

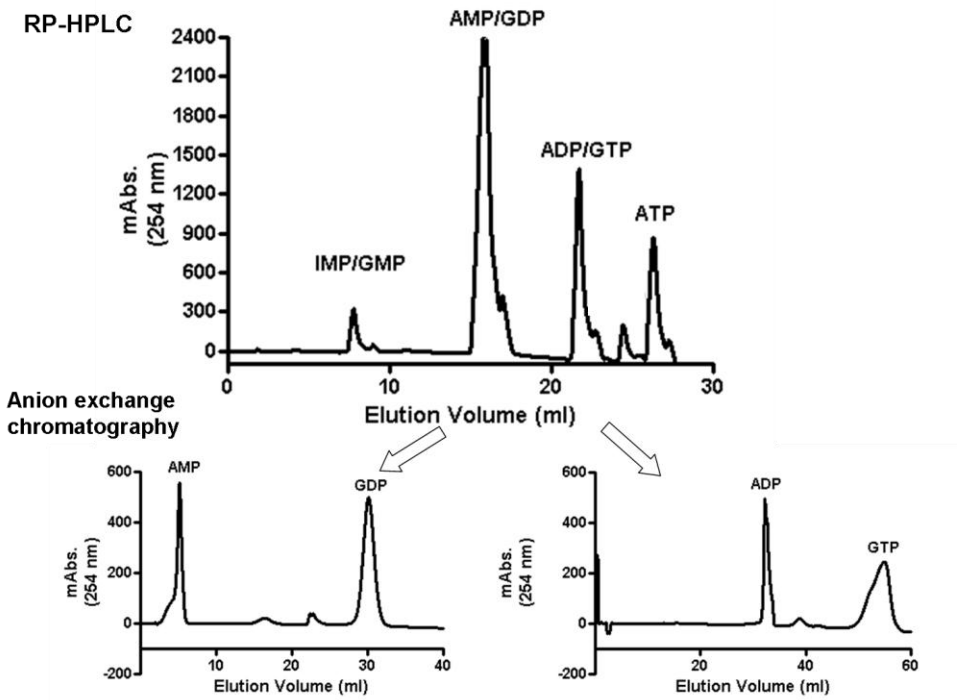

B

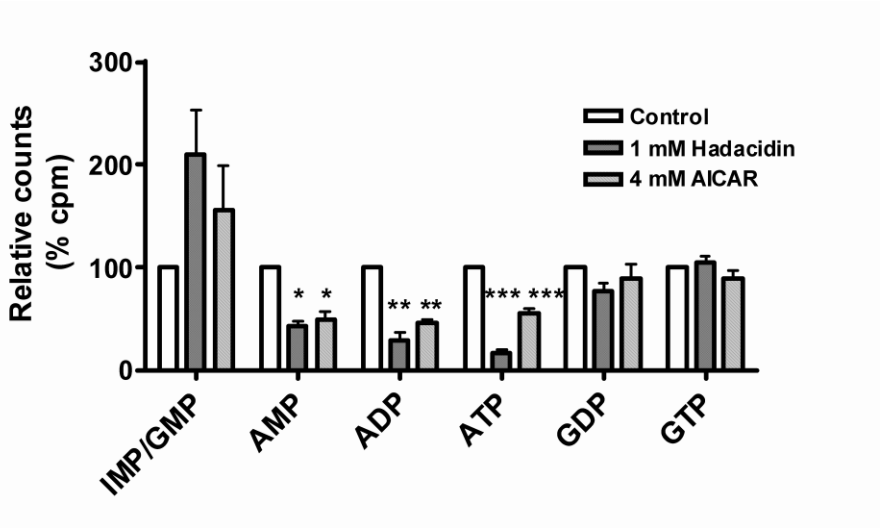

Fig. 3.11: Purine nucleotide labeling, separation and comparison across untreated, hadacidin and AICAR treated parasitized erythrocytes

*(A) Elution profiles of purine nucleotide standards separated by a combination of ion-paired RP-HPLC and Q-sepharose anion exchange chromatography. (B) Radioactive counts under each fraction was counted and plotted as % cpm with respect to the untreated culture. Data were evaluated statistically by two tailed paired student's t-test using Graph Pad Prism software, version 4.0. * indicates p < 0.05, ** p<0.005 and *** p<0.0005.*

3.3.10 AICAR pretreated erythrocytes are refractory to *P. falciparum* growth

Mass spectrometry analysis indicated that erythrocytes accumulate ZMP in their cytosol after treatment with AICAR (Fig. 3.6B). Therefore, erythrocytes were pretreated with AICAR and were tested for their ability to support *P. falciparum* merozoite growth. Prior to use in culture, the pretreated erythrocytes were washed extensively to remove extracellular AICAR. Interestingly, a dramatic drop in parasitemia was seen in cultures with AICAR pretreated erythrocytes with hardly any intraerythrocytic parasites being detected after 48 h (Fig. 3.12A). On the other hand, erythrocytes treated with solvent control for the same period and washed in the same way as done for AICAR treated erythrocytes supported a normal parasite growth with parasitemia increasing from 1 % to 20 % at the end of 96 h (Fig. 3.12A). The latter observation supported that erythrocytes were not damaged during the incubation and the washing steps. The metabolic viability of the parasites was also quantified by their ability to incorporate [^{3}H]-hypoxanthine. As can be seen from Fig. 3.12B, while parasites growing in untreated erythrocytes showed significant incorporation of [^{3}H]-hypoxanthine, AICAR pretreated erythrocytes showed no [^{3}H]-hypoxanthine incorporation indicating complete parasite death and hence, supporting the microscopic observation.

Inhibition of *P. falciparum* growth in AICAR pretreated erythrocytes could be because of either (1) inhibition of erythrocyte invasion by *P. falciparum* merozoites, or (2) inhibition of development of parasites in AICAR pretreated erythrocytes or a combination of both. To check this, parasite culture was first synchronized by 5 % D-sorbitol treatment and then, at the schizont stage, parasitized erythrocytes were enriched to 80-90 % parasitemia by centrifugation on 70 % percoll solution. The schizont enriched

parasitized erythrocytes were then used to infect either normal or AICAR pretreated erythrocytes. In the normal course of *P. falciparum* development, after 24 h, schizonts rupture the erythrocytes releasing merozoites that infect new erythrocytes and develop into ring stages. Thus, invasion efficiency was calculated as the ratio of parasitemia (calculated only for rings or merozoites) in the culture after 24 h to the initial parasitemia. As can be seen from Fig. 3.12C, there was a 50 % decrease in the invasion efficiency in AICAR pretreated erythrocytes compared to the untreated erythrocytes. Rabbit erythrocytes, known to be refractory to *P. falciparum* invasion (Breuer *et al.*, 1983), were used to correct for invasion of carried over erythrocytes from percoll enriched culture by *P. falciparum* merozoites. The significant drop in the invasion rate upon using rabbit erythrocytes over the untreated erythrocytes indicates that the carried over uninfected erythrocytes from the percoll enriched culture were very less and hence, insignificant. As this experiment was done in 10 % rabbit serum, human erythrocytes resuspended in complete RPMI medium containing 10 % rabbit serum were infected with the percoll enriched culture. After 24 h, the invasion rate was found to be slightly higher in comparison to the untreated erythrocytes thereby ruling out the effect of rabbit serum in blocking *P. falciparum* invasion.

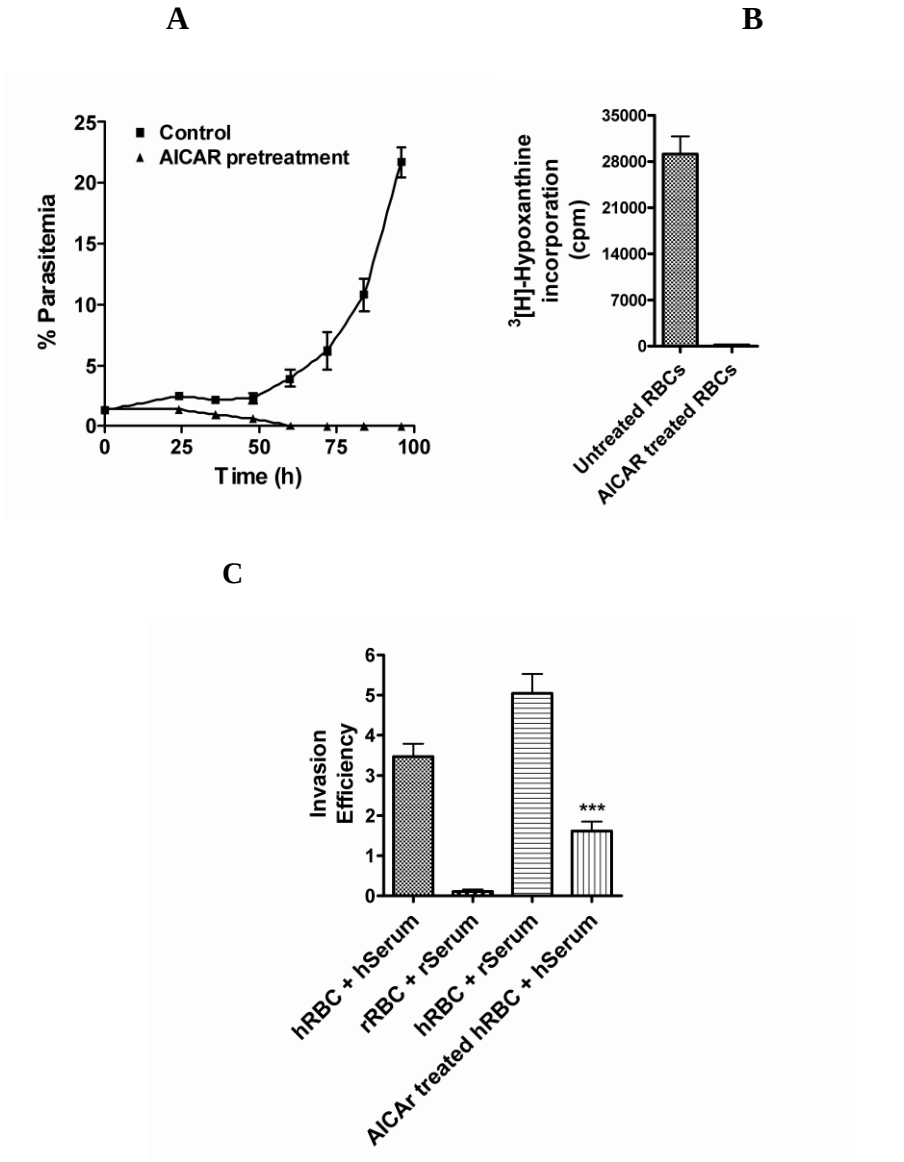

Fig. 3.12: Effect of erythrocyte pretreatment with AICAR on *P. falciparum* growth and invasion.

*(A) P. falciparum growth in control and AICAR pretreated erythrocytes monitored by microscopic examination of Giemsa stained smears and represented as % parasitemia post infection, (B) [^{3}H]-hypoxanthine incorporation measured at the end of 96 h by parasites in culture containing AICAR pretreated or normal erythrocytes. (C) Invasion efficiency of AICAR pretreated erythrocytes by P. falciparum merozoites. Untreated human erythrocytes in human serum (hRBC + hSerum), rabbit erythrocytes in rabbit serum (rRBC + rSerum) and human erythrocytes in rabbit serum (hRBC + rSerum) were mixed with the percoll enriched parasitized culture containing schizonts and used as controls. Following infection, Giemsa stained smears were made after 24 h and slides examined for merozoites and rings. Invasion efficiency was calculated for both the control and treated erythrocytes by dividing the parasitemia after 24 h by the initial parasitemia. Data were plotted and evaluated statistically by two tailed paired student's t-test using Graph Pad Prism software, version 4.0. *** p<0.0005.*

Several events occur during the course of the invasion process, which include merozoite release, its attachment to the erythrocyte membrane, followed by entry and ring formation. A decrease in generation of new ring forms may result from inhibition of any of these events (Hadley, 1986). Though further studies are needed to distinguish the effect(s) of AICAR on these individual processes, it is clear that in addition to the purine salvage pathway in the parasite, AICAR is affecting a vital metabolic process in the erythrocyte that is crucial for the parasite survival. Possible mechanism for AICAR toxicity could be depletion of ATP levels as a consequence of conversion of AICAR to ZMP by adenosine kinase. This enzyme transfers a phosphate from ATP to AICAR to produce ADP and ZMP and hence, incubation of erythrocytes with AICAR would result in a depletion of ATP levels. Previously, erythrocytes from individuals with pyruvate kinase deficiency have been shown to be more resistant to invasion by *P. falciparum* parasites (Durand and Coetzer, 2008) and the molecular basis for this has been attributed to decreased glycolysis and as a consequence, depletion of ATP levels in the erythrocytes (Ayi *et al.*, 2009). One of the main targets of ZMP in mammalian cells is AMP-activated protein kinase (AMPK) (Hardie, 2007). AMPK is a serine/threonine protein kinase, which functions as a heterotrimeric enzyme with α, β and γ subunits being encoded by separate genes. The enzyme is present in most eukaryotic cells, but no report exists for the presence of the same in *Plasmodium spp*.

3.4 CONCLUSIONS

AICAR has been used extensively *in vivo*, both in rodents and human beings for metabolic and therapeutic investigations at doses as high as 10-100 mg kg^{-1} body weight with no toxic side effects. AICAR has been used in humans as a potential drug for use during myocardial ischemia and cardiac bypass surgery (Mangano, 1997). Administration of AICAR in humans results in its accumulation in plasma at a concentration of 0.16 mM (Boon *et al.*, 2008) and has been shown to be rapidly taken up and phoshorylated to ZMP by erythrocytes (Dixon *et al.*, 1991). Recently, AICAR infusion in mice has shown to increase their muscle endurance (Narkar *et al.*, 2008). Thus, it remains interesting to see the effect of AICAR or its analogues on the parasite growth under in *vivo* conditions in a mice model.

Previously, several nucleoside analogs such as tubericidin, sangivamycin have been shown to have an inhibitory effect on *P. falciparum* growth (Coomber *et al.*, 1994). However, the mechanism of action of these molecules at the level of individual enzymes and metabolism in *P. falciparum* has not been elucidated (Riegelhaupt *et al.*, 2010). The studies carried out here emphasize the need to consider these aspects, particularly the role played by the erythrocyte metabolism on the mode of anti-parasitic action of these nucleoside analogs. Also, as AICAR accumulation is seen in individuals with in born errors in purine metabolism like Lesch-Nyhan syndrome (Lopez, 2008) and AICARibosiduria (Sandrine *et al.*, 2008), it would be interesting to survey the susceptibility of such populations to malaria infections.

CHAPTER 4

Metabolic fate of fumarate during the intraerythrocytic stages of *Plasmodium falciparum*

Metabolic fate of fumarate during the intraerythrocytic stages of *Plasmodium falciparum*

Abstract

Energy metabolism in aerobic respiration involves a complete breakdown of carbohydrates, proteins and lipids to CO_2 and H_2O by the TCA cycle and in this process, reducing equivalents in the form of NADH and $FADH_2$ are generated, which are used in the electron transport chain to generate ATP. Besides this, the TCA cycle also serves biosynthetic roles for many metabolic pathways. During the intraerythrocytic stages of P. falciparum, the TCA cycle is believed to be dysfunctional as a cycle with most of the ATP requirements being met by glycolysis. It is also proposed that the only biosynthetic role of P. falciparum TCA cycle is to generate succinyl-CoA for heme biosynthesis. This chapter highlights another critical role for the cycle in the metabolism of fumarate, a side product of purine salvage pathway.

4.1 INTRODUCTION

In the purine salvage pathway, AMP is synthesized by the concerted actions of adenylosuccinate synthetase and adenylosuccinate lyase. The ADSS reaction involves the addition of a molecule of aspartate to the 6-oxo group of IMP to generate SAMP, which is then cleaved by ASL to generate AMP and fumarate. Excess AMP is deaminated back to IMP by AMP deaminase. The rest of the carbon skeleton of aspartate is released as fumarate (Fig. 4.1). The net result of this cyclic series of reactions (known as the purine

nucleotide cycle) is the generation of a molecule of fumarate from aspartate at the expense of one GTP molecule.

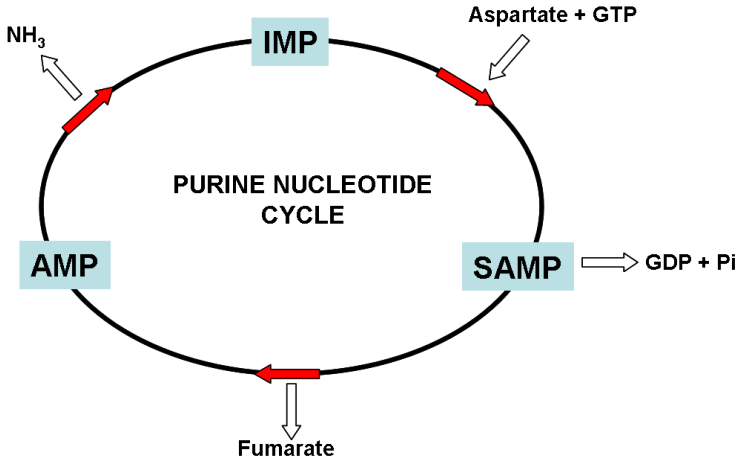

Fig. 4.1: The purine nucleotide cycle

Adenylosuccinate synthetase (ADSS) adds a molecule of aspartate to IMP with a concomitant hydrolysis of GTP to GDP to generate SAMP. Adenylosuccinate lyase (ASL) cleaves SAMP to AMP and fumarate. AMP is deaminated back to IMP by AMP deaminase (AMPDA). The net reaction of this cycle is to generate a molecule each of GDP, Pi, NH_3 and fumarate.

The purine nucleotide cycle becomes active under conditions requiring excess ATP production such as in the muscle tissue. Aragon and Lowenstein found that the contents of TCA cycle intermediates increased in rat hind limb muscle during exercise (Aragon and Lowenstein, 1980). The increase was more pronounced for fumarate and malate. Interestingly, addition of hadacidin reduced the increase of fumarate and malate and also increased IMP accumulation (Aragon and Lowenstein, 1980). These observations clearly implicate the vital role played by the purine nucleotide cycle. The cycle ensures a maximal production of ATP by two mechanisms: (1) fumarate being produced enters the TCA cycle and replenishes the intermediates, malate and

oxaloacetate and (2) depletion of AMP by the action of AMP deaminase drives the equilibrium of adenylate kinase reaction towards ATP formation (Van den Berghe *et al.*, 1992).

The TCA cycle operating in the mitochondria generates fumarate from succinate by the action of succinate dehydrogenase (E.C. 1.3.5.1), an enzyme present on the inner mitochondrial membrane. This reaction involves the reduction of ubiquinone (CoQ) to ubiquinol ($CoQH_2$) and is one of the four reactions in the TCA cycle that generates reducing equivalents for the electron transport chain. Fumarate is then converted to malate by fumarate hydratase (E.C. 4.2.1.2). Malate is converted to oxaloacetate by malate dehydrogenase (E.C. 1.1.1.37) in a reaction that involves the reduction of NAD^+ to NADH. Oxaloacetate then combines with acetyl-CoA by the action of citrate synthase (E.C. 2.3.3.1) to form citrate to initiate the cycle again.

The purine nucleotide cycle should be functional in *P. falciparum* as the parasite contains homologues of the three enzymes constituting the cycle. Further, numerous studies have shown that incubation of free parasites with [^{3}H]-hypoxanthine leads to labeling of AMP indicating ADSS and ASL activities. Evidence for the activity of AMP deaminase comes from the observation of Cassera *et al.*, who found radioactivity incorporation in IMP when free parasites were incubated with [^{33}P]-AMP (Cassera *et al.*, 2008). Thus, fumarate produced in the parasite as a consequence of this cycle is expected to be high. Metabolite analyses of *P. falciparum* during the intraerythrocytic stages by NMR (Teng *et al.*, 2009) and ESI-MS/MS (Olszewski *et al.*, 2009) have shown the presence of fumarate and its intracellular concentration is estimated to be about 0.2 mM (Teng *et al.*, 2009). Perhaps the most convincing evidence of the presence of intracellular

pool of fumarate comes from the study by Painter *et al.*, (Painter *et al.*, 2007). The study involved generation of transgenic *P. falciparum* parasites in which the endogenous gene for dihydroorotate dehydrogenase (DHODH) was replaced with *Saccharomyces cerevisiae* dihydroorotate dehydrogenase (ScDHODH). The authors found that while the parental parasites were susceptible to atovaquone (complex III inhibitor) the transgenic parasites were completely resistant to the drug at doses as high as 1 μM (< 1000 times IC_{50} value). The study implicates that the sole role of electron transport chain is to regenerate oxidized ubiquinone, which is utilized by DHODH in pyrimidine biosynthesis. It should be noted that both the enzymes oxidize dihydroorotate to orotate, but unlike PfDHODH that transfers the reducing equivalents to ubiquinone (CoQ), *Sc*DHODH transfers reducing equivalents to fumarate. The other difference between the two enzymes is their subcellular localization. While PfDHODH is localized to the mitochondrial inner membrane (Krungkrai, 1995), ScDHODH-GFP fusion protein is localized to the cytoplasm in *P. falciparum* (Painter *et al.*, 2007). Although the authors have not speculated on the source of fumarate, these results implicate that there is sufficient intracellular pool of cytosolic fumarate to sustain the activity of ScDHODH in the transgenic parasites. Purine salvage pathway is operational in the cytosol and therefore, there is a good reason to believe that the source of cytosolic fumarate is indeed the purine salvage pathway.

As mentioned in Chapter 1, the TCA cycle in *P. falciparum* is dysfunctional as a cycle. Hence, the metabolic fate of fumarate generated from the purine salvage pathway in *P. falciparum* is unknown and needs investigation. Fry and Beesley observed that isolated mitochondria of *P. yoelli* and *P. falciparum* could reduce cytochrome c in the

presence of NADH, alpha-glycerophosphate and succinate (Fry and Beesley, 1991), which are substrates for NADH dehydrogenase, alpha-glycerophosphate dehydrogenase and succinate dehydrogenase respectively. Oxidation of these substrates generates reduced ubiquinone ($CoQH_2$), which is used by complex III in the reduction of cytochrome c. Interestingly, the reduction of cytochrome c was inhibited by fumarate. On the other hand, Uyemura *et al.,* (Uyemura *et al.,* 2004) found that fumarate increased the membrane potential in isolated *P. yoelli* parasites. These two results are completely contradictory with respect to the direction of fumarate metabolism. Fry and Beesley's results implicate a fumarate reductase activity in which, fumarate is reduced to succinate with a concomitant oxidation of reduced ubiquinone ($CoQH_2$) to ubiquinone (CoQ). However, no gene encoding fumarate reductase is found in *P. falciparum* genome (Gardner *et al.*, 2002). It is therefore believed that this activity could be a consequence of the reverse reaction of succinate dehydrogenase (Fisher *et al.*, 2008). However, results shown by Uyemura *et al.* implicate that fumarate is converted to malate by the action of fumarate hydratase, which is a substrate for malate quinone oxidoreductase and hence, would be oxidized to oxaloacetate. The oxidation of malate to oxaloacetate generates reduced ubiquinone ($CoQH_2$), which then feeds the electron transport chain at complex III.

Studies reported in this chapter therefore, were aimed to trace the metabolic fate of fumarate during the intraerythrocytic stages of *P. falciparum*.

4.2 MATERIALS AND METHODS

All reagents and chemicals unless mentioned otherwise were obtained from Sigma Chemical Co., St. Louis, USA. U-[^{14}C]-aspartate (200 mCi mmol^{-1}) was obtained from Board of Radiation and Isotope Technology, India (BRIT, India). 2,3-[^{14}C]-fumarate (10 mCi mmol^{-1}), 2,3-[^{13}C]-fumarate and 1-[^{13}C]-D-glucose were obtained from Sigma Chemical Co., St. Louis, USA. 8-[^{3}H]-hypoxanthine (19.2 Ci mmol^{-1}) was obtained from GE Healthcare, UK. Primers for gene cloning were custom synthesized at Sigma, Bangalore, India. Human O^{+} serum and erythrocytes for maintenance of the 3D7 strain of *P. falciparum* were obtained from healthy volunteers from a local hospital.

4.2.1 *P. falciparum* culture maintenance

The 3D7 strain of *P. falciparum* was maintained and cultured *in vitro* as described in chapter 3. Protocols used for isolation of free parasites and enrichment of parasitized erythrocytes for mature stages were the same as described in chapter 3.

4.2.2 Spent medium analysis of cells incubated with U- [^{14}C]-aspartate and 2, 3-[^{14}C]-fumarate

1 µCi of U-[^{14}C]-aspartate (200 mCi mmol^{-1}) and 2,3-[^{14}C]-fumarate (10 mCi mmol^{-1}) were added to erythrocytes, parasitized erythrocytes (2 % hematocrit and 6-8 % parasitemia, 200 µl) or saponin released free parasites (total protein: 2-3 mg ml^{-1}). Parasites were predominantly in the trophozoite stage before labeling. While erythrocytes and parasitized erythrocytes were incubated for 24 or 48 h, saponin released free parasites were incubated for 8 h at 37 ºC in a 96 well flat-bottomed plate placed in a candle jar. At the end of incubation, the spent medium of each cell type was collected and was treated

with 10 % trichloroacetic acid (TCA) for 15 min. on ice followed by boiling for 10 min. The protein precipitate was removed by centrifugation for 30 min. at 4 ºC. The supernatant was collected, lyophilized and reconstituted in 10-20 µl of distilled water. 2-3 µl of the concentrated media was spotted on a 10 x 5 cm TLC silica gel 60 F_{254} plate (Merck, Germany) and air dried. A mobile phase consisting of n-butanol, acetic acid and water in the ratio of 4: 1: 1 was used to run the TLC following which the TLC plate was dried and developed using a Fuji FLA 5000 phosphorimager.

4.2.3 Nucleic acid and protein labeling with U-[^{14}C]-aspartate and 2,3-[^{14}C]-fumarate

1 µCi of U-[^{14}C]-aspartate (200 mCi mmol^{-1}), 2,3-[^{14}C]-fumarate (10 mCi mmol^{-1}) and 8-[^{3}H]-hypoxanthine (19.2 Ci mmol^{-1}) were added to erythrocytes, parasitized erythrocytes (2 % hematocrit and 2-3 % parasitemia, 200 µl) or saponin released free parasites (total protein: 2-3 mg ml^{-1}). While erythrocytes and parasitized erythrocytes were incubated for 24 or 48 h, saponin released free parasites were incubated for 8 h at 37 ºC in a 96 well flat-bottomed plate placed in a candle jar. At the end of incubation, the contents of each well were harvested onto glass fiber filters using a Combi-12 automated cell harvester (Molecular Devices, Sunnyvale, CA), washed extensively with distilled water and dried. The incorporated radioactivity was measured as disintegrations per minute using a Wallac 1409 (Wallac Oy, Turku, Finland) liquid scintillation counter.

To check the incorporation of radioactivity in proteins, the parasite culture was treated with 0.15 % saponin solution for 2-3 min. to release the parasites from the erythrocytes. The parasite pellet was washed 5-6 times in PBS, resuspended in 1X SDS-

gel loading buffer, boiled for 10 minutes and subjected to 10 % SDS-PAGE. The gel was dried and developed on a Fuji FLA 5000 phosphorimager. The experiments were done in duplicate and repeated twice.

4.2.4 Metabolite extraction

Free parasites after incubation with the radioactive tracers, U-[^{14}C]-aspartate, 2,3-[^{14}C]-fumarate and 8-[^{3}H]-hypoxanthine were washed thrice with 1 X PBS to remove excess radioactive label, resuspended in distilled water and lysed by rapid freeze thawing. Soluble metabolites were extracted from the lysate by treatment with 0.5 M $HClO_4$ for 30 min. on ice using published protocols (Cassera *et al.*, 2008). Samples were then neutralized with 5 M KOH and centrifuged to remove the precipitate. The supernatant was concentrated by lyophillization and stored at –80 ºC till further use.

4.2.5 Reverse phase high performance liquid chromatography for separation of nucleotides

Purine and pyrimidine nucleotide monophosphates were separated using reverse phase (Genesis C18, 4µm, 150mm X 4.6mm, Grace Davison Discovery Sciences^{TM}) ion-pair HPLC. The mobile phases were 8 mM tetrabutylammonium bisulfate (Spectrochem, India) and 100 mM KH_2PO_4, pH 6.0 (solution A) and 30 % acetonitrile containing 8 mM tetrabutylammonium bisulfate and 100 mM KH_2PO_4 (pH 6.0) (solution B). The cell extracts were resuspended in a small volume of solution A and spiked with nucleotide monophosphate standards. After injection, the column was washed with 2 column volumes of buffer A and then a gradient from 0 % to 100 % solution B in 60 min. was run. The eluate was monitored at 254 nm with the flow rate set at 0.7 ml min^{-1}. Peaks

corresponding to the nucleotide fraction were collected and the radioactive counts were measured as counts per minute using a Wallac 1409 (Wallac Oy, Turku, Finland) liquid scintillation counter.

4.2.6 Carbon-13 nuclear magnetic resonance experiments

Free parasites obtained from saponin treatment of parasitized erythrocytes were washed thrice in 1X PBS and incubated with either 25 mM D-1-[^{13}C]-glucose or 10 mM D-2,3-[^{13}C]-fumarate for 2 h at 37 °C. Erythrocytes incubated with similar quantities of ^{13}C-tracers for the same amount of time served as controls. Following incubation, cell suspensions were directly frozen in liquid nitrogen and stored at -80 ºC till further use. Before acquiring NMR spectra, the cell suspensions were disrupted by sonication, centrifuged and the supernatants collected for analyses.

After centrifugation for 30 min, the volume of the supernatant was made up to 450 µl with H_2O and 50 µl of D_2O was added to obtain final volume of 500 µl. ^{13}C NMR spectra were collected on a 500 MHz Bruker NMR spectrometer equipped with a 5-mm broad-band probe head. Measurements were recorded at 25 °C under a bi-level broad-band gated proton decoupling with D_2O lock.

4.2.7 Cloning, expression and purification of *P. falciparum* malate dehydrogenase and *P. falciparum* aspartate aminotransferase

P. falciparum malate dehydrogenase gene (single exon) was amplified using parasite genomic DNA as template with a forward primer, Pf $MDH_{fwd.}$ with *Nco* I and reverse primer, $PfMDH_{rev.}$ with *Xho* I restriction sites.

$PfMDH_{fwd.}$: $^{5'}$GCT**CCATGG**CTAAAATTGCCTTAATAGGTAGTGGTCAAATCGG $^{3'}$

PfMDH$_{rev.}$: $^{5'}$ATC**CTCGAG**TTTAATTAAGTCGAAAGCTTTTTGTGTGTTGC $^{3'}$

Similarly, *P. falciparum* aspartate amintransferase (AAT) gene was amplified using the forward primer PfAAT$_{fwd.}$ with *Nco* I and reverse primer PfAAT$_{rev.}$ with *Xho* I restriction sites.

PfAAT$_{fwd.}$: $^{5'}$CATG**CCATGG**ATAAGTTATTAAGCAGCTTAGAAAATATCG $^{3'}$

PfAAT$_{rev.}$: $^{5'}$ CCG**CTCGAG**TATTTGACTTAGCGAAAGACAAATTTTGTCGGC $^{3'}$

Amplification yielded DNA fragments corresponding to 0.9 Kb for PfMDH and 1.2 Kb for PfAAT that were digested with *Nco* I and *Xho* I and cloned in pET28b expression vector. The identity of the clone was confirmed by sequencing. PfMDH protein was expressed with a hexahistidine tag at the C-terminus in *E. coli* BL21-CodonPlus™ (DE3)-RIL cells (Stratagene, USA). Transformed cultures were grown in terrific broth containing kanamycin (50 µg ml^{-1}) and chloramphenicol (40 µg ml^{-1}) and induced with IPTG at a final concentration of 0.75 mM. Induction was carried out at 16 °C for 12 hours. PfAAT was expressed in C41 DE3 strain of *E. coli* (Miroux and Walker, 1996). Induction was carried out for 12 hours at 27 °C. For protein purification, the cell pellets were resuspended in lysis buffer containing 50 mM potassium phosphate, pH 7.4, 100 mM NaCl, 2 mM dithiothreitol (DTT) and 10 % glycerol, lysed using French press and centrifuged. The supernatant was incubated with nickel-nitrilotriacetic acid (Ni-NTA) agarose beads after which the beads were washed extensively with wash buffer (50 mM potassium phosphate, pH 7.4, 100 mM NaCl, 30 mM imidazole, 2 mM DTT, 10 % glycerol). Bound proteins were eluted with elution buffer, pH 7.4 (wash buffer containing

200 mM imidazole). The eluted protein was concentrated and further purified on Sephacryl 200 gel filtration column pre-equilibrated with 50 mM potassium phosphate pH 7.4, 100 mM NaCl, 2 mM DTT, 1 mM EDTA and 10 % glycerol. The eluted protein was again concentrated and used for further experiments. Protein concentrations were determined by the method of Bradford (Bradford, 1976) with bovine serum albumin (BSA) as standard.

PfAAT was assayed as described by Winter and Dekker (Winter and Dekker, 1989). The consumption of oxaloacetate was monitored as a time dependent decrease in absorbance at 270 nm with a molar extinction coefficient of 782 M^{-1} cm^{-1}.

4.2.8 Generation of polyclonal antibodies against *P. falciparum* malate dehydrogenase (MDH) and aspartate aminotransferase (AAT).

The purified PfMDH (100 µg) was injected subcutaneously into a healthy New Zealand White rabbit after emulsification in complete Freund's adjuvant followed by two boosters in incomplete Freund's adjuvant each separated by 14 days. Purified PfAAT (100 µg) was injected into mice (BALB/c) and subsequent injections were same as in the case of PfMDH. Antiserum was collected from the animals at the end of 14 days after second booster and was stored at 4 ºC to allow complete coagulation of blood. The serum was separated by centrifugation for 30 min. The supernatant was aliquoted into sterile eppendorff tubes and stored at -20 ºC till further use.

4.2.9 Western blotting

PfMDH and PfAAT antisera were characterized for their specificity against purified recombinant proteins and were also tested on the parasite lysate. The proteins

were separated on a 10 % SDS-polyacrylamide gel and were transferred onto a PVDF membrane using a Hoefer wet transfer apparatus (Hoefer®, Inc., MA, USA). The PVDF membrane was activated with methanol for 10 min. before use. The PVDF membrane was then blocked for 12 h at 4 ºC with blocking solution containing 5 % skim milk in 1 X PBS. The membrane was then incubated with PfMDH or PfAAT antiserum in 2.5 % skim milk solution at dilutions of 1:5000 for recombinant proteins or 1:1000 for parasite lysate for 3 h at 4 ºC. The membrane was washed thrice with washing solution containing 0.1 % Tween 20 in 1 X PBS. Anti-rabbit IgG (Sigma Chemical Co., St. Louis, USA) or anti-mouse IgG (Sigma Chemical Co., St. Louis, USA) antibodies conjugated with horse raddish peroxidase (HRP) were used as secondary antibodies at a dilution of 1:1000 for PfMDH and PfAAT, respectively. Following incubation with the secondary antibodies for 3 h at 4 ºC and washing three times with the wash solution, the membrane was developed using the chromogenic substrate, 3-amino-9-ethyl-carbazole (Sigma Chemical Co., St. Louis, USA). For parasite lysates, the membrane was developed using Pierce Super Signal West Pico Chemiluminiscent kit as described by the manufacturer. The blot was exposed to TMS (Kodak) films for different time points and developed using GBX-Developer-Fixer solutions (Premier Kodak reagents).

4.2.10 Indirect immunofluorescence

Indirect immunofluorescence was done as described earlier (Tonkin *et al.*, 2004) with minor modifications. Parasitized erythrocytes were washed thrice in 1 X PBS and then fixed with 4 % paraformaldehyde and 0.0075 % glutaraldehyde in PBS for 30 min. Following washing with 1 X PBS, the cells were permeabilized with 0.05 % saponin solution (prepared in 1 X PBS) for 2 min. Following another PBS wash, cells were

blocked with 3 % BSA in 1 X PBS for one hour. Anti-PfMDH (diluted 1:200) or anti-PfAAT antiserum (diluted 1:200) was added to the blocking solution and cells were incubated for further one hour. Following washing, the cells were incubated with anti-rabbit IgG (for MDH) or anti-mouse IgG (for AAT) conjugated with AlexaFluor dyes (Molecular Probes®, USA) for one hour. After washes with wash buffer the nuclei were stained with Hoechst stain (Molecular Probes®, USA) (1:10,000 dilution) for 20 min. After washing, the cell suspension placed on poly-lysine coated coverslips and were then mounted on a glass microscope slide in 50 % glycerol (in 1X PBS) and sealed. The glass slides were visualized by using a Carl-Zeiss laser scanning confocal microscope (Carl Zeiss, Inc., USA).

4.2.11 Digitonin permeabilization of free parasites and Western blotting

Free parasites were treated with increasing concentrations of digitonin as described earlier (Hodges *et al.*, 2005) with minor modifications. Total protein lysates were separated by SDS-PAGE (12 %) and blotted onto a PVDF membrane using a Hoefer wet transfer apparatus (Hoefer®, Inc., MA, USA). Immunodetections were performed using the primary antibodies, mouse anti-PfAAT (1:2000), rabbit anti-PfMDH (1:2000), and rabbit anti-PfHSP60 (1:1000). As secondary antibodies, anti-mouse or anti-rabbit IgG conjugated to horseraddish peroxidase (Sigma Chemical Co., St. Louis, USA) were used. Western blots were developed using Pierce Super Signal West Pico Chemiluminiscent kit as described by the manufacturer. The blot was exposed to TMS (Kodak) films for different time points and developed using GBX-Developer-Fixer solutions (Premier Kodak reagents).

4.2.12 Effect of hadacidin on the mitochondrial membrane potential

Parasite culture was enriched for mature stages by centrifugation on a 70 % Percoll solution. The enriched stages were then treated with 1 mM hadacidin for 2 h and were then stained with 100 nM of Tetramethyl Rhodamine Methyl ester (TMRM) for 30 min at 37 ºC in a candle jar. The culture was washed thrice and was then imaged using Carl Zeiss confocal laser scanning microscope (Carl Zeiss, Inc., USA). Intact mitochondria were visualized from ten independent fields in control and hadacidin treated samples and the intensity of TMRM fluorescence was compared by student's t-test.

4.3 RESULTS AND DISCUSSION

4.3.1 Fumarate is not a metabolic waste for intraerythrocytic *P. falciparum* parasites.

Prior to metabolic labeling of erythrocytes and parasitized erythrocytes, U-[^{14}C]-aspartate was spotted and analyzed for radiochemical purity on a TLC silica gel 60 F_{254} plate (Merck, Germany). Under the conditions described for TLC in materials and methods, U-[^{14}C]-aspartate showed predominantly a single spot (Fig. 4.2A) with no other contaminating radioactive chemical.

Erythrocytes (RBCs) and *P. falciparum* infected erythrocytes (PRBCs) were incubated with 1 µCi of 8-[^{3}H]-hypoxanthine and U-[^{14}C]-aspartate in separate wells in a 96 well flat bottomed plate kept in a glass candle jar at 37 ºC for 24 and 48 h. After incubation, the cells were harvested onto glass fiber filters as described in materials and methods section. A significant amount of radioactivity was obtained in the nucleic acid fractions of parasitized erythrocytes incubated with 8-[^{3}H]-hypoxanthine (Fig. 4.2B) and U-[^{14}C] aspartate (Fig. 4.2C) while it was not associated with erythrocytes. Aspartate incorporation in nucleic acids could be explained by the fact that *P. falciparum* synthesizes pyrimidines by the *de novo* pathway in which, the carbon skeleton of aspartate forms the backbone of the pyrimidine ring. Further, radioactive incorporation could also be seen in the protein fraction of PRBCs that were incubated with U-[^{14}C]-aspartate (Fig. 4.2D). These results indicate that aspartate is taken up and metabolized by the parasite.

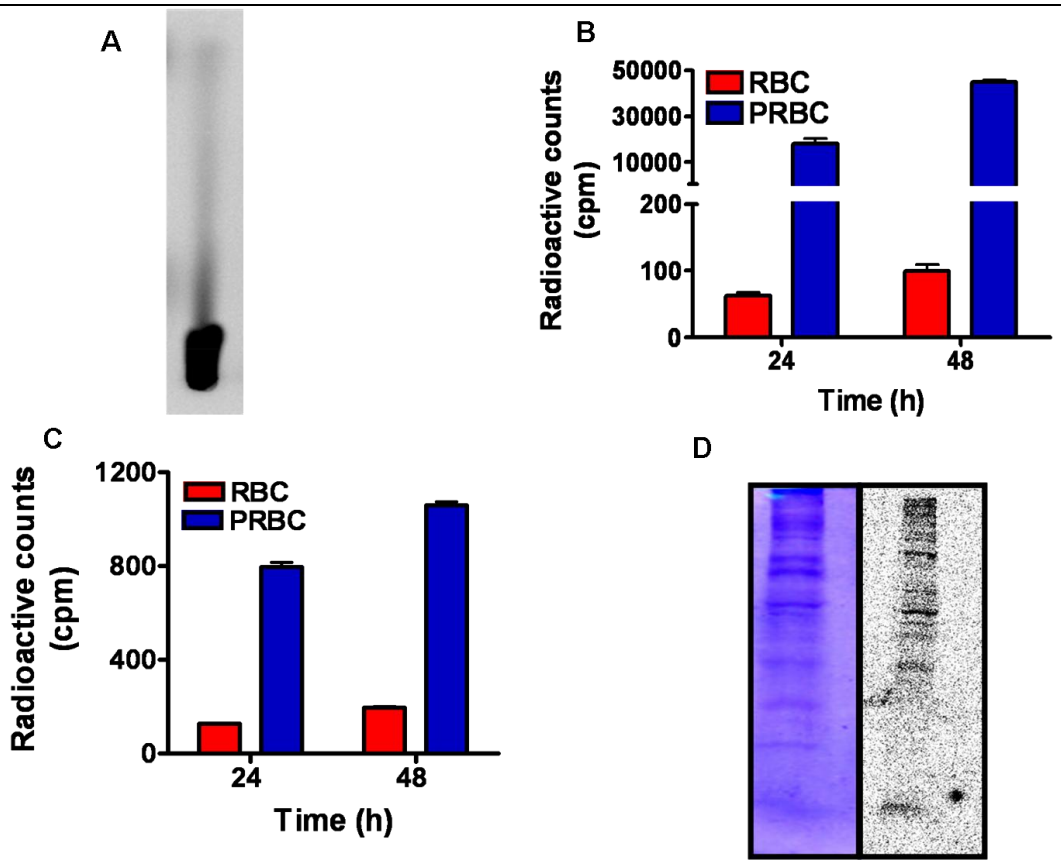

Fig. 4.2: U-[^{14}C]-aspartate incorporation in nucleic acids and proteins by parasitized erythrocytes.

(A) Radio-TLC of U-[^{14}C]-aspartate (200 mCi mmol^{-1}). (B) 8-[^{3}H]-hypoxanthine incorporation and (C) U-[^{14}C]-aspartate incorporation into nucleic acids by parasitized erythrocytes after 24 and 48 h incubation with the radioactive tracer. 1 μCi of 8-[^{3}H]-hypoxanthine or U-[^{14}C]-aspartate was added to parasitized erythrocytes (2 % hematocrit and 2 % parasitemia) and erythrocytes (2 % hematocrit) and incubated for 24 and 48 h. Cells were harvested onto glass fiber filters using a Combi-12 automated cell harvester (Molecular Devices, Sunnyvale, CA), washed extensively with distilled water and dried. The incorporated radioactivity was measured as counts per minute (cpm) using a Wallac 1409 (Wallac Oy, Turku, Finland) liquid scintillation counter. Experiments were done in duplicate and repeated thrice. (D) Parasitized erythrocytes were incubated with 1 μCi of U-[^{14}C]-aspartate for 24 h and were then treated with 0.15 % saponin solution to release parasites from the erythrocytes. The parasite pellet was washed 3-4 times in 1 X PBS and was resuspended in 1X SDS loading dye, boiled and loaded on a 10 % SDS-polyacrylamide gel. Following electrophoresis, the gel was stained with Coomassie Brilliant Blue and was dried and developed using a Fuji FLA 5000 phosphorimager.

^{14}C-aspartate incorporation in the pyrimidine bases has been shown earlier in *Plasmodium lophurae* by Walsh and Sherman (Walsh and Sherman, 1968) and thereby establishing the presence of *de novo* pyrimidine biosynthesis. The overall reaction of adenylosuccinate synthetase (ADSS) and adenylosuccinate lyase (ASL) involves the transfer of an α amino group from aspartate to the 6-oxo group of IMP to generate AMP, with the rest of the carbon skeleton of aspartate being released as fumarate. To check whether fumarate produced by this metabolic pathway is secreted by *P. falciparum* as a waste, erythrocytes and *P. falciparum* infected erythrocytes were incubated with U-[^{14}C] aspartate (1 µCi) for 24 h. Apart from being incorporated into proteins and nucleic acids, U-[^{14}C] aspartate should be converted to U-[^{14}C]-fumarate by the enzymatic action of ADSS and ASL (Fig. 4.3A). U-[^{14}C]-fumarate formed may be secreted out by parasitized erythrocytes if fumarate is a metabolic waste. Under the TLC conditions described, a mixture of [^{14}C]-aspartate and 2,3-[^{14}C]-fumarate could be separated (Fig. 4.3B). However, on examination of the spent medium of RBCs and PRBCs by TLC, a radioactive spot corresponding to the mobility of [^{14}C]-fumarate could not be observed (Fig. 4.3B). These results implicate that fumarate generated by the purine salvage pathway in *P. falciparum* is not secreted out in the medium and hence, is not a metabolic waste.

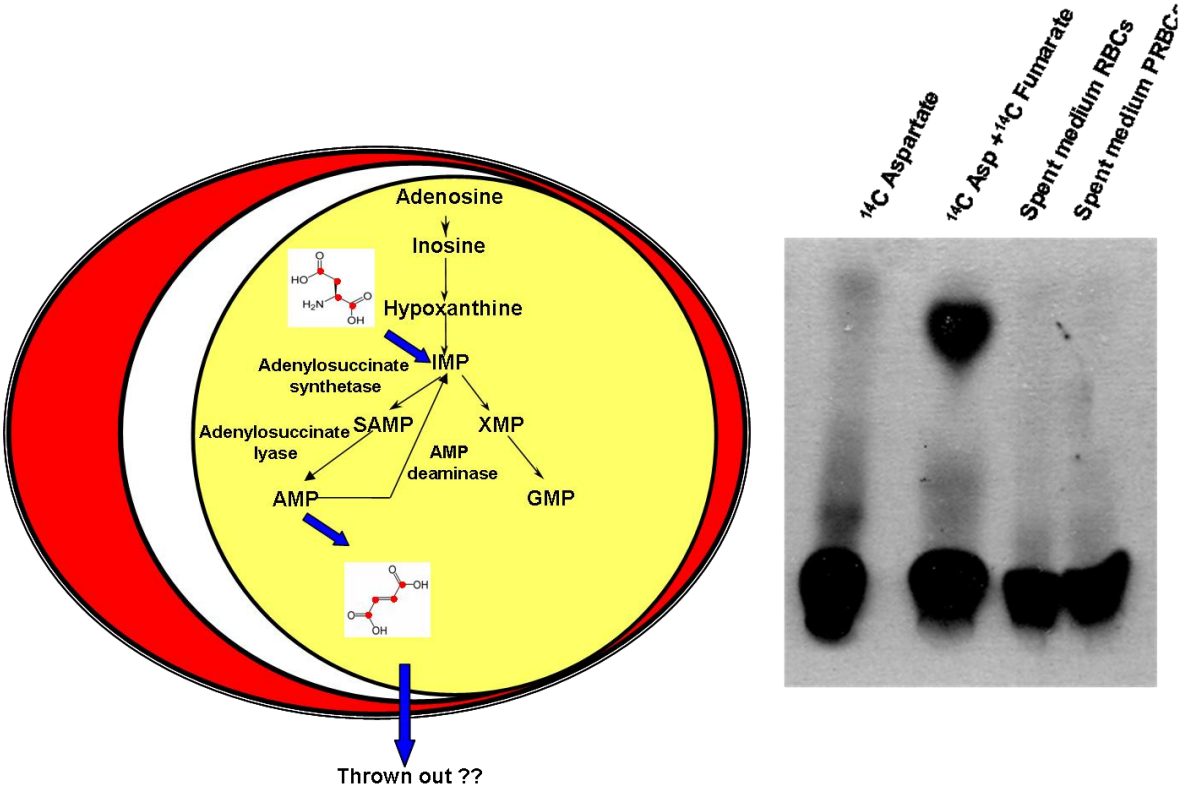

Fig. 4.3: Analysis of spent medium of parasitized erythrocytes incubated with U-[^{14}C]-aspartate.

(A) Schematic of purine salvage pathway in the intraerythrocytic P. falciparum in which a molecule of aspartate is utilized in the conversion of IMP to AMP. The carbon skeleton of U-[^{14}C]-aspartate (in which all the carbon atoms are enriched in ^{14}C and shown as red circles) is converted to U-[^{14}C]-fumarate in the parasite by the concerted actions of adenylosuccinate synthetase and adenylosuccinate lyase. Fumarate, if a metabolic waste for P. falciparum should be thrown out into the culture medium. (B) Radio-TLC analysis of the spent medium of erythrocytes (2 % hematocrit) and parasitized erythrocytes (2 % hematocrit and 8 % parasitemia) incubated with 1 μCi of U-[^{14}C]-aspartate for 24 h. U-[^{14}C]-aspartate and a mixture of U-[^{14}C]-aspartate and 2,3- [^{14}C]-fumarate were used as TLC markers. A solvent mixture of n-butanol, acetic acid and water in the ratio of 4:1:1 was used as the mobile phase for TLC. The silica-TLC plate was dried and developed using a Fuji FLA 5000 phosphorimager.

4.3.2 Putative metabolic fates of fumarate

Kyoto Encyclopedia of Genes and Genomes (KEGG) pathway database (Kanehisa and Goto, 2000) was examined for the different metabolic routes involved in the production and consumption of fumarate across all organisms. A large number of metabolic reactions generate fumarate (Fig. 4.4) while only a small number of reactions are involved in its consumption. *P. falciparum* genome does not encode enzymes for most of these reactions (highlighted as dotted arrows) and are hence, presumed to be absent.

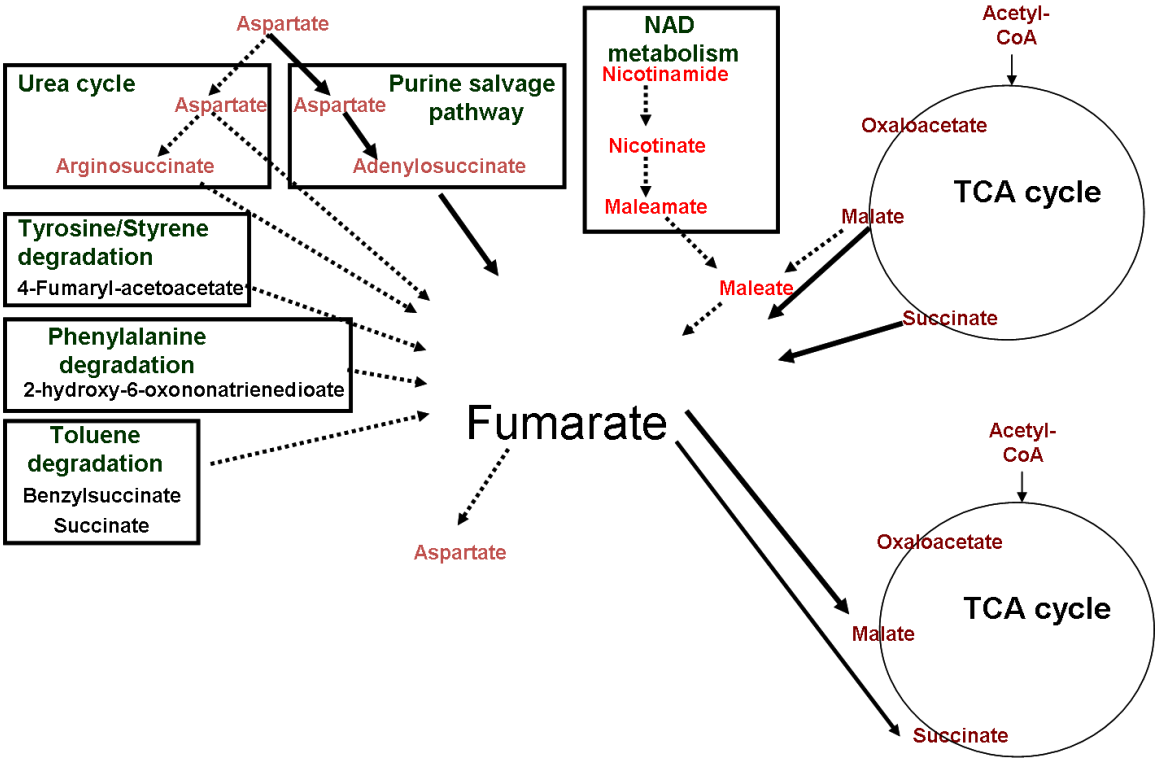

Fig. 4.4: Metabolic pathways involved in fumarate metabolism

Reactions involved in the generation and consumption of fumarate are obtained from KEGG pathway database (Kanehisa and Goto, 2000). Highlighted in dotted arrows are reactions that are expected to be absent in P. falciparum as genes encoding enzymes for these reactions are absent from the P. falciparum genome.

4.3.3 Parasitized erythrocytes incorporate 2,3-[^{14}C]-fumarate into their proteins and nucleic acids.

In a molecule of 2,3-[^{14}C]-fumarate, the second and third carbon atoms are enriched in ^{14}C. Prior to metabolic labeling of erythrocytes and parasitized erythrocytes, 2,3-[^{14}C]-fumarate was spotted and analyzed for radiochemical purity on a TLC silica gel 60 F_{254} plate (Merck, Germany). Under the conditions described for TLC in materials and methods, 2,3-[^{14}C]-fumarate showed predominantly a single spot (Fig. 4.5 A) with no other contaminating radioactive chemical.

To trace the metabolic fate of fumarate, RBCs and PRBCs were incubated with 2, 3-[^{14}C]-fumarate (1 µCi) for 24 and 48 h. Incorporation of radioactivity was seen in the nucleic acid fraction of PRBCs while control RBCs treated in a similar manner yielded low radioactive counts (Fig. 4.5B). Radioactive incorporation was also seen in the protein fraction of the PRBCs with almost all the protein bands obtained from the cell lysate being radiolabeled (Fig. 4.5 C).

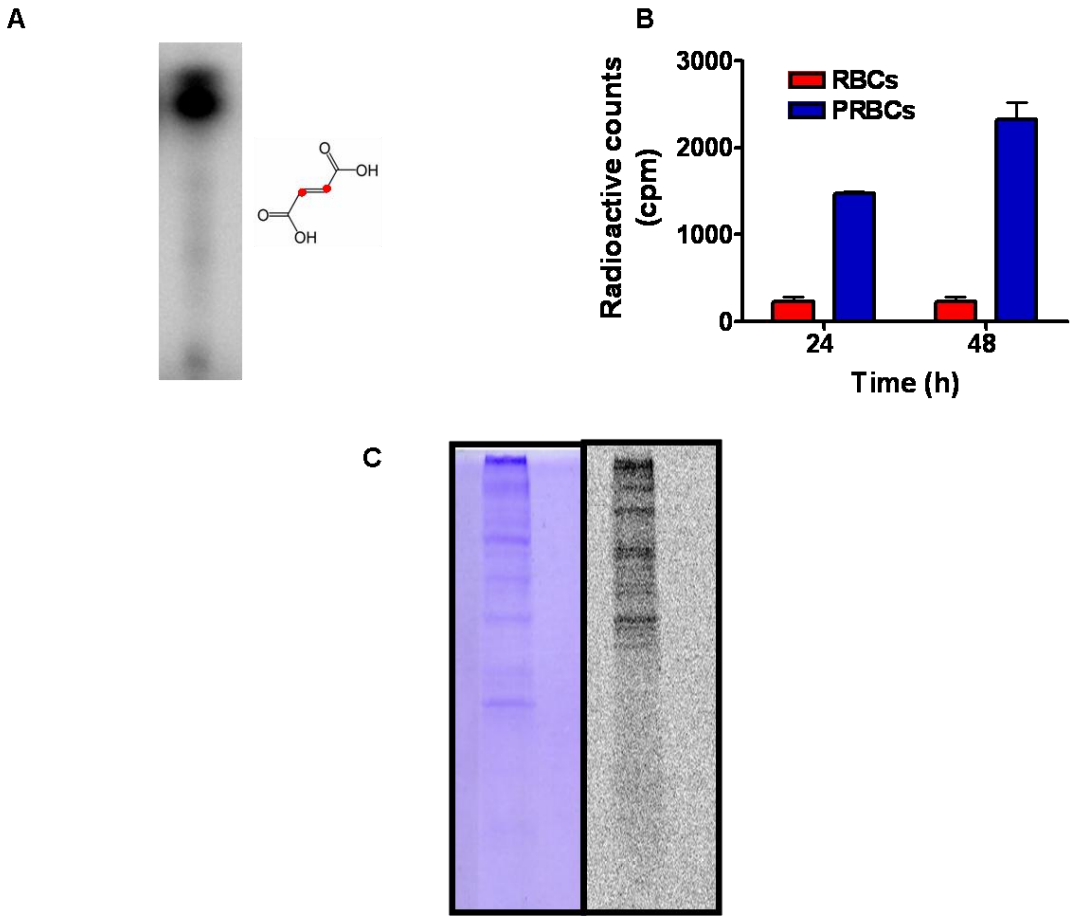

Fig. 4.5: 2,3-[^{14}C]-fumarate incorporation in nucleic acids and proteins by parasitized erythrocytes.

(A) Radio-TLC of 2,3-[^{14}C]-fumarate (10 mCi mmol^{-1}). (B) 2,3-[^{14}C]-fumarate incorporation by parasitized erythrocytes after incubation with the radioactive label for 24 and 48 h. 1 µCi of 2,3-[^{14}C]-fumarate was added to parasitized erythrocytes (2 % hematocrit and 2 % parasitemia) and erythrocytes (2 % hematocrit) and were incubated for 24 and 48 h. Cells were harvested onto glass fiber filters using a Combi-12 automated cell harvester, washed extensively with distilled water and dried. The incorporated radioactivity was measured as counts per minute (cpm) using a Wallac 1409 liquid scintillation counter. (D) Parasitized erythrocytes incubated with 1 µCi of 2,3-[^{14}C]-fumarate for 24 h were treated with 0.15 % saponin solution to release free parasites from erythrocytes. The parasite pellet was washed 3-4 times in 1 X PBS and was resuspended in 1X SDS loading dye, boiled and loaded on a 10 % SDS-polyacrylamide gel. Following electrophoresis, the gel was stained with Coomassie Brilliant Blue, dried and developed using a Fuji FLA 5000 phosphorimager.

4.3.4. 2,3-[^{14}C]-fumarate incorporation in protein and nucleic acid fractions by free parasites.

During the intraerythrocytic stages of *P. falciparum* life cycle, an extensive metabolic cross talk exists between the erythrocyte and the parasite. Thus, to implicate the exclusive role of parasite metabolism in the incorporation of 2,3-[^{14}C]-fumarate, metabolic labeling studies were done on free parasites released from erythrocytes. Here, the time of incubation was reduced to 8 h with the labels (2, 3-[^{14}C]-fumarate or U-[^{14}C]-aspartate) and radioactivity in the nucleic acids was counted as described above. A dose dependent increase in radioactive counts was obtained in the nucleic acid fractions (Fig. 4.6) implicating that parasite metabolism is sufficient for the incorporation 2,3-[^{14}C]-fumarate.

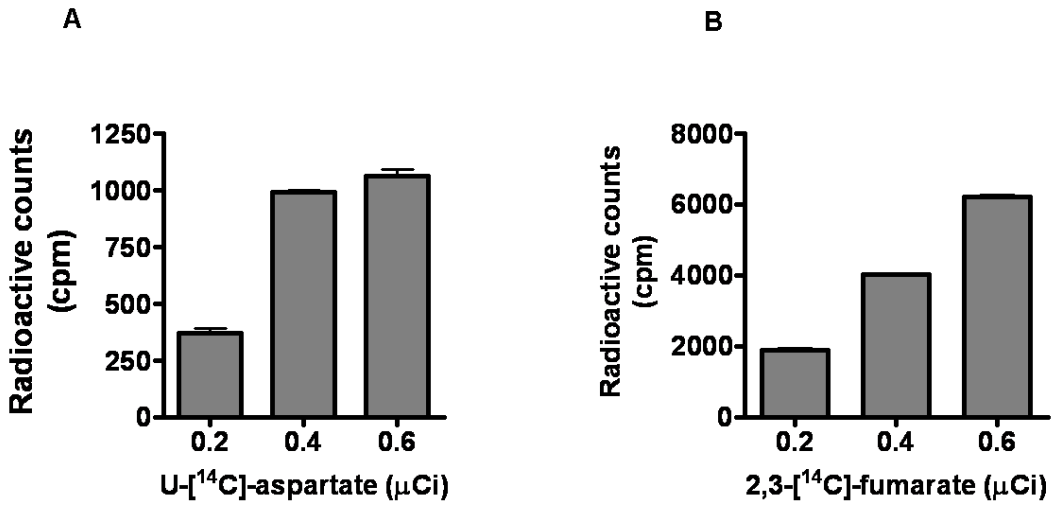

Fig. 4.6: Nucleic acid labeling of free *P. falciparum* parasites with ^{14}C-U-aspartate and 2,3-[^{14}C]-fumarate.

(A) U-[^{14}C]-aspartate and (B) 2,3-[^{14}C]-fumarate were added to saponin released free parasites (total protein: 2-3 mg ml $^{-1}$) and incubated in complete RPMI medium for 8 h. Cells were harvested onto glass fiber filters using a Combi-12 automated cell harvester washed extensively with distilled water and dried. The incorporated radioactivity was measured as counts per minute (cpm) using a Wallac 1409 liquid scintillation counter.

4.3.5. 2,3-[^{14}C]-fumarate incorporates into pyrimidines and not purines.

The incorporation of fumarate into the nucleic acids, DNA and RNA could be either through the nitrogenous base (purine or pyrimidine) or through the ribose moiety. If the incorporation is through the ribose group, then both purine and pyrimidine nucleotides would be labeled as the ribose sugar is common to them. However, if the incorporation is specifically through the nitrogenous base, then either purine or pyrimidine nucleotides would be labeled, but not both. In order to probe this, saponin released free parasites were labeled with 2,3-[^{14}C]-fumarate for 4 h. Following metabolite extraction as described in materials and methods, the samples were spiked with nucleotide monophosphate standards, which were then separated by ion-pair RP-HPLC (Fig. 4.7A). As controls, nucleotide labeling pattern was assessed in parasites incubated with 1 µCi each of 8-[^{3}H]-hypoxanthine and U-[^{14}C] aspartate. Free parasites incubated with 8-[^{3}H]-hypoxanthine showed radioactive labeling of the purines, GMP and AMP (Fig. 4.7B) while parasites treated with U-[^{14}C]-aspartate showed maximum radioactivity in the UMP fraction (Fig. 4.7C). Parasites incubated with 2,3-[^{14}C]-fumarate showed maximum radioactivity incorporation in UMP, followed by CMP with counts in GMP and AMP fractions being insignificant (Fig. 4.7D). These results indicate that fumarate incorporation into nucleic acids is not through the ribose moiety, but more specifically through the pyrimidine backbone.

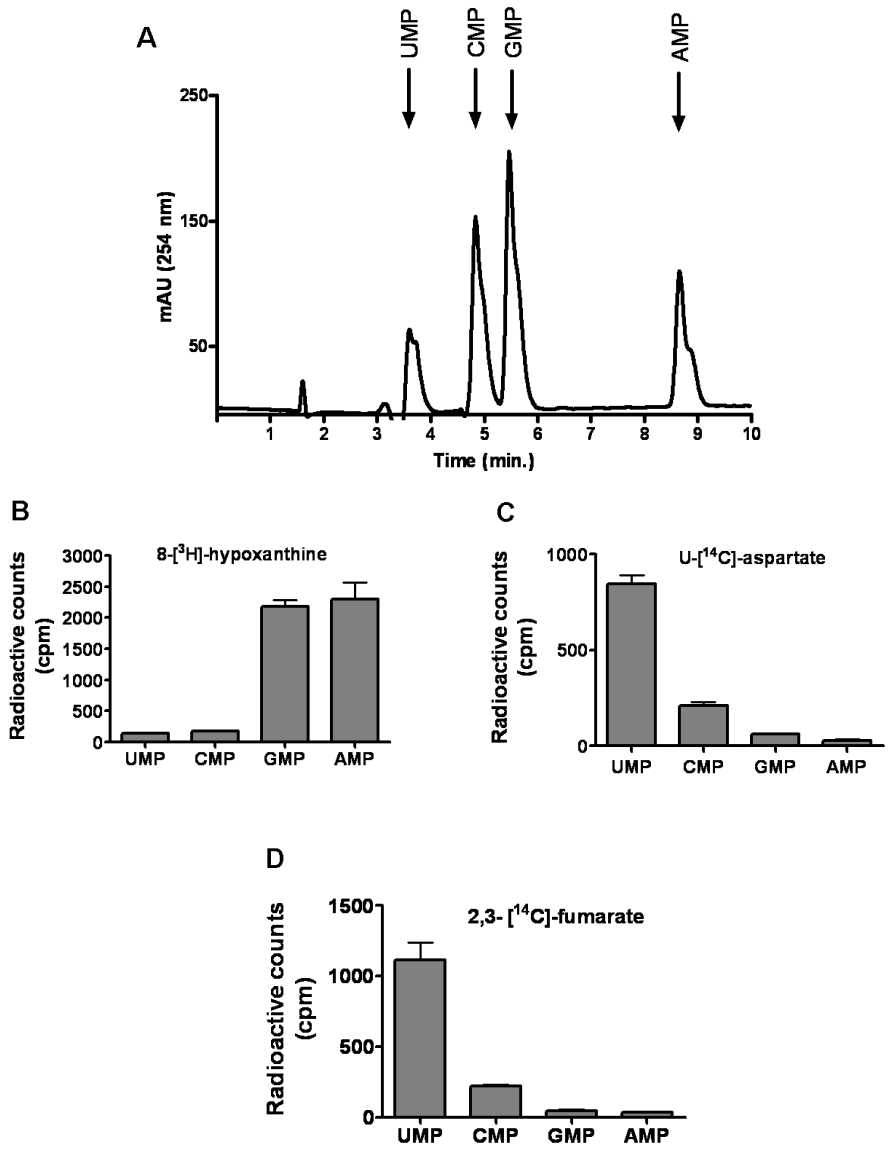

Fig. 4.7: Purine and pyrimidine nucleotide labeling in free parasites by 8-[^{3}H]-hypoxanthine, U-[^{14}C]-aspartate and 2,3-[^{14}C]-fumarate.

(A) Separation of pyrimidine (UMP and CMP) and purine (GMP and AMP) mononucleotides on C18-RP-HPLC. A mixture of nucleotide monophosphates was injected into the column and eluted with a linear gradient of solution B (30 % acetonitrile containing 8 mM tetrabutylammonium bisulfate and 100 mM KH_2PO_4 (pH 6.0)). Soluble metabolites were extracted from free parasites that were incubated with (B) 1 µCi of [^{3}H]-hypoxanthine, (C) 1 µCi of U-[^{14}C]-aspartate and (D) 1 µCi of 2,3-[^{14}C]-fumarate and were spiked with the nucleotide standards prior to HPLC. Peaks corresponding to the pyrimidine and purine nucleotide fractions were separately collected, concentrated and radioactivity incorporated was measured as counts per minute (cpm) using a Wallac 1409 liquid scintillation counter.

Studies on *P. falciparum* (Blum and Ginsberg, 1984), *P. knowlesi* (Sherman and Ting, 1968; Polet *et al.*, 1969) and *P. lophurae* (Sherman and Ting, 1966) have shown that the parasites fix free radiolabelled CO_2 into the amino acids glutamate and aspartate. The first step involving the fixation of CO_2 is mediated through the enzymatic action of carboxykinases (pyruvate carboxykinase or phosphoenolpyruvate carboxykinase) followed by the action of transaminases (alanine or aspartate transaminase). However, such a pathway is ruled out here because in the experiments reported here, 2,3-[^{14}C]-fumarate was used and not 1,4-[^{14}C]-fumarate (in which the carboxylic acid group carbons are labeled). Only 1,4-[^{14}C]-fumarate can give rise to $^{14}CO_2$ and not 2,3-[^{14}C]-fumarate and hence, such an indirect pathway for radioactive incorporation is ruled out. Thus, radioactivity incorporation in the protein and nucleic acid fractions of parasitized erythrocytes seen here is through a direct incorporation of the fumarate backbone.

4.3.6 Metabolic intermediates in fumarate metabolism

As aspartate forms the backbone of pyrimidines, we predicted that fumarate could be getting converted to aspartate prior to its incorporation in proteins and nucleic acids. Examination of the KEGG metabolic pathway database (Kanehisa and Goto, 2000) highlights two possible routes for the formation of aspartate from fumarate (Fig. 4.8A). The first includes the metabolic intermediates, malate and oxaloacetate while the second is a direct conversion of fumarate to aspartate catalyzed by the enzyme aspartase. To distinguish between these two pathways, nucleic acid labeling by 2,3-[^{14}C]-fumarate was done in the presence of 0.5 mM fumarate, malate, oxaloacetate and aspartate. If malate and oxaloacetate are not intermediates in the metabolism of fumarate to aspartate, and only a direct conversion operates in *P. falciparum*, then the presence of malate and

oxaloacetate should not dilute the radioactive counts arising from 2,3-[^{14}C]-fumarate incorporation. However, the radioactive counts in cultures incubated with both cold 0.5 mM fumarate/malate/ aspartate and 1 μCi of 2,3-[^{14}C]-fumarate dropped to nearly 30-50 % of the counts obtained in culture in which only 2,3-[^{14}C]-fumarate was added (Fig. 4.8B). The drop in radioactive counts could be because of the existence of a common pathway that metabolizes both the radioactive tracer (2,3-[^{14}C]-fumarate) and its corresponding unlabelled metabolite and further downstream metabolic intermediates or, alternately, the drop in counts could be because of their toxicity of the *P. falciparum* growth in the presence of these metabolic intermediates. To check this, 8-[^{3}H]-hypoxanthine labeling of nucleic acids was done in the presence or absence of these intermediates (Fig. 4.8C). As can be seen clearly, no difference in the % incorporation was observed across untreated and treated parasite cultures ruling out the toxicity of these intermediates on *P. falciparum* growth and thus, supporting the existence of a common pathway for the metabolism of ^{14}C-fumarate, malate and oxaloacetate.

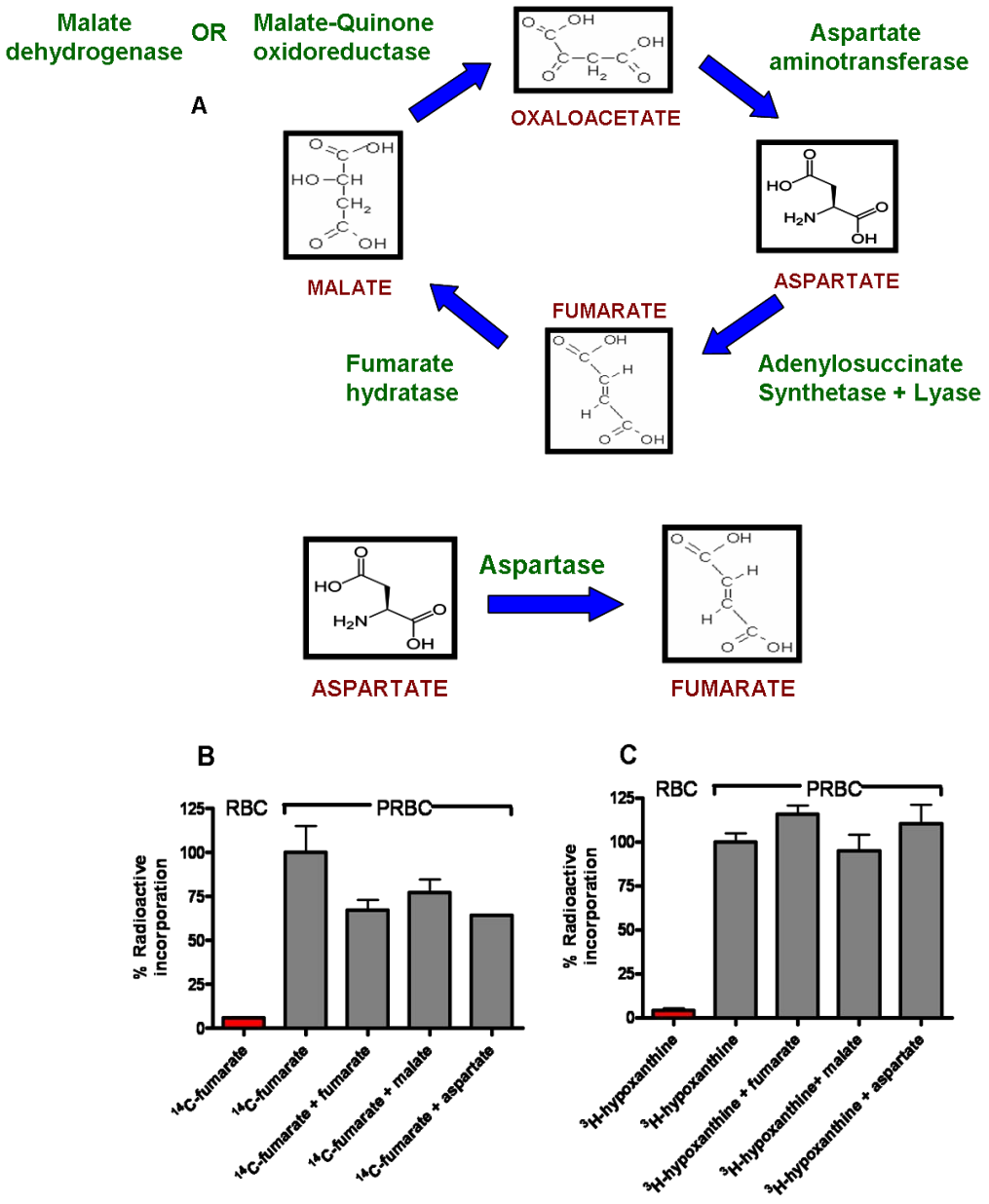

Fig. 4.8: ^{14}C-2,3-fumarate dilution by fumarate, malate and aspartate

(A) Two putative metabolic routes for the conversion of fumarate to aspartate. (B) ^{14}C-2,3-fumarate incorporation by parasitized erythrocytes in the presence or absence of 0.5 mM fumarate, malate and aspartate. (C) [^{3}H]-hypoxanthine incorporation by parasitized erythrocytes in the presence or absence of 0.5 mM fumarate, malate and aspartate.

4.3.7 ^{13}C-NMR analysis of free parasites incubated with 1-[^{13}C]-glucose

A study by Lian *et al.* showed that when free parasites were incubated with 1-^{13}C-glucose; glycerol, pyruvate, lactate and alanine were enriched in ^{13}C (Lian *et al.*, 2009). However, apart from pyruvate and lactate, no other organic acids were found to be enriched. This study therefore, supported the earlier observations by Bryant *et al.*, in which, U-^{14}C-glucose failed to label significantly any TCA cycle intermediates in *P. falciparum* parasites (Bryant *et al.*, 1964).

Prior to experiments with ^{13}C-2,3-fumarate, ^{13}C-NMR spectra were recorded on lysates of free parasites incubated with 1-^{13}C-glucose. This was done to ensure that the process of isolation of free parasites from parasitized erythrocytes does not alter the metabolic activity of the parasites. Standard ^{13}C-NMR spectra for 1-[^{13}C]-glucose and lactate are shown (Fig. 4.9 A & B). In solution, glucose exists in two different isoforms, α and β based on the position of hydroxyl group at C-1 of glucose. In α isoform, the hydroxyl group is below the plane of the ring while in β, it is above the plane of the ring. This process of interconversion is called mutarotation and the C-1 of glucose is called the anomeric carbon atom. Due to these two forms, there are two different chemical shifts for the anomeric carbon atom (for α isoform, C-1 chemical shift: 93 ppm and for β isoform, C-1 chemical shift: 97 ppm). The glucose used in the experiments here is 1-^{13}C-glucose in which, the anomeric carbon is enriched for ^{13}C (> 99 atom % ^{13}C). NMR spectra of the standard solution of 1-^{13}C-glucose show these two chemical shift resonances.

A

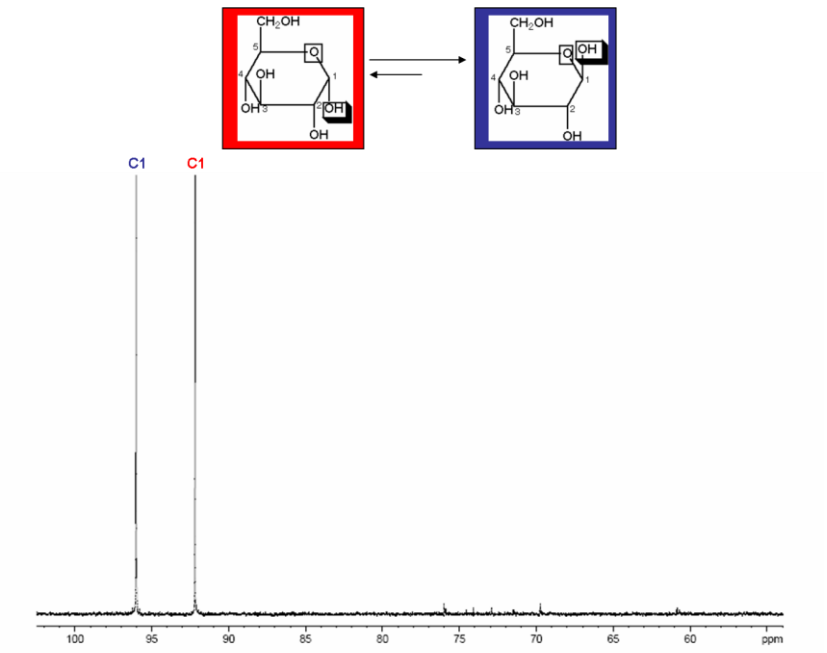

B

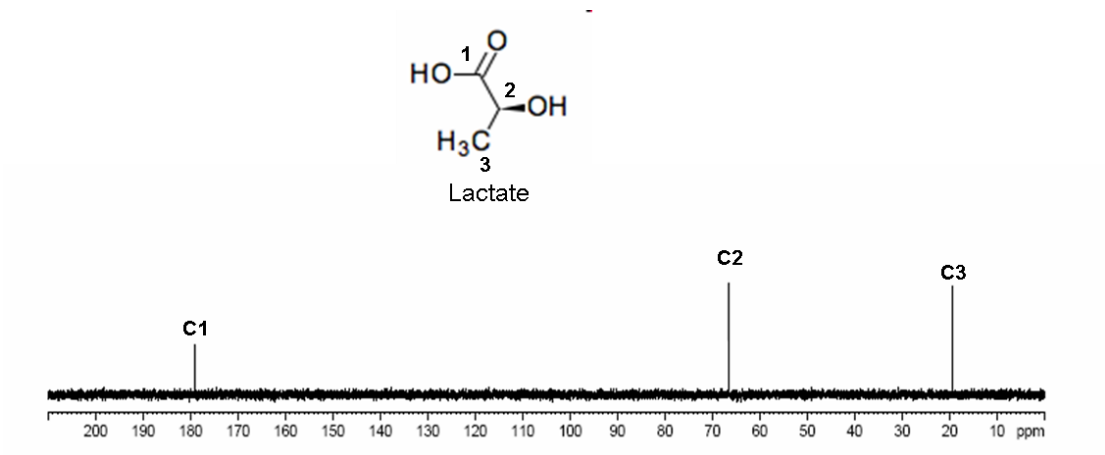

Fig. 4.9: Carbon-13 proton decoupled NMR spectra

(A) ^{13}C-proton decoupled NMR spectrum of 1-^{13}C-glucose. The interconversion between α (red) and β (blue) anomers of glucose is shown. Chemical shifts of C-1 of α and β anomers of glucose are 93 and 97 ppm respectively. (B) ^{13}C-proton decoupled NMR spectrum of lactate. Chemical shifts of C-1, C-2 and C-3 of lactate are 180 ppm, 69 ppm and 20 ppm, respectively.

Erythrocytes incubated with 25 mM 1-^{13}C-glucose for 2 h showed formation of 3-^{13}C-lactate (Fig. 4.10 A) while free parasites showed the additional formation of 3-^{13}C-pyruvate and 3-^{13}C-glycerol (Fig. 4.10 B). The formation of glycerol was also observed by Lian *et al.* (Lian *et al.*, 2009) and it was proposed to be formed through glycerol-3-phosphate. The enrichment of the third carbon of lactate, pyruvate and glycerol from 1-^{13}C-glucose could be explained from the glycolytic pathway as outlined in Fig. 4.10C. As can be seen, no TCA cycle intermediates were enriched in ^{13}C indicating again the discontinuity of glycolysis from the TCA cycle in *P. falciparum*.

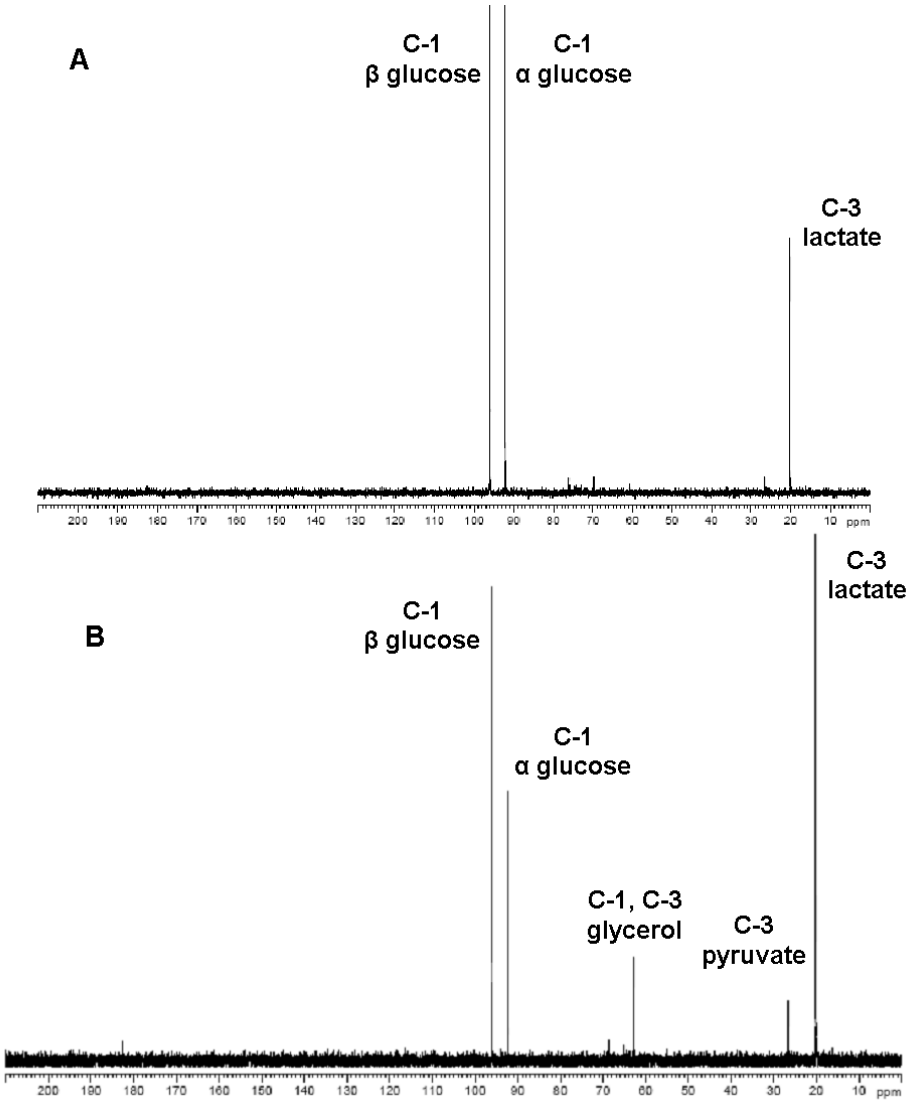

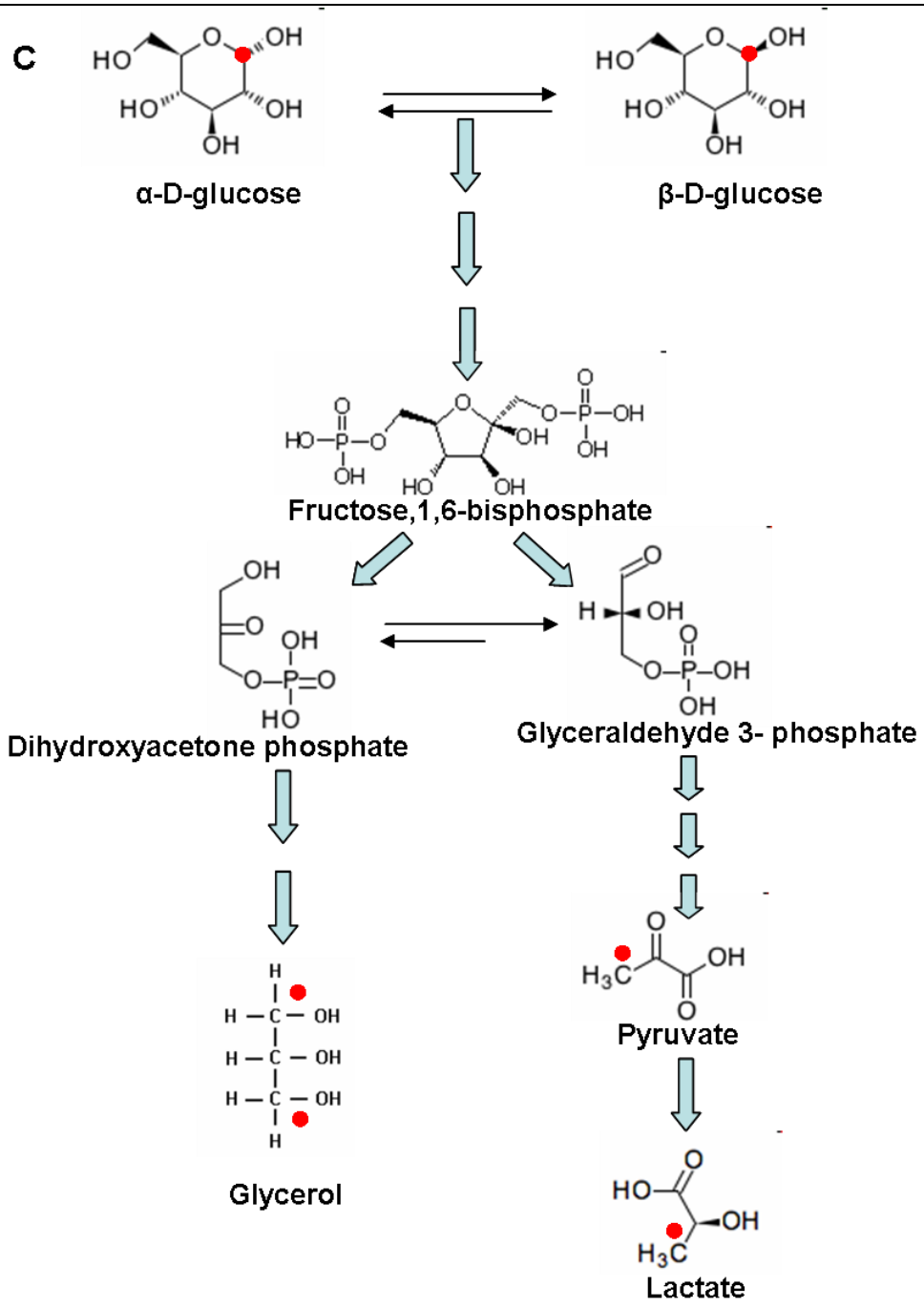

Fig. 4.10: Metabolism of 1-[^{13}C]-glucose in erythrocytes and *P. falciparum* parasites

(A) Erythrocytes and (B) free parasites incubated with 25 mM of 1-[^{13}C]-glucose in 1 X PBS at 37 ºC for 2 h. Cell suspension was lysed and processed as described. D_2O was added to a final concentration of 10 % of the cell lysate and NMR spectra recorded. (C) Glucose metabolism in P. falciparum

4.3.8 Malate is a metabolic intermediate in fumarate metabolism to aspartate

To further confirm the nature of the intermediary metabolites and thereby, to establish the pathway of fumarate metabolism, free parasites were incubated with 10 mM of ^{13}C-2,3-fumarate for 2 h in 1 X PBS. Further, ^{13}C-NMR of standard solutions of fumarate, malate, aspartate, succinate and glutamate were acquired (Fig. 4.11 A-E). These spectra were used as reference spectra to assign the peaks in the cell suspensions.

A

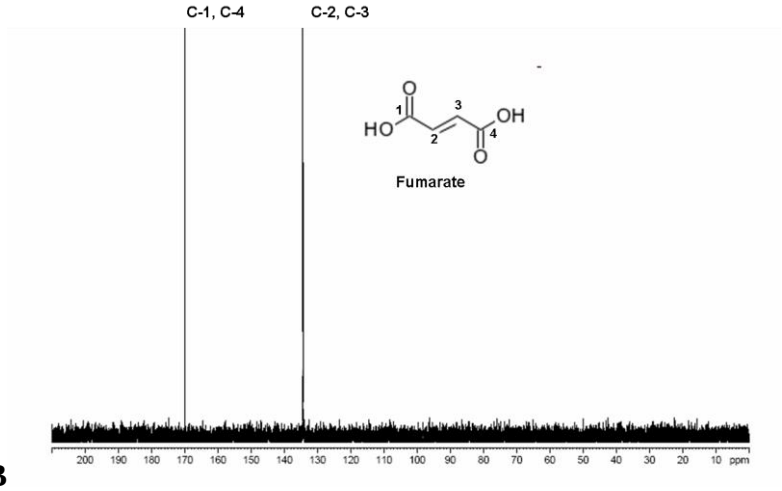

B

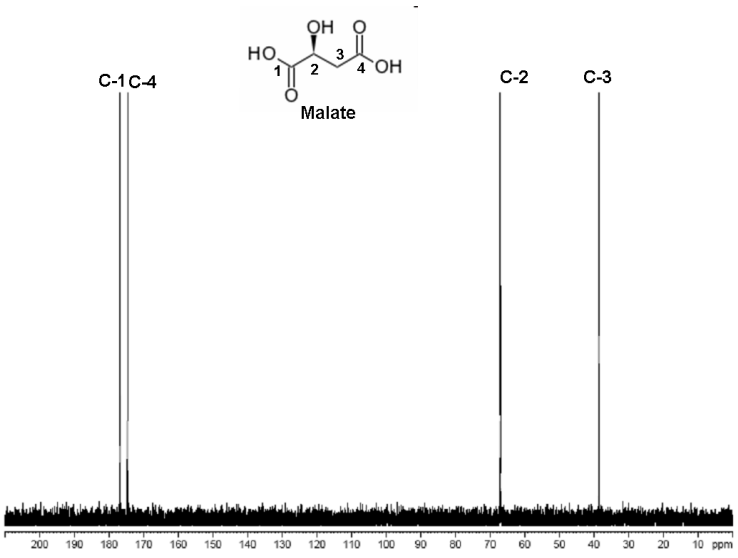

C

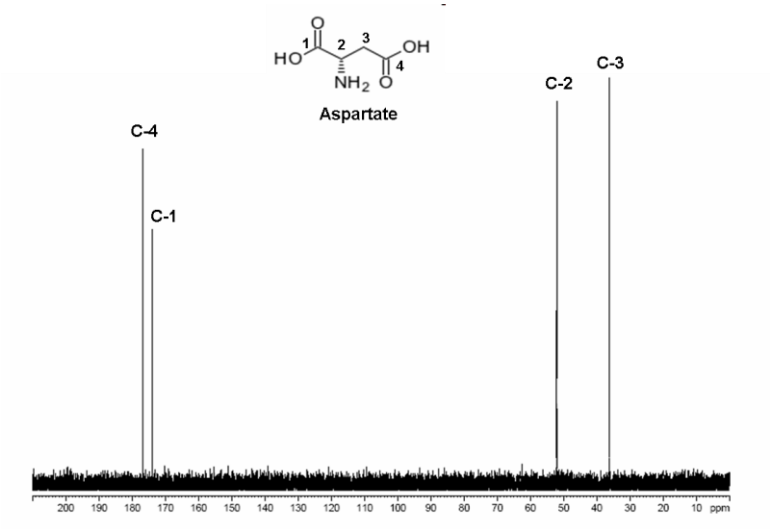
Aspartate
C-4
C-1
C-2
C-3
200 190 180 170 160 150 140 130 120 110 100 90 80 70 60 50 40 30 20 10 ppm

D

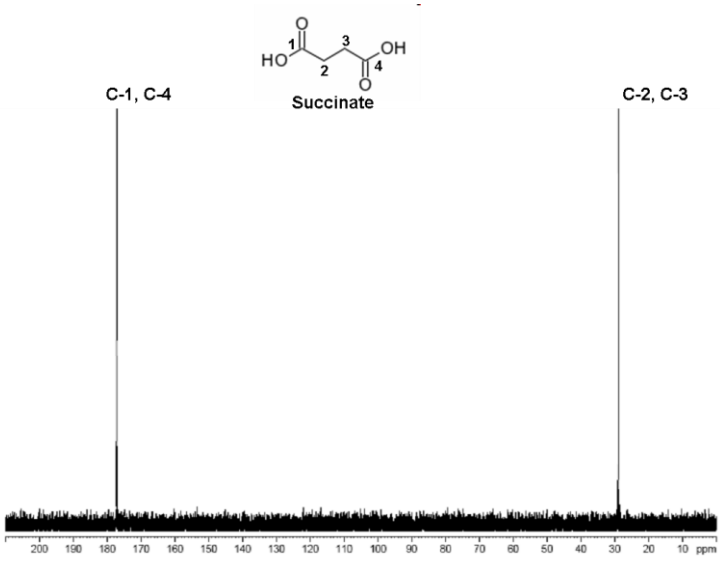
Succinate
C-1, C-4
C-2, C-3
200 190 180 170 160 150 140 130 120 110 100 90 80 70 60 50 40 30 20 10 ppm

E

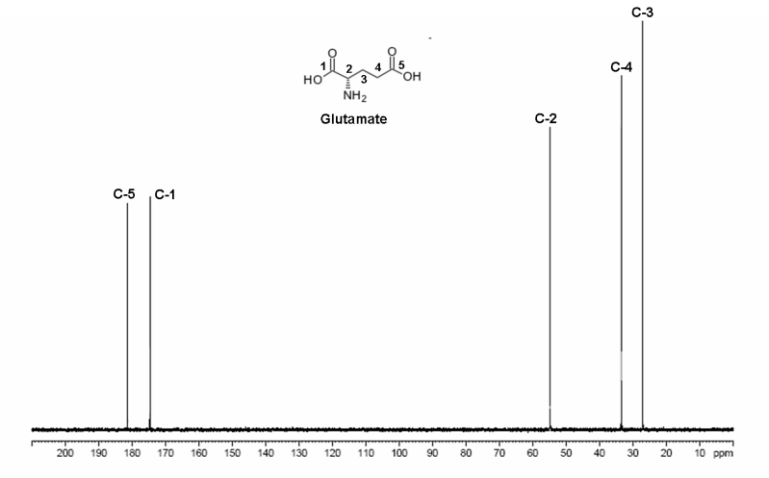

Fig. 4.11: Standard carbon-13 proton decoupled NMR spectra

(A) Fumarate; (B) Malate; (C) Aspartate; (D) Succinate and (E) Glutamate. Stock solutions were dissolved in water containing 10 % D_2O.

^{13}C proton decoupled NMR spectra of free parasites incubated with 10 mM of ^{13}C-2,3-fumarate for 2 h in 1 X PBS showed a peak at 135 ppm corresponding to the 2,3-carbon atoms of ^{13}C-2,3-fumarate. The other dominant peaks were found at 70 ppm and 42 ppm, which correspond to C-2 and C-3 of malate, respectively. In addition to these, peaks arising from aspartate (C-2: δ = 52 ppm and C-3: δ = 36 ppm), pyruvate (C-2: δ = 206 ppm and C-3: δ = 26 ppm) and lactate (C-2: δ = 69 ppm and C-3: δ = 20 ppm) were also detected. On the other hand, erythrocytes incubated with 10 mM of ^{13}C-2,3-fumarate showed only the presence of malate and lactate (C-2: δ = 69 ppm and C-3: δ = 20 ppm) (Fig. 4.12). These observations support the existence of a metabolic pathway for the conversion of fumarate to aspartate through malate in the free parasites. The doublet nature of the peak resonances of malate, aspartate, pyruvate and lactate is a confirmation that these intermediates are formed from 2,3-^{13}C-fumarate.

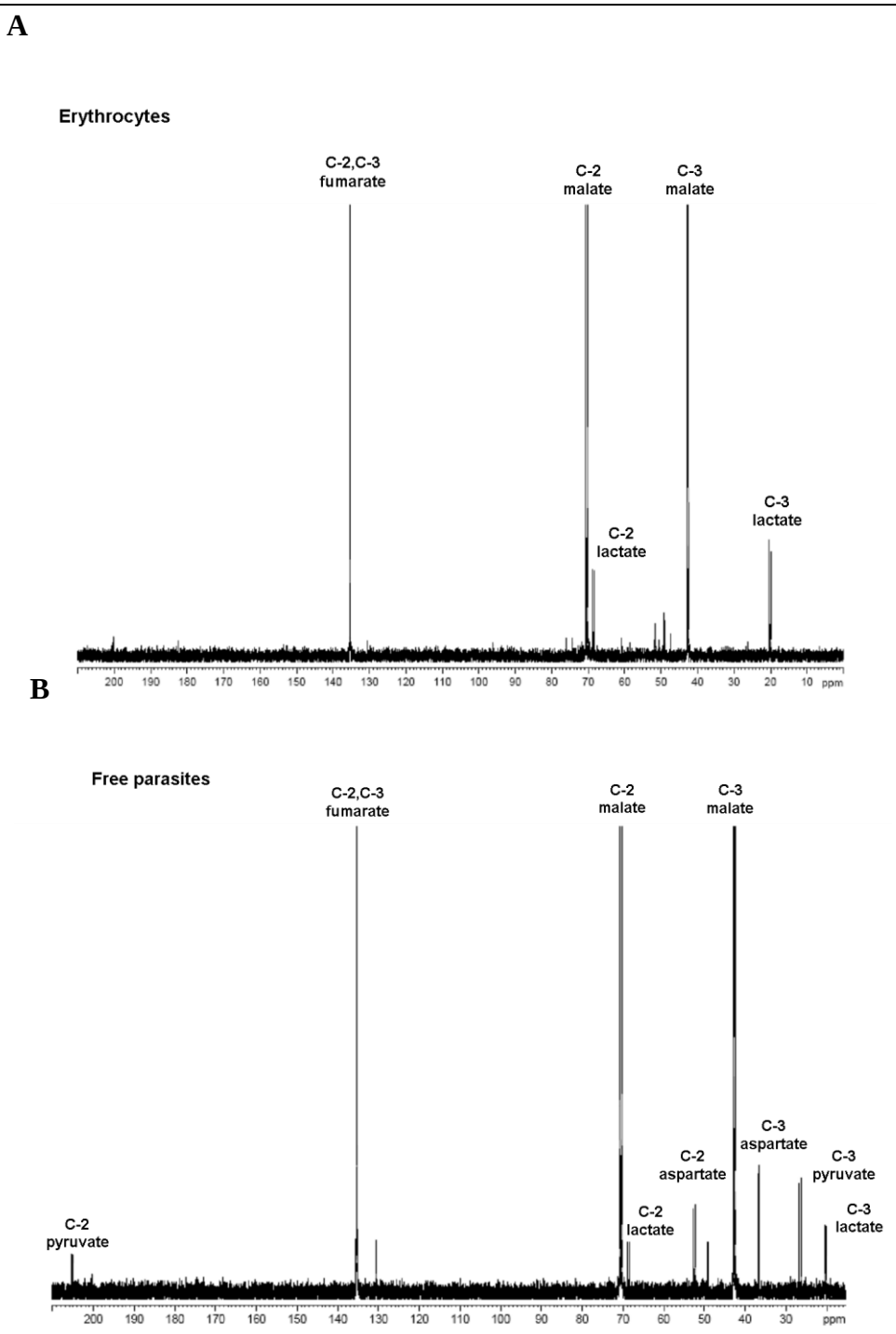

Fig. 4.12: ^{13}C-2,3-fumarate metabolism in erythrocytes and parasites

(A) Erythrocytes and (B) free parasites incubated with 10 mM of 2,3-[^{13}C]-fumarate in 1 X PBS at 37 ºC for 2 h. Cell suspension was lysed and processed as described. D_2O was added to a final concentration of 10 % to the cell lysate and NMR spectra recorded.

Enzymes catalyzing the conversion of fumarate to aspartate are fumarate hydratase, malate dehydrogenase or malate-quinone oxidoreductase and aspartate aminotransferase. *P. falciparum* genome contains homologues of all these enzymes. Except malate dehydrogenase, the biochemical characterization and subcellular localization of the other enzymes is unknown and needs investigation.

4.3.9 Fumarate hydratase activity is localized to the mitochondria

Fumarate hydratase is an enzyme that catalyzes the reversible conversion of fumarate to malate. Free parasites were treated with increasing concentrations of digitonin to prepare distinct cytosolic and organellar protein fractions. Digitonin is a non-ionic detergent used to solubilize cellular and organellar membranes. At lower concentrations of digitonin, cell membrane is permeabilized and cytosolic proteins are released whereas at higher concentrations, the organellar and nuclear membranes are solubilized and organellar extracts can be obtained. It has been shown that PfMDH is cytosolic (Lang-Unnasch, 1992; Pradhan *et al.*, 2009). Digitonin concentration required to fully release cytoplasmic proteins in free plasmodium parasites was obtained by using antisera against the cytoplasmic marker protein, malate dehydrogenase. Pf MDH protein purification and antisera generation in the rabbit is described in the appendix at the end of the chapter. On the other hand, antisera against *P. falciparum* Heat Shock Protein 60 (Pf HSP 60) (a kind gift from Prof. G. Padmanabhan, Indian Institute of Science, Bangalore, India) were used as mitochondrial marker. From Western blotting analysis, the values for digitonin concentration for selective permeabilization of cytosolic and organellar membranes were found to be 0.17 mM and 3.5 mM respectively (Fig. 4.13A).

The digitonin extracts were probed for Pf fumarate hydratase (PfFH) through its enzymatic activity for formation of ^{14}C-malate from ^{14}C-fumarate. Porcine heart fumarase (Sigma Chemical Co., St. Louis, USA) was used as a positive control. PfFH activity was found to be more in the cell extracts obtained by permeabilization with the higher digitonin concentrations (Fig. 4.13B). This indicates that PfFH is not cytosolic, but probably mitochondrial. In support of this, PfFH sequence upon analysis by MitoProt II 1.0a4 program (Claros and Vincens, 1996) yields a high probability value of 0.89 for it being targeted to the mitochondrion (Fig. 4.13C).

A

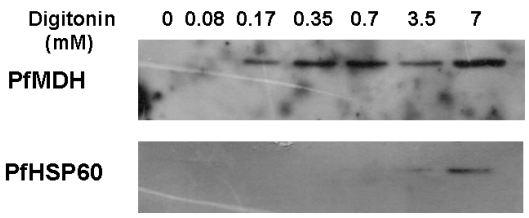

B

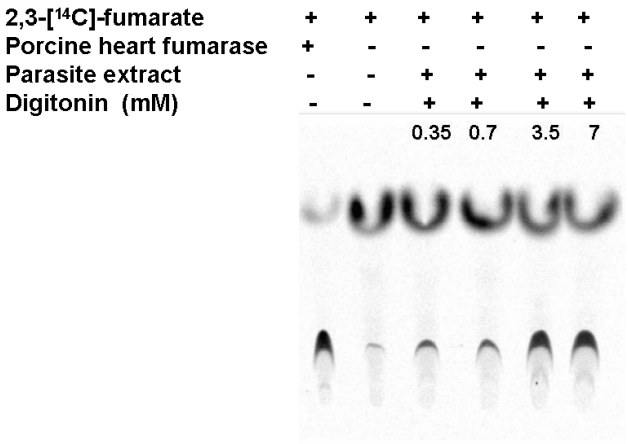

C

Enzyme	Probability of mitochondrial localization
Adenylosuccinate synthetase	0.0954
Adenylosuccinate lyase	0.0427
Fumarate hydratase	0.8939

Fig. 4.13: Fumarate hydratase activity in cytosolic and mitochondrial fractions of *P. falciparum*

(A) Western blotting of the different subcellular fractions of P. falciparum parasites obtained with increasing concentrations of digitonin with anti-PfMDH and anti-PfHsp60 antisera. (B) Radio-TLC analysis for fumarate hydratase activity in different parasite cellular fractions obtained by digitonin treatment. Activity was assessed by the formation of ^{14}C-malate from 2,3-[^{14}C]-fumarate. The mobile phase consisted of 4:1:1 mixture of n-butanol, acetic acid and water. (C) MitoProt II (1.0a4 program) (Claros and Vincens, 1996) analysis of P. falciparum adenylosuccinate synthetase, adenylosuccinate lyase and fumarate hydratase protein sequences.

4.3.10 Malate quinone oxidoreductase and not malate dehydrogenase catalyzes the conversion of malate to oxaloacetate

The conversion of malate to oxaloacetate can be mediated through malate dehydrogenase (MDH) or through another dehydrogenase, malate quinone oxidoreductase (MQO). *P. falciparum* genome contains a single copy of malate dehydrogenase, which has been shown to be localized in the cytosol (Lang-Unnasch, 1992; Pradhan *et al.*, 2009). At the physiological pH, recombinant PfMDH was unable to catalyze the oxidation of malate to oxaloacetate, but exhibited high activity in the reduction of oxaloacetate to malate (Tripathi *et al.*, 2004). Malate oxidation however, could be observed at pH > 9.5 and only with high concentrations of malate. These observations indicate that PfMDH has a preferential bias for the reduction of oxaloacetate rather than oxidation of malate.

MQO catalyses the conversion of malate to OAA using CoQ as the electron acceptor. MQO was originally identified in *Corynebacterium glutamicum* and subsequently reported in several other bacteria (Molenaar *et al.*, 2000). A functional annotation for MQO is present in the *P. falciparum* genome (Gardner *et al.*, 2002), which has also been subsequently shown to be expressed in the intraerythrocytic stages of *P. falciparum* (Tripathi *et al.*, 2004). Thus, PfMQO could provide an alternate route for the oxidation of malate to oxaloacetate.

MQO generates reduced coenzyme Q ($CoQH_2$), from coenzyme Q (CoQ) along with the oxidation of malate to oxaloacetate. $CoQH_2$ is then oxidized directly by complex III and the reducing equivalents are transferred to cytochrome C. Atovaquone is a

specific and a potent inhibitor of the enzymatic activity of *P. falciparum* complex III (Mather *et al.*, 2005) and thus, treatment of *P. falciparum* parasites should lead to a depletion of CoQ. It was therefore, of interest to examine the effect (if any) of this depletion on the conversion of 2,3-^{13}C-fumarate to aspartate. For this, free parasites were treated with 1 μM of atovaquone (~1000 times the IC_{50} value) for 2 h and were then pulsed with 10 mM of 2,3-^{13}C-fumarate. While control parasites showed ^{13}C-enrichment in aspartate (peak resonances at 52 and 36 ppm), atovaquone treated parasites did not show the same (Fig. 4.14). ^{13}C-enrichment in malate was unaffected across control and atovaquone treated parasites, which was quite expected as fumarate hydratase activity will be unaltered by atovaquone.

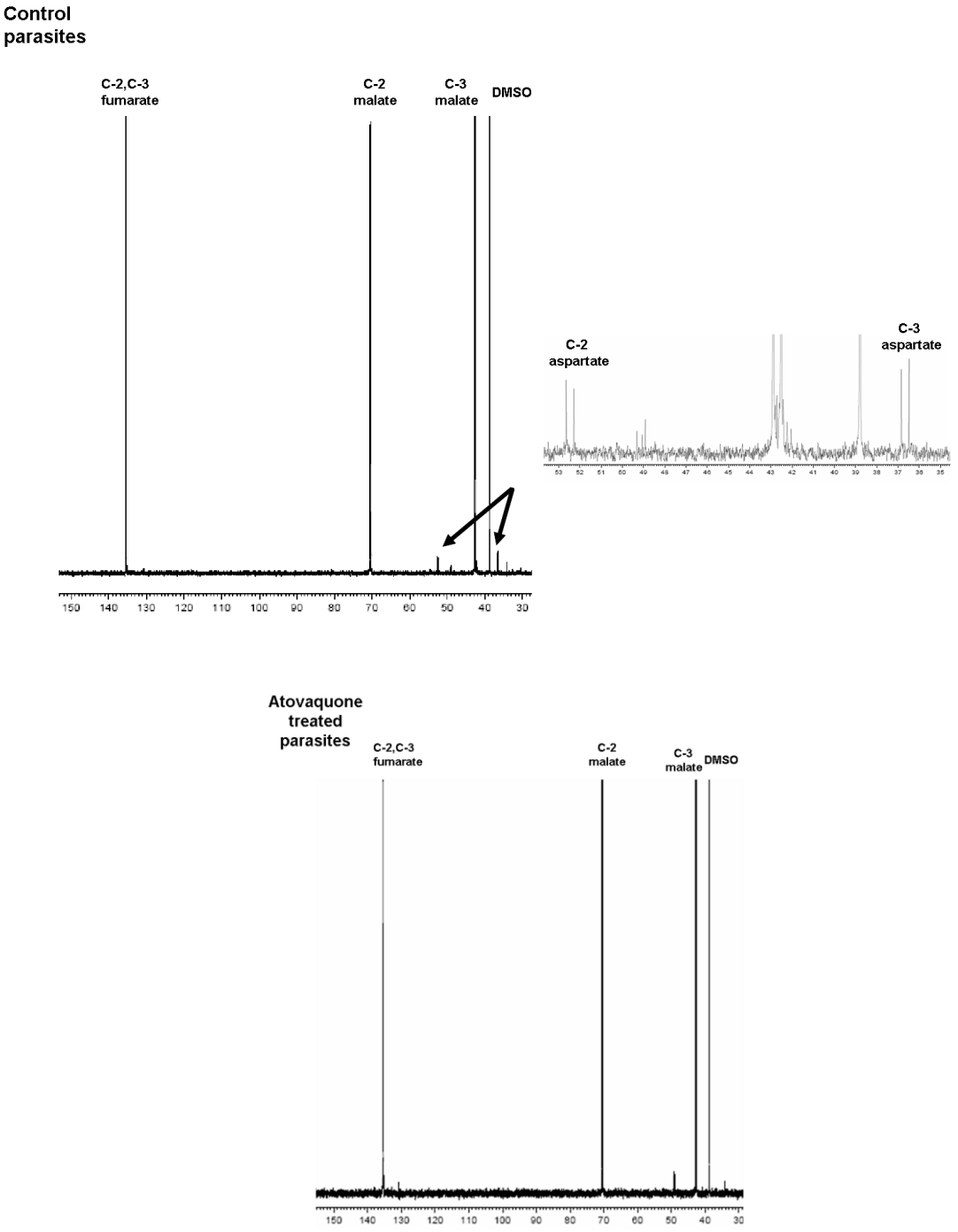

Fig. 4.14: Atovaquone treatment inhibits the formation of aspartate

Free parasites were untreated (control) or treated with 1 μM of atovaquone for 2 h and were then pulsed with 10 mM of 2,3-[^{13}C]-fumarate for 2 h. Following incubation, the parasites were processed as described in materials and methods section. The region from 35-55 ppm has been blown up in the NMR spectra of the control parasites to show the formation of 2,3-[^{13}C]-aspartate.

4.3.11 *P. falciparum* aspartate aminotransferase is cytoplasmic and catalyzes the reversible conversion of oxaloacetate to aspartate

PfAAT was expressed and purified as a C-terminal hexahistidine tagged protein through Ni-NTA affinity and gel permeation chromatography. The purified protein showed a single band with a molecular mass of around 50 kDa (Fig. 4.15A). PfAAT was used to generate anti-PfAAT antisera in mice as described in materials and methods. Antisera were then characterized for the specificity against PfAAT. Purified PfAAT was serially diluted (1 µg, 0.5 µg and 0.25 µg) and loaded on a 10 % SDS-PAGE for western blot analysis with anti-PfAAT antisera used at a dilution of 1:5000 (Fig. 4.15B).

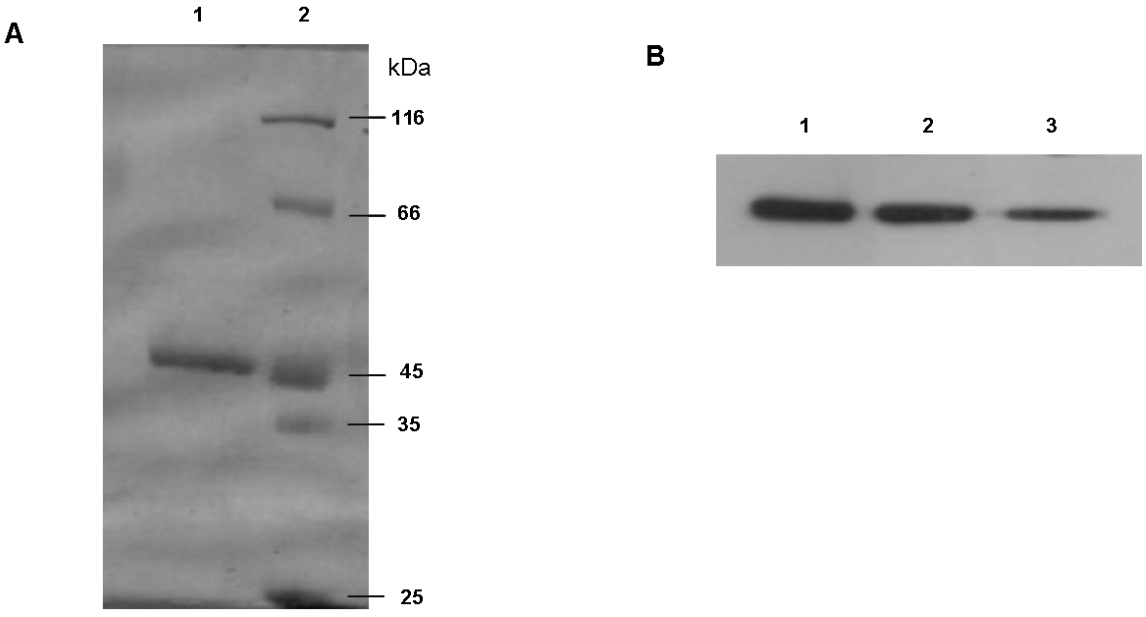

Fig. 4.15: Expression, purification and antibody characterization for PfAAT

(A) SDS-PAGE analysis of PfAAT purification. Recombinant PfAAT was purified from bacterial lysate by Ni-NTA affinity chromatography followed by gel filtration chromatography. Lane 1, Protein fraction eluted from sephacryl S-200 gel filtration column. Lane 2, Protein molecular weight marker; (B) Western blot analysis of PfAAT with anti-PfAAT antisera used at a dilution of 1:5000. Lanes 1-3, recombinant PfAAT in varying amounts (1-0.25 µg).

Previously, cloning, expression and substrate specificity studies on the recombinant PfAAT revealed that the enzyme catalyzes the transamination of α-ketomethylthiobutyrate to generate methionine (Berger *et al.*, 2001). This study reported the expression of PfAAT in BL21DE3 RIL strain of *E.coli*. The authors mention that the yield of the protein was very low and it was proposed that PfAAT might probably be toxic for the host bacterium. For expressing PfAAT, C41DE3 strain of *E. coli* has been used here that gave very high yield of the protein.

The authors speculated that this enzyme has an important role in methionine recycling. However, the subcellular localization of this enzyme was not known. Western blotting analysis on digitonin extracts show that PfAAT is localized to the cytoplasmic fractions of *P. falciparum* (Fig. 4.16 A). This was further confirmed by confocal microscopy (Fig. 4.16 B) in which, PfHSP 60 was used as a mitochondrial marker.

Previously, K_m and k_{cat} values for the conversion of α-ketoglutarate to glutamate by PfAAT were reported by Berger *et al.*, (Berger *et al.*, 2001). The K_m for aspartate was found out to be 6 mM when α-ketoglutarate was used at a concentration of 10 mM. However, it was not known whether the enzyme could catalyze the reverse reaction of oxaloacetate to aspartate. Hence, recombinant purified PfAAT was characterized for its ability to catalyze the conversion of oxaloacetate to aspartate. As can be seen in Table 4.1, the enzyme has got similar propensity to catalyze the reaction in both the forward and reverse reactions.

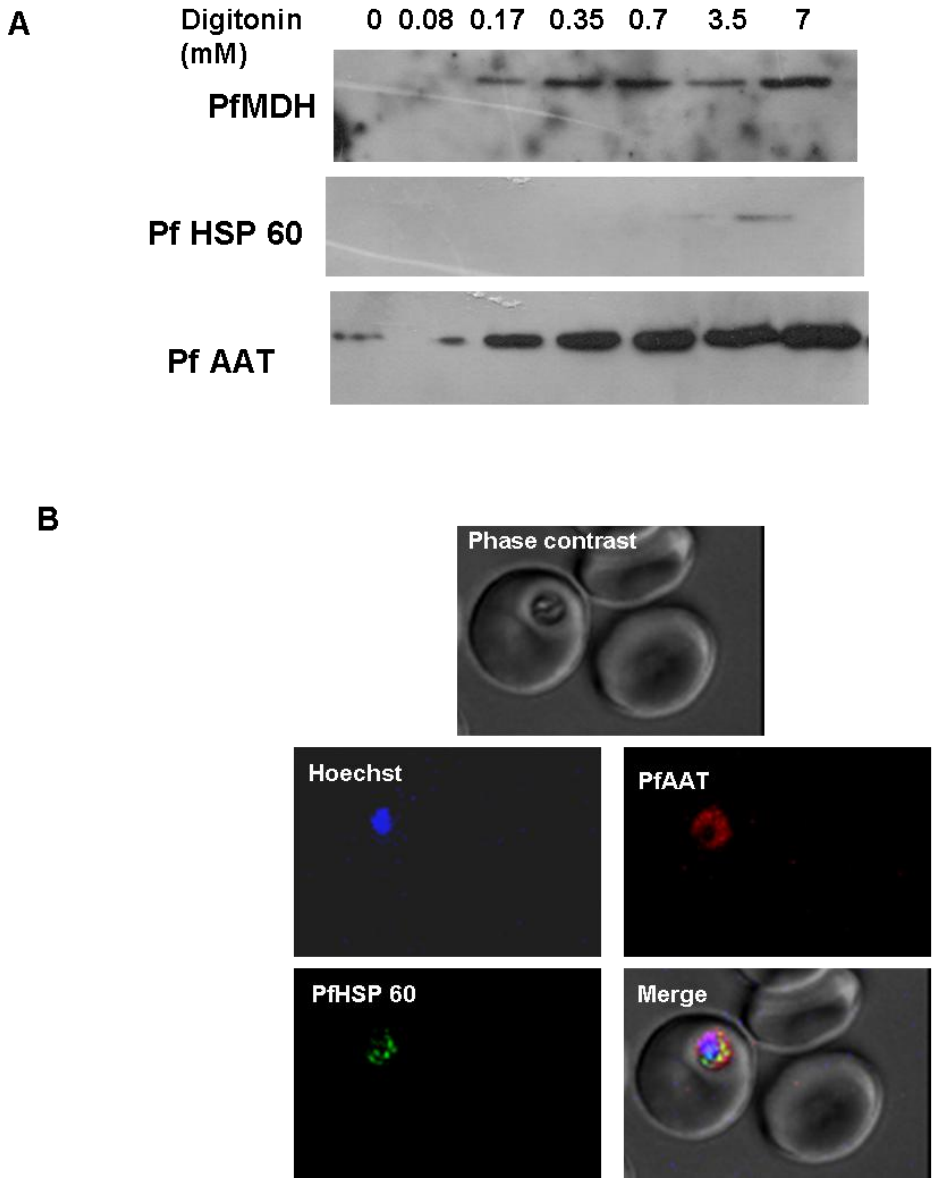

Fig. 4.16: Subcellular localization of Pf aspartate aminotransferase

(A) Western blotting of subcellular fractions of P. falciparum by anti-PfMDH, anti-PfHsp60 and anti-PfAAT antisera. (B) Indirect immunofluorescence analysis of parasitized erythrocytes with anti-PfAAT and anti-PfHsp60 antisera. Anti-mouse and anti-rabbit IgG antibodies conjugated with Alexa-Fluor dyes were used as secondary antibodies. Hoechst was used as a nuclear stain.

Substrate	K_m (mM)	k_{cat} (s^{-1})	k_{cat}/K_m (s^{-1} mM^{-1})
Glutamate	8.1±1	161± 45	19.9
Oxaloacetate	5.0 ±0.5	367 ± 100	73.5
Aspartate	14.8 ± 1.2	122 ± 20	8.3
α-ketoglutarate	1.1 ± 0.2	85 ± 18	77.5

Table 4.1: Kinetic parameters for PfAAT catalyzed reversible transamination reactions[a]

[a] *Reaction was monitored as a decrease or increase in absorbance at 270 nm due to the consumption or formation of oxaloacetate with an extinction coefficient of 782 M^{-1} cm^{-1} (Winter and Dekker, 1989)*

4.3.12 Hadacidin reduces the mitochondrial membrane potential

NMR spectra show the enrichment of ^{13}C in malate when free parasites were incubated with 2,3-^{13}C-fumarate. Further formation of aspartate is explained by the enzymatic action of malate quinone oxidoreductase to generate oxaloacetate followed by transamination by aspartate aminotransferase. If the conversion of malate to oxaloacetate is through Pf malate quinone oxidoreductase (MQO), then alteration of fumarate levels by hadacidin should perturb the flux across the electron transport chain. Hadacidin is a specific inhibitor of adenylosuccinate synthetase (ADSS) (Shigeura and Gordon, 1962) and has been shown to inhibit PfADSS with a K_i of 5.6 µM (Raman *et al.*, 2004). Previously, hadacidin was used to reduce fumarate levels through the purine nucleotide cycle in the rat hind limb muscle (Aragon and Lowenstein, 1980) and in cardiomyocytes

(Sridharan V *et al.*, 2008). In order to test the effect of depletion of fumarate levels on the flux across the electron transport chain, we treated percoll enriched parasitized erythrocytes with 1 mM hadacidin for 2 h and assayed for the mitochondrial membrane potential with tetramethyl rhodamine methyl ester (TMRM). TMRM is a Nernstian cationic dye, which distributes across membranes having a negative potential gradient. It is used for quantitative measurements of membrane potentials using Nernst equation. TMRM does not form aggregates in cell membranes nor does it interact with membrane proteins. Thus, the transmembrane distribution of TMRM is directly related to the membrane potential via Nernst equation. Parasitized erythrocytes stained with TMRM treated with hadacidin showed more than 50 % drop (p value <0.0001) in the mitochondrial membrane potential compared to the control untreated culture (Fig. 4.17).

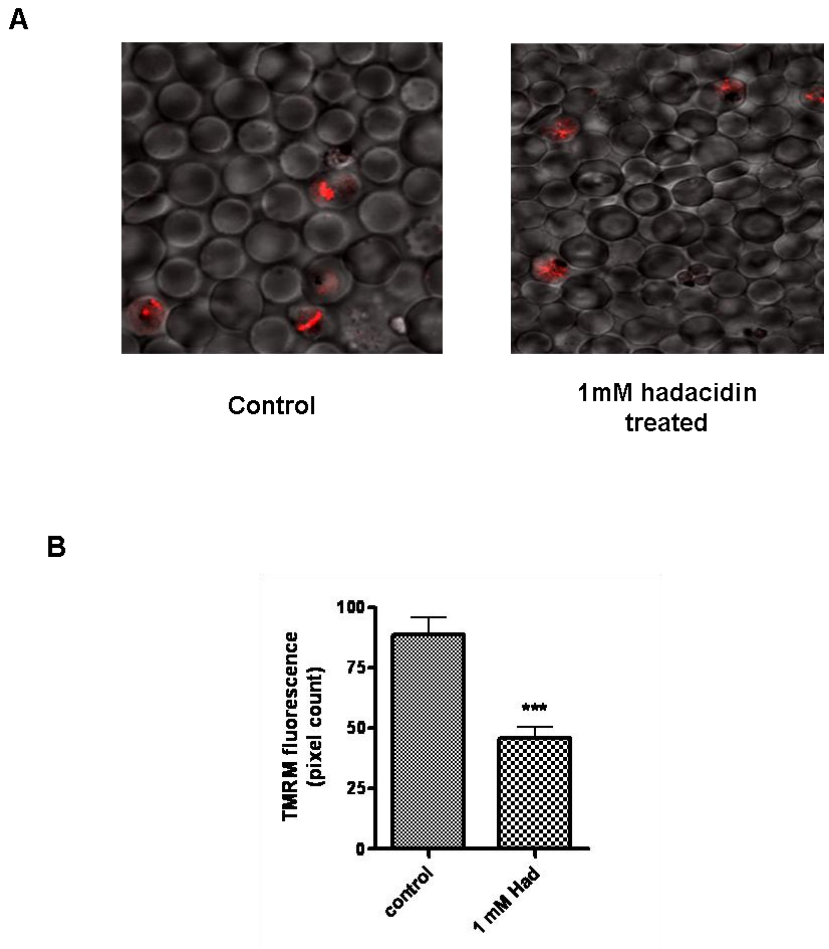

Fig. 4.17: Tetramethyl rhodamine methyl ester staining of hadacidin treated and untreated parasitized erythrocytes

*(A) Confocal images of parasitized erythrocytes stained with TMRM. The parasitized erythrocytes were either untreated (control) or treated with 1 mM hadacidin prior to staining. (B) Fluorescence intensity was obtained from ten different fields across untreated and treated samples and was compared by student's t-test. *** indicates p value <0.0001*

4.3.13 Metabolic pathway for fumarate to aspartate conversion

Based on all these studies, it can be concluded that the cytosolic fumarate generated from the purine salvage pathway is metabolized to aspartate by a metabolic route shown in Fig. 4.18. However, not all fumarate is metabolized to aspartate as bulk of the ^{13}C enrichment is seen in malate. Recently, malate efflux was also found in the spent medium of Chinese Hamster Ovary (CHO) fed batch reactor cultures (Chong *et al.*, 2010). Further, this study also showed ^{13}C enrichment in malate when the CHO cultures were pulsed with C-13 aspartate.

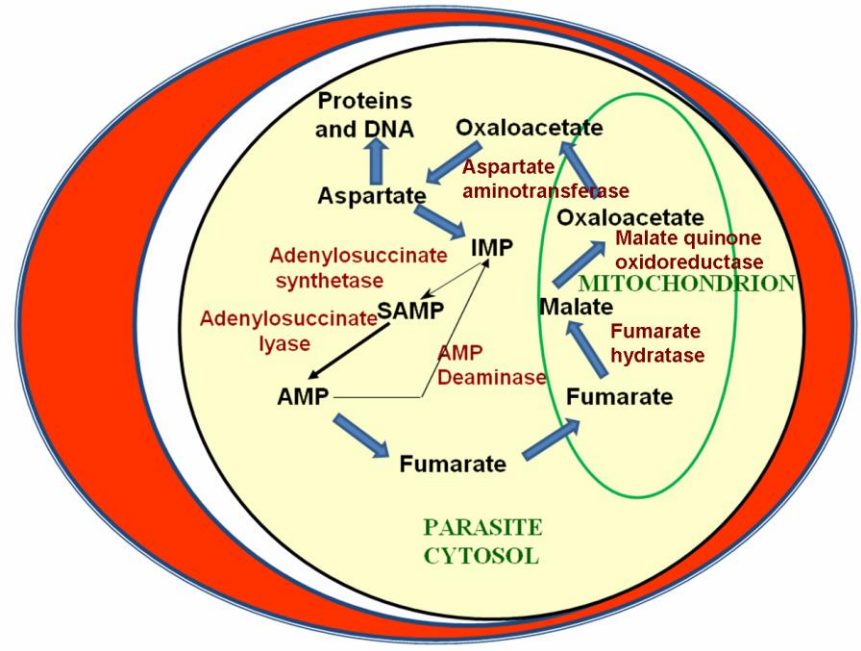

Fig. 4.18: Fumarate metabolism in *P. falciparum*

Fumarate generated in the cytosol is transported into the mitochondria, where it is acted upon by fumarate hydratase to generate malate. Malate is then catalyzed by malate quinone oxidoreducatse to oxaloacetate and in this process also generates $CoQH_2$. Oxaloacetate is then probably transported to the cytosol where it is acted upon by aspartate aminotransferase to generate aspartate or it could also be catalyzed to malate by malate dehydrogenase regenerating NAD^+.

Interestingly, succinate (C-2, C-3: δ = 29 ppm) formation was not observed in parasites incubated with ^{13}C-2,3-fumarate. This indicates that fumarate reductase activity to convert fumarate to succinate is absent or if present, very low. Earlier, Fry and Beesley proposed the presence of fumarate reductase activity in isolated mitochondria of *Plasmodium spp.* (Fry and Beesley, 1991). However, no direct biochemical proof exists for this activity, which is warranted especially in the absence of a gene encoding fumarate reductase in Plasmodium genome.

Peak resonances for glutamate (C-2, δ = 54 ppm and C-3, δ = 27 ppm) were also absent. ^{13}C enrichment of glutamate is expected if 2,3-[^{13}C]-fumarate is initially converted to citrate, which then forms α-ketoglutarate. The latter is converted to glutamate by the action of aspartate aminotransferase. The lack of ^{13}C enrichment in glutamate indicates that oxaloacetate is diverted mainly to produce aspartate by aspartate aminotransferase, and to an extent pyruvate by phosphoenol pyruvate carboxykinase and pyruvate kinase. This is unlike the normal TCA cycle in which, oxaloacetate is combined with acetyl-CoA to yield citrate by citrate synthase. As mentioned in chapter 1, acetyl-CoA produced from pyruvate dehydrogenase fuels the fatty acid biosynthesis in the apicoplast and not the TCA cycle in the mitochondria. Thus, the acetyl-CoA concentration in the mitochondria of *P. falciparum* seems to be very low to carry out the oxaloacetate to citrate conversion.

P. falciparum obtains its amino acids from host hemoglobin degradation (Sherman, 1979) and thus, the parasite may not completely rely on this metabolic pathway for aspartate. The conversion of fumarate to aspartate may then serve two important roles for the parasite: (1) metabolism of fumarate ensures a mechanism to

prevent feed back inhibition of purine salvage pathway through inhibition of SAMP to AMP conversion by ASL and (2) conversion of malate to oxaloacetate would replenish the electron transport chain and also maintain the mitochondrial membrane potential, which has been speculated to play an important role in the transport of proteins, solutes, ions across the mitochondria (van Dooren *et al.*, 2006). However, further studies involving gene knockout of one or more of the enzymes involved will undoubtedly, provide more insights.

4.4 CONCLUSIONS

Fumarate is a metabolic end product of purine salvage pathway and its intracellular concentration in *P. falciparum* is estimated to be about 0.2 mM (Teng *et al.*, 2009). Metabolic fate of fumarate has been delineated by the use of ^{14}C radioactive and ^{13}C-NMR sensitive tracers. It was found that fumarate is converted to aspartate through the metabolic intermediate malate by a pathway that involves the enzymatic action of fumarate hydratase, malate quinone oxidoreductase and aspartate aminotransferase. The conversion also feeds the electron transport chain as treatment with atovaquone inhibits the ^{13}C enrichment of aspartate from fumarate. This is the first report to show functionality to a portion of TCA cycle in *P. falciparum*. Further studies on this pathway should highlight the essentiality of this pathway to parasite survival.

APPENDIX

P. falciparum malate dehydrogenase: Expression, purification and generation of polyclonal antisera

PfMDH was expressed and purified as a C-terminal hexahistidine tagged protein through Ni-NTA affinity and gel permeation chromatography. The purified protein showed a single band with a molecular mass of around 34 kDa (Fig. 4.19 A). PfMDH was used to generate anti-Pf MDH antisera in rabbit as described in materials and methods. Antisera was then characterized for the specificity against PfMDH. Purified PfMDH was serially diluted (1 µg, 0.5 µg and 0.25 µg) and loaded on a 10 % SDS-PAGE for western blot analysis with anti-PfMDH antisera used at a dilution of 1:5000 (Fig. 4.19 B).

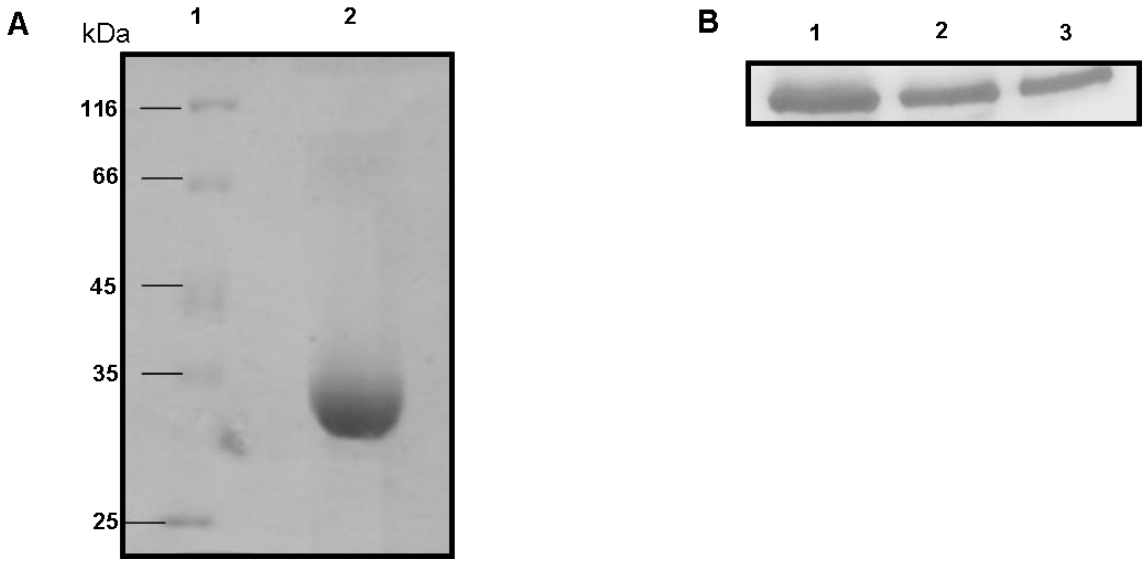

Fig. 4.19: Expression, purification and antibody characterization for PfMDH

(A) SDS-PAGE analysis of PfMDH purification. Recombinant PfMDH was purified from bacterial lysate by Ni-NTA affinity chromatography followed by gel filtration chromatography. Lane 1, Protein molecular weight marker; Lane 2, Protein fraction eluted from sephacryl S-200 gel filtration column. (B) Western blot analysis of PfMDH with anti-PfMDH antisera used at a dilution of 1:5000. Lanes 1-3, recombinant PfMDH in varying amounts (1-0.25 μg).

Summary and Future Perspectives

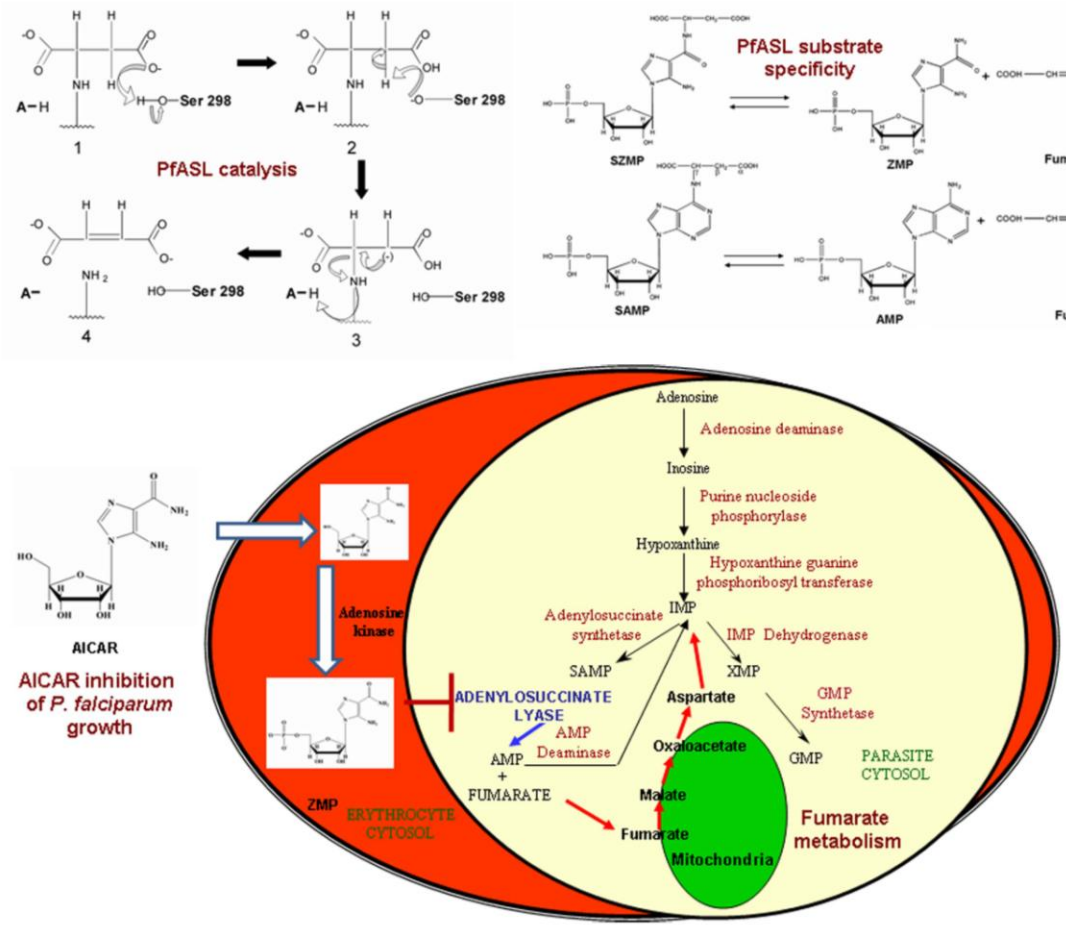

Schematic representation of the various aspects of *P. falciparum* biochemistry presented in this thesis

"Genome sequencing efforts followed by transcriptional and proteomic profiling of *Plasmodium falciparum* have generated a vast amount of data for malariologists. It was predicted that in exploring this morass of predicted genes and proteins, there is a danger of simply re-inventing any other cell". This is a quote taken from a paper written by Wilson (Wilson, 2004). However, several studies in the post genomic era have highlighted unique features about the basic biology of the malarial parasite that not only pave way for new licensed therapies in the future but also ignite broader scientific interests (Winzeler, 2008).

In the absence of a *de novo* pathway, the salvage pathway is the sole mechanism for *P. falciparum* to satisfy its purine nucleotide requirements. Enzymes of this pathway have been predicted to be promising candidates for the design of novel antimalarial drugs. Adenylosuccinate lyase is the last enzyme of the pathway, which converts adenylosuccinate (SAMP) to AMP and fumarate. The enzyme has not been characterized from any of the pathogenic protozoa and hence, a detailed kinetic and catalytic characterization of this enzyme from *P. falciparum* was carried out. The enzyme was found to catalyze the cleavage of SAMP to AMP and fumarate by a Uni-Bi Rapid Equilibrium Ordered Kinetic model. The overall rate of the reaction was limited by the C-N bond cleavage in the substrate, SAMP. Most importantly, the evidence of serine acting as the catalytic base has indeed proven to be very similar to the *E. coli* ASL thereby indicating the catalytic mechanism to be conserved across diverse species. However, a unique feature of PfASL that emerged from this study is 'substrate assisted catalysis' in which, the substrate carboxylic group assists in the ionization of the catalytic base, Ser 298. SAMP liganded crystal structure of *E. coli* ASL highlighted several residues being hydrogen bonded to the substrate carboxylic group (Tsai *et al.,* 2007). Hydrogen bonding can facilitate proton transfer in certain directions and retard proton transfer in certain other directions. This

directed proton transfer along strategically oriented hydrogen bonds in the enzyme-substrate complex plays an important role in determining the efficiency and specificity of an enzyme (Wang, 1970). Further studies involving site-directed mutagenesis of these residues should therefore; give an insight into the role of these individual hydrogen bonded networks in catalysis in PfASL.

PfASL was found to catalyze the reversible cleavage of 5-aminoimidazole-4(N-succinylcarboxamide) ribonucleotide (SZMP) to 5-aminoimidazole-4-carboxamide ribonucleotide (ZMP) and fumarate, a reaction that forms the eighth step of the *de novo* purine biosynthetic pathway**.** The physiological significance of this reaction in *P. falciparum* is unknown especially in the absence of a *de novo* purine biosynthetic pathway. However, this catalytic feature of PfASL was effectively used to inhibit the intraerythrocytic growth of *P. falciparum* using the cell permeable metabolite, AICAR. This study also highlighted the important role played by the erythrocyte compartment in mediating AICAR toxicity. Previously, several nucleoside analogs such as tubericidin, sangivamycin have been shown to have an inhibitory effect on *P. falciparum* growth (Coomber *et al.*, 1994). However, the mechanism of action of these molecules at the level of individual enzymes and metabolism in *P. falciparum* has not been elucidated (Riegelhaupt *et al.*, 2010). The studies carried out here emphasize the need to consider these aspects, particularly the role played by the erythrocyte metabolism on the mode of anti-parasitic action of these nucleoside analogs. Although, the IC_{50} of AICAR to inhibit *P. falciparum* growth was obtained at a higher concentration of 167 μM, this metabolite has been used extensively in humans at far higher doses with no toxic side effects. Thus, our findings implicate the possibility of using a naturally occurring human metabolite as a potential

antimalarial. In this regard, it also remains to be determined, the susceptibility of patients who exhibit abnormal accumulation of AICAR and ZMP in their body fluids to malaria.

Lastly, the side product of PfASL reaction, fumarate was extensively studied to elucidate its role within the parasite. It was found that fumarate is not a metabolic waste but is rather a metabolite integrating the purine salvage, *de novo* pyrimidine biosynthesis and the electron transport chain in *P. falciparum*. ^{14}C-fumarate was incorporated in proteins and DNA through its conversion to aspartate and in this process also replenishes the electron transport chain. However, the most interesting aspect of this study was the elucidation of the function of a part of TCA cycle, which was considered dysfunctional as a cycle. Fumarate hydratase, malate quinone oxidoreductase and aspartate aminotransferase are involved in the conversion of fumarate to aspartate and further studies involving genetic knockout of one or more of these enzymes would highlight the essentiality of this metabolic conversion to *P. falciparum* life cycle.

From our results, we find that *P. falciparum* aspartate aminotransferase (PfAAT) is cytosolic. Thus, oxaloacetate has to be transported out into the cytosol from the mitochondrion for it to get converted to aspartate by PfAAT. The protein most likely to be involved in this process is the malate oxoglutarate translocator.

In bean mitochondria, this translocator was found to exchange oxoglutarate for succinate, malate, malonate and oxaloacetate but not for phosphate or phosphoenolpyruvate (De Santis *et al.*, 1976). The function of this translocator in animals is to participate in the malate aspartate shuttle, a key process for the transport of reducing equivalents, NADH and NADPH across the mitochondrial membrane. In plants, the physiological function of this translocator is to export 2-oxo-glutarate to the cytosol for the biosynthesis of amino acids (Laloi, 1999). However, in *P.*

falciparum this transporter has not been characterized for its substrate specificity and it is possible that this translocator might be involved in the transport of fumarate from the cytosol to the mitochondria in exchange for oxaloacetate. It was also proposed that such a transporter could export oxaloacetate in exchange for citrate, thus bypassing the acetyl-CoA requiring step catalyzed by citrate synthase (van Dooren *et al.*, 2006). It was found that animal mitochondria under normal physiological conditions do not transport oxaloacetate significantly and a minor amount can be transported through the dicarboxylate or oxoglutarate/malate translocator. On the other hand, plant mitochondria transports oxaloacetate at rapid rates across the inner mitochondrial membrane (Laloi, 1999). Our observations reported here could imply the presence of a specific oxaloacetate transporter in *P. falciparum*, which needs identification and characterization. A BLAST search highlighted several translocators in *P. falciparum* whose functions are not known (van Dooren *et al.*, 2006). It might be possible that one of them might be involved in the export of oxaloacetate from the mitochondria into the cytosol.

After submission of this thesis (dated 09.07.10) a study was published by Olszewski *et al.*, (Olszewski *et al.*, 2010) which showed that the TCA cycle in the intraerythrocytic stages of *P. falciparum* is highly divergent from that operating in the human host. As mentioned in the thesis, it was earlier believed that there is minimal carbon flow from the cytoplasm to the mitochondria in *P. falciparum* (Vaidya and Mather, 2009). Bulk of the glucose is secreted out by the parasite as lactate (Bryant *et al.*, 1964) and there is a minimal labeling of the TCA cycle intermediates by labeled glucose (Lian *et al.*, 2009). The study by Olszewski *et al.*, however highlights that glutamine feeds the TCA cycle intermediates through 2-oxo-glutarate. The latter is metabolized in two opposite routes (Fig. 1) with one generating Succinyl-CoA (which is the conventional TCA cycle direction) and the other generating isocitrate. Because of this, the TCA

cycle in *P. falciparum* exists as a branched pathway. The study also shows that this branched pathway converges at malate, which is then secreted out by the parasite as a metabolic waste (Fig. 1).

Our studies show that fumarate is also metabolized to aspartate and pyruvate through malate and oxaloacetate. The conversion to aspartate is clearly evident from both ^{13}C-NMR experiments and from the incorporation of radiolabeled fumarate into both proteins and nucleic acids. As proposed by Olszewski *et al.*, if oxaloacetate is solely converted to malate in the mitochondrion, the formation of ^{13}C and radiolabelled aspartate would not have been evident in our experiments. Our study shows for the first time that one more step of the oxidative arm of the TCA cycle, namely the conversion of malate to oxaloacetate does occur in the parasite.

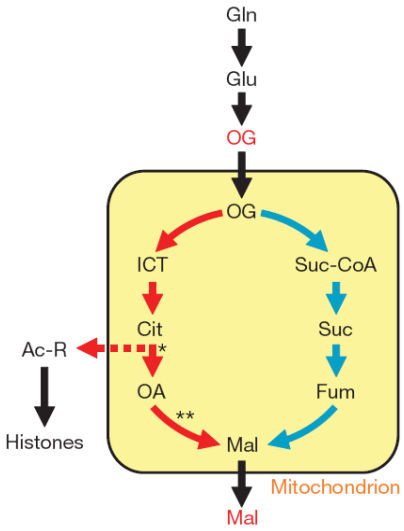

Image adapted from Olszewski *et al.*, (2010) *Nature* **466**:774-8.

Fig. 1: Branched TCA cycle in *P. falciparum*

Cytosolic glutamine (Gln) generates 2-oxoglutarate (OG) which is converted to Succinyl-CoA (Suc-CoA) or isocitrate (ICT). The pathway converges at malate (Mal). The metabolic intermediates are abbreviated as: Cit:Citrate;OA:Oxaloacetate;Fum:Fumarate;Suc:Succinate.

This conversion, of malate to oxaloacetate cannot not occur through *P. falciparum* malate dehydrogenase as it has been shown to catalyze only the reduction reaction. We also examined different conditions that are known to activate MDH from other organisms to catalyze malate to oxaloacetate conversion namely presence of citrate and aspartate aminotransferase. But these failed to alter the direction of conversion by recombinant *P. falciparum* MDH (data not shown). Malate Quinone Oxidoreductase (MQO) is a CoQ dependent dehydrogenase and the absence of ^{13}C enrichment in aspartate in parasites incubated with atovaquone and 2,3-^{13}C-fumarate indicates that this enzyme from the parasite catalyses the oxidation of malate to oxaloacetate. Indeed *P. falciparum* MQO exhibits high homology to MQO from *Helicobacter pylori* (Kather *et al.*, 2000), which has been shown to convert malate to oxaloacetate and not the reverse. A genetic approach that obliterates fumarate production would throw more light on the importance of this pathway.

Overall, the research work carried out in this thesis was focused towards understanding the enzyme adenylosuccinate lyase, with respect to its kinetic mechanism and substrate specificity. Most importantly, one of the reaction products of this enzyme, fumarate served as a tool in deciphering the functionality of few of the TCA cycle proteins within the parasite.

Agbenyega T, Angus BJ, Bedu-Addo G, Baffoe-Bonnie B, Guyton T, Stacpoole PW and Krishna S (2000) Glucose and lactate kinetics in children with severe malaria. *J. Clin. Endocrinol. Metab.* **85**:1569–76.

Albers E. (2009) Metabolic characteristics and importance of the universal methionine salvage pathway recycling methionine from 5'-methylthioadenosine. *IUBMB Life* **61**:1132-42.

Antoniou D, Basner J, Núñez S and Schwartz SD. (2006) Computational and theoretical methods to explore the relation between enzyme dynamics and catalysis. *Chem. Rev.* **106**: 3170-87.

Aragon JJ and Lowenstein JM (1980) The purine-nucleotide cycle. Comparison of the levels of citric acid cycle intermediates with the operation of the purine nucleotide cycle in rat skeletal muscle during exercise and recovery from exercise. *Eur. J. Biochem.* **110**:371-7.

Aragón JJ, Tornheim K, Goodman MN and Lowenstein JM. (1981) Replenishment of citric acid cycle intermediates by the purine nucleotide cycle in rat skeletal muscle. *Curr. Top. Cell Regul.* **18**:131-49.

Atamna H, Pascarmona G and Ginsburg H. (1994) Hexose-monophosphate shunt activity in intact Plasmodium falciparum-infected erythrocytes and in free parasites. *Mol. Biochem. Parasitol.* **67**:79-89.

Ayi K, Liles WC, Gros P and Kain KC. (2009) Adenosine triphosphate depletion of erythrocytes simulates the phenotype associated with pyruvate kinase deficiency and confers protection against Plasmodium falciparum in vitro. *J. Infect. Dis.* **200**:1289-99.

Bannister L and Mitchell G (2003) The ins, outs and roundabouts of malaria. *Trends Parasitol.* **19:**209-13.

Berger BJ, Dai WW, Wang H, Stark RE and Cerami A. (1996) Aromatic amino acid transamination and methionine recycling in trypanosomatids. *Proc. Natl. Acad. Sci. USA.* **93**:4126-30.

Berger LC, Wilson J, Wood P and Berger BJ (2001) Methionine regeneration and aspartate aminotransferase in parasitic protozoa. *J. Bacteriol.* **183**:4421-34.

Berman PA, Human L and Freese JA. (1991) Xanthine oxidase inhibits growth of Plasmodium falciparum in human erythrocytes in vitro. *J. Clin. Invest.* **88**:1848-55.

Bhat JY, Shastri BG and Balaram H. (2008) Kinetic and biochemical characterization of Plasmodium falciparum GMP synthetase. *Biochem. J.* **409**:263-73.

Biagini GA, Viriyavejakul P, O'neill PM, Bray PG and Ward SA (2006) Functional characterization and target validation of alternative complex I of Plasmodium falciparum mitochondria. *Antimicrob. Agents Chemother.* **50**:1841-51.

Blum JJ and Ginsberg H (1984) Absence of α-ketogluterate dehydrogenase activity and presence of CO2-fixing activity in *Plasmodium falciparum* grown in vitro in human erythrocytes. *J. Protozool.* **31**:167–69.

Booden T and Hull RW (1973) Nucleic acid precursor synthesis by Plasmodium lophurae parasitizing chicken erythrocytes. *Exp. Parasitol.* **34**:220-8.

Boon H, Bosselaar M, Praet SF, Blaak EE, Saris WH, Wagenmakers AJ, McGee S L, Tack CJ, Smits P, Hargreaves M and van Loon LJ. (2008) Intravenous AICAR administration reduces hepatic glucose output and inhibits whole body lipolysis in type 2 diabetic patients. *Diabetologia* **51**:1893-900.

Bozdech Z, Llinás M, Pulliam BL, Wong ED, Zhu J and DeRisi JL. (2003) The transcriptome of the intraerythrocytic developmental cycle of Plasmodium falciparum. *PLoS Biol.* **1**:E5.

Bradford MM. (1976) A rapid and sensitive method for the quantitation of microgram quantities of protein utilizing the principle of protein-dye binding. *Anal. Biochem.* **72**:248–254.

Breuer WV, Ginsburg H and Cabantchik ZI (1983) An assay of malaria parasite invasion into human erythrocytes: the effects of chemical and enzymatic modification of erythrocyte membrane components. *Biochim. Biophys. Acta* **755**:263-271.

Bridger WA and Cohen LH. (1968) The kinetics of adenylosuccinate lyase. *J. Biol. Chem.* **243**: 644–650.

Bryant C, Voller A and Smith MJ (1964) The incorporation of radioactivity from (14c) glucose into the soluble metabolic intermediates of malaria parasites. *Am. J. Trop. Med. Hyg.* **13**:515-9.

Brosius JL and Colman RF. (2002) Three subunits contribute amino acids to the active site of tetrameric adenylosuccinate lyase: Lys268 and Glu275 are required. *Biochemistry*. **41**:2217-26.

Brosius JL and Colman RF. (2000) A key role in catalysis for His89 of adenylosuccinate lyase of Bacillus subtilis. *Biochemistry* **39**:13336–13343.

Bungener W and Nielsen G. (1968) Nucleic acid metabolism in experimental malaria. 2. Incorporation of adenosine and hypoxanthine into the nucleic acids of malaria parasites (*Plasmodium berghei* and *Plasmodium vinckei*). *Z. Tropenmed Parasitol*. **19:**185–197.

Carlson J, Helmby H, Hill AVS, Brewster D, Greenwood BM and Wahlgren M (1990) Human cerebral malaria: association with erythrocyte rosetting and lack of anti-rosetting antibodies. *Lancet* **336:**1457-1460.

Carter NS, Ben Mamoun C, Liu W, Silva EO, Landfear SM, Goldberg DE and Ullman B. (2000) Isolation and functional characterization of the PfNT1 nucleoside transporter gene from Plasmodium falciparum. *J. Biol. Chem.* **275**:10683-91.

Carter CE and Cohen LH. (1956) The preparation and properties of adenylosuccinase and adenylosuccinic acid. *J. Biol.Chem.* **222**:17–30.

Cassera MB, Hazleton KZ, Riegelhaupt PM, Merino EF, Luo M, Akabas MH and Schramm VL (2008) Erythrocytic adenosine monophosphate as an alternative purine source in Plasmodium falciparum. *J. Biol. Chem.* **283**:32889-99.

Chaudhary K, Darling JA, Fohl LM, Sullivan WJ Jr, Donald RG, Pfefferkorn ER, Ullman B, and Roos DS. (2004) Purine salvage pathways in the apicomplexan parasite Toxoplasma gondii. *J. Biol. Chem.* **279**:31221-7.

Chong WP, Reddy SG, Yusufi FN, Lee DY, Wong NS, Heng CK, Yap MG and Ho YS (2010) Metabolomics-driven approach for the improvement of Chinese hamster ovary cell growth: overexpression of malate dehydrogenase II. *J. Biotechnol.* **147**:116-21

Christopherson RI, Cinquin O, Shojaei M, Kuehn D and Menz RI. (2004) Cloning and expression of malarial pyrimidine enzymes. *Nucleosides Nucleotides Nucleic Acids.* **23**:1459-65.

Claros MG and Vincens P (1996) Computational method to predict mitochondrially imported proteins and their targeting sequences. *Eur. J. Biochem.* **241**:779-86.

Collins FH and Paskewitz SM (1995) Malaria: current and future prospects for control. *Annu. Rev. Entomol.* **40**:195-219.

Coomber DW, O'Sullivan WJ and Gero AM. (1994) Adenosine analogues as antimetabolites against Plasmodium falciparum malaria. *Int. J. Parasitol.* **24**:357-65.

Daddona PE, Wiesmann WP, Lambros C, Kelley WN and Webster HK. (1984) Human malaria parasite adenosine deaminase. Characterization in host enzyme-deficient erythrocyte culture. *J. Biol. Chem.* **259**:1472-5.

Daily JP, Scanfeld D, Pochet N, Le Roch K, Plouffe D, Kamal M, Sarr O, Mboup S, Ndir O, Wypij D, Levasseur K, Thomas E, Tamayo P, Dong C, Zhou Y, Lander ES, Ndiaye D, Wirth D, Winzeler EA, Mesirov JP and Regev A (2007) Distinct physiological states of Plasmodium falciparum in malaria-infected patients. *Nature* **450**:1091-5.

Davies M, Heikkilä T, McConkey GA, Fishwick CW, Parsons MR and Johnson AP. (2009) Structure-based design, synthesis, and characterization of inhibitors of human and Plasmodium falciparum dihydroorotate dehydrogenases. *J. Med. Chem.* **52**:2683-93.

David PH, Handunnetti SM, Leech JH, Gamage P and Mendis KN (1988) Rosetting: a new cytoadherence property of malaria-infected erythrocytes. *Am. J. Trop. Med. Hyg.* **38**:289-297.

De Santis A, Arrigoni O and Palmieri F. (1976) Carrier mediated transport of metabolites in purified bean mitochondria. *Plant Cell Physiol.* **17:**1221–1233.

Desjardins RE, Canfield CJ, Haynes JD and Chulay JD. (1979) Quantitative assessment of antimalarial activity in vitro by a semiautomated microdilution technique. *Antimicrob. Agents Chemother.* **16**:710-8.

Dinglasan RR and Jacobs-Lorena M (2008) Flipping the paradigm on malaria transmission-blocking vaccines. *Trends Parasitol.* **24**:364-370.

Divo AA, Geary TG, Davis NL, Jensen JB (1985) Nutritional requirements of Plasmodium falciparum in culture. I. Exogenously supplied dialyzable components necessary for continuous growth. *J. Protozool.* **32**:59-64.

Divo AA and Jensen JB. (1982) Studies on serum requirements for the cultivation of Plasmodium falciparum. 2. Medium enrichment. *Bull World Health Organ.* **60**:571-5.

Dixon R, Gourzis J, McDermott D, Fujitaki J, Dewland P and Gruber H. (1991) AICA-riboside: safety, tolerance, and pharmacokinetics of a novel adenosine-regulating agent. *J. Clin. Pharmacol.* **31**:342-7.

Downie MJ, Kirk K and Mamoun CB. (2008) Purine salvage pathways in the intraerythrocytic malaria parasite Plasmodium falciparum. *Eukaryot Cell.* **7**:1231-7.

Downie MJ, El Bissati K, Bobenchik AM, Nic Lochlainn L, Amerik A, Zufferey R, Kirk K, and Ben Mamoun C. (2010) PfNT2, a permease of the equilibrative nucleoside transporter family in the endoplasmic reticulum of Plasmodium falciparum. *J.Biol. Chem.* **285**:20827-33.

Durand PM and Coetzer TL (2008) Pyruvate kinase deficiency protects against malaria in humans. *Haematologica* **93**:939-40.

Eastman RT and Fidock DA (2009) Artemisinin-based combination therapies: a vital tool in efforts to eliminate malaria. *Nat. Rev. Microbiol.* **7**:864-74.

Eaazhisai K, Jayalakshmi R, Gayathri P, Anand RP, Sumathy K, Balaram H and Murthy MR. (2004) Crystal structure of fully ligated adenylosuccinate synthetase from Plasmodium falciparum. *J. Mol. Biol.* **335**:1251-64.

Eisenmesser ZE, Bosco DA, Akke M and Kern D. (2002) Enzyme Dynamics During Catalysis. *Science* **295**: 1520-23.

El Bissati K, Downie MJ, Kim SK, Horowitz M, Carter N, Ullman B and Mamoun CB. (2008) Genetic evidence for the essential role of PfNT1 in the transport and utilization of xanthine, guanine, guanosine and adenine by Plasmodium falciparum. *Mol. Biochem. Parasitol.* **161**:130-9.

El Bissati K, Zufferey R, Witola WH, Carter NS, Ullman B and Ben Mamoun C. (2006) The plasma membrane permease PfNT1 is essential for purine salvage in the human malaria parasite Plasmodium falciparum. *Proc. Natl. Acad. Sci. U S A.* **103**:9286-91.

el Kouni MH. (2007) Adenosine metabolism in Toxoplasma gondii: potential targets for chemotherapy. *Curr. Pharm. Des*. **13**:581-97.

el Kouni MH (2002) Trends in the design of nucleoside analogues as anti-HIV drugs.*Curr. Pharm. Des*. **8**:581-93.

Falco EA, Goodwin LG, Hitchings GH, Rollo IM and Rusell PB (1951) 2:4-diaminopyrimidines- a new series of antimalarials *Br. J. Pharmacol. Chemother.* **6**:185-200.

Fatumo S, Plaimas K, Mallm JP, Schramm G, Adebiyi E, Oswald M, Eils R and König R. (2009) Estimating novel potential drug targets of Plasmodium falciparum by analysing the metabolic network of knock-out strains in silico. *Infect. Genet. Evol.* **9**:351-8.

Fisher N, Bray PG, Ward SA and Biagini GA. (2007) The malaria parasite type II NADH:quinone oxidoreductase: an alternative enzyme for an alternative lifestyle. *Trends Parasitol.* **23**:305-10.

Fisher N, Bray PG, Ward SA and Biagini GA. (2008) Malaria-parasite mitochondrial dehydrogenases as drug targets: too early to write the obituary. *Trends Parasitol.* **24**:9-10.

Florens L, Washburn MP, Raine J D,. Anthony R M, Grainger M, Haynes JD, Moch JK, Muster N, Sacci J B., Tabb DL,. Witney AA, Wolters, D, Wu Y, Gardner M J,Holder AA, Sinden RE, Yates JR and Carucci DJ (2002) A proteomic view of the Plasmodium falciparum life cycle. *Nature* **419**:520-526.

Flores MV, Atkins D, Wade D, O'Sullivan WJ and Stewart TS. (1997) Inhibition of Plasmodium falciparum proliferation in vitro by ribozymes. *J. Biol. Chem.* **272**:16940-5.

Flores MV, O'Sullivan WJ and Stewart TS. (1994) Characterisation of the carbamoyl phosphate synthetase gene from Plasmodium falciparum. *Mol. Biochem. Parasitol.* **68:** 315-8.

Foth BJ, Stimmler LM, Handman E, Crabb BS, Hodder AN and McFadden GI (2005) The malaria parasite Plasmodium falciparum has only one pyruvate dehydrogenase complex, which is located in the apicoplast. *Mol. Microbiol.* **55**:39-53.

Fragasso G, Sanvito F, Baratto F, Martinenghi S, Doglioni C and Margonato A (2009) Cardiotoxicity after low-dose chloroquine antimalarial therapy. *Heart Vessels* **24**:385-7.

Franco-Paredes C, Santos-Preciado JI. (2006) Problem pathogens: prevention of malaria in travellers. *Lancet Infect Dis.* **6**:139-49.

Freese JA, Sharp BL, Ridl FC and Markus MB. (1988) In vitro cultivation of southern African strains of Plasmodium falciparum and gametocytogenesis. *S. Afr. Med. J.* **73**:720-2.

Friedecky D, Vyskocilova P, Kuchynova H, Hornik P and Adam T. (2005) Nucleotides in Erythrocytes – Incorporation Study. *Klin. Biochem. Metab.***13**:182–183.

Fry M and Beesley JE. (1991) Mitochondria of mammalian Plasmodium spp. *Parasitology* **102 Pt 1**:17-26.

Fry M, Webb E and Pudney M. (1990) Effect of mitochondrial inhibitors on adenosinetriphosphate levels in Plasmodium falciparum. *Comp. Biochem. Physiol. B* **96**:775-82.

Frydman B, de los Santos C, Cannata JJ and Cazzulo JJ (1990) Carbon-13 nuclear magnetic resonance analysis of [1-13C] glucose metabolism in Trypanosoma cruzi. Evidence of the presence of two alanine pools and of two CO2 fixation reactions. *Eur. J. Biochem.* **192**:363-8.

Galmarini CM, Mackey JR and Dumontet C. (2002) Nucleoside analogues and nucleobases in cancer treatment. *Lancet Oncol.* **3**:415-24.

Gardner MJ, Hall N, Fung E, White O, Berriman M, Hyman RW, Carlton JM, Pain A, Nelson KE, Bowman S, Paulsen IT, James K, Eisen JA, Rutherford K, Salzberg SL, Craig A, Kyes S, Chan MS, Nene V, Shallom SJ, Suh B, Peterson J, Angiuoli S, Pertea M, Allen J, Selengut J, Haft D, Mather MW, Vaidya AB, Martin DM, Fairlamb AH, Fraunholz MJ, Roos DS, Ralph SA, McFadden GI, Cummings LM, Subramanian GM, Mungall C, Venter JC, Carucci DJ, Hoffman SL, Newbold C, Davis RW, Fraser CM and Barrell B (2002) Genome sequence of the human malaria parasite Plasmodium falciparum. *Nature* **419**:512-9.

Gero AM, Brown GV and O'Sullivan WJ. (1984) Pyrimidine de novo synthesis during the life cycle of the intraerythrocytic stage of Plasmodium falciparum *J. Parasitol.* **70:** 536-41.

Gherardi A and Sarciron ME. (2007) Molecules targeting the purine salvage pathway in Apicomplexan parasites. *Trends Parasitol.* **23**:384-9.

Giles NH, Partridge CW and Nelson NJ. (1957) The genetic control of adenylosuccinase in Neurospora crassa. *Proc. Natl. Acad. Sci. U. S. A.* **43**:305–317.

Ginsburg H, Ward SA and Bray PG (1999) An integrated model of chloroquine action. *Parasitol. Today* **15**:357-60.

Hadley TJ (1986) Invasion of erythrocytes by malaria parasites: a cellular and molecular overview *Annu. Rev. Microbiol.* **40**:451-77.

Haldar K, Kamoun S, Hiller NL, Bhattacharje S and van Ooij C (2006) Common infection strategies of pathogenic eukaryotes. *Nat. Rev. Microbiol.* **4**:922-31.

Haldar K, Murphy SC, Milner DA and Taylor TE (2007) Malaria: mechanisms of erythrocytic infection and pathological correlates of severe disease. *Annu. Rev. Pathol.* **2:** 217-49.

Hardie DG (2007) AMP-activated/SNF1 protein kinases: conserved guardians of cellular energy. *Nat. Rev. Mol. Cell Biol.* **8**:774-85.

Hassan HF and Coombs GH. (1988) Purine and pyrimidine metabolism in parasitic protozoa. *FEMS Microbiol. Rev.* **4**:47-83.

Hawkins CF and Bagnara AS (1987) Adenosine kinase from human erythrocytes: kinetic studies and characterization of adenosine binding sites. *Biochemistry* **26**:1982-7.

Hay SI, Guerra CA, Tatum AJ, Atkinson PM and Snow RW (2005) Urbanization, malaria transmission and disease burden in Africa. *Nat. Rev. Microbiol*. **3**:81-90.

Hayakawa T, Culleton R, Otani H, Horii T and Tanabe K (2008) Big bang in the evolution of extant malaria parasites. *Mol. Biol. Evol.* **25**:2233-9.

Higgins D, Thompson J, Gibson T, Thompson JD, Higgins DG and Gibson TJ. (1994) CLUSTALW: improving the sensitivity of progressive multiple sequence alignment through sequence weighting, position-specific gap penalties and weight matrix choice, *Nucleic Acids Res.* **22**:4673–4680.

Hill B, Kilsby J, McIntosh RT, Wrigglesworth R and Ginger CD. (1981) Pyrimidine biosynthesis in Plasmodium berghei. *Int. J. Biochem*. **13**:303-10.

Hinman A (1999) Eradication of vaccine preventable diseases. *Annu. Rev. Public Health.* **20**:211-29.

Hodges M, Yikilmaz E, Patterson G, Kasvosve I, Rouault TA, Gordeuk VR and Loyevsky M. (2005) An iron regulatory-like protein expressed in Plasmodium falciparum displays aconitase activity. *Mol. Biochem. Parasitol.* **143**:29-38

Hyde JE. (2007) Targeting purine and pyrimidine metabolism in human apicomplexan parasites *Curr. Drug Targets* **8**:31-47.

Jaeken J and Van den Berghe G. (1984) An infantile autistic syndrome characterised by the presence of succinylpurines in body fluids. *Lancet* **2**:1058-1061.

Jayalakshmi R, Sumathy K and Balaram H. (2002) Purification and characterization of recombinant Plasmodium falciparum adenylosuccinate synthetase expressed in Escherichia coli. *Protein Expr. Purif.* **25**:65-72.

Jongwutiwes S, Putaporntip C, Iwasaki T, Sata T and Kanbara H (2004) Naturally acquired *Plasmodium knowlesi* malaria in human, Thailand. *Emerg Infect Dis.* **10**:2211–3.

Kandeel M, Miyamoto T and Kitade Y. (2009) Bioinformatics, enzymologic properties, and comprehensive tracking of Plasmodium falciparum nucleoside diphosphate kinase. *Biol. Pharm. Bull.* **32**:1321-7.

Kanehisa M and Goto S (2000) KEGG: kyoto encyclopedia of genes and genomes. *Nucleic Acids Res.* **28**:27-30.

Kather B, Stingl K, van der Rest ME, Altendorf K and Molenaar D. (2000) Another unusual type of citric acid cycle enzyme in Helicobacter pylori: the malate:quinone oxidoreductase. *J.Bacteriol.* **182**:3204-9.

Kedzierski L, Escalante AA, Isea R, Black CG, Barnwell JW and Coppel RL. (2002) Phylogenetic analysis of the genus Plasmodium based on the gene encoding adenylosuccinate lyase. *Infect. Genet. Evol.* **1**:297-301.

Keough DT, Ng AL, Winzor DJ, Emmerson BT and de Jersey J. (1999) Purification and characterization of Plasmodium falciparum hypoxanthine-guanine-xanthine phosphoribosyltransferase and comparison with the human enzyme. *Mol. Biochem. Parasitol.* **98**:29-41.

Keough DT, Skinner-Adams T, Jones MK, Ng AL, Brereton IM, Guddat LW and de Jersey J. (2006) Lead compounds for antimalarial chemotherapy: purine base analogs discriminate between human and P. falciparum 6-oxopurine phosphoribosyltransferases. *J. Med. Chem.* **49**:7479-86.

Khersonsky O, Roodveldt C and Tawfik DS. (2006) Enzyme promiscuity: evolutionary and mechanistic aspects. *Curr. Opin. Chem. Biol*. **10**:498–508.

[a]Kicska GA, Tyler PC, Evans GB, Furneaux RH, Kim K and Schramm VL. (2002) Transition state analogue inhibitors of purine nucleoside phosphorylase from Plasmodium falciparum. *J. Biol. Chem.* **277**:3219-25.

[b]Kicska GA, Tyler PC, Evans GB, Furneaux RH, Schramm VL and Kim K. (2002) Purine-less death in Plasmodium falciparum induced by immucillin-H, a transition state analogue of purine nucleoside phosphorylase. *J. Biol. Chem*. **277**:3226-31.

Kim YA, King MT, Teague WE Jr, Rufo GA Jr, Veech RL and Passonneau JV. (1992) Regulation of the purine salvage pathway in rat liver. *Am. J. Physiol.* **262**:E344-52.

Kirk K, Horner HA and Kirk J (1996) Glucose uptake in Plasmodium falciparum-infected erythrocytes is an equilibrative not an active process. *Mol. Biochem. Parasitol.* **82**:195-205.

Kita K, Hirawake H, Miyadera H, Amino H and Takeo S (2002) Role of complex II in anaerobic respiration of the parasite mitochondria from Ascaris suum and Plasmodium falciparum. *Biochim. Biophys. Acta*. **1553**:123-39.

Koshland DE. (1958). Application of a Theory of Enzyme Specificity to Protein synthesis. *Proc. Natl. Acad. Sci.* **44**: 98–104.

Krungkrai J. (1995) Purification, characterization and localization of mitochondrial dihydroorotate dehydrogenase in Plasmodium falciparum, human malaria parasite. *Biochim. Biophys. Acta.* **1243**:351-60.

Krungkrai J. (2004) The multiple roles of the mitochondrion of the malarial parasite. *Parasitology*. **129**:511-24.

[a] Krungkrai SR, Aoki S, Palacpac NM, Sato D, Mitamura T, Krungkrai J and Horii T. (2004) Human malaria parasite orotate phosphoribosyltransferase: functional expression, characterization of kinetic reaction mechanism and inhibition profile. *Mol Biochem Parasitol*. **134**:245-55.

[b]Krungkrai SR, Prapunwattana P, Horii T and Krungkrai J. (2004) Orotate phosphoribosyltransferase and orotidine 5'-monophosphate decarboxylase exist as multienzyme complex in human malaria parasite Plasmodium falciparum. *Biochem. Biophys. Res. Commun.* **318**:1012-8.

Krungkrai SR, Wutipraditkul N and Krungkrai J. (2008) Dihydroorotase of human malarial parasite Plasmodium falciparum differs from host enzyme. *Biochem. Biophys. Res. Commun.* **366**:821-6.

Kyte J. (1995) Mechanism in Protein Chemistry, Garland Publishing, New York.

Laloi M. (1999) Plant mitochondrial carriers: anoverview. *Cell Mol. Life Sci*. **56**(11-12):918-44.

Lambros C and Vanderberg JP. (1979) Synchronization of Plasmodium falciparum erythrocytic stages in culture. *J. Parasitol.* **65**:418-20.

Lang-Unnasch N (1992) Purification and properties of Plasmodium falciparum malate dehydrogenase. *Mol. Biochem. Parasitol.* **50**:17-25.

Larsen NA, Heine A, Crane L, Cravatt BF, Lerner RA and Wilson IA. (2001) Structural basis for a disfavored elimination reaction in catalytic antibody 1D4. *J. Mol. Biol.* **314:**93–102.

Lee TT, Worby C, Dixon JE and Colman RF (1997) Identification of His141 in the active site of Bacillus subtilis adenylosuccinate lyase by affinity labeling with 6-(4-Bromo2,3 dioxobutyl)thioadenosine 5-monophosphate. *J. Biol. Chem.* **272:**458–465.

Lee TT, Worby C, Bao ZQ, Dixon JE and Colman RF. (1999) His68 and His141 are critical contributors to the intersubunit catalytic site of adenylosuccinate lyase of Bacillus subtilis. *Biochemistry*. **38**:22-32.

Lemieux JE, Gomez-Escobar N, Feller A, Carret C, Amambua-Ngwa A, Pinches R, Day F, Kyes SA, Conway DJ, Holmes CC and Newbold CI. (2009) Statistical estimation of cell-cycle progression and lineage commitment in Plasmodium falciparum reveals a homogeneous pattern of transcription in ex vivo culture. *Proc. Natl. Acad. Sci. U S A.* **106**:7559-64.

Lian LY, Al-Helal M, Roslaini AM, Fisher N, Bray PG, Ward SA and Biagini GA (2009) Glycerol: an unexpected major metabolite of energy metabolism by the human malaria parasite. *Malar J*. **8**:38.

Lopez MJ. (2008) Is ZMP the toxic metabolite in Lesch–Nyhan disease? *Med. Hypotheses* **71**:657–663.

Luthy R, Bowie JU and Eisenberg D. (1992) Assessment of protein models with three dimensional profiles. *Nature* **356**: 83–85.

Mackintosh CL, Beeson JG and Marsh K. (2004) Clinical features and pathogenesis of severe malaria *Trends Parasitol.* **20**:597-603.

Madrid DC, Ting LM, Waller KL, Schramm VL and Kim K. (2008) Plasmodium falciparum purine nucleoside phosphorylase is critical for viability of malaria parasites. *J. Biol. Chem.* **283**:35899-907.

Mangano DT (1997) Effects of acadesine on myocardial infarction, stroke, and death following surgery. A meta-analysis of the 5 international randomized trials. The Multicenter Study of Perioperative Ischemia (McSPI) Research Group. *JAMA* **277**:325-32.

March J. (1992) Advanced Organic Chemistry, John Wiley & Sons, New York,.

Marshall VM and Coppel RL. (1997) Characterisation of the gene encoding adenylosuccinate lyase of Plasmodium falciparum. *Mol. Biochem. Parasitol*. **88**:237-41.

Marshall JM and Taylor CE (2009) Malaria control with transgenic mosquitoes. *PLoS Med.* **6**:e20

Martin RE, Henry RI, Abbey JL, Clements JD and Kirk K. (2005) The 'permeome' of the malaria parasite: an overview of the membrane transport proteins of Plasmodium falciparum. *Genome Biol.* **6**:R26.

Mather MW, Darrouzet E, Valkova-Valchanova M, Cooley JW, McIntosh MT, Daldal F and Vaidya AB (2005) Uncovering the molecular mode of action of the antimalarial drug atovaquone using a bacterial system *J. Biol. Chem.* **280**:27458-65.

McConkey GA. (2000) Plasmodium falciparum: isolation and characterisation of a gene encoding protozoan GMP synthase. *Exp Parasitol.* **94**:23-32.

McCormick GJ, Canfield CJ and Willet GP. (1974) In vitro antimalarial activity of nucleic acid precursor analogues in the simian malaria Plasmodium knowlesi. *Antimicrob. Agents Chemother.* **6**:16-21.

McGhee RB (1953) The infection by Plasmodium lophurae of duck erythrocytes in the chicken embryo. *J. Exp. Med.* **97**:773-82.

Mehrotra S, Bopanna MP, Bulusu V and Balaram H. (2010) Adenine metabolism in Plasmodium falciparum. *Exp. Parasitol.* **125**:147-51.

Miroux B and Walker JE (1996) Over-production of proteins in Escherichia coli: mutant hosts that allow synthesis of some membrane proteins and globular proteins at high levels. *J. Mol. Biol.* **260**:289-98.

Molenaar D, van der Rest ME, Drysch A and Yucel R (2000) Functions of the membrane-associated and cytoplasmic malate dehydrogenases in the citric acid cycle of Corynebacterium glutamicum. *J. Bacteriol.* **182**:6884–6891.

Müller S and Kappes B (2007) Vitamin and cofactor biosynthesis pathways in Plasmodium and other apicomplexan parasites *Trends Parasitol.* **23**:112-21.

Nakamura J and Lou L. (1995) Biochemical characterization of human GMP synthetase. *J. Biol. Chem.* **270**:7347-53.

Narkar VA, Downes M, Yu RT, Embler E, Wang YX, Banayo E, Mihaylova MM, Nelson MC, Zou Y, Juguilon H, Kang H, Shaw RJ and Evans RM (2008) AMPK and PPARdelta agonists are exercise mimetics. *Cell* **134**:405-15.

Nayar A (2009) Malaria vaccine enters phase III clinical trials. *Nature* **459**:627.

Newbold C, Craig A, Kyes S, Rowe A, Fernandez-Reyes D and Fagan T (1999) Cytoadherence, pathogenesis and the infected red cell surface in Plasmodium falciparum. *Int. J. Parasitol.* **29**:927-37.

Ng OT, Ooi EE, Lee CC, Lee PJ, Ng LC, Pei SW, Tu TM, Loh JP and Leo YS (2008) Naturally acquired human *Plasmodium knowlesi* infection, Singapore. *Emerg. Infect. Dis.* **14**:814–6.

Nobeli I, Favia A D and Thornton JM. (2009) Protein promiscuity and its implications for biotechnology. *Nat. Biotechnol.* **27**:157-67.

Nuiry II, Hermes JD, Weiss PM, Chen CY and Cook PF. (1984) Kinetic mechanism and location of rate-determining steps for aspartase from Hafnia alvei. *Biochemistry* **235**:168–175.

Nussenzweig RS, Vanderberg J, Most H and Orton C (1967) Protective immunity produced by the injection of x-irradiated sporozoites of plasmodium berghei. *Nature* **216** 160-2.

Nzila A (2006) The past, present and future of antifolates in the treatment of Plasmodium falciparum infection. *J. Antimicrob. Chemother.* **57**:1043-54.

Olszewski KL, Morrisey JM, Wilinski D, Burns JM, Vaidya AB, Rabinowitz JD and Llinás M. (2009) Host-parasite interactions revealed by Plasmodium falciparum metabolomics. *Cell Host Microbe* **5**:191-9.

Olszewski KL, Mather MW, Morrisey JM, Garcia BA, Vaidya AB, Rabinowitz JD, Llinás M. (2010) Branched tricarboxylic acid metabolism in Plasmodium falciparum. *Nature* **466**:774-8.

Painter HJ, Morrisey JM, Mather MW and Vaidya AB. (2007) Specific role of mitochondrial electron transport in blood-stage Plasmodium falciparum. *Nature.* **446**:88-91.

Palenchar JB and Colman RF. (2003) Characterization of a mutant Bacillus subtilis adenylosuccinate lyase equivalent to a mutant enzyme found in human adenylosuccinate lyase deficiency: asparagine 276 plays an important structural role. *Biochemistry*. **42**:1831–1841.

Palenchar JB, Crocco JM and Colman RF. (2003) The characterization of mutant Bacillus subtilis adenylosuccinate lyases corresponding to severe human adenylosuccinate lyase deficiencies. *Protein Sci.* **12**:1694-705.

Parker WB and Long MC. (2007) Purine metabolism in Mycobacterium tuberculosis as a target for drug development. *Curr. Pharm. Des.* **13**:599-608.

Patel V, Booker M, Kramer M, Ross L, Celatka CA, Kennedy LM, Dvorin JD, Duraisingh MT, Sliz P, Wirth DF and Clardy J. (2008) Identification and characterization of small molecule inhibitors of Plasmodium falciparum dihydroorotate dehydrogenase. *J. Biol. Chem.* **283**:35078-85.

Pegg AE. (2009) Mammalian polyamine metabolism and function. *IUBMB Life.* **61**:880-94.

Pei Y, Tarun AS, Vaughan AM, Herman RW, Soliman JM, Erickson-Wayman A and Kappe SH (2010) Plasmodium pyruvate dehydrogenase activity is only essential for the parasite's progression from liver infection to blood infection. *Mol. Microbiol.* **75**:957-71.

Pérignon JL, Hamet M and Druilhe P. (1994) Cytidine triphosphate synthetase activity in asexual blood stages of Plasmodium falciparum. *Mol. Biochem. Parasitol.* **67**:179-82.

Polet H and Barr CF. (1968) DNA, RNA, and protein synthesis in erythrocytic forms of Plasmodium knowlesi. *Am. J. Trop. Med. Hyg.* **17**:672-9.

Polet H, Brown ND and Angel CR (1969) Biosynthesis of amino acids from 14C-U-glucose, pyruvate, and acetate by erythrocytic forms of *P. knowlesi* in vitro. *Proc. Soc. Exp. Biol. Med.* **131**:1215–18.

Porter DJ, Rudie NG and Bright HJ. (1983) Nitro analogs of substrates for adenylosuccinate synthetase and adenylosuccinate lyase. *Arch. Biochem. Biophys.* **225**: 157–163.

Pradhan A, Mukherjee P, Tripathi AK, Avery MA, Walker LA and Tekwani BL (2009) Analysis of quaternary structure of a [LDH-like] malate dehydrogenase of Plasmodium falciparum with oligomeric mutants. *Mol. Cell Biochem.* **325**:141-8.

Pradines B, Spiegel A, Rogier C, Tall A, Mosnier J, Fusai T, Trape JF and Parzy D (2000) Antibiotics for prophylaxis of Plasmodium falciparum infections: in vitro activity of doxycycline against Senegalese isolates. *Am. J. Trop. Med. Hyg.* **62**:82-5.

Quashie NB, Dorin-Semblat D, Bray PG, Biagini GA, Doerig C, Ranford-Cartwright LC, and De Koning HP. (2008) A comprehensive model of purine uptake by the malaria parasite Plasmodium falciparum: identification of four purine transport activities in intraerythrocytic parasites. *Biochem J.* **411**:287-95.

Queen SA, Jagt DL and Reyes P. (1990) In vitro susceptibilities of Plasmodium falciparum to compounds which inhibit nucleotide metabolism. *Antimicrob. Agents Chemother.* **34**:1393-8.

Radzicka A and Wolfenden R (1997) A proficient enzyme. *Science* **276**:942-5.

Rager N, Mamoun CB, Carter NS, Goldberg DE and Ullman B. (2001) Localization of the Plasmodium falciparum PfNT1 nucleoside transporter to the parasite plasma membrane. *J. Biol. Chem.* **276**:41095-9.

Raman J, Mehrotra S, Anand RP and Balaram H. (2004) Unique kinetic mechanism of Plasmodium falciparum adenylosuccinate synthetase. *Mol. Biochem. Parasitol*. **138**:1-8.

Raman J, Sumathy K, Anand RP and Balaram H. (2004) A non-active site mutation in human hypoxanthine guanine phosphoribosyltransferase expands substrate specificity. *Arch. Biochem. Biophys*. **427**:116-22.

Ratner S, (1972) In: P.D. Boyer (Ed.), 3rd ed., The Enzymes, Vol.7, Academic Press, New York, , pp. 167–197.

Riegelhaupt PM, Cassera MB, Fröhlich RF, Hazleton KZ, Hefter JJ, Schramm VL, and Akabas MH. (2010) Transport of purines and purine salvage pathway inhibitors by the Plasmodium falciparum equilibrative nucleoside transporter PfENT1. .*Mol. Biochem. Parasitol.* **169**:40-9.

Reyes P, Rathod PK, Sanchez DJ, Mrema JE, Rieckmann KH, and Heidrich HG. (1982) Enzymes of purine and pyrimidine metabolism from the human malaria parasite, Plasmodium falciparum. *Mol. Biochem. Parasitol.* **5:**275–290.

Roberts F, Roberts CW, Johnson JJ, Kyle DE, Krell T, Coggins JR, Coombs GH, Milhous WK, Tzipori S, Ferguson DJ, Chakrabarti D and McLeod R. (1998) Evidence for the shikimate pathway in apicomplexan parasites**.** *Nature*. **393**:801-5.

Roestenberg M, McCall M, Hopman J, Wiersma J, Luty AJ, van Gemert GJ, van de Vegte-Bolmer M, van Schaijk B, Teelen K, Arens T, Spaarman L, de Mast Q, Roeffen W, Snounou G, Rénia L, van der Ven A, Hermsen CC and Sauerwein R. (2009) Protection against a Malaria Challenge by Sporozoite Inoculation. *N. Engl. J. Med.* **361:**468-77.

Roth E Jr, Ogasawara N and Schulman S. (1989) The deamination of adenosine and adenosine monophosphate in Plasmodium falciparum-infected human erythrocytes: in vitro use of 2'deoxycoformycin and AMP deaminase-deficient red cells. *Blood* **74**:1121-5.

Roth EF Jr, Ruprecht RM, Schulman S, Vanderberg J, Olson JA. (1986) Ribose metabolism and nucleic acid synthesis in normal and glucose-6-phosphate dehydrogenase-deficient human erythrocytes infected with Plasmodium falciparum. *J. Clin. Invest.* **77**:1129-35.

Saliba KJ and Kirk K. (2001) Nutrient acquisition by intracellular apicomplexan parasites: staying in for dinner. *Int. J. Parasitol.* **31**:1321-30.

Sali A and Blundell TL (1993) Comparative protein modelling by satisfaction of spatial restraints. *J. Mol. Biol.* **234**: 779–815.

Salter AF and Cerami A (1992) Inhibition by chloroquine of a novel haem polymerase enzyme activity in malaria trophozoites. *Nature* **355**:108-109.

Sandrine MB, Heron P, Bitoun T, Timmerman Van den Berghe G and Vincent MF (2004) AICA-Ribosiduria: A Novel, Neurologically Devastating Inborn Error of Purine Biosynthesis Caused by Mutation of ATIC. *Am. J. Hum. Genet.* **74**:1276–1281.

Schlitzer M (2008) Antimalarial Drugs – What is in Use and What is in the Pipeline. *Arch. Pharm. Chem. Life Sci.* **341**:149-163.

Schwartz SD and Schramm VL. (2009) Enzymatic transition states and dynamic motion in barrier crossing. *Nat. Chem. Biol.* **5**: 551 – 558.

Segel IH. (1975) Enzyme kinetics, Behavior and Analysis of Rapid Equilibrium and Steady-State Enzyme Systems, John Wiley & Sons, Inc., NY, , pp. 320–329.

Sharma P, Bharadwaj A, Bhasin VK, Sailaja VN and Chauhan VS. (1996) Antibodies to a conserved-motif peptide sequence of the Plasmodium falciparum thrombospondin-related anonymous protein and circumsporozoite protein recognize a 78-kilodalton protein in the asexual blood stages of the parasite and inhibit merozoite invasion in vitro. *Infect. Immun.* **64**:2172-9.

Shenoy AR and Visweswariah SS. (2003) Site-directed mutagenesis using a single mutagenic oligonucleotide and DpnI digestion of template DNA. *Anal. Biochem.* **319:**335–336.

Sherman IW (1979) Biochemistry of Plasmodium (malarial parasites) *Microbiol. Rev.* **43**:453-95.

Sherman IW (1998) Malaria: Parasite biology, pathogenesis and protection. American Society for Microbiology, Washington D.C.

Sherman IW and Ting IP (1968) Carbon dioxide fixation in malaria. II. *Plasmodium knowlesi* (monkey malaria). *Comp. Biochem. Physiol.* **24**:639–42.

Sherman IW and Ting IP (1966) Carbon dioxide fixation in malaria (*Plasmodium lophurae*). *Nature* **212**:1387–88.

Shi W, Dunbar J, Jayasekera MM, Viola RE and Farber GK. (1997) The structure of L-aspartate ammonia-lyase from Escherichia coli. *Biochemistry* **36**: 9136–44.

Shi W, Ting LM, Kicska GA, Lewandowicz A, Tyler PC, Evans GB, Furneaux RH, Kim K, Almo SC and Schramm VL. (2004) Plasmodium falciparum purine nucleoside phosphorylase: crystal structures, immucillin inhibitors, and dual catalytic function. *J. Biol. Chem.* **279**:18103-6.

Shigeura HT and Gordon CN (1962) The mechanism of action of hadacidin *J. Biol. Chem.* **237**:1937–1940.

Showen KB and Showen RL. (1982) Solvent isotope effects of enzyme systems. *Methods Enzymol.* **87**:551–606.

Simpson A, Bateman O, Driessen H, Lindley P, Moss D, Mylvaganam S, Narebor E and Slingsby C. (1994) The structure of avian eye lens-crystallin reveals a new fold for a superfamily of oligomeric enzymes, *Nat. Struct. Biol.* **1:** 724–733.

Singh B, Kim Sung L, Matusop A, Radhakrishnan A, Shamsul SS, Cox-Singh J, Thomas A and Conway DJ (2004) A large focus of naturally acquired *Plasmodium knowlesi* infections in human beings. *Lancet.* **363**:1017–24.

Sivendran S and Colman RF. (2008) Effect of a new non-cleavable substrate analog on wildtype and serine mutants in the signature sequence of adenylosuccinate lyase of Bacillus subtilis and Homo sapiens. *Protein Sci.* **17**:1162–1174.

Spiegel EK, Colman RF and Patterson D. (2006) Adenylosuccinate lyase deficiency. *Mol. Genet. Metab.* **89**:19–31.

Sridharan V, Guichard J, Li CY, Muise-Helmericks R, Beeson CC and Wright GL (2008) O(2)-sensing signal cascade: clamping of O(2) respiration, reduced ATP utilization, and inducible fumarate respiration. *Am. J. Physiol. Cell Physiol.* **295**:C29-37.

Srivastava IK, Rottenberg H and Vaidya AB. (1997) Atovaquone, a broad spectrum antiparasitic drug, collapses mitochondrial membrane potential in a malarial parasite. *J. Biol. Chem.* **272**:3961-6.

Srivastava IK and Vaidya AB (1999) A mechanism for the synergistic antimalarial action of atovaquone and proguanil. *Antimicrob Agents Chemother*. **43**:1334-9.

Stone RL, Zalkin H and Dixon JE. (1993) Expression, purification, and kinetic characterization of recombinant human adenylosuccinate lyase. *J. Biol. Chem.* **268**:19710–19716.

Striepen B, Pruijssers AJ, Huang J, Li C, Gubbels MJ, Umejiego NN, Hedstrom L, and Kissinger JC. (2004) Gene transfer in the evolution of parasite nucleotide biosynthesis. *Proc. Natl. Acad. Sci. U S A.* **101**:3154-9.

Sufrin JR, Meshnick SR, Spiess AJ, Garofalo-Hannan J, Pan XQ and Bacchi CJ. (1995) Methionine recycling pathways and antimalarial drug design. *Antimicrob. Agents Chemother.* **39**:2511-5.

Surolia N and Surolia A (2001) Triclosan offers protection against blood stages of malaria by inhibiting enoyl-ACP reductase of Plasmodium falciparum. *Nat. Med.* **7**:167-73.

Targett GA and Greenwood BM (2008) Malaria vaccines and their potential role in the elimination of malaria. *Malar. J.* **7**:S10.

Teng R, Junankar PR, Bubb WA, Rae C, Mercier P and Kirk K. (2009) Metabolite profiling of the intraerythrocytic malaria parasite Plasmodium falciparum by (1)H NMR spectroscopy. *NMR Biomed.* **22**:292-302.

Ting LM, Gissot M, Coppi A, Sinnis P and Kim K. (2008) Attenuated Plasmodium yoelii lacking purine nucleoside phosphorylase confer protective immunity. *Nat. Med.* **14**:954-8.

Ting LM, Shi W, Lewandowicz A, Singh V, Mwakingwe A, Birck MR, Ringia EA, Bench G, Madrid DC, Tyler PC, Evans GB, Furneaux RH, Schramm VL and Kim K. (2005) Targeting

a novel Plasmodium falciparum purine recycling pathway with specific immucillins. *J. Biol. Chem.* **280**:9547–9554.

Tonkin CJ, van Dooren GG, Spurck TP, Struck NS, Good RT, Handman E, Cowman AF and McFadden GI. (2004) Localization of organellar proteins in Plasmodium falciparum using a novel set of transfection vectors and a new immunofluorescence fixation method. *Mol. Biochem. Parasitol.* **137**:13-21.

Tornheim K and Lowenstein JM. (1972) The Purine Nucleotide Cycle: the production of ammonia from aspartate by extracts of rat skeletal muscle. *J. Biol.Chem.* **247:**162–169.

Toth EA, Worby C, Dixon JE, Goedken ER, Marqusee S and Yeates TO (2000) The crystal structure of adenylosuccinate lyase from Pyrobaculum aerophilum reveals an intracellular protein with three disulfide bonds. *J. Mol. Biol.* **301**: 433-50.

Toth EA and Yeates TO (2000) The structure of adenylosuccinate lyase, an enzyme with dual activity in the de novo purine biosynthetic pathway. *Structure* **8:**163–174.

Trager W and Jensen JB. (1976) Human malaria parasites in continuous culture *Science* **193:** 673–675.

Tripathi AK, Desai PV, Pradhan A, Khan SI, Avery MA, Walker LA and Tekwani BL (2004) An alpha-proteobacterial type malate dehydrogenase may complement LDH function in Plasmodium falciparum. Cloning and biochemical characterization of the enzyme. *Eur. J. Biochem.* **271**:3488-502.

Tsai M, Koo J, Yip P, Colman RF, Segall ML, and Howell PL (2007) Substrate and product complexes of Escherichia coli adenylosuccinate lyase provide new insights into the enzymatic mechanism. *J. Mol. Biol.* **370**: 541-54.

Turner MA, Simpson A, McInnes RR and Howell PL. (1997) Human argininosuccinate lyase:a structural basis for intragenic complementation, *Proc. Natl. Acad. Sci.* **94:** 9063–9068.

Tyler PC, Taylor EA, Fröhlich RF and Schramm VL. (2007) Synthesis of 5'-methylthio coformycins: specific inhibitors for malarial adenosine deaminase. *J. Am. Chem. Soc.* **129**:6872-9.

Umejiego NN, Li C, Riera T, Hedstrom L and Striepen B. (2004) Cryptosporidium parvum IMP dehydrogenase: identification of functional, structural, and dynamic properties that can be exploited for drug design. *J. Biol. Chem.* **279**:40320-7.

Umejiego NN, Gollapalli D, Sharling L, Volftsun A, Lu J, Benjamin NN, Stroupe AH, Riera TV, Striepen B and Hedstrom L. (2008) Targeting a prokaryotic protein in a eukaryotic pathogen: identification of lead compounds against cryptosporidiosis. *Chem. Biol.* **15**:70-7.

Uyemura SA, Luo S, Moreno SN and Docampo R. (2000) Oxidative phosphorylation, Ca(2+) transport, and fatty acid-induced uncoupling in malaria parasites mitochondria. *J. Biol. Chem.* **275**:9709-15.

Uyemura SA, Luo S, Vieira M, Moreno SN and Docampo R. (2004) Oxidative phosphorylation and rotenone-insensitive malate- and NADH-quinone oxidoreductases in Plasmodium yoelii yoelii mitochondria in situ. *J. Biol. Chem.* **279**:385-93.

Vaidya AB and Mather MW. (2009) Mitochondrial evolution and functions in malaria parasites. *Annu. Rev. Microbiol*. **63**:249-67.

Van den Berghe G, Bontemps F, Vincent MF and Van den Bergh F. (1992) The purine nucleotide cycle and its molecular defects. *Prog. Neurobiol.* **39**:547-61.

Van den Bergh F, Vincent MF, Jaeken J and Van den Berghe G. (1991) Radiochemical assay of adenylosuccinase: demonstration of parallel loss of activity toward both adenylosuccinate and succinylaminoimidazole carbamide ribotide in liver of patients with the enzyme defect. *Anal. Biochem.* **193**:287–291.

Van den Bergh F, Vincent MF, Jaeken J and Van den Berghe G. (1993) Residual adenylosuccinase activities in fibroblasts of adenylosuccinase-deficient children: parallel deficiency with adenylosuccinate and succinyl-AICAR in profoundly retarded patients and non-parallel deficiency in a mildly retarded girl. *J. Inherit. Metab. Dis*.**16**:415-24.

van Dooren GG, Marti M, Tonkin CJ, Stimmler LM, Cowman AF, and McFadden GI (2005) Development of the endoplasmic reticulum, mitochondrion and apicoplast during the asexual life cycle of Plasmodium falciparum. *Mol. Microbiol.* **57:***405–419.*

van Dooren GG, Stimmler LM and McFadden GI (2006) Metabolic maps and functions of the Plasmodium mitochondrion. *FEMS Microbiol. Rev.* **30**:596-630.

Van Dyke K, Tremblay GC, Lantz CH and Szustkiewicz C. (1970) The source of purines and pyrimidines in Plasmodium berghei. *Am. J. Trop. Med. Hyg.* **19**:202-8.

Vriend G. (1990) WHAT IF: a molecular modeling and drug design program. *J.Mol.Graph.* **8**:52–56.

Walsh CJ and Sherman IW (1968) Purine and pyrimidine synthesis by the avian malaria parasite, Plasmodium lophurae. *J. Protozool*. **15**:763-70.

Wang JH. (1970) Directional character of proton transfer in enzyme catalysis. *Proc. Natl. Acad. Sci. U S A.* 66:874-81.

Wang CC, and Aldritt S. (1983) Purine salvage networks in *Giardia lamblia*. *J. Exp. Med.* **158:**1703–1712.

Weaver TM, Levitt DG, Donnelly MI, Stevens PP, Wilkens and Banaszak LJ. (1995) The multisubunit active site of fumarase C from Escherichia coli. *Nat. Struct. Biol.***2**:654–662.

Webster HK, Whaun JM, Walker MD and Bean TL. (1984) Synthesis of adenosine nucleotides from hypoxanthine by human malaria parasites (Plasmodium falciparum) in continuous erythrocyte culture: inhibition by hadacidin but not alanosine. *Biochem. Pharmacol.* **33**:1555–1557.

Webster HK and Whaun JM. (1982) Antimalarial properties of bredinin. Prediction based on identification of differences in human host-parasite purine metabolism. *J. Clin. Invest.* **70**:461-9.

Westheimer FH. (1961) The magnitude of the primary kinetic isotope effect for compounds of hydrogen and deuterium. *Chem. Rev.* **61**:265–273.

White NJ, Warrell DA, Chanthavanich P, Looareesuwan S, Warrell MJ, Krishna, S, Williamson DH, and Turner RC (1983) Severe hypoglycemia and hyperinsulinemia in falciparum malaria. *N. Engl. J. Med.* **309**:61–6.

Wilson RJ. (2004) The transcriptome: malariologists ride the wave. *Bioessays* **26**:339-42.

Winter HC and Dekker EE (1989) Specificity of Aspartate Aminotransferases from Leguminous Plants for 4-Substituted Glutamic Acids. *Plant Physiol.* **89**:1122-1128.

Winzeler EA. (2008) Malaria research in the post-genomic era. *Nature.* **455**:751-6.

Wittmann JG, Heinrich D, Gasow K, Frey A, Diederichsen U and Rudolph MG. (2008) Structures of the human orotidine-5'-monophosphate decarboxylase support a covalent mechanism and provide a framework for drug design. *Structure* **16**:82-92.

Woodward DO and Braymer HD. (1966) Purification and properties of Neurospora adenylosuccinase, *J. Biol. Chem.* **241**:580–587.

Wrenger C and Muller S (2003) Isocitrate dehydrogenase of Plasmodium falciparum. *Eur. J. Biochem.* **270**:1775-83.

Wu CY, Lee HJ, Wu SH, Chen ST, Chiou SH and Chang GG. (1998) Chemical mechanism of the endogenous argininosuccinate lyase activity of duck lens delta2-crystallin. *Biochem. J.* **333**:327–334.

Yu M, Kumar TR, Nkrumah LJ, Coppi A, Retzlaff S, Li CD, Kelly BJ, Moura PA, Lakshmanan V, Freundlich JS, Valderramos JC, Vilcheze C, Siedner M, Tsai JH, Falkard B, Sidhu AB, Purcell LA, Gratraud P, Kremer L, Waters AP, Schiehser G, Jacobus DP, Janse CJ, Ager A, Jacobs WR Jr, Sacchettini JC, Heussler V, Sinnis P, and Fidock DA (2008) The fatty acid biosynthesis enzyme FabI plays a key role in the development of liver-stage malarial parasites. *Cell Host Microbe.* **4**:567-78.

Yuan P, Hendriks EF, Fernandez HR, O'Sullivan WJ and Stewart TS. (2005) Functional expression of the gene encoding cytidine triphosphate synthetase from Plasmodium falciparum which contains two novel sequences that are potential antimalarial targets. *Mol. Biochem. Parasitol.* **143**:200-8.

Zeuthen T, Wu B, Pavlovic-Djuranovic S, Holm LM, Uzcategui NL, Duszenko M, Kun JF, Schultz JE and Beitz E. (2006) Ammonia permeability of the aquaglyceroporins from Plasmodium falciparum, Toxoplasma gondii and Trypansoma brucei. *Mol. Microbiol.* **61**:1598-608.

Zimmermann TP and Deeprose RD (1978) Metabolism of 5-amino-1-beta-D-ribofuranosylimidazole-4-carboxamide and related five-membered heterocycles to 5'-triphosphates in human blood and L5178Y cells. *Biochem. Pharmacol.* **27**:709-716.

Zolg JW, MacLeod AJ, Dickson IH and Scaife JG. (1982) Plasmodium falciparum: modifications of the in vitro culture conditions improving parasitic yields. *J. Parasitol*. **68**:1072-80.